INTERFACIAL PHENOMENA OF CRUDE OIL/BRINE/ROCK/SURFACTANT SYSTEMS IN LOWER 48 SHALE RESERVOIRS AND THEIR OPTIMUM SURFACTANT STRUCTURES FOR ENHANCED OIL RECOVERY PROCESS

A Dissertation

by

I WAYAN RAKANANDA SAPUTRA

Submitted to the Graduate and Professional School of
Texas A&M University
in partial fulfillment of the requirements for the degree of

DOCTOR OF PHILOSOPHY

Chair of Committee,	David S. Schechter
Committee Members,	Jenn Tai-Liang
	Sara Abedi
	Mahmoud El-Halwagi
Head of Department,	Jeff Spath

May 2022

Major Subject: Petroleum Engineering

ABSTRACT

This study investigates how the structure of surfactant molecules interacts with the crude oil/rock/brine system characteristic of unconventional liquid reservoirs. In most cases, the interaction results in the improvement of oil recovery. There also exists cases where it negatively influences oil recovery. Recovery improvement by surfactant could be applied to the field, especially on unconventional oil wells that are depleted and in terminal decline. As reported in Enverus (Accessed September 3rd, 2021) in June of 2020, the number of these prospective oil wells is more than 150,000 located in the lower 48., thus making the application of Surfactant-Assisted Spontaneous Imbibition (SASI) even more attractive. However, due to the fact that improperly chosen surfactants can negatively affect recovery, a robust understanding of how different surfactant molecules behaves in the shale system is crucial.

The utilization of unconventional reservoirs is relatively recent when compared to conventional reservoirs. While interfacial studies can be commonly found in conventional reservoirs, the same cannot be said for unconventional reservoirs. In the first part of this study, the heterogeneity of crude oil composition, brine characteristics, and rock mineralogy of the Lower 48 shale is presented. Fifteen crude oil samples, five rock samples, and four brines are incorporated in this study. Characterization method such as gas chromatography (GC), Saturates, Aromatics, Resins, and Asphaltenes (SARA) analysis, X-Ray Diffraction (XRD), density, etc., are incorporated. The aim is to provide

a detailed description of the shale heterogeneity. It is found that shale is highly heterogenous from one reservoir to another.

The next step is to investigate the interaction between the three phases, oil, brine, and rock. Oil and brine interaction is analyzed by studying the trend of interfacial tension value with varying oil and brine composition that can be found in unconventional reservoirs. Then, the rock-phase is added to investigate the wettability of a crude oil/brine/rock system with varying composition and mineralogy. And finally, spontaneous imbibition experiments for base case conditions are performed on multiple combination of crude oil, rock mineralogy, and brine salinity. Interfacial tension and wettability provide the greatest insight of interfacial phenomena in shale reservoir systems. Spontaneous imbibition is important as it provides context, it captures how the effects of crude oil/brine/rock properties to the interfacial tension and wettability are translated to the fluid flow in a porous media setting. Spontaneous imbibition is the ultimate experiment for understanding surfactant additives as it encapsules all aspects that are relevant in producing an oil reservoir.

Once the base scenario is determined, the next step is to incorporate surfactant. Twelve surfactants are systematically investigated the effect of tailgroup and headgroup structure. The same methodology previously described is performed. First, the effect of surfactant to an oil/brine system is investigated with IFT. Then, the effect of surfactant to an oil/brine/rock system is investigated with wettability. Finally, oil recovery as a function of surfactant structure is analyzed through imbibition experiments.

DEDICATION

This dissertation is dedicated to my parents.

ACKNOWLEDGEMENTS

I would like to thank my committee chair, Dr. Schechter. For providing an amazing research group that allows me to learn, grow my confidence, and sharpen my surfactant knowledge. I would like to thank for all the advice and guidance, both academically and in life, that has been provided through the six years of working in his research group.

I also would like to thank my committee members, Dr. Liang, Dr. Abedi, and Dr. El-Halwagi, for their guidance and support throughout the course of this research.

I would like to thank my mother and father for their continuous support and encouragement throughout my graduate studies. I would like to thank my sister for manning the home base while I am pursuing my degree.

I would like to thank Elizabeth Saputra for her patience, love, and support throughout my PhD study.

I would like to thank the department faculty and staff for making my time at Texas A&M University a great experience. Especially to John Maldonado, for his help and his friendship.

I would like to thank Johannes Alvarez and Manoj Valluri for their guidance during the early time of my graduate study. I would like to thank Denise Benoit for her mentorship that completely revolutionize my analytical and experimental design skill. As well as for her introduction to JMP.

I would like to thank Fan Zhang and Imad Adel for the friendship, discussion, and camaraderie during the first two years of my PhD study.

I would like to thank my research group for enabling a collaborative and conducive research atmosphere. Stefano Tagliaferi, for all the help designing and manufacturing HPHT set up in the lab and all the friendship. Weidong Chen, for all our discussion of surfactant in the early time of my research. Elsie Ladan and Tobi Adebisi, for their help in the laboratory and all our discussion on nonionic and ionic surfactants. Especially for Elsie Ladan, for her help on the cloud point measurement. Aashrit Bagareddy, for his help on one of the projects we are involved in the group.

I would like to thank all companies that provided surfactant, crude oil, produced water, sidewall core plug samples. These samples are highly crucial to ensuring the representability of the condition variation of this study.

I would like to thank my keyboards and synthesizers for their help to unwind after long days in the laboratory.

And lastly, I would like to thank my friends and for making my Texas A&M University experience whole, in the class, in the laboratory, in Kyle Field, and outside of campus.

CONTRIBUTORS AND FUNDING SOURCES

Contributors

This work was supervised by a dissertation committee consisting of Professor David Schechter, Jenn-Tai Liang, and Sara Abedi of the Department of Petroleum Engineering and Professor Mohammad El-Halwagi of the Department of Chemical Engineering.

The work of Chapter IV has been published in a journal, SPE Journal SPE-206721-PA.

The work of Chapter V is captured from a joint paper from multiple students in the groups. The paper is published in ACS Omega acsomega.1c03940. Contact angle data measured by Elsie Ladan, Tobi Adebisi, Aashrit Bagareddy, and Abhishek Sarmah are included in the chapter.

The work of Chapter VI is based on experimental data gathered by Elsie Ladan.

The work of Chapter VIII contains experimental data gathered by Tobi Adebisi.

All other work conducted for the dissertation was completed individually by the student.

Funding Source

This work was made possible through Crisman Institute for Petroleum Research, project number ER.10.19B. The student was funded half through the same project and the rest from BPS JET.

NOMENCLATURE

15S	Secondary pentadecanol
CA	Contact Angle
CMC	Critical Micelle Concentration
EO	Ethylene Oxide
GC	Gas Chromatography
IFT	Interfacial Tension
NP	Nonylphenol
SARA	Saturates, Aromatics, Resins, and Asphaltenes
TD	Tridecanol

TABLE OF CONTENTS

Page

LIST OF FIGURES

Page

LIST OF TABLES

Page

CHAPTER I

INTRODUCTION

The Lower 48 shale reservoirs are low porosity and ultra-low permeability reservoirs. Economic production can be achieved only by hydraulic fracture and extensive lateral well. The hydraulic fractures interact with natural fractures to create flow path from crude oil in the matrix to the well (Afra et al. 2019, Bao and Gildin 2017, Bao et al. 2017, Deng and King 2018, Kou et al. 2018). The shale reservoirs are scattered around the continent. In the North we have Middle Bakken and Three Forks, in the Mid-Con there is Niobrara and SCOOP-STACK, and in the South, there is Wolfcamp, Delaware, and Eagle Ford. The number of wells producing from these reservoirs are larger than 120,000, showing how prolific these reservoirs are. However, the recovery factor of these reservoirs is typically less than 15% of the original oil in place (OOIP). This induces the pursuit of methods to improve the recovery of the shale oil reservoir.

Surfactant has been implemented in shale reservoirs since the early development of shale reservoirs in early 2010s. Initially, it was added to the fracturing fluid as a flowback aid chemical (Zhou et al. 2014, Yue et al. 2016, Yang et al. 2014, Xu et al. 2015, Roychaudhuri et al. 2013, Rostami and Nasr-El-Din 2014, Paktinat et al. 2006, Mahmoudkhani et al. 2015, Liang, Zhou, et al. 2017, Liang, Achour, et al. 2017, Kim, Omur-Ozbek, et al. 2016, Kim, Zhang, et al. 2016, Howard et al. 2010, Houston et al. 2009, He et al. 2017, Ge et al. 2015, Champagne et al. 2012, Blauch et al. 1993). The argument was that with large volume of water injected to frac a shale well, some of the

water might block the pore which inhibits production of hydrocarbon. Surfactant was added to reduce the IFT of water and the hydrocarbon, presumably it would reduce the pore blockage and enhances the production.

Afterwards, surfactant application was further expanded as a production enhancement chemical (HanZhao et al. 2020, Lotfollahi et al. 2017, Patil et al. 2018, Quintero, Hawkes, et al. 2018, Xu et al. 2019, Alvarez, Tovar, et al. 2018, He and Xu 2017, Quintero, Mattucci, et al. 2018, Singh and Miller 2021, Uzun et al. 2020, Wang et al. 2019, Zeng et al. 2018a, Alvarez and Schechter 2016a, B. Alamdari et al. 2018, Bui et al. 2016, Gupta et al. 2020, Yarveicy et al. 2018, Yassin et al. 2018, Alvarez, Saputra, et al. 2017b, Chen and Schechter 2021, Habibi et al. 2020, Haghighi et al. 2020, Liang et al. 2021, Miller et al. , Miller et al. 2019, Das et al. 2019, Liu and Sheng 2019, Mirchi et al. 2017, Mukhina et al. 2021, Saputra et al. 2019, Wang et al. 2017, Wang et al. 2020, Alvarez and Schechter 2017, Liang et al. 2018, Sheng 2017, Takbiri-Borujeni et al. 2019, Teklu et al. 2018, Wijaya and Sheng 2020, SalahEldin Hussien et al. 2019, Yekeen et al. 2019). The delivery mechanism was still through addition to the fracturing fluid. However, this application relies more on the detergency properties of the surfactant molecule rather than the IFT reduction. Detergency properties or wettability alteration is believed to cause the wettability of the shale reservoir from oil-wet initially to water-wet. Oil-wet reservoir traps more oil in its pore, prohibiting it to be produced. While water-wet reservoir would allow more oil to be produced and traps water more. An abundance of studies on this type of surfactant application can be found in the literature. Most, if not all, of these studies was performed in the laboratory. This presents a problem since, as will be presented later,

surfactant molecule is highly sensitive to the condition of the system it is applied to. Especially with temperature and salinity, which is often disregarded on a laboratory-scale study. There is a high chance that surfactant that performs well in laboratory condition does not respond in the same way when applied in the field.

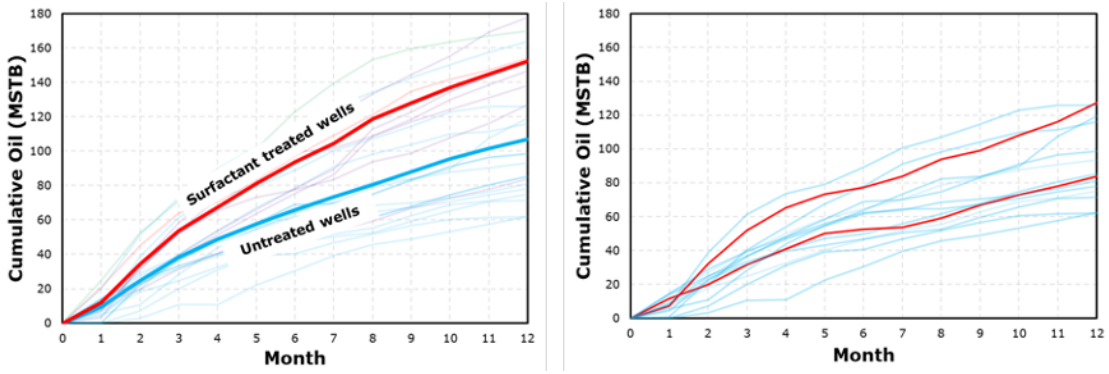

Figure 1 - Cumulative recovery of a well stack in the Permian basin, comparing surfactant-treated and untreated wells.

One example where this occurs is the field case presented in Figure 1. The presented production data were gathered from a field application in the Permian basin. There were 20 wells in these well stack, all were completed in the Wolfcamp B interval. Out of 20, eight wells were completed with surfactant in its fracturing fluid. Wells without surfactants are presented in blue and all the other color represent different surfactants that were applied in this stack. From the right figure, surfactant treated wells performed significantly better than the untreated wells. This result is one evidence of the efficacy of surfactant application in the fracturing fluid as a production enhancement chemical. However, further investigation into the data revealed a problem. The eight surfactant-

treated wells used various surfactants. Some of the surfactants used did not improve the oil recovery, with the cumulative production similar to the untreated wells (left figure).

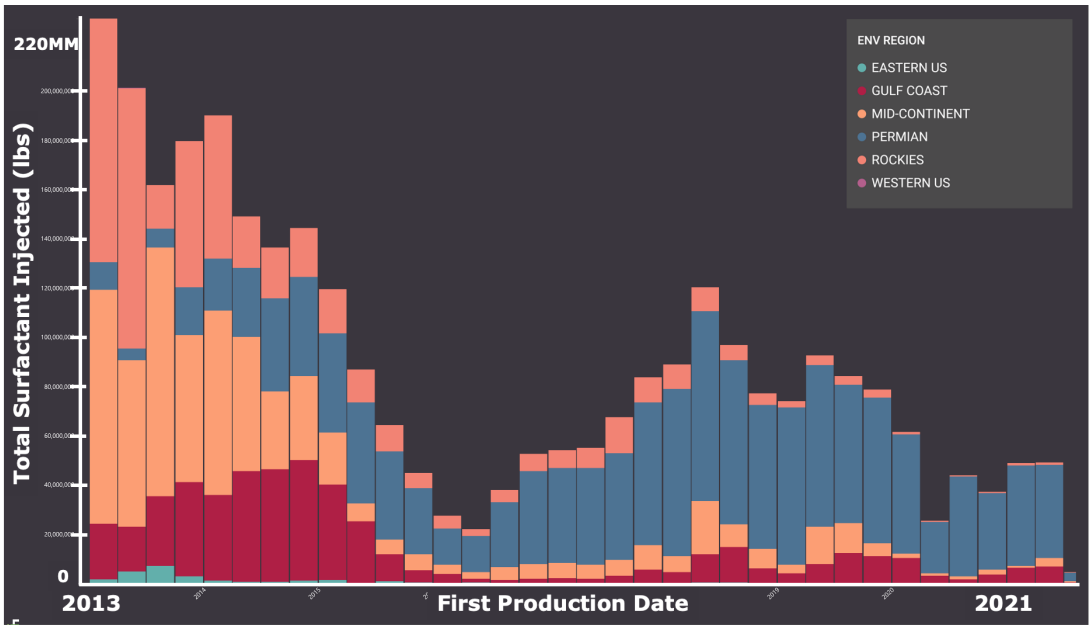

Figure 2 - Total surfactant injected in wells completed from 2013.

The field result shows that surfactant performance in improving the oil recovery varies. The performance inconsistency, combined with the surfactant cost, left a bad impression to operators. Additionally, often times laboratory data presented to substantiate the surfactant application does not correlate well to the field performance. Compounded with the oil price crash in mid 2010s, less and less operators include surfactant from part of their completion fluid (Figure 2).

Surfactant application in shale does not stop there. Currently, there is an ongoing effort to apply surfactant as an EOR agent. There are two reasons why this method of surfactant application in shale reservoir is promising.

First, less chemical interaction that could harm the surfactant performance. Fracturing fluid contains chemical other than the surfactant, i.e., polymer as friction reduction agent, biocide, and clay inhibitor. These chemicals react with the surfactant. Polyacrylamide is often used for the friction reducer polymer. Cationic and/or anionic compound could be added to the polymer backbone. Having ionic surfactant in the same fluid system would result in ineffective surfactant due to the interaction with the polymer. Additionally, the polymer is often added in the form of emulsified polymer. In its emulsified form, an emulsion inversion package is added. This package is a surfactant. Adding surfactant to this system would damage not only the surfactant performance to improve the oil recovery, but also damage the emulsion inversion of the polymer.

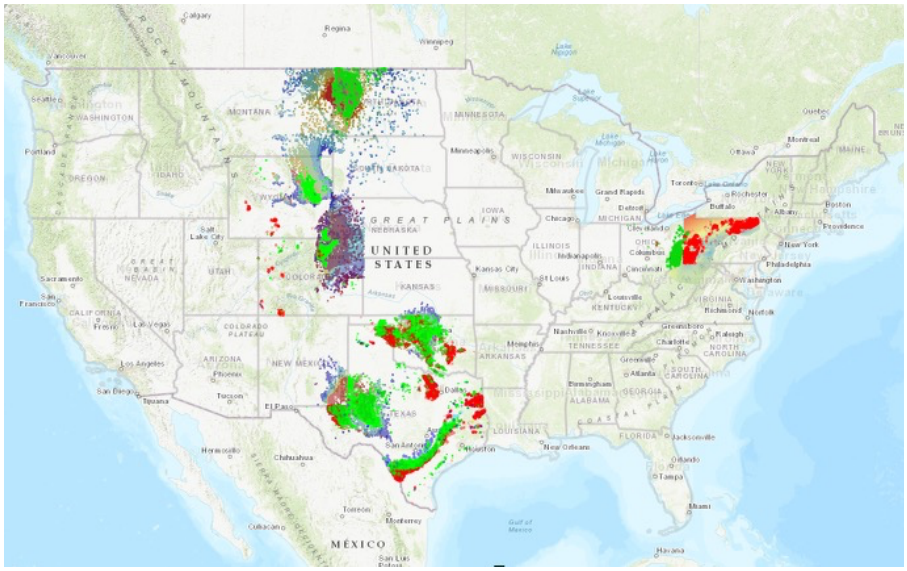

Figure 3 - Distribution of shale oil wells drilled in the Lower 48.

The second reason is the potential economic impact. Since 2010, there have been more than 168,000 shale oil drilled in the US (Figure 3). Out of the 168,000, only 49,627 wells are still actively producing per June 2021. Out of all the remaining active wells, each well on average produces 90 STB/d of oil and 144 STB/d of water. The problem of late-life shale oil wells is highlighted here, high water cut. The high water production is also a reason why almost 120,000 wells are already shut-in even though the oldest well is only 10 years old. It is well-known that each shale oil well only recovers less than 15% of their OOIP. This means that there is an enormous resource being left behind in the reservoir. Surfactant application as an EOR agent on these wells, after their primary recovery lift, could be highly profitable.

Currently, there is an ongoing effort to investigate the feasibility of the surfactant shale EOR method. To avoid the same fate of surfactant application in the fracturing fluid, this study aims to support the ongoing effort by answering the following questions:

Since surfactant is sensitive to the system condition, what is the range of heterogeneity of Lower 48 shale reservoir systems? This includes the crude oil characteristic, brine salinity, rock mineralogy, and reservoir temperature

- Does the same oil/water interfacial interaction in the conventional reservoir system apply to shale? If not, what is the mechanism?
- What drives wettability in Lower 48 shale oil reservoir system?
- Is there a systematic behavior between the molecular structure of the surfactant and the surfactant performance in:
    - Reducing oil/water IFT?

    - Altering rock surface wettability from oil-wet to water-wet?
    - Improving oil recovery from imbibition?
- Based on all the previous bullet points, how to optimize surfactant system for shale EOR?

CHAPTER II

LITERATURE REVIEW

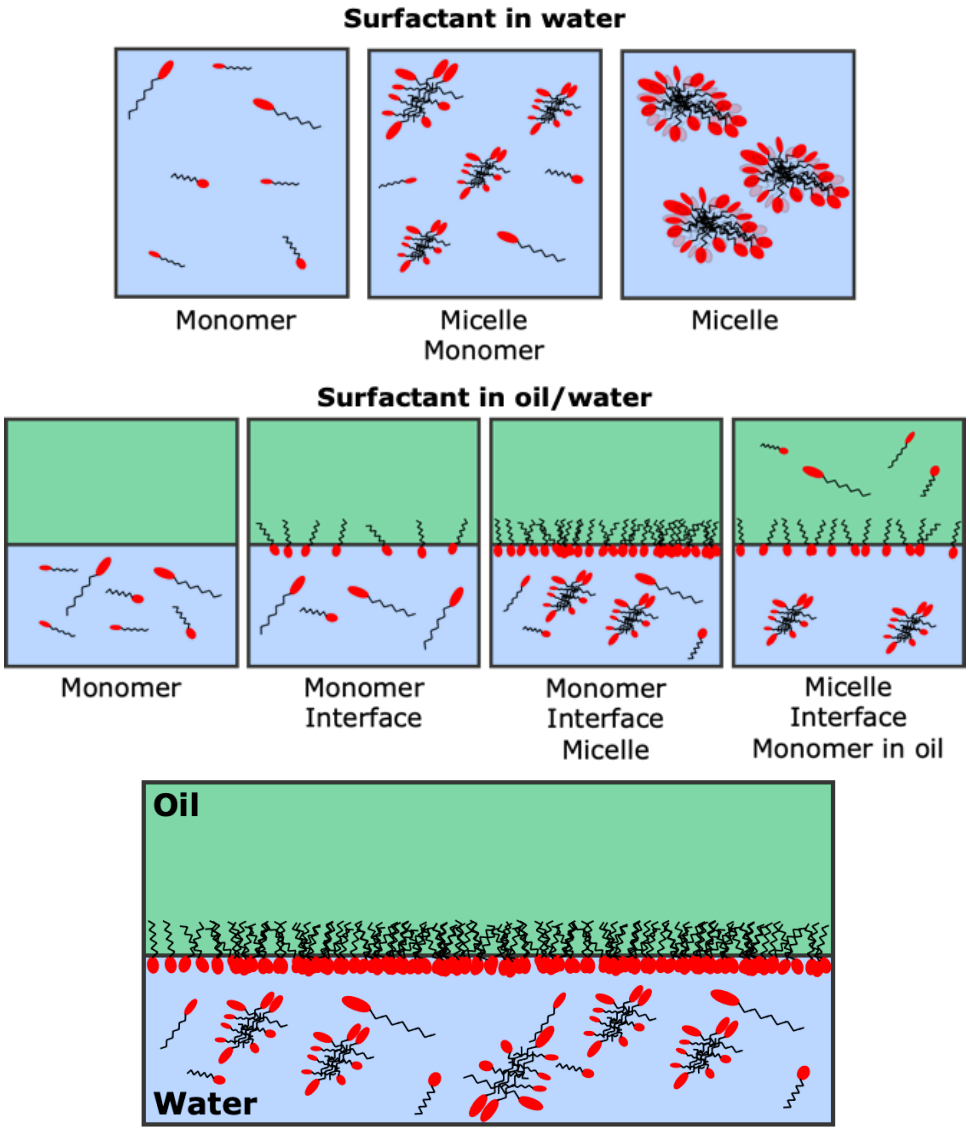

Figure 4 - Possible surfactant molecule configuration in water and in oil/water system (top) and optimum surfactant partitioning, saturating the interface (bottom).

Surfactant's amphiphilicity causes the molecule to be soluble in various phases. As a result, the surfactant molecule can virtually be present in all of the phases in an crude oil/brine system. Additionally, the surfactant is also able to form micelle where the hydrophobic part of the surfactant interacts to form a "complete hydrophilic" molecule. The top part of Figure 4 shows some configuration that the surfactant might exist in a given system. The simplest form is for the surfactant to be in monomers when diluted into an aqueous-phase. When the surfactant hydrophobicity is increased, the surfactant will start to form micelle. It is important to note that the term increased hydrophobicity is used instead of increased concentration here. This is because the drive to micellization can be caused by other factor than increasing the surfactant concentration. Salinity increase, temperature increase (nonionics), or temperature decrease (ionics) could all drive the formation of micelle. Initially, both micelle and monomers exist. When the system is pushed again, monomers will cease to exist, and all surfactant molecules will be present in solution as micelles. Next, is the surfactant configuration as it is added into an oil/brine system. Here, the surfactant will start in the aqueous-phase. Once the hydrophobicity is increased or the hydrophilicity is decreased, surfactant molecules will start progressing to the interface. This is driven by the amphiphilicity nature of the surfactant. Pushing the system further, more surfactant will be transferred to the interface and at the same time micellization starts in the aqueous-phase. Further pushing the system condition results in the transfer of the surfactant molecule to the oleic-phase where the surfactant starts to become not soluble in the aqueous-phase. Notice how the amount of surfactant in the molecule also decreases during this point.

This visualization of surfactant activities in a complex system is important. The goal of putting surfactant into the system is to perturb the interface of crude oil/brine and/or crude oil/brine/rock to the direction that would improve oil recovery. The surfactant molecule will only alters the interface when the surfactant molecule is actually positioned to be on the interface. The configuration is presented in the bottom figure of Figure 4. It is also important to realize that concentration increment is not the only way to induce micellization or transfer of surfactant into the aqueous-phase. The main driver is change in the hydrophobicity and hydrophilicity of the surfactant. And this is strongly affected by the condition of the system that the surfactant is applied to. This could be a problem since the system condition of domestic shale reservoirs is heterogenous. Meaning that surfactant system that works in one reservoir might not work in another reservoir.

Factors Affecting Surfactant Performance

There are six variables that control the surfactant performance, presented in Figure 5. The surfactant headgroup and tailgroup structure would strongly affect this. Not just by the degree of hydrophilicity and hydrophobicity, but also on how the surfactant would interact with the system. The surfactant tailgroup can vary from a primary linear alcohol to hydrocarbon chain with branches and aromatic rings. While the headgroup is typically what the surfactant is categorized as. Nonionic has EO group and cationic, anionic, and zwitterionic has ion as the headgroup. The next variable is the brine of the system, or more specifically, the salinity of the system. Salinity increase will generally push the surfactant to be less hydrophilic as it reduces the ability of the surfactant molecule to bond with the

water molecule. However, salinity could also interact with the tailgroup of the surfactant, affecting its hydrophobicity. Next is the reservoir temperature. Temperature increase could both increase and decrease the hydrophilicity of the surfactant, depends on the structure of the headgroup. Next, crude oil of the reservoir system. This variable will mostly interact with the tailgroup of the surfactant. And lastly, the mineralogy of the rock. Rock surface with different minerals would have different level of charge on its surface. This charge would affect how surfactant molecule is interacting with the system.

Figure 5 - Six variables affecting surfactant performance in a shale reservoir system.

As can be seen, the surfactant interaction with the system it is applied to is complex. There have been efforts published in the literature to elucidate this interaction. The upcoming section of the literature review will cover some of the most important studies performed on this matter.

Surfactant Characterization and Optimization Past Studies

Salager with his publications in the early 1980s was one of the pioneers in the journey to optimize surfactant formulation for EOR purpose. He did not start the study, but he was one of the very first that understands the complex interaction between salinity, oil properties, temperature, and surfactant structure and its effect to IFT. Salager et al. with bottle tests performed variable sweep of all the mentioned variables to map the range of which Winsor Phase-II is created. Conductance and viscosity measurements were first used to detect the phase creation (Salager et al. 1982, Salager, Mi~ ana-Pérez, et al. 1983). In the next study, Winsor Phase diagram was expanded to include phase transition observed that was not driven by physio-chemical effect (Salager, Minana-Perez, et al. 1983). With nonionic surfactant, increasing the temperature resulted in the shift of emulsion from oil-in-water to water-in-oil (Antón et al. 1986). Heavier crude oil increased the oil alkane carbon number which widen the three-phase zone (Salager et al. 1990). Increase of viscosity with heavier crude also makes it more difficult to invert into water-in-oil emulsion. Salager et al. also looked at the phase behavior of mixed surfactant systems that contain nonionic-anionic and cationic-anionic surfactants (Antón et al. 1992, Antón et al. 1993, Antón et al. 1996). With nonionic-anionic mixtures, better salinity

resistance compared to anionic alone was observed and better temperature resistance than nonionic by itself was observed. However, on the cationic-anionic mixtures, liquid crystalline was formed between 0.25 to 0.75 mole ratio of either surfactant. This crystal is not soluble in oil, water, or emulsion phase. In their early work, mostly linear alkane was used as the oil-phase. Later, the study advanced into a more representative oil system that contains carboxylic acid. By utilizing pH as the variable, the model was able to be applied on these crude oils. Increasing pH resulted in the increase of hydrophilicity of the crude oil (Mendez et al. 1999).

Salager et al. derived a formula to optimize surfactant/water/oil/alcohol system to reach the lowest IFT value possible (Salager, Morgan, et al. 1979). Anionic sulfonates surfactants were used in this study along with simple linear alkane as the oleic-phase. In their correlation, salinity, oil-phase characteristic, alcohol molecular weight, surfactant structure, and temperature were included as variables. Based on experimental data, they observed the following: Optimum salinity varies linearly with the carbon number of the oil-phase after salinity is transformed with natural log. Surfactant structure can be defined by using the slope of the optimum salinity vs oil carbon number in a semi-natural-log plot. Temperature was observed to show linear trend. Surfactant concentration only affect the system through concentration shift. And lastly water-oil-ratio was observed to not significantly affect the optimum formulation. Additionally, they also noticed optimum behavior where at the optimum condition, lowest IFT or Winsor Phase-III was observed. It is interesting to note that performing variable sweep at with different variables results in heterogenous trend. Increasing salinity, alcohol molecular weight, and surfactant

hydrophobicity shift the phase behavior from Phase I to III to II. Increasing the oil carbon number and temperature resulted in shift from II to III to I.

$$\ln S^* = K(ACN) + f(A) - \sigma$$

As a follow up, Salager et al. tested their characterization equation to systems containing mixtures (Salager, Bourrel, et al. 1979). They tested mixtures of anionic-anionic surfactants, anionic-nonionic surfactants, and multiple alkane length as the oleic-phase. They found that with the correct mixing rule, by applying percentage of surfactant composition to the natural log of the optimum salinity of each surfactant, the equation can still be applied on mixture of anionic-anionic surfactants. The same cannot be said to anionic-nonionic surfactant mixtures due to the dissimilarity between the response of anionic and nonionic to temperature and salinity. Mixing rule can also be applied to represent oil-phase containing multiple alkane length.

Marquez et al. measured the effect of EO number and chain length of alkylphenol to the partition coefficient in a distilled water/n-heptane. Both increasing EO number and decreasing the alkyl length results in the increasing value of the partition coefficient. However, the effect of EO is more significant as adding a single EO group has the equal effect of decreasing the length of the alkyl chain by ten carbon atom (Marquez et al. 1995). In the same study, Marquez et al. had one branched surfactant with two C9. They observed a deviation from the other linear alkyl where the two C9 actually falls into linear C16 instead of C18. On the second series of their publication, Marquez et al. investigated the effect of tailgroup branching and structure (Márquez et al. 1998). Branching was observed

to increase the partition coefficient as it reduces the hydrophobicity of the surfactant molecule. Shifting from linear to branching in C4 alkyl chain resulted in 20% increase in the partition coefficient. The trend continued from two branches to three branches. This result was confirmed with the increasing CMC with branched surfactants. Marquez et al. also investigated the effect of temperature and composition of the oleic-phase (Márquez et al. 2002). With EO group on nonionic surfactants, a decrease by one order of magnitude on the partition coefficient was observed for every 86°-122° F increment of temperature. While on the oil side, the logarithmic of the partition coefficient increases by 0.03 unit per carbon atom added to the oleic-phase. Of course, in this simple mode, only single length linear alkane was used as the oleic-phase. Increasing salinity interestingly resulted in the decrease of partition coefficient. However, this was attributed to the formation of micelle. Adding alcohol also decreased the partition coefficient as the alcohol moves into the oleic-phase and reduces the oleic-phase hydrophobicity which allows the surfactant to progress to the oleic-phase easier.

Surfactant Headgroup and Tailgroup Configuration

Puerto et al. investigated the phase behavior of alkoxyglycidylether sulfonates (AGES) surfactants under a range of salinity, temperature, tailgroup, headgroup, and tailgroup (Puerto et al. 2011). The surfactant blends were designed for high salinity and high temperature system (>20 wt% NaCl and up to 120° C). Increasing the EO group results in higher optimum salinity. While increasing the PO group decreases it. Using longer hydrophobes also leads to lower optimum salinity. With lighter oil, a viscous, waxy

phase was observed (like what observed here), increasing temperature and/or changing the oil amount in the system removes this phase.

Ghosh et al. designed surfactant-polymer cocktails for High-Temp (80° C) and High-Sal (>90000 ppm) (Ghosh et al. 2018). They observed the trend of increasing oil solubilization and increasing optimum salinity when the hydrophobe was extended from 13 to 28.

Bera et al. measured wettability of secondary C15 nonionic surfactant with EO ranging from 5 to 12 (Bera et al. 2012). The solid-phase was a cleaned quartz surface, and the oleic-phase was a 34° API oil. The wettability was measured by dispensing an oil droplet on the surface of the quartz which is submerged in the tested surfactant solution. Oil-wetness of the clean surface was observed with increasing EO number. The difference between 5 EO to 12 EO is only 10° which is only 10% of the contact angle value. The authors attributed this trend to the increasing hydrophilicity of the surfactant with higher EO number and the formation of surfactant double layer on the rock surface.

Santos et al. investigated the micelle formation phenomena of nonionic and anionic surfactants, Figure 6 (Santos et al. 2009). The nonionic surfactant consisted of DD-10, DD-23, NP-20, and NP-100. While saponified coconut oil and castor oil were the two anionics tested. Brines with salinity ranging up to 8 wt%, containing only KCl salt, were included in this study. Increasing the EO length results in lower CMC value due to the increase of micelle size at longer EO group. Heavier tailgroup, moving from dodecyl to nonylphenol, also decreases the surfactant CMC

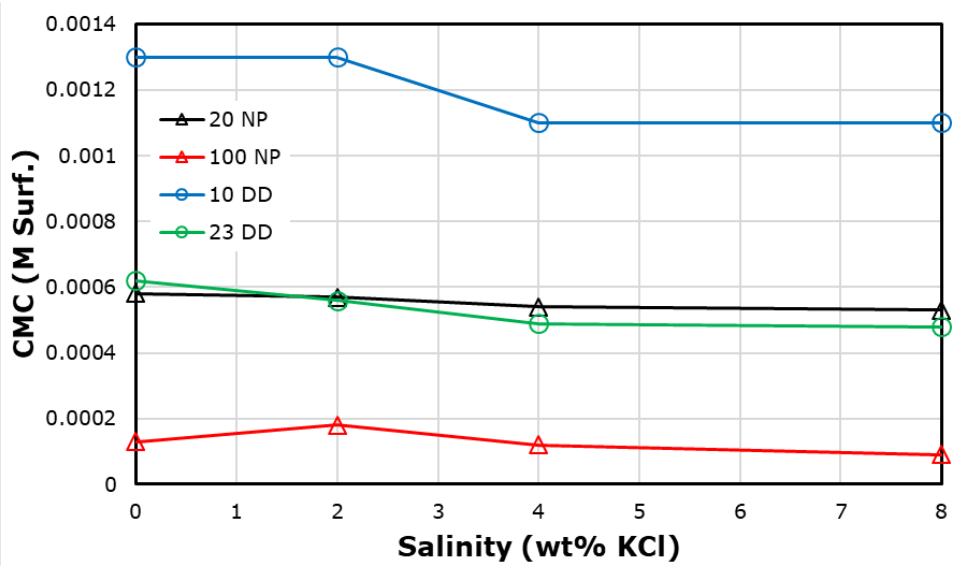

Figure 6 – CMC of surfactants as affected by salinity, data captured from (Santos et al. 2009).

Cao et al. investigated the effect of surfactant molecular structure to its IFT reduction performance (Cao et al. 2012). Two branched alkyl benzene sulfonates were used, one with dodecyl one with hexadecyl. The authors specifically looked at the effect of size ratio between the hydrophilic and the hydrophobic part of the surfactant. The two surfactants were mixed in different ratio to extend the variation of the size ratio. Minimum IFT was observed when the size of the two parts of the surfactant is similar. Below the minima, increasing the hydrophobic size results in gradual reduction in IFT. Passing the minima, larger hydrophobic size results in steep increase in IFT.

Jia et al. observed both minima and maxima trend on their investigation of salinity effect to a cationic/anionic surfactant mixture (Jia et al. 2017). A minimum of IFT was observed at 2.5 wt% NaCl when the cationic dominated the mixture. On the other hand, a maxima was observed at 1 wt% NaCl when the mixture contained more anionic surfactant.

For the cationic surfactant at lower salt concentration, the surfactants were loosely packed on the interface. Increasing salinity compresses the surfactant and added more surfactant on the interface. Increasing the salinity further would induces the solubility of the surfactant in the oleic-phase, hence the minima behavior. While for the anionic, the surfactant was already packed initially. Increasing the salinity induced salting-out effect, resulting in the increase of IFT value. Further salinity increments then added more surfactant on the interface, resulting in the reduction of IFT.

Aqueous-phase

Strand et al. performed spontaneous imbibition experiment using C12TAB surfactant on calcite-rich core plugs (Strand et al. 2003). Salinity ranging from 0.9 wt% to 4.5 wt% was used in the study. Two temperatures were applied on the experiment, 40° and 70° C. At 40° C, a negative trend between salinity and oil recovery was observed on 1 wt% C12TAB concentration (65% to 5% OOIP from 0% salinity to 10%). However, the recovery factor was not affected by salinity at 70°C. The authors explained the results to the shift of CMC value at the different test condition. For the surfactant tested, increase in salinity reduces the CMC while increase in temperature increase the CMC. Surfactant concentration must be well below the CMC to ensure monomers presence in the system.

Yuan et al. investigated surfactant blends for low-IFT conventional EOR flooding application (Yuan et al. 2015). Blends of nonionic and anionic surfactants were tested at salinity ranging from 1 to 2 wt%. Lower IFT was observed when salinity was increased and was attributed to the charge neutralization of the adsorbed anionic surfactant molecule

on the oil-water interface. Cationic salt ion reduces the repulsion of adsorbed anionics which in turn increase the number of surfactant molecule adsorbed, ultimately reducing the IFT.

Leung and Shah investigated the effect of salinity to the phase equilibria of a water-in-oil emulsion system (Leung and Shah 1987). An optimum salinity was determined. At the optimum salinity, maximum brine solubilization occurs. The optimum nature exists due to the balancing act of attractive inter-droplet interaction and interfacial bending stress. Below the optimum point, solubilization increases due to the increase of alcohol partitioning, driven by salting-out process. Above the optimum point, the solubilization decreases due to the increase in interfacial rigidity. Leung and Shah also observed the shift of optimum salinity to higher salt concentration when the alkane length was increased.

Al-Sahhaf et al. measured the oil/water IFT of three surfactants, SDBS, SDOSS, and HTAB (Al-Sahhaf et al. 2005). The oleic-phase is n-octane and the salinity of the aqueous-phase is up to 4 wt%. The IFT of SDBS was observed to be unaffected by the salinity increase. While both SDOSS and HTAB showed negative trend of IFT and salinity.

Kedar and Bhagwat measured the oil/water IFT and partition coefficient of SLES, DD-23, and DTAB surfactants (Kedar and Bhagwat 2018). NaCl, $MgCl_2$, and $CaCl_2$ brines were used at 5 wt% and 10 wt% TDS. Heavy oil with 1.8 mg-KOH/gr-oil TAN was used as the oleic-phase. Increasing salinity results in lower IFT and, interestingly, lower partition coefficient. This means that increasing the brine salinity pushes the surfactant molecule to the oil/water interface but increasing the salinity up to 10% does not push the

surfactant to be soluble in the oleic-phase. Magnesium chloride salt was observed to cause the most impact at the same salinity level.

Saha et al. investigated the effect of salinity to surfactant adsorption on a rock surface (Saha et al. 2017). The adsorption of Triton X-100, an octylphenol nonionic surfactant, on a quartz-rich surface was measured. Increasing the salinity of the brine from 0 to 0.4 wt% already increase the surfactant adsorption by almost 50% at 30° C. At higher temperature, the effect of salinity is decreased, an increase of 25% at 70° C.

Saxena et al. measured the adsorption of anionic natural surfactant on bentonite, carbonaceous, and siliceous rocks (Saxena et al. 2019). Observed consistent increase of adsorption at higher brine salinity. They tested up to 3 wt% NaCl salinity

Belhaj et al. measured the partition coefficient of anionic alkyl ether carboxylate, anionic AOS and nonionic APG into 45° API oil (Belhaj et al. 2020). Salinity range up to 3.2 wt% seawater. They observed increase of partition coefficient when the salinity is increased. Anionic AEC has the most sensitive response to increase in salinity. This positive trend contradicts the result from Kedar and Bhagwat.

Rizwan et al. measured adsorption of anionic surfactant on crushed Berea (Azam et al. 2013). Increasing the brine salinity from 1 wt% to 2 wt% NaCl increase the adsorption.

Bansal and Shah measured optimum salinity and interfacial tension data of surfactant/surfactant mixtures as well as surfactant/alcohol mixtures (Bansal and Shah 1978). With brine concentration up to 25 wt% NaCl. Up to 25 wt%, the general trend is that higher salinity reduces the oil/water IFT.

Akhlaghi et al. measured oil/water IFT with a 33° API oil and Triton X-100 nonionic surfactant (Akhlaghi et al. 2021). Four salts at salinity of 0.1, 0.5, and 1 wt% were used, NaCl, $CaCl_2$, $MgCl_2$, and Na_2SO_4. Increasing brine salinity decreases the IFT. The IFT from NaCl was the smallest, then $MgCl_2$, $CaCl_2$, and Na_2SO_4.

Paternina et al. investigated the effect of total salinity (0 – 5 wt %) and the hardness of the brine (0 – 0.1) to the static adsorption of anionic Petrostep S13D (Paternina et al. 2020). Higher TDS results in more surfactant to be adsorbed. But due to the nature of the extended surfactant, the adsorption isotherm is not as straight forward. Extended surfactant has tendency to form strong hydrophobic-hydrophobic bond as well as hydrogen bond on the PO structure. With hardness, the content of calcium ion, the effect could be both increase and decrease depending on the TDS. At low TDS, increasing hardness induces adsorption driven by salting out. At intermediate, increasing reduces adsorption, driven by competing adsorption. While at high TDS, increasing hardness also reduces adsorption. At these high TDS, it was predicted that the surfactant prefers to form micelle or hemimicelle rather than adsorbed.

Phaodee et al. found an optimum point of coconut oil detergency at 10° C when the salinity is between 7 – 8 wt% NaCl (Phaodee et al. 2019). Anionic surfactant C14-15-8PO-SO4Na was used.

Gupta and Mohanty measured the IFT of surfactant C12-157EO and NP-30 with a 28° API oil (Gupta and Mohanty 2010). With salinity increased from 2.9 wt% to 8.8 wt% NaCl, IFT was observed to be the lowest at 7 wt% when surfactant C12-15-7EO was used. While on surfactant NP-30 and brine Na_2CO_3, the IFT was observed to be the lowest at 1

wt% Na_2CO_3. Did not continue the measurement to look at the effect of salinity to wettability alteration.

Curbelo et al. measured the cloud point of nonylphenol surfactant with four EO group length (Curbelo et al. 2013). The length of the EO group was from 9.5 to 20 and the salinity was varied from 0 to 15 wt% KCl. Lower cloud point with higher brine salinity was observed. Initially at 78°C at 2 wt% KCl, the cloud point went down to 53°C when the salinity was increased to 15 wt%.

Zhang et al. measured IFT with 43° API Bakken crude oil with salinity up to 30 wt% (Zhang et al. 2013). Cationic Tallow Amines, anionic S-2, zwitterionic dimethyl amine oxide, and nonionic C12-15_12 EO surfactants were used. Optimum salinity to reach the minimum IFT was observed for all except the zwitterionic. At 90°C, nonionic reaches its lowest IFT at 8 wt% salinity, anionic at 11 wt%, and cationic at 12 wt%. While the zwitterionic maintains the highest IFT and consistent decrease with increasing salinity.

Sammalkorpi et al. performed molecular dynamics simulations to investigate the micellization of anionic surfactant SDS in the presence of NaCl and $CaCl_2$ salt (Sammalkorpi et al. 2009). In the presence of salt ions, SDS micelle was observed to be more packed. Comparing the two salts, micelles formed in the presence of $CaCl_2$ salt were more packed compared to NaCl. This is driven by the charge density of the counterion condensation and the stronger ion bridge of calcium ion for two SDS adjacent SDS headgroup.

Mandal et al. measured wettability of Tween-80/SDBS nonionic-anionic surfactant mixture on an oil-wet aged quartz rock surface (Mandal et al. 2016). The measurement is

quite unique as surfactant solution droplet is deposited on the aged rock surface in the presence of air, unlike any other sessile drop method. An optimum wetting condition was observed at 4 wt% NaCl salinity. Below and above this salinity level, the wetting is more oil-wet. A large jump from 0% to 2%, then to 4% was observed but the decrease from 4% to 8% was in lower magnitude.

Dehghan et al. performed coreflood experiment using a 19° API heavy oil with Berea sandstone (Dehghan et al. 2015). A nonionic-anionic surfactant mixture was tested, specifically designed for high salinity application of up to 15 wt% NaCl. Corefloods were performed at the surfactant's optimum salinity (15%) and below (4%). Two sets of core plugs, oil-wet and water-wet, were used. Injecting the surfactant at its optimum salinity results in higher recovery factor and more effective on the oil-wet core plugs. Differential pressure build up was observed due to micro-emulsion formation.

Gupta and Mohanty investigated the wettability alteration capability of anionic surfactants on calcite surface using a model oil (cyclohexanepentanoic acid and n-decane mix) and a 28° API oil (Gupta and Mohanty 2008). The range of salinity was only up to 4.5 wt% NaCl. Optimum salinity point was observed at 1.4 wt% when Sulfate-8PO anionic surfactant was used on model oil. Similar optimum salinity was observed on the 28° API oil. Increasing the salinity up to this optimum point results in rapid shift into water-wet region. Increasing the salinity above the optimum point returns the wettability back to oil-wet with a more gradual trend

Souayeh et al. investigated nonionic surfactants application to alter the wettability of a carbonate-rich surface and 35° API oil system (Souayeh et al. 2018). The brine salinity

was varied up to 12 wt% TDS. Two nonionic surfactants, TD-7 and TD-20, which are ethoxylated tridecanol with 7 and 20 EO were tested. Consistent decrease of IFT at higher salinity level was observed, no optimum salinity behavior was observed. Similarly, increasing the brine salinity enhances the water-wetness of the surface when surfactant solution was used. It is interesting to note that without surfactant presence, an optimum point where the surface is the most water-wet is observed when the salinity is at 2 wt%. Increasing the salinity beyond this level gradually returned the wettability to oil-wet. At 10 wt% the wettability was similar to at 2 wt% and increasing the salinity even more results in surface with stronger oil-wetness than the 2 wt % brine. Hydrophobic-hydrophobic interaction between adsorbed oil and the tailgroup of the surfactant which ultimately results in the surfactant headgroup facing the bulk-phase was hypothesized to be one of the wettability alteration mechanisms. Another proposed mechanism was the replacement of adsorbed oil with the EO group adsorption on the rock surface.

Santos et al. investigated the effect of salinity to surfactant CMC (Santos et al. 2009). Ionic surfactant's CMC were more dependent to the salinity of the aqueous-phase, ranging from 50-70% decrease when the salinity was increased to 4 wt % KCl. Nonionic surfactants on the other hand showed less dependence to salinity.

Mohammadi et al. investigated the effect of salinity to the wettability alteration performance of CTAB, SDS, and TX-100 surfactants (Mohammadi et al. 2014). Carbonate-rich surface was aged in a crude oil and used in inversed pendant drop contact angle measurement. Brine salinity was varied from 0.1 up to 10 wt % NaCl. Optimum salinity, most water-wet condition, was observed. CTAB and Triton X-100 were at 3 wt%

NaCl. While SDS was observed at 5 wt% NaCl. The optimum behavior was attributed to the balancing act of surfactant partitioning. At the optimum salinity, the amount of surfactant at the interface was at its highest, allowing to alter wettability more effectively.

Liu et al. measured AAS surfactant adsorption on clay surface using the QCMD methodology (Liu et al. 2019). Salinity increases the adsorption. Shifting to $CaCl_2$ salt resulted in higher surfactant adsorption, while shifting to NaCl decreased the adsorption. This trend was attributed to the formation of ion bridging between the negatively-charged clay surface and the negative surfactant headgroup with the calcium ion.

Temperature

Deng et al. compiled a literature review study of wettability alteration studies that have been performed in the literature that encompasses more than 120 published manuscripts, the data is presented in Figure 7 (Deng et al. 2020). It is interesting to see that the effect of surfactant structure is easily identified from their review work. While the same cannot be said in investigating the temperature effect to wettability alteration by surfactant. This is seems to be a trend for all other studies that has been published. Mostly due to the fact most surfactant study was performed to optimize surfactant for a specific reservoir system. With most system is considered as isothermic, it is natural to simply omit the temperature effect. In their summary, Deng et al. compiled the temperature variable which I have transformed into the following graph. Unfortunately, the confidence band is too wide to discern a meaningful trend.

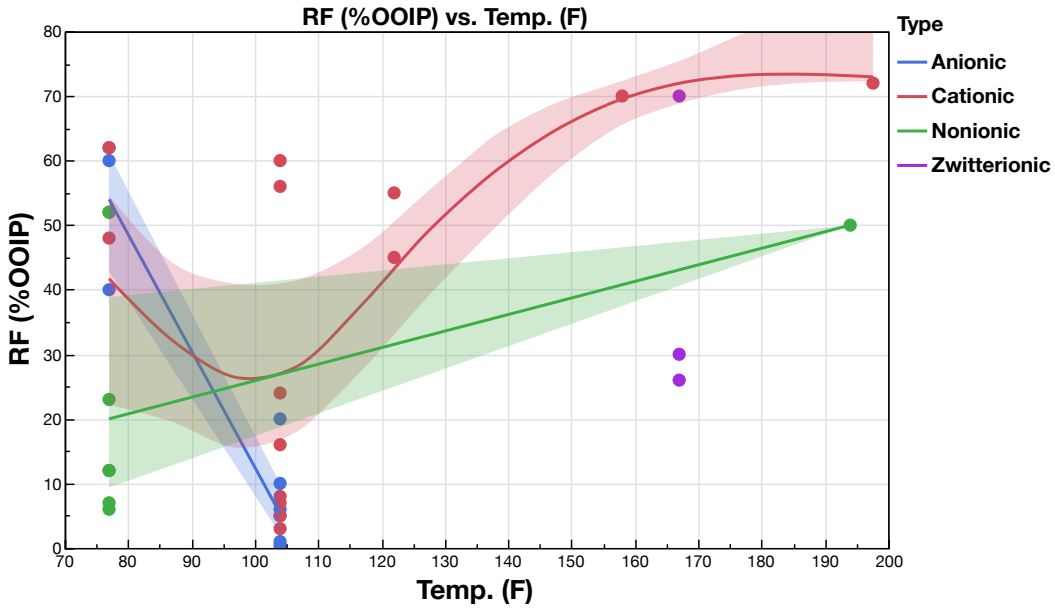

Figure 7 – Compilations of imbibition recovery data at various temperature for four types of surfactants, data gathered from Deng et al. 2020.

Arachchilage et al. measured the shift of optimum salinity and solubilization ratio due to temperature change (Pinnawala Arachchilage et al. 2018). For surfactant that has cloud point characteristic, increasing the temperature results in lower optimum salinity. While for surfactant that only has Kraft point characteristic, temperature increase causes the optimum salinity to increase as well. This is all due to the solubility of the surfactant

Velasquez et al. observed the linear trend of optimum salinity with temperature (Velásquez et al. 2010). The trend is strongly negative with nonionic surfactant (NP group). Longer EO started at higher salinity but with stronger gradient. Propoxylated anionic surfactant also showed negative trend, only in a lesser degree. While SDS and SDBS had positive trend, increasing optimum salinity concentration when the temperature is higher.

Karnanda et al. measured the interfacial tension reduction of surfactant Zonyl FSE, Triton X-100, and Triton X-405 on 27° API oil (Karnanda et al. 2013). Higher IFT was observed with surfactant Zonyl FSE when the temperature was increased, expected for an anionic surfactant. Decreasing trend of IFT and temperature was observed on surfactant Triton X-405, a characteristic of nonionic surfactant. However, the other nonionic, Triton X-100 shows increasing trend.

Ziegler and Handy measured the adsorption of sodium dodecyl benzene sulfate anionic surfactant and NP-20 nonionic surfactant on Berea with temperature ranging from 77° to 194° F (Ziegler and Handy 1981). Increasing adsorption was observed when the temperature was increased for the nonionic surfactant. While adsorption decreased for higher temperature on the anionic surfactant.

Ye et al. investigated the effect of temperature to the IFT reduction performance of two gemini surfactants (Ye et al. 2008). Gemini surfactant is a type of surfactant that is constructed by combining two surfactants at its head using a spacer molecule. Increasing temperature resulted in lower IFT due to the increasing solubility of the oleic-phase and the aqueous-phase. Then at one temperature point (158°F), a positive trend between the IFT and temperature was observed for temperature higher than this point. The shift of trend was attributed to the Phase Inversion Temperature (PIT) theory. Above the PIT, increasing the temperature results in the partitioning of surfactant molecule into the oleic-phase which reduces the number of surfactant on the interface, ultimately decreasing the magnitude of IFT reduction. The authors also observed that temperature increase accelerates the equilibrium time for dynamic IFT measurement.

Ivanova et al. investigated the temperature effect to the IFT reduction on the molecular level (Ivanova et al. 2020). Two cationic surfactants, CTAC and EHAC (ethoxylated and cationic), were used on n-decane and DI water system. The temperature range was from 77° to 203° F. The IFT of the CTAC surfactant was found to be lower at higher temperature, which is surprising. Surfactant EHAC showed negative trend as well. However above 149°F, the IFT increased. The shift was attributed to the lowering of hydrogen bond strength at higher temperature. As a result, the surfactant molecule was pushed into the oleic-phase more and less IFT reduction was observed.

Mosayebi et al. measured the IFT of NP surfactant with four and nine EO group on a 37° API oil (Mosayebi et al. 2016). Increasing the temperature resulted in lower IFT value. A minimum, at 86°F and 93°F for NP-4 and NP-9 respectively, was observed on both surfactants. Above this temperature, a positive trend between IFT and temperature was observed.

Kumar et al. investigated the temperature effect to surfactant Petrostep 420 IFT using pure alkane from C4 to C10 (Kumar et al. 1985). With C4, positive trend of IFT and temperature was observed. With C5, C9, and C10 no trend was observed. And lastly with C6, C7, and C8, a negative trend was observed. A minimum was observed when lignosulfate was added and C7 was used. However, based on conductivity measurement, the PIT theory did not cause this minima as how other publications have indicated.

Wang et al. performed imbibition experiments with Middle Bakken samples at temperature ranging from 120° to 248°F (Wang et al. 2012). Sulfonate surfactants were used in their study. Surfactant improved the recovery from the imbibition experiment.

However, no significant trend between the surfactant performance and the temperature was observed.

Pu et al. measured the wettability alteration change due to temperature with Alpha-Olefin Sulfonates, Amphocaroxymethy Imidazoline, Alcohol Ether Sulfate, and Ethoxylated Alcohol Carboxylate surfactant mixtures (Pu et al. 2016). Contact angle measurements were performed on quartz-rich core plug to assess the wettability. Surfactants were able to alter the initially oil-wet surface into water-wet. Stronger wettability alteration was observed at higher temperature. This trend was attributed to the diminishing of hydrogen bond, pushing the surfactant to go to the surface and alter the wettability.

Standnes and Austad performed imbibition on chalk/crude oil system at 104° and 158°F using C12TAB surfactant (Standnes and Austad 2000). The crude oil was diluted in heptane. Imbibition recovery was higher at base case when the temperature was increased. When surfactant was added, higher temperature results in faster oil recovery. However, at lower surfactant concentration, higher temperature leads to faster recovery but smaller final recovery. It is also important to note that the recovery improvement is not significant. The author attributed the recovery improvement to the enhancement of surfactant diffusion at higher temperature.

Vatanparast et al. performed imbibition experiments on various surfactants, including Tide, on carbonate core/39° API oil system (Vatanparast et al. 2011). Most surfactants showed recovery improvement. On CTAB, increasing the temperature from 77° to 131°F improved the surfactant performance by 200% in improving the oil recovery. On the IFT

measurement, the author observed that below the surfactant CMC (measured at 77°), increasing the temperature results in IFT reduction. While above the CMC, temperature increase resulted in higher IFT values. Based on this observation, the authors attributed the performance enhancement with higher temperature to the increase in capillary pressure after wettability alteration as a result of the higher IFT value.

Aoudia et al. developed two surfactants for a wide temperature application range (Aoudia et al. 2006). Both surfactants are anionic, specifically ether sulfonates family. Spinning drop tensiometer was used to measure the IFT as the IFT values were in below 0.1 mN/m. Oman crude oil and brine from Yibal formation was used as the oleic- and aqueous-phase. The surfactants were able to reduce the IFT below 0.01 mN/m at 131° - 176°F temperature range. At the same time, this range was also the minima. Above and below this temperature range, the IFT was higher. It was also observed that the IFT increment with temperature was more significant at temperature above the window.

Jia et al. investigated the effect of temperature to cationic/anionic surfactant mixtures (Jia et al. 2017). A 16° API crude oil with a NaCl brine was used. The cationic surfactant was N-dodecyl-N-methylpyrrolidinium bromide and the anionic was SDS. The authors varied the ratio of the two surfactants from 10:1 to 1:10. At the temperature window of 86° to 158°F, a positive trend between IFT and temperature was observed. The observed trend was stronger when the composition of cationic surfactant was larger than the anionic. The authors attributed the trend to the increasing solubility of the cationic surfactant at higher temperature. When SDS composition was higher than the cationic, the surfactant layer was denser which lessen the effect of solubility/temperature to the IFT.

Alasiri et al. performed DPD simulation on SDS/water/octane system(Alasiri et al. 2019). Increasing the system temperature from 77° to 185° F decreased the IFT by 8%, a relatively insignificant change. The negative trend is unusual for an ionic surfactant. The authors attributed the trend to the reduction of tailgroup-water interaction. The DPD simulation showed increase of saturated area of the surfactant at the interface which should result in positive trend between IFT and temperature but the IFT reading as presented before showed negative trend.

Mohammadshahi et al. measured the dynamic IFT of two large nonionic surfactants, Tween 80 and Behamid D (Mohammadshahi et al. 2020). Crude oil from a reservoir in the Southwest of Iran along with its 3 wt% brine was used as the brine/oil system. The temperature was varied from 77° to 153° F. Initial IFT decline was observed during the early time of the drop age. However, an IFT increment occurred after one minute drop age. These two trends were hypothesized to be the result of surfactant transfer. On the initial decline, surfactant molecules progress to the oil/water interface which causes reduction of IFT. However, the surfactant then advances from the interface into the oleic-phase. The last transport results in less surfactant molecule available on the interface which causes the IFT value to increase. On the effect of temperature to the surfactant performance, negative trends between IFT and temperature were observed at all surfactant concentration tested. After equilibrium, the IFT of surfactant Tween 80 decreased from 7 to 1 mN/m when the temperature was increased from 77° to 122°F. While surfactant Behamid D was observed to have IFT reduction from 9 to 5 mN/m with temperature change from 77° to 153°F.

Novosad measured the effect of temperature to surfactant retention on Berea sandstone cores and the surfactant transfer to the oleic-phase from the aqueous-phase (Novosad 1982). Two anionic surfactants were used. Sodium chloride salt dissolved in DI water was the brine-phase. Octane was the oleic-phase. The measurements were performed at temperature from 77° to 158°F. Surfactant was contacted with the Berea sandstone under coreflooding experiments. Higher temperature resulted in lower surfactant retention in the rock. The reduction of surfactant retention reduces by 50% on average on the two surfactants on the minimum and maximum temperature. The amount of surfactant moved from the aqueous-phase to the octane also was lower at higher temperature. Surfactant lost to the oleic-phase was also observed to be more sensitive to the temperature; reduction of up to 71% at the same temperature range. This trend is in line with the fact that in general, more surfactant is lost to retention on the rock than to the oleic-phase.

Cloud Point Problem for Nonionic Surfactants

Surfactants are amphiphilic organic compounds with a chemical structure composed of a hydrophilic group and a hydrophobic group. The hydrophile exhibits affinity for polar solvents while the hydrophobe is non-polar. When introduced into a multi-component system, like a hydrocarbon reservoir's brine/oil/rock system, surfactant molecules align at the interface because of their amphiphilic nature. This behavior alters the dynamic between phases and can improve oil recovery in one, or both, of two ways. First, altering fluid/fluid interactions which is often observed as IFT reduction. Second, altering

fluid/rock properties via wettability alteration. Where IFT is high, the hydrocarbon forms large spherical globules that possess cross-sectional areas that make flow through the nanoporous shale throats extremely difficult. A decrease in IFT reduces the differential pressure, which distorts the oil drop and allows flow of oil through the shale pore throats (Sheng 2013, Wilson et al. 2019). When the reservoir is oil-wet, the hydrocarbon is trapped in the smaller pores while the brine is in the larger pores. This distribution means the injected fluid must overcome negative capillary pressure to invade the matrix and displace oil. Adsorption of surfactant at the rock interface changes the surface affinity to oil, i.e., alters wettability which is the second process. Wettability alteration towards water-wet shifts the capillary pressure to positive, allowing spontaneous imbibition of the aqueous solution into the matrix, promoting oil recovery (Singh and Miller 2021, Zhang, Saputra, et al. 2018a).

When selecting the appropriate surfactant type, nonionic surfactants are considered the second most used class, after anionics, with about 45% overall industrial production (Salager 2002). Nonionic surfactants are an exciting class of surfactants for a few reasons. They do not ionize in an aqueous solution because their hydrophilic group is of a non-dissociable type. This implies that electrostatic interactions do not play a significant role in their behavior, thus making them suitable for several reservoir types and allowing for relatively constant properties in the presence of salts (Souayeh et al. 2021). Also, nonionic surfactants possess significantly lower critical micelle concentration (CMC) when compared to ionic surfactants, which allows less volume of the former to be as effective as the latter, making them cheaper for conventional EOR flooding application. Lastly,

nonionic surfactants display temperature-dependent physiochemical properties, one of which is cloud point. With increasing temperature, the degree of hydration of the hydrophilic portion is insufficient to solubilize the remaining hydrocarbon portion of a nonionic surfactant (Sharma et al. 2003). Therefore, at cloud point temperature (CPT), the surfactant losses sufficient water solubility, creating a cloudy dispersion, with phase separation into a surfactant rich phase and a brine rich phase in some situations.

The surfactants' cloud point should be an important consideration when deploying nonionics because above the CPT, the surfactant ceases to perform some or all its normal detergency, wettability, and IFT alteration functions (Huibers et al. 1997). For surfactants with short ethylene oxide (EO) groups, the increased hydrophobicity leads to a decrease in solubility in water and a low CPT, while increased hydrophilicity (due to longer EOs) leads to better solubility and increase in CPT. The increased hydrophobicity does imply higher adsorption on rock surfaces at high temperatures which improves wettability alteration while the reverse is the case for more hydrophilic molecules (Das et al. 2020).

Previous cloud point studies have shown that surfactant structure, electrolytes in the aqueous phase, and other oilfield chemicals affect nonionic surfactants' CPT. Gu and Sjöblom demonstrated a linear relationship between the cloud point and the logarithm of ethylene oxide number for alkyl ethoxylates, alkyl phenyl ethoxylates and methyl capped alkyl ethoxylates esters, as well as a linear relationship between the cloud point and alkyl carbon number (Gu and Sjöblom 1992). Nonionic surfactants with low EO numbers, between 2.5 and 3 are observed to form turbid solutions at ambient conditions due to the short polar head, which strongly limits dissolution in water. While surfactants with large

EOs, between 40 and 50, have high cloud points, usually above 212˚F (Al-Sabagh et al. 2011, Mirchi et al. 2015). Li et al. revealed that polar compounds like Cl^-, Br^-, I^- and NO_3^- improve CPT due to their ability to enhance water's solvent property, which increases the solubility of the surfactant molecules in solution (Li et al. 2009). Acids and short-chain alcohols also increase the cloud point by increasing the concentration of hydrogen ions present in solution which enhances nonionic surfactant solubility via hydrogen bond formation (Nasr-El-Din and Al-Ghamdi 1996).

Nonionic surfactants in blends are usually co-surfactants that enhance ionic species' activity (Alvarez, Saputra, et al. 2018a). However, in studies in which the primary surfactant is the nonionic species, small amounts of ionic surfactant have significantly increased the CPT; with the increase becoming more significant as the co-surfactant mass fraction increases to match that of the primary surfactant (Das et al. 2020, Gu et al. 1989, Lindman et al. 2016, Sadaghiania and Khan 1991, Valaulikar and Manohar 1985). The introduction of the ionic co-surfactant leads to the formation of mixed micelles which possess electrostatic charges. The surface charge increases the repulsion between micelles, hindering the formation of the surfactant-rich phase. The cloud-point-increasing effect is stronger with ionic co-surfactant where the nonionic surfactant is more hydrophobic. This is because hydrophobic interactions aid the interaction between the ionic monomer and nonionic micelle. The mixed surfactant systems are noted to behave similarly to the single nonionic surfactant. With increasing electrolyte concentration leading to a detrimental effect on cloud point. And the presence of co-solvents like short-chain alcohols improving cloud point.

This study explores the issue of cloud point to better understand how the primary and co-surfactant structure and salinity affect CPT. We use three types of nonionic surfactant, nonylphenol, tridecanol, and secondary alcohol ethoxylates; as single surfactant systems and in combination with ionic co-surfactants. The temperature ranges targeted are above 212˚F with the aim of designing thermally stable surfactant solutions for use in high-temperature unconventional liquid-rich reservoirs.

Oil/Water IFT

Oil/water IFT determines the interaction potential between the oleic and the aqueous phase. Larger IFT indicates that a larger force is required to break the interface between the two phases, in order to mix them. Oil/water interfaces exists due to contrasting polarity of the two phases, which explains why they are immiscible. IFT also controls the flow of fluid in porous media and it directly affects the relative permeability and capillary pressure. Several dimensionless groups, i.e., capillary number and Bond number, directly demonstrates the effect of IFT on flow behavior and oil recovery.

IFT is an important parameter when surfactants are injected in a reservoir. Surfactants are unique molecules with a polar component on one portion of the molecule and a non-polar component on the other. This means that surfactant is soluble in both water and oil. But more importantly, this amphiphilic nature results in surfactant molecules aligning themselves at the oil/water interface. Once at the interface, the surfactant molecules reduce the oil/water IFT and alters the wettability of the oil/water/rock system. These effects are responsible for increasing the oil recovery of the reservoir.

IFT is typically obtained from laboratory experiments. The inverse pendant drop method measures IFT by calculating the size of an oil droplet at the tip of a needle submerged in the aqueous phase. Du Nuoy ring method measures IFT by measuring the force generated by pulling a metal ring in-between the two phases. Spinning drop method measures IFT by measuring the deformation of an oil drop in the presence of aqueous phase due to applied centrifugal force.

IFT can also be obtained from correlations. Most IFT correlations available in the literature are based on the relationship presented by Macleod (Macleod 1923). Firoozabadi and Ramey investigated the Macleod-based correlation on a range of standard crude oil samples from the literature (Livingston's Texas oil and Mobil crude oil samples) and found that it accurately predicts the IFT value, even with reservoir brine (Firoozabadi and Ramey 1988, Ramey 1973). Sutton revisited the correlation and improved its accuracy for higher temperatures (Sutton 2009). Several authors improved the Macleod-based IFT correlation by applying machine learning on thousands of data points from the literature (Nait Amar et al. 2019, Najafi-Marghmaleki et al. 2016).

The Macleod-based correlations are known to be accurate on certain cases. Their accuracy is believed to come from the close relationship between the density difference between the oil/water and their IFT (Ramey 1973). The correlations are stronger when approaching the miscibility point, because the two variables tend to zero at different rates (Schechter et al. 1994). However, the correlations and their derivatives do not account for the surface-active molecules contained in the crude oils, and their interactions with the system, which is affected by salt concentration, temperature, and pH. Buckley and Fan

investigated these correlations with IFT data from 42 oil samples. They concluded that it was inaccurate to predict the IFT solely from density difference. This was caused by the presence of surface-active components in the oil (Buckley and Fan 2007).

The effect of temperature and pressure on the IFT is one of the most complex experiments to perform, due to the requirement of a high pressure-high temperature cell. Higher temperature and lower pressure generally decrease oil/water IFT (Barati-Harooni et al. 2016, Hjelmeland and Larrondo 1986). The temperature effect is driven by the increase of the system entropy at higher temperature, resulting in the decrease of the Gibbs free energy. Lower Gibbs energy reduces the IFT. The pressure effect can be explained by the reduction of molecule-to-molecule distance at higher pressures, which result in an increase in the cohesion tension and ultimately, the IFT. Interestingly, in the same study, Harooni et al. also presented increasing IFT when the system temperature was increased on one of the oil samples. It was concluded that the higher asphaltene content on the particular oil caused this discrepancy; higher temperature resulted in lower asphaltene solubility. An inverse relationship between IFT and pressure has also been reported in the literature (Hassan et al. 1953, Michaels and Hauser 1951). A benzene system showed decreasing IFT when the pressure increased was observed. It was hypothesized that at higher pressure, benzene was adsorbed in the aqueous phase, causing the IFT to decrease. On the same study however, the n-decane system showed a positive correlation. It was concluded that the effect of temperature and pressure on the oil/water IFT was a response to the composition of the oleic phase.

The relationship between IFT and salinity is one of the most investigated IFT related topics due to its implication to EOR applications in conventional reservoirs. The general trend presented in the literature is a positive correlation between the two variables (Alotaibi and Nasr-El-Din 2009, Barati-Harooni et al. 2016, Kumar 2012, Okasha and Alshiwaish 2009). Heavier and higher valence salt ions result in larger IFT increase in systems with the same salt concentration (Weissenborn and Pugh 1996). The mechanism behind the IFT/salinity behavior is known as "salting-out" (Moeini et al. 2014). Several authors also observed independency of IFT to the brine salinity, when pure alkane was used as the oleic phase (Sayed et al. 2019). Interestingly, IFT reduction has also been observed when the brine was investigated at lower salinity (Khaksar Manshad et al. 2016, Lashkarbolooki et al. 2016, Rostami et al. 2019). The low salinity EOR concept is based on this phenomenon. It is important to note that most of the studies in the literature presenting this behavior were performed with crude oil containing significant asphaltenes content. Asphaltenes are the most surface-active components in crude oil, meaning that the mechanism of low-salinity IFT reduction is exactly the same as the mechanism of optimal salinity in surfactant applications. To summarize, oil/water IFT can increase, decrease, or even be unaffected when the salinity is varied. The trend is highly dependent on the oil composition used in the study.

It has been established that the oil/water IFT is a function of the oil composition. Furthermore, the effect of pressure, temperature, and salinity to the IFT is also controlled by the oil composition. The effect of the oil composition on IFT has not been deeply explored in the literature. This can be explained by the fact that it is uncommon to have a

wide variety of oil samples when analyzing a single reservoir. It seems to be more common to alter only the salinity, temperature, and pressure, when studying the interfacial properties. Several authors have performed IFT measurement on various pure components such as alkanes with different carbon number, or cyclic hydrocarbon (Cai et al. 1996, Zeppieri et al. 2001). However, actual crude oil sample always contain hundreds of various hydrocarbon molecules that interact with each other. There are several publications looking at the IFT of various crude oil compositions. Buckley and Fan performed a robust and comprehensive study with 42 crude oil samples, and derived a good relationship between the oil acid number, base number, asphaltene content and IFT (Buckley and Fan 2007). Lashkarbolooki and Ayatollahi went a step further, by separating the resins and asphaltenes component of two crude oil samples, to investigate the effect of oil components on the IFT (Lashkarbolooki and Ayatollahi 2018). In their study, asphaltene content was observed to dictate dominantly the IFT value. They also observed the opposite effect of salinity and IFT, depending on the hydrogen-to-carbon ratio contained in asphaltene and resin component of the crude oil.

This study aims to correlate the combined polarity of the oil and the water to the IFT. Actual crude oil samples are included in this study to capture the range of hydrocarbon molecular composition. The polarity of the oil is gauged from the composition of its saturates, aromatics, resins and asphaltenes components (SARA). SARA analysis was performed on the oil to extract each component, using solvents with various polarity levels. All crude oil samples came from a wide range of unconventional shale reservoirs in the US.

There are two versions of the novel SARA-based oil/water IFT correlation included in this study. The first version is constructed based on data acquired at room temperature (80°F). The second version accounts for changes in the temperature. This distinction results in better understanding of the effects of SARA components on IFT, and the interaction caused by the salinity and temperature on the SARA components and ultimately on the IFT.

Wettability

Wettability is defined as the affinity of a solid surface to a certain fluid phase in the presence of another immiscible fluid phase. A shale oil reservoir is a perfect case for wettability investigation because it contains all three phases required for wettability effect to exist. In this system, interstitial water acts as the polar liquid phase. The water phase always contains salt ions which makes it more polar. Crude oil that contains a vast variety of hydrocarbon chain acts as the non-polar liquid phase. These two liquid phases coexist inside the pore space of a rock, the solid phase. Wettability affects oil recovery factor, the efficiency of oil production from the reservoir, since it influences the flow pattern of fluids flowing through a reservoir (Zhang, Saputra, et al. 2018b). There has been significant focus in recent years on shale reservoir's wettability, which has been determined to be mostly oil-wet (Alvarez and Schechter 2016b). The oil-wetness is believed to cause a greater effect in a tighter reservoir, i.e., shale oil reservoirs, due to the stronger boundary effect from the pore wall to the pore throat. To solve this problem, several authors have investigated the application of surfactant as an EOR technique by altering the shale

wettability from oil-wet to water-wet (Akbarabadi et al. 2015b, Liang et al. 2015a, Alharthy et al. 2018, Alvarez, Saputra, et al. 2018b, Zeng et al. 2018b, Zhang and Wang 2018b, Bidhendi et al. 2019a, Tu and Sheng 2019b, Zhang et al. 2019b, Park and Schechter 2020). To design a surfactant system with strong wettability alteration performance, we must first understand the surface oil-wetting mechanism. This is important because minerals commonly found in the reservoir, i.e., quartz, calcite, dolomite, and clay, are actually water-wet after deposition. Additionally, the effect of oil composition, rock mineralogy, and salinity must also be investigated, especially with the heterogeneity of these three parameters observed in shale reservoirs in the US.

Several authors have investigated the mechanism behind the oil-wetting mechanism of a rock surface. Buckley and Liu (1998) proposed four mechanisms for oil-wet surface creation; 1) polar interactions, 2) surface precipitation, 3) acid/base interaction, and 4) ion binding (Buckley and Liu 1998). Polar interaction occurs due to the adsorption of the polar components of crude oil on the rock surface. Zhong et al. (2013) supported this mechanism based on their observation of the adsorption of pyridine on a silica surface from a molecular dynamic simulation (Zhong et al. 2013). Interestingly, other studies have also reported the adsorption of non-polar saturates of the crude oil on both silica and calcite surfaces (Liu et al. 2012, Yuan et al. 2016). However, due to the weak nature of the interaction, it is hypothesized that the rock surface must be free of water molecules during the adsorption process. Surface precipitation occurs when the asphaltene component of the crude oil becomes less soluble. The asphaltene precipitation occurs when the concentration of the lighter components in the crude oil are increased, which results in

stronger oil-wetness observed with lighter crude oil (Tang and Morrow 1997, Al-Maamari and Buckley 2003). The acid/base interaction occurs when crude oil has significant acid and/or base content. Calcite surfaces are believed to be positively charged, which will attract crude oil with acid content. Quartz, on the other hand, is negatively charged, which attracts the basic components. This interaction is highly dependent on the pH of the system (Brown and Neustadter 1980). Temperature has been observed to have a variable impact on oil-wetness caused by the acid/base interaction. An increase in temperature could increase the oil-wetness due to stronger electrostatic bonds (Rao 1999, Strand et al. 2003, Strand et al. 2008, Bai, Kubelka, et al. 2020). In contrast, higher temperatures could also decrease the oil-wetness due to the general onset of desorption and, in the case of calcite surfaces, the reduction of calcium adsorption sites (Hamouda and Rezaei Gomari 2006, Hirasaki and Zhang 2004, Tang and Morrow 1997). The last mechanism, ion binding, occurs due to the presence of salt ions on the rock surface which bridges the polar components of crude oil to the rock. This mechanism was observed to occur only with divalent ions (Brown and Neustadter 1980, Buckley et al. 1996).

Another approach to investigate the mechanism behind the surface oil-wet rendering is through molecular simulation. Atomic-scale simulation provides insight into the different forces that govern the wettability of a rock surface. The initial wettability of a rock surface is a function of oil and rock composition. In the absence of carboxylic acid, van der Waals forces cause oil adsorption on both siliceous and carbonaceous surfaces (Liu et al. 2012, Tang et al. 2019, Yuan et al. 2016). This force is, however, weaker than the electrostatic interaction between the water molecule and the solid surface. Therefore,

according to molecular simulation, the creation of a hydrophobic surface with oil can only occur when water is not present in the system. With a carboxylic acid group present in the crude oil, the surface oil-wetting is driven by the electrostatic interaction between the acid to positive calcium ions (calcite-rich surface) and the hydrogen atoms of the hydroxyl group (quartz-rich surface). This interaction was found to be stronger than the interaction between the water molecule and the rock (Zhong et al. 2013, Pantelides et al. 2017, Bai, Kubelka, et al. 2020).

Contamination of reservoir rock samples during the sampling process is inevitable. Before the experiment, reservoir rock samples are often cleaned and conditioned. In the area of wettability or surfactant research, rock samples are aged to restore the reservoir's initial wettability. The aging process consists of submerging rock samples in their corresponding crude oil at high temperature for an extended period. A look through the available literature indicates that the duration of the aging process that was employed for surfactant studies in shale varied from zero time up to a year, Figure 8 (Adel et al. 2018, Akbarabadi et al. 2015a, Alharthy et al. 2015, Alhashim et al. 2019, Alvarez, Saputra, et al. 2017a, Alvarez, Tovar, et al. 2017, Argüelles-Vivas et al. 2020, Benoit et al. 2020, Bidhendi et al. 2019b, Buckley and Liu 1998, Fu et al. 2019, Huang et al. 2020, Jin et al. 2017, Kurz et al. 2018, Liang et al. 2015b, Liu et al. 2018, Mohanty et al. 2019, Mohanty et al. 2017, Neog and Schechter 2016, Park and Schechter 2020, Peng et al. 2019, Sorensen et al. 2015, Tovar et al. 2018, Tu and Sheng 2019a, Tuero et al. 2017, Wang et al. 2014, Wang et al. 2015, Yu et al. 2016, Yu and Sheng 2015, Zeng et al. 2018a, Zhang, Adel, et al. 2018, Zhang et al. 2019a, Zhang and Wang 2018a). This is worrying because several

authors have presented the effect of the aging process on flow behavior. Jia et al. (Jia et al. 1991) investigated the effect of the aging time on the rock wettability measured on the Amott-Harvey index. They established the required aging time on their specific rock and oil system to be at least 12 days. They also found that higher aging temperature could decrease the minimum aging time. Drexler et al. (Drexler et al. 2019) reported that 30 days of aging is the minimum requirement to render their sample oil-wet. It is important to note that these two studies were performed mostly using heavy crude with high asphaltene and high acid/base content. These studies, therefore, might not apply to typical shale crude oil characterization because of the lack of asphaltenes. Sample wettability, as affected by the aging protocol, also controls the water imbibition profile. Zhou et al. (Zhou et al. 1995) performed spontaneous imbibition on Berea sandstone samples with various aging periods. Their study showed that although the aging time does not affect the final recovery volume, it reduces the rate of recovery. In another study, Zhou et al. (Zhou et al. 2000) further investigated the effect of aging on waterflood performance. They found a positive correlation between aging time and final recovery. Jadhunandan and Morrow (Jadhunandan and Morrow 1995) also reported similar results in a separate study. It is important to note that these studies limited their aging time to a maximum of ten days.

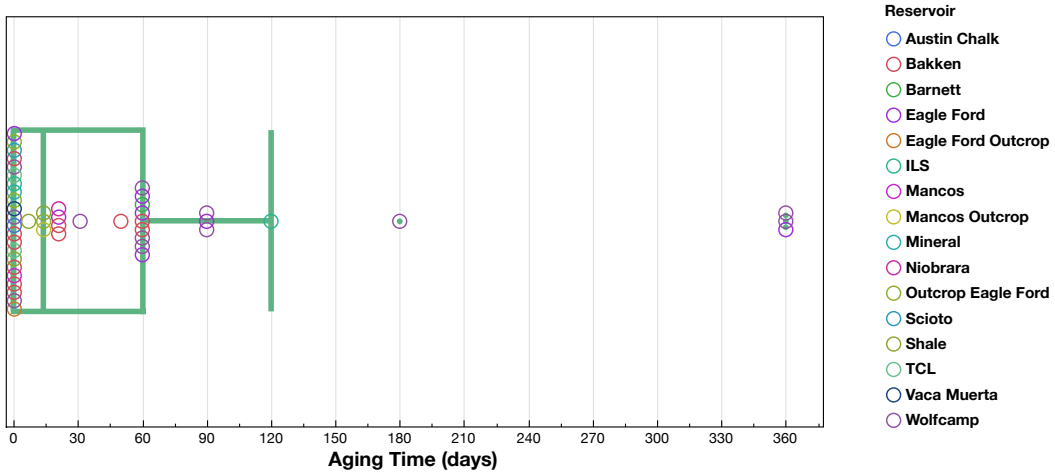

Figure 8 - Distribution of aging time from 44 publications of shale EOR involving aging procedure.

Brine is initially in contact with the sediment that forms reservoir rock. Therefore, during the formation of hydrocarbon in shale rock, water molecules are presumably still present in the reservoir. This hypothesis is often cited as a weakness of the aging procedure. The aging process has been criticized to over-estimate the oil-wetness of the shale rock surface as the process is preceded by a solvent (toluene and/or methanol) cleaning procedure. The cleaning process is therefore believed to remove all the water molecules from the rock surface, thereby rendering it unrepresentative of the original reservoir conditions. Additionally, it is believed that the water molecules would "block" the oil from rendering the surface oil-wet, especially with the presence of salt ions in reservoir brine. Studies have shown that monovalent and divalent cations (Na^+, K^+, Ca^{2+}, Mg^{2+}) affect shale's wettability by adsorbing onto the shale surface and providing additional sites for polar interactions on the shale surface (Mugele et al. 2015, Bai, Kang, et al. 2020). To understand the in-situ wettability of shale, it is important to understand the conditions which the reservoir rock is subjected. The effect of the presence of an initial

in-situ bulk brine phase and the shale hydration effect caused by this aqueous phase on the wettability of complex heterogeneous shale rock is critical in understanding the wettability alteration of shale rock by polar components in the oil.

This study is a continuation of previous work directed towards the effort to understand the polar/non-polar interaction between various phases in a shale system. In the previous study, we investigated the interaction occurring in a two-phase oil-brine system by interfacial tension (Saputra and Schechter 2021). This paper expands the research by adding the rock variable to the system, making it a three-phase system; oil, brine, and rock. The concept of mutual solubility, which was found to clearly explain the oil and brine interaction, was tested again in the three-phase system. Additionally, this study also aims to investigate the relevance of the surface oil-wetting mechanism available in the literature. Most, if not all, of the literature performed investigations on the crude oil/brine/rock systems of conventional reservoirs. As stated previously, the shale system has a very distinctive feature from conventional reservoirs. That is the absence of asphaltene, acid, and basic content in the crude oil and the high salinity characteristic of the brine. Lastly, this study is also intended to develop a standardized aging time protocol for preparing shale rock samples for wettability- or surfactant-related experiments.

CHAPTER III

METHODOLOGY

In this section, all the materials and measurement methodologies incorporate in this study are covered. Samples collection was performed to a great extend to fulfil the objective of comprising the wide distribution of Lower 48 shale oil/brine/rock system properties. Almost all of the samples used, except for the outcrop core plugs, was retrieved from the reservoir. This was performed to recreate shale reservoir condition as accurate as possible. Samples from multiple zones of the Eagle Ford, multiple depths of the Wolfcamp, Middle Bakken, Three Forks, multiple section of the Niobrara, and SCOOP/STACK were collected and incorporated in this study.

We will start with the description of all materials used in this study along with all characterization methods that were performed on the samples. Then the methods applied to prepare the rock samples which includes aging process is presented. Following the preparation method, interfacial tension, wettability, and cloud point measurement methods are described. And finally, the method used to quantify oil recovery is reported

Materials

Oil Samples

Fifteen oil samples from various reservoirs were collected for this study. Table 1 contains the density coefficient for density vs temperature equation presented in $\rho(T) = \rho_0 + \rho_1 * T$ ……Equation **1**. In the same table, API gravity along with the

source of the crude oil samples are also presented. As can be seen, although all samples came from shale reservoirs in the US, the crude oil from one reservoir has contrasting different to oil from another reservoir. The difference is presented clearly in Figure 9. In the figure, Lower 48 shale produces all sort of crude oil, from really light oil on the left to a black oil, shown on the right. Heterogeneity also presents in the same reservoir. For example, in the Eagle Ford, going from shallow to deep already results in the API gravity change from 25 to 55° API. In the Wolfcamp, similar trend also exists in smaller magnitude. Moving from the shallower Lower Spraberry to the deeper Wolfcamp D shifts the API gravity from 41 to 48° API.

$\rho(T) = \rho_0 + \rho_1 * T$ ……Equation 1

Table 1 – Oil samples density, API gravity, and reservoir

Oil	$\boldsymbol{\rho_0}$	$\boldsymbol{\rho_1}$	°API	Reservoir	Other Name
1	0.7801	-0.0004071	55.8	Eagle Ford (Deep)	EF-C
2	0.8038	-0.0004142	50.2	Eagle Ford (Deep)	EF-C-S
3	0.8151	-0.0004327	47.8	Wolfcamp D	W-D
4	0.8193	-0.0004206	46.7	Caney	C
5	0.8186	-0.0003900	46.5	Eagle Ford (Deep)	EF-M
6	0.8240	-0.0004000	45.4	Wolfcamp B	3H
7	0.8294	-0.0004287	44.6	Wolfcamp B	2H
8	0.8328	-0.0004060	43.5	Wolfcamp	W
9	0.8362	-0.0004135	42.9	Canyon Lime	CL-1
10	0.8387	-0.0003924	42.1	Niobrara B	N-B
11	0.8410	-0.0004000	41.7	Wolfcamp A	W-A
12	0.9500	-0.0022000	41.5	Wolfcamp	WC
13	0.8450	-0.0004000	40.9	Lower Spraberry	LSS
14	0.8647	-0.0004018	36.8	Middle Bakken	MB
15	0.9098	-0.0003798	28.0	Eagle Ford (Shallow)	EF-Au

Figure 9 – Crude oil samples used in this study, left-to-right is oil 1 – 15.

SARA analysis was performed on each of the oil samples to understand better the difference between the oil samples. The SARA results are presented in Figure 10. Composition heterogeneity is reflected here as well. For the fifteen crude oil samples this study has, the Saturates ranges from 34% to 91%, the Aromatics ranges from 4% to 49%, and the Resins ranges from 5% to 15%. Oil with higher API gravity contains more Saturates, while oil with lower API gravity has higher composition of Aromatics and Resins. In a shale crude oil reservoir system, the hydrocarbon is generated in-situ. The in-situ generation results in deeper reservoir to produce lighter hydrocarbon; in comparison, deeper conventional oil reservoir produces heavier hydrocarbon compared to shallower conventional reservoir. This trend can be observed in the API gravity trend and reflected in the SARA data. Higher temperature induces the cracking of complex hydrocarbon molecule (aromatics, resins, ring-structure, double-bond) into simpler linear hydrocarbon. Therefore, higher Saturates composition is obtained with lighter oil from deeper shale reservoir. It is also believed that this phenomena occurs to an extreme as almost none of the oil samples in this study contain any asphaltene molecule. Asphaltene is the most complex hydrocarbon molecule and would be broken down to simpler form first at higher

temperature. The asphaltene-free nature of these crude oil could be a strong signature of shale oil system and is expected to cause different interaction with rock and brine in the reservoir. It is important to note that one of the oil sample, oil#15, contains a small amount of asphaltene. This oil sample comes from the shallowest part of the Eagle Ford and also the heaviest crude oil in this study.

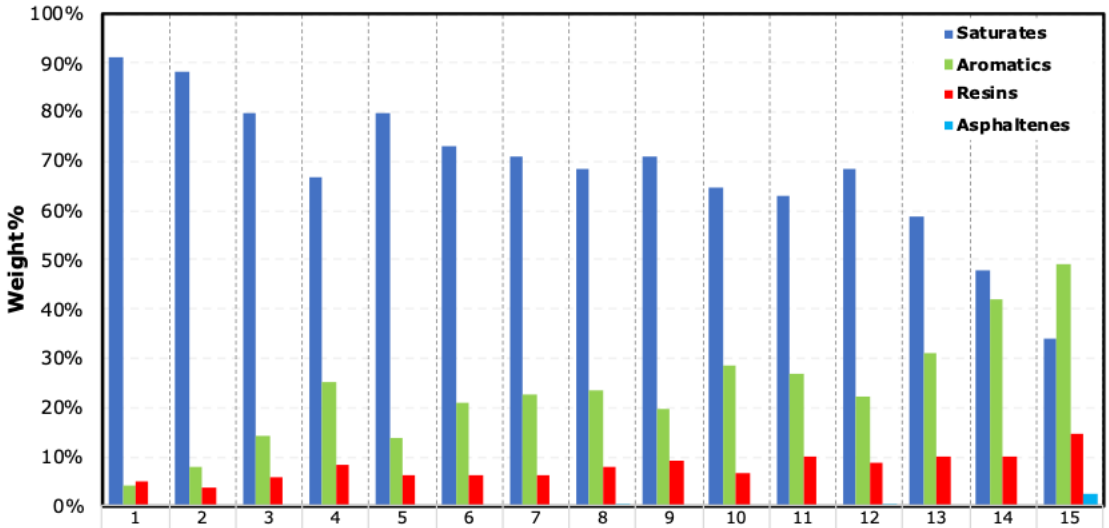

	1	2	3	4	5	6	7	8	9	10	11	12	13	14	15
Saturates	91.2%	88.4%	79.8%	66.7%	80.0%	72.9%	70.9%	68.4%	71.2%	64.7%	63.2%	68.5%	58.9%	48.0%	34.0%
Aromatics	4.0%	7.9%	14.3%	25.1%	13.9%	20.9%	22.7%	23.5%	19.7%	28.6%	26.9%	22.2%	30.9%	42.0%	49.0%
Resins	4.8%	3.7%	5.9%	8.2%	6.1%	6.2%	6.4%	7.8%	9.1%	6.7%	10.0%	8.8%	10.2%	9.9%	14.7%
Asphaltenes	0.0%	0.0%	0.0%	0.0%	0.0%	0.0%	0.0%	0.2%	0.0%	0.0%	0.0%	0.4%	0.0%	0.0%	2.3%

Figure 10 – SARA composition data.

These crude oil samples were collected either from the wellhead or the oil/water separator. Therefore, impurities were expected. To remove any impurities, Crude oil samples were centrifuged at 6000 rpm for 30 minutes. Then each sample was vacuumed for 4 hours. Density and SARA analysis were performed on the sample after it went through this sample preparation process

All fifteen crude oil samples will only be used in CHAPTER IV (page 72). The interaction of oil and brine at different temperature is covered in the chapter. With fifteen samples, a correlation to predict the oil/brine IFT that covers Lower 48 shale oil properties distribution was able to be constructed. In chapters following CHAPTER IV, only four oil samples will be used to simplify the experiment matrix. With the inclusion of rock and surfactant variables which each contains three to 15 variations, using four crude oil instead of 15 would exponentially reduce the experiment matrix. The four crude oils are Oil 1, 6, 14, and 15. These oils were picked to cover the extremes of Lower 48 shale crude oil properties.

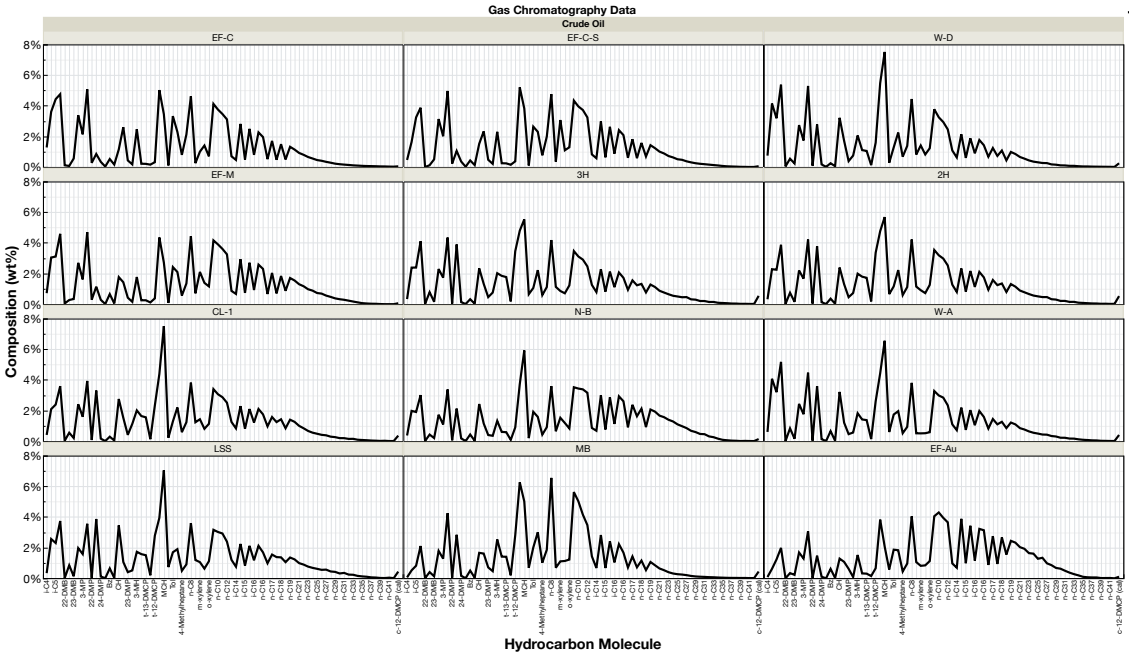

Figure 11 – Summary of Gas Chromatography results

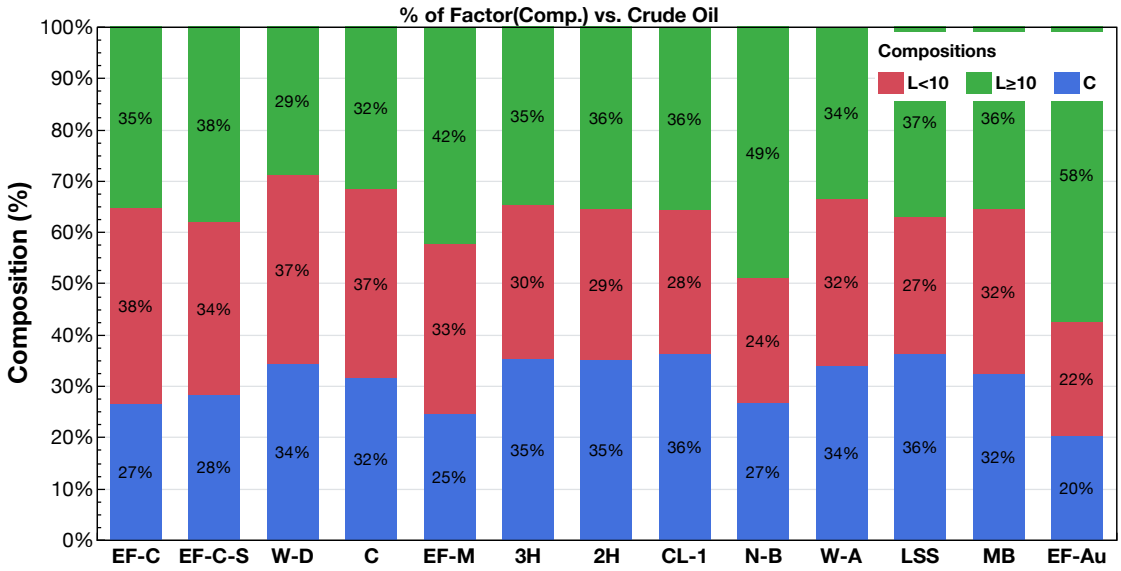

Figure 12 – Compiled GC results based on the shape of the hydrocarbon chain (linear vs cyclical) and the number of carbon atom.

Gas chromatography (GC) is also performed on the crude oils included in this study. A summary of the GC is presented in Figure 11. The composition (y-axis) is plotted for each of the hydrocarbon molecules (x-axis) found in the crude oil. GC provides a thorough information on the make-up of the crude oil by presenting the content of more than 50 hydrocarbon molecules in each crude oil. This level of detail can be hard to utilize. Therefore, the hydrocarbon molecules are compiled into three groups based on their structure. The first group is molecules containing 10 carbon atoms with linear chain as the main feature (L<10). The second group is linear molecule, but with more than and equal to 10 carbon atoms (L≥10). And lastly, molecules with a hydrocarbon ring as its main feature (C). The composition of each crude oils under this categorization is presented in Figure 12. This grouping is based on the expected polarity/polarizability. Linear hydrocarbon chain is more non-polar when compared to the cyclical hydrocarbon chain

due to the orbital configuration of the electrons on the cyclical chain. In linear hydrocarbon chain group, shorter hydrocarbon chain is expected to have stronger non-polarity.

Based on the GC grouping above, a new oil characterization variable is constructed. This variable is denoted as $\boldsymbol{R_{oil}}$. The definition of the variable is presented in $R_{oil} = \frac{L_{C<10}{}^{*}}{L_{C\geq 10}{}^{*}+C^{*}}$..... Equation **2**. As can be seen, the formula compares the two compositions of the three hydrocarbon groups. Larger values indicate a more non-polar crude oil as the amount of short linear hydrocarbon in the crude oil is higher. Smaller values indicate a more polarizable crude oil since the crude oil is dominated by the cyclical an longer linear hydrocarbon molecules. The $\boldsymbol{R_{oil}}$ values of the crude oil included in this study are presented in Figure 13.

$R_{oil} = \frac{L_{C<10}{}^{*}}{L_{C\geq 10}{}^{*}+C^{*}}$..... Equation 2

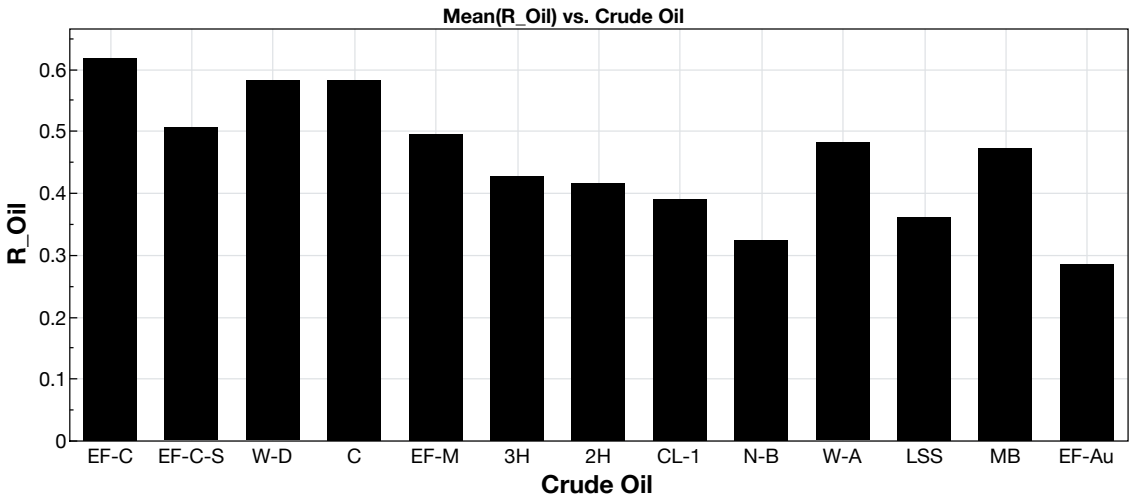

Figure 13 – $\boldsymbol{R_{oil}}$ values of the crude oils.

Brine Samples

Produced water from shale reservoir ranges from as low as 20000 ppm TDS to as high as 320000 ppm TDS, Figure 14. The figure was constructed from mostly USGS produced water data that was combined with several produced water composition data that was generated in-house. The lowest salinity for shale oil reservoirs is from the deeper section of the Eagle Ford with 20000 ppm TDS; this is where oil#2 in Table 1 was produced from. The salinity in the Eagle Ford increases with decreasing depth. Up to 16000 ppm TDS was produced from the reservoir depth of oil#15. In the Wolfcamp, the salinity of the produced water ranges from 10000 ppm to 15000 ppm TDS. The most extreme condition was from the Middle Bakken/Three Forks area where the TDS reaches the value of 320000 TDS which is virtually the saturation limit of salt in water.

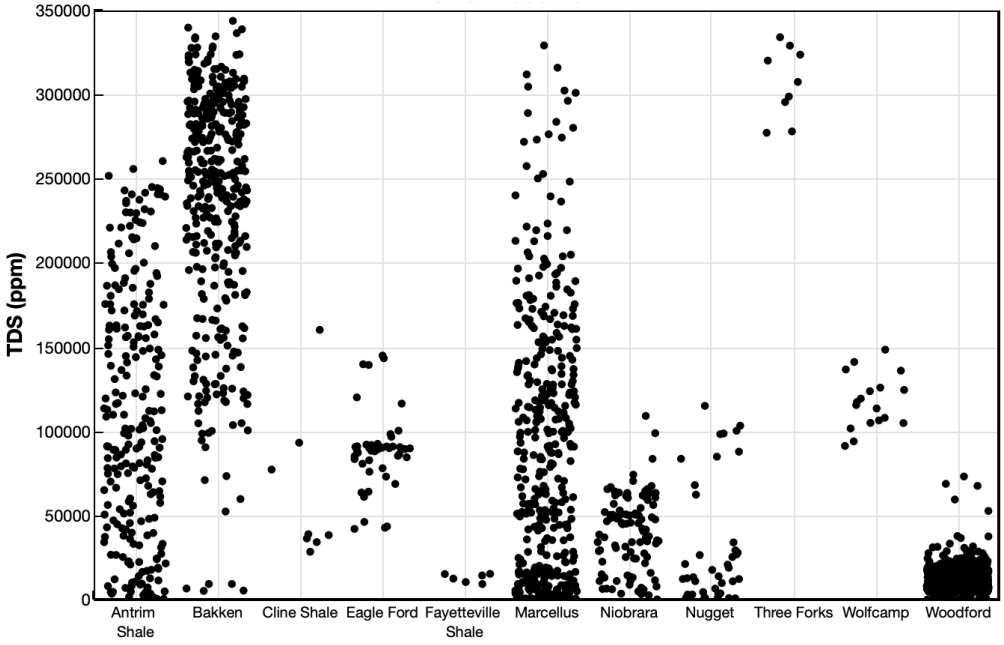

Figure 14 – TDS distribution of shale produced water from USGS (Engle et al. 2019) and in-house data.

It is interesting to note however that even though the TDS is widely varied from one reservoir to another, salt ion from all produced water is composed of more than 90% NaCl salt. This observation is presented in Figure 15 where the concentration of NaCl ion in the brine is normalized to the TDS and plotted on the y-axis. Simplification of the brine salt ion make up to only contain NaCl salt is applied in this study. This simplification is justifiable since NaCl dominates the salt ion composition.

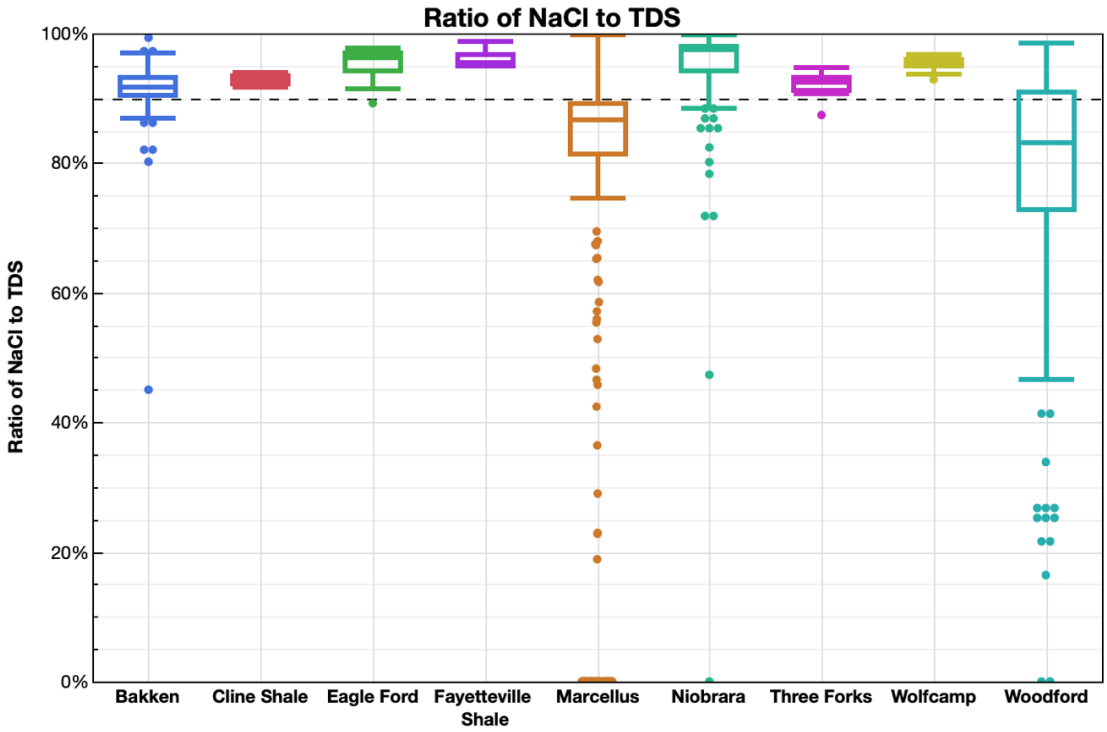

Figure 15 – Composition of NaCl in the salt ion making up 100% TDS of shale produced water.

To summarize, in this study four brines are included. The salinity ranges from 0 wt% to 24 wt% with 8 wt% increment. As mentioned earlier, only NaCl salt was used in the brine. To make the brine, DI water is used as the starting fluid, then NaCl salt is added according to the required concentration. Table 2 contains a recipe example to make 1L of each of the four brines in this study. The solution then is mixed overnight with a magnetic stirrer at room temperature to ensure the complete solubility of the salt.

Table 2 – Brine recipe to create 1L brine

Brine	NaCl weight (gr)	DI weight (gr)
0% NaCl	0	1000
8% NaCl	80	920
16% NaCl	160	840

24% NaCl	240	760

Rock Samples

The mineralogy of shale reservoir rock is heterogenous from one reservoir to another. In the past four to five years, numerous rock samples have been encountered from various reservoirs. A summary of the mineralogy of these rocks are presented in Figure 16. Generally, shale reservoir can be categorized into two, quartz-rich and carbonate-rich. The latter category then can be specified into calcite-rich and dolomite-rich.

Eagle Ford reservoir is generally calcite-rich with calcite composing between 50% to 93% of the rock mineralogy. Less than 20% of quartz can be found, considerable low compared to the calcite amount. While zero dolomite is found in this reservoir. In the Wolfcamp, both quartz-rich and calcite-rich rock can be found depending on the depth of the reservoir. This can be seen by the overlapping quartz and calcite box-whisker in the figure. Moving to Middle Bakken, rock mineralogy is more heterogeneous with dominant quartz, calcite, and dolomite can be found depending on the location and the depth of the reservoir. In the same basin, the deeper Three Forks reservoir is mostly dominated by dolomite-rich rock as can be seen by the dominant green box-whisker plot. In the rest of the samples, a wide range of calcite-rich and quartz-rich samples is observed.

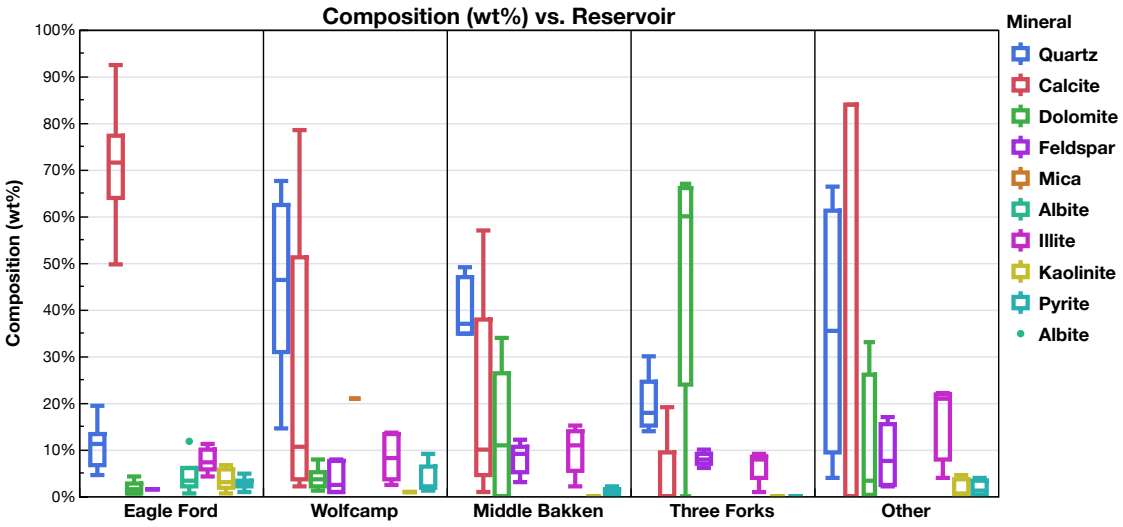

Figure 16 – Mineralogy distribution of in-house shale reservoir rock samples.

To accommodate for the vast distribution of mineralogy shown in Figure 16, this study employs both quartz-rich and calcite-rich rock samples. For wettability measurements, presented in CHAPTER V (page 91) and CHAPTER VIII (page 166), three rock samples are used. These three samples were obtained from either sidewall core or whole core of Eagle Ford and Wolfcamp reservoirs. The mineralogy of these samples is presented in Figure 17. Eagle Ford sample (EF-M) is carbonate-rich. Two Wolfcamp samples, Wh-84xx and Wh-86xx, are included. These two samples are quartz-rich and carbonate-rich respectively.

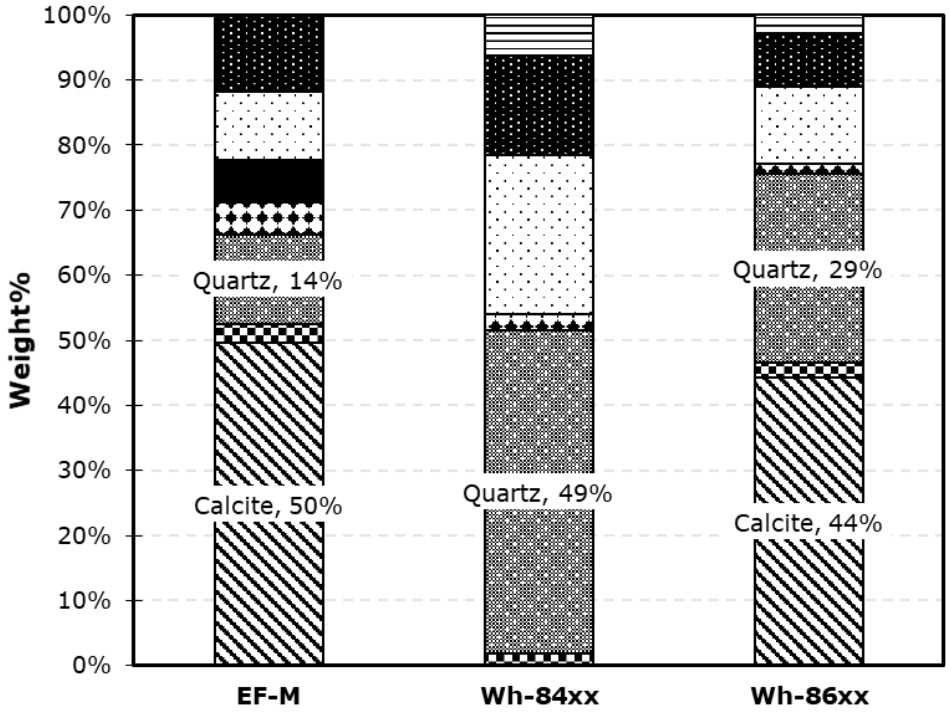

Figure 17 – Mineralogy composition of EF-M, Wh-84, and Wh-86 rocks.

This study employs more than 100 spontaneous imbibition experiments. Therefore, to ensure the availability of core samples for this massive effort, outcrop samples are used. Outcrop samples are also used to reduce the heterogeneity of actual shale reservoir sample which is notorious for having wide range of porosity and permeability, even in the same reservoir. The two outcrop samples used are Indiana Limestone and Scioto, the properties of these outcrops are given in Table 3.

Both reservoir and outcrop samples undergo careful sample preparation process before they can be used for the experiment. The preparation process includes cleaning, saturating, and aging. More detail on the process will be presented in upcoming sections.

Table 3 – Rock mineralogy, porosity, and permeability of ILS and Sc rocks.

Rock	Alias	Mineralogy	Porosity	Permeability
Indiana Limestone	ILS	Carbonaceous	13-14%	2-4 md
Scioto	Sc	Siliceous	16%	0.01 – 0.1 md

Temperature Range

Reservoir temperature of shale reservoirs varies widely. In the Eagle Ford, the temperature ranges from 180° F to 330° F depending on the depth of the reservoir; Eagle Ford is dipping towards the South-East. In the Wolfcamp, the temperature ranges from 150° F to 190° F when going deeper from Wolfcamp A to Wolfcamp D. In the Middle Bakken and Three Forks, the temperature is relatively consistent at 240° F. And finally, in the Niobrara, the temperature is 225° F. To better represent this wide variation, experiments in this study are performed at temperature range from 70° F up to 300° F.

Surfactant Samples

To investigate how surfactant headgroup and tailgroup structure are affecting the surfactant performance in enhancing oil recovery in a shale oil/brine/rock system, thirteen surfactants listed in Table 4 are included in this study.

The effect of headgroup charge to the surfactant performance will be investigated by comparing the performance of surfactant TD-12, S-13A, C12TAC, and CB. Each of these surfactants has different charge on the headgroup, nonionic, anionic, cationic, and zwitterionic respectively. The effect of tailgroup will be investigated by comparing the performance of surfactant NP-30, TD-30, and 15S-30. These three surfactants have 30 EO

groups as their headgroup. However, they all have different tailgroup, nonylphenol, tridecanol, and secondary pentadecanol, respectively. The effect of EO group length will be investigated by comparing the performance of surfactant NP-12, NP-20, NP-30, and NP-55 or surfactant TD-12, TD-30, and TD-50. These two groups have the same tailgroup, nonylphenol and tridecanol respectively. Each surfactant in each group has different EO group length as indicated by the number in their alias.

Table 4 – Surfactants tested in this study.

Alias	Name	Charge	Tail	Head	Manufacturer
NP-12	SURFONIC N-120	N	Nonylphenol	12 EO	HUNTSMAN
NP-20	SURFONIC N-200	N	Nonylphenol	20 EO	HUNTSMAN
NP-30	SURFONIC NB-307	N	Nonylphenol	30 EO	HUNTSMAN
NP-55	SURFONIC NB-557	N	Nonylphenol	55 EO	HUNTSMAN
TD-12	MAKON TD-12	N	Tridecanol	12 EO	Stepan
TD-30	MAKON TD-30	N	Tridecanol	30 EO	Stepan
TD-50	Makon TD-50	N	Tridecanol	50 EO	Stepan
15S-20	Tergitol 15-S-20	N	Secondary C15	20 EO	Dow Chemical
15S-30	Tergitol 15-S-30	N	Secondary C15	30 EO	Dow Chemical
S-13A	PETROSTEP S-13A HA	A	C12-C13 + 7PO	Sulfate	Stepan
C12TAC	STEPANQUAN 3712-W	C	Dodecanol	TAC	Stepan
CB	PETROSTEP CG-50	Z	Dodecanol	Betaine	Stepan

Aging and Rock Samples Preparation

Rock samples in this study goes through a rigorous preparation methodology. For rock chips used in contact angle experiment, the chip is cut from reservoir core sample. The chip has a dimension of 1 cm by 1 cm with 5mm thickness. Then chips are submerged in toluene for three days and in methanol for two days to remove any impurities. After methanol soak, chips are dried in a vacuum oven for one day. Then chips are aged in their corresponding oil for five weeks period and finally ready to be used for contact angle

measurement. In CHAPTER V (page 91), aging study is performed to establish the optimum aging duration to prepare shale samples. For this particular section of this study, the aging time is varied from zero to 120 days.

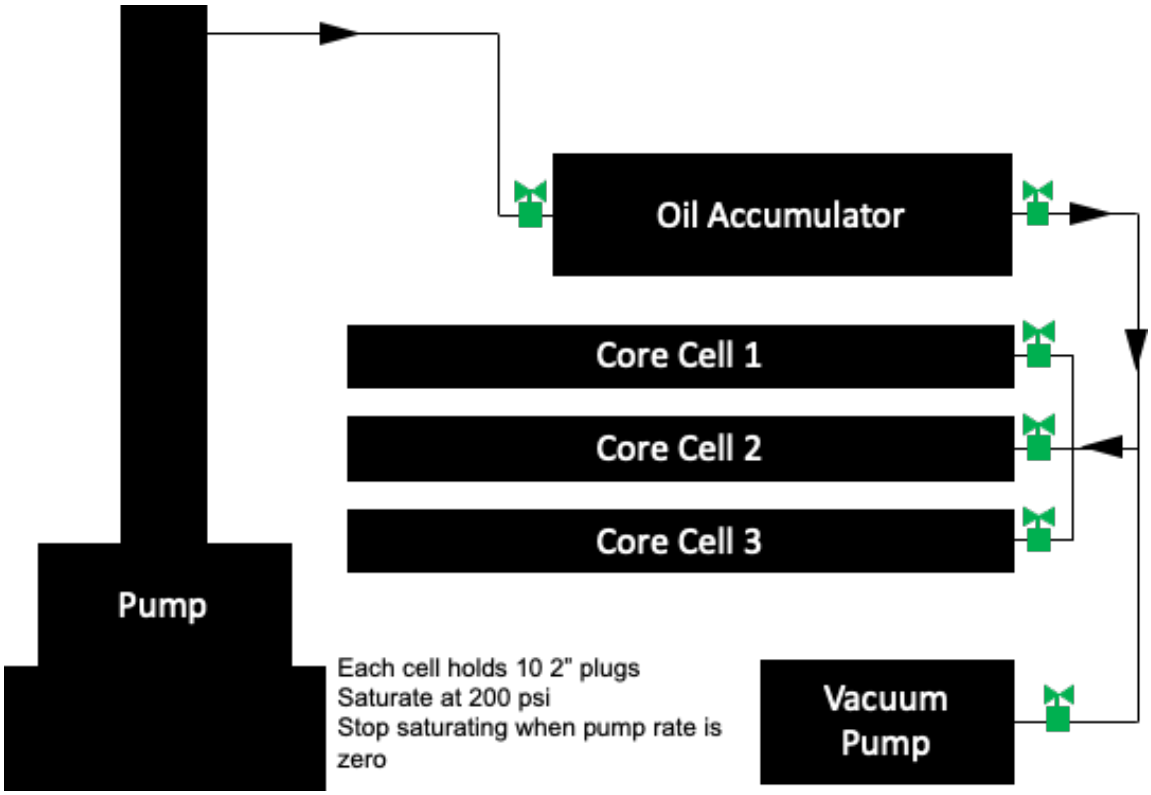

Figure 18 – Core plug saturation set-up.

For core plugs used in spontaneous imbibition experiment, core plugs are cut from an outcrop block to a 2” length by 1” diameter size. Then core plugs go through similar process. First, core plugs are cleaned of any non-polar impurities using the Dean-Stark apparatus with toluene for two weeks. Then, methanol is used in the Dean-Stark for one week to remove any polar impurities from the core plugs. Then, core plugs are dried in the

vacuum oven for another week. To saturate core plugs, a saturation setup shown in Figure 18 is used. Core plugs are loaded into the core cells, each core cell takes 10 core plugs. Then a vacuum pump is used to pull vacuum in the whole system overnight. Once vacuumed, the vacuum pump is disconnected, and the oil is pumped into the system. The system is then pressurized to 200 psi and left running until the pump rate reaches 0.00 mL/min which shows that all cores are fully saturated. Then core plugs are taken out of the cell and aged in their corresponding oil for three months. Finally, core plugs are ready to be used for spontaneous imbibition experiment.

OOIP is important for the spontaneous imbibition experiment as it determines the recovery factor of the experiment. Weight difference of the core plug before saturation and after aging is combined with the oil density to measure the OOIP of each core plug.

Interfacial Tension Measurement

Interfacial tension data is measured using the inversed pendant drop method. In this method, an oil drop is formed at the tip of a needle that dispenses upward. The needle is submerged in the aqueous-phase and the whole system is heated to the desired temperature. Figure 19 shows the configuration of this experimental method. Once the oil drop is formed, Young-Laplace curve fit is performed to approximate the oil drop shape and dimension. Then, IFT is calculated using the parameter from the curve fit and the density difference between the oil and the aqueous-phase at each salinity and temperature condition. This is where $\rho(T) = \rho_0 + \rho_1 * T$ ……Equation **1** and Table 1 play an important role to accurately calculate the density at the condition of the measurement.

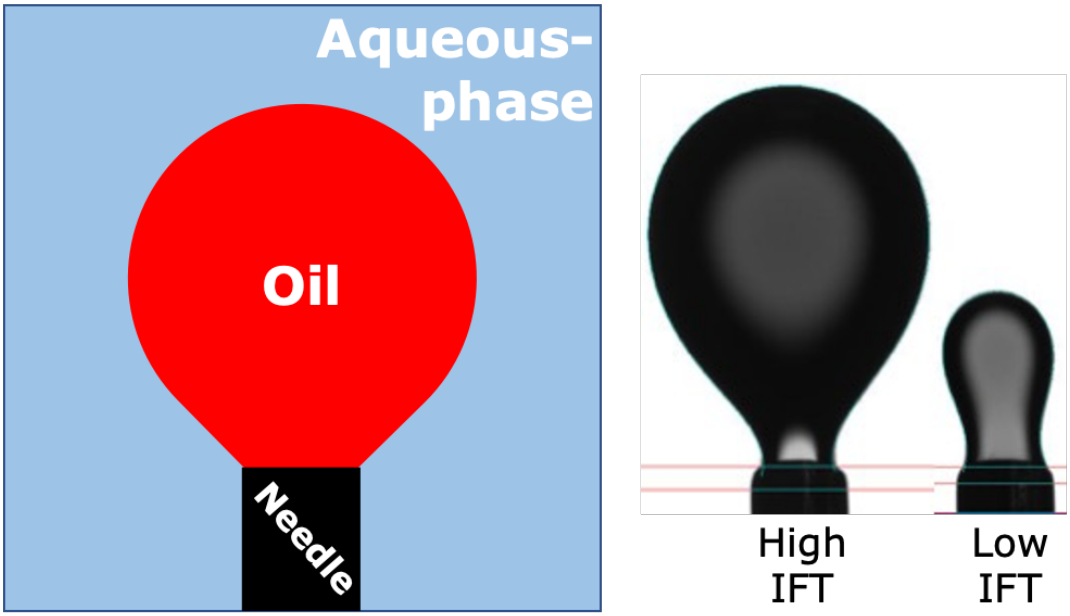

Figure 19 – Inversed pendant drop method (left), example of high IFT system (middle), example of low IFT system (right).

In this study, the IFT measurements are performed instantaneously without aging the oil drop in the aqueous-phase. The curve fitting calculation is performed at the maximum drop volume before it detaches from the needle. For temperature scan data, measurement is repeated at an interval of 10° F from room temperature until the maximum temperature of the machine, 195° F, is reached

Wettability Measurement

Wettability data are measured with the captive bubble method. This method is performed on aged rock chips that were cut from reservoir rock sample. To measure the contact angle, one chip is removed from their aging vial. Excess oil is removed from the chip and the chip is placed on a stage that is submerged in the aqueous-phase. For the

standard temperature, the aqueous-phase is preheated to the measurement temperature before the chip is placed. Once placed, a drop of oil is dispensed and placed at the bottom of the rock chip. Contact angle is defined as the angle formed by the drop with the rock surface, measured from the aqueous-phase (Figure 20).

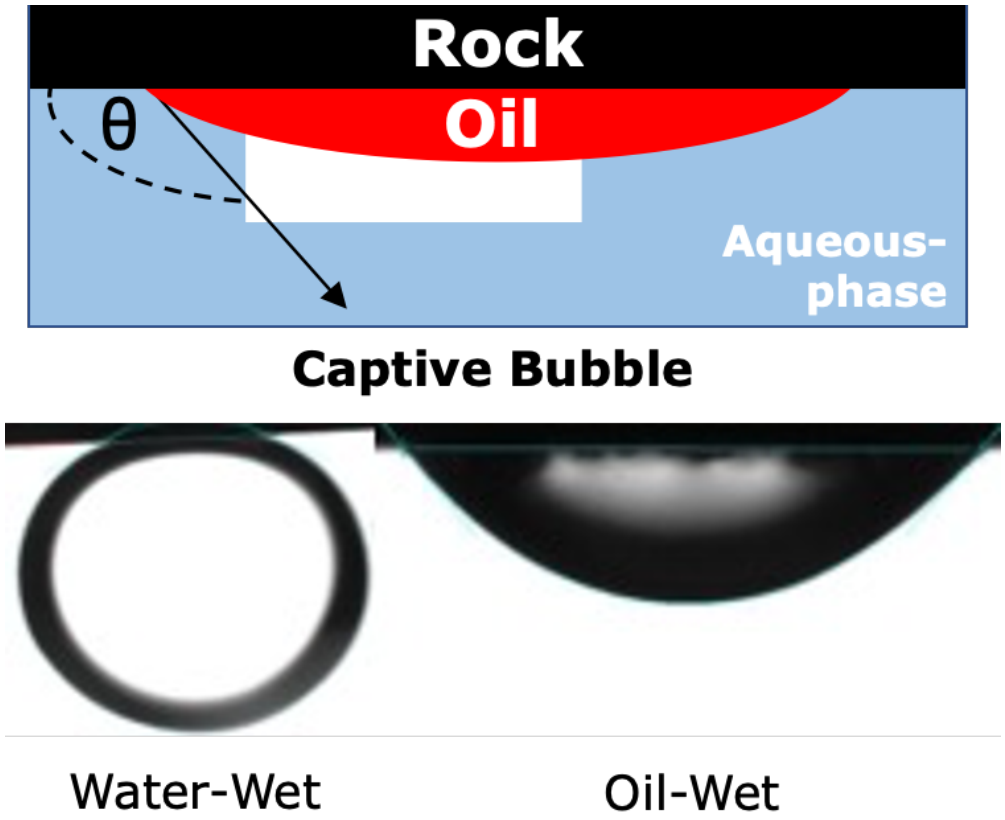

Figure 20 – Captive bubble method (top), example of water-wet system (bottom-left), and example of oil-wet system (bottom-right).

As described earlier, shale reservoir like the Eagle Ford and the Middle Bakken has reservoir temperature above the boiling point of water. For contact angle measurement

above the boiling temperature of water, the system needs to be pressurized to prevent the water from boiling. A Biolin Theta Flex apparatus is used for this HPHT measurement. With this machine, system condition up to 392° F and 5,000 psi can be replicated for the measurement.

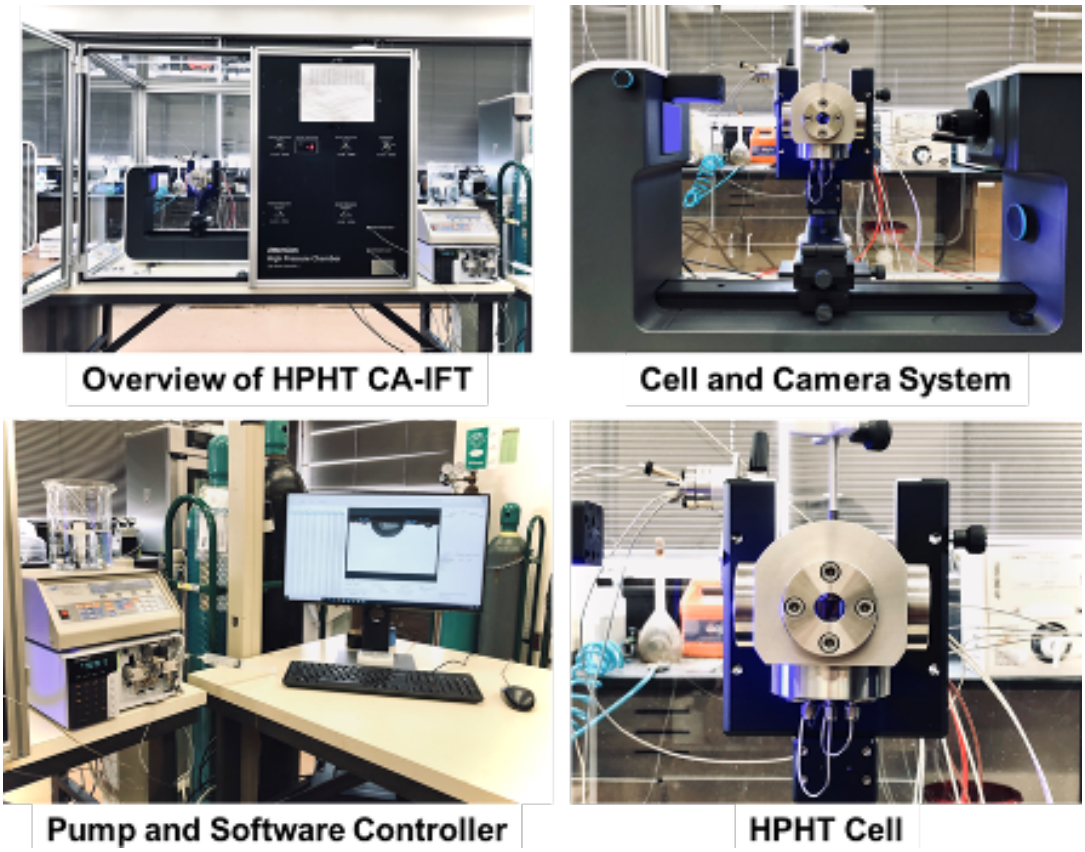

Figure 21 – Biolin Theta Flex apparatus to measure contact angle at HPHT.

In essence, the Biolin system follows the exact same methodology as the standard temperature. And Oil drop is still formed at the bottom of the aged rock chip that is submerged in the aqueous-phase. The only difference is that in the Biolin system, the

whole set up is placed inside a pressure vessel. The other difference is that oil drop is placed on the rock surface at room temperature. Then, the cell is heated to the desired temperature.

Cloud Point Measurement

Cloud point is the temperature where nonionic surfactants lose their hydrophilicity and become insoluble in the aquoues-phase. This phase transition can be observed clearly by the change in turbidity of the sample, Figure 22. For cloud point lower than the boiling point of water, cloud point measurement is a simple procedure. Several bottles filled with the tested surfactant are placed inside a water bath. The water bath then is heated and the temperature where the surfactant becomes completely turbid is recorded as the cloud point temperature.

Figure 22 – Cloud point measurement for temperature below 200° F, showing before cloud point (left) and after cloud point (right).

Some surfactant has cloud point above the boiling point of water. To measure cloud point of these surfactants, a special device was constructed (Figure 23). This device is in essence a pressure cell with heating and viewing port. To measure the cloud point, the surfactant solution is loaded into the device. Then the system is pressurized to 200 psi and the system is heated. A camera system is installed at the viewing port to improve the safety rating of the device. This device is rated to cloud point measurement up to 500 psi and temperature up to 400° F. Compared to the bottle test method in the cloud point measurement below the boiling point of water, the HPHT method is significantly slower as only one fluid at a time can be tested.

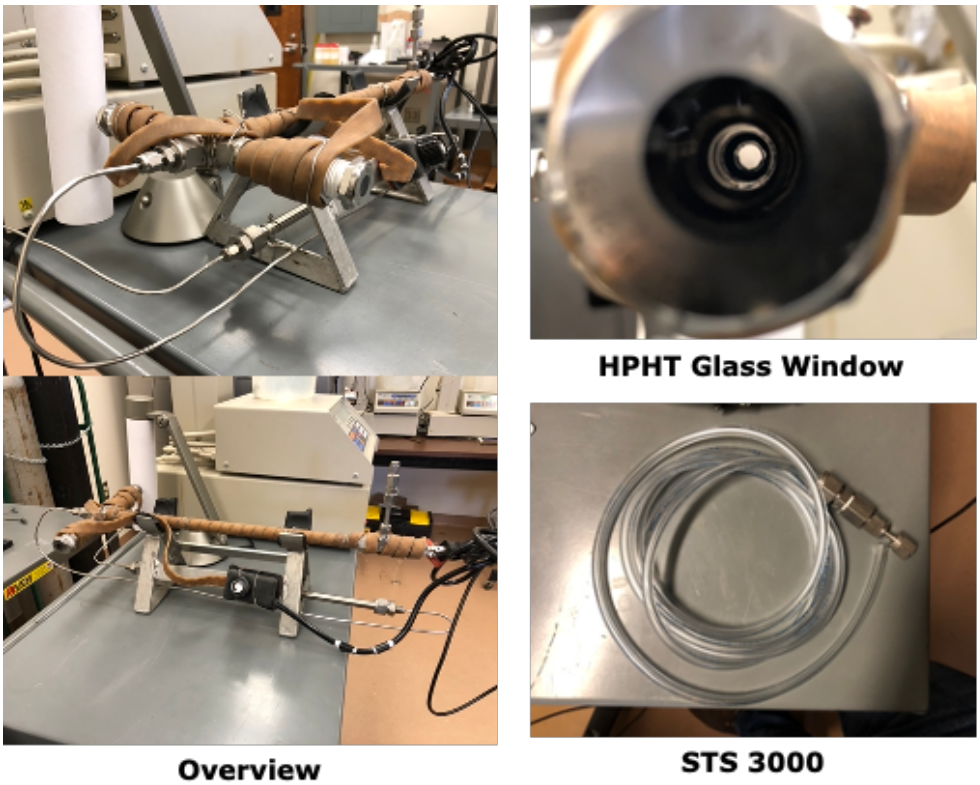

Figure 23 – HPHT cloud point measurement apparatus, “The Trombone”, to measure cloud point up to 400° F.

Oil Recovery Factor Measurement

Spontaneous imbibition experiment is the method used in this study to quantify the oil recovery. This method is relatively simple compared to the other method employed in this study. However, the preparation takes more than four months, mostly in aging the core plug. Once started, it typically only takes 10 days to finish.

Figure 24 – Custom Amott cells, "The Taj", to perform spontaneous imbibition experiments.

Aged core sample is placed horizontally at the bottom of the cell, see Figure 24. The bottom PTFE part of the cell has built-in stand to hold the core plug. Then the glass top is screwed on the bottom plug. Then the cell is filled with the aqueous-phase that is being tested. The whole cell is placed inside an oven, set at the experiment temperature. Produced oil will come out of the rock and accumulated at the top of the cell, see Figure 25. The top part of the cell is graduated so the volume of the oil can be measured. Oil production typically occurs fast at the early time and gradually slows down at later time. Therefore, in the first 24 hours of the experiment, the oil recovery is recorded every four

hours. Then every 6 hours for the next 48 hours and every 12 hours for the next 48 hours. And finally, every 24 hours until the end of the experiment.

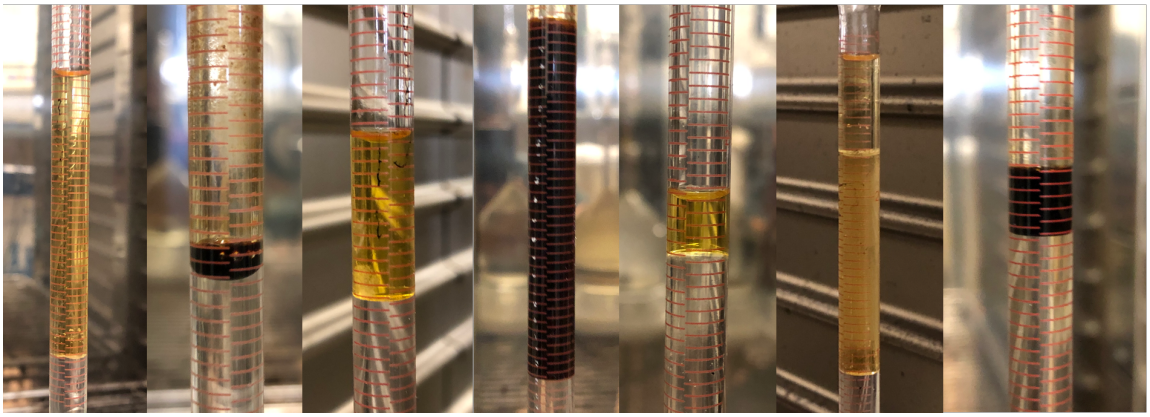

Figure 25 – Examples of produced oil accumulated at the top of Amott cells.

Often time, some oil drop would stick on the core plug and does not go to the top. For this case, the cell is shaken until the oil drop detaches and accumulate at the top. This process is justified as this study only looks at the performance of surfactant in producing oil from the pores of the core plug. Another problem that might arise during the spontaneous imbibition experiment is the formation of Winsor Phase-III emulsion. When this happens, oil recovery will only be recorded for the oil-phase produced at the top. Emulsion will not be accounted for as it is known that the oil content of these emulsions is very low.

CHAPTER IV

LOWER 48 SHALE RESERVOIRS OIL/BRINE INTERACTION

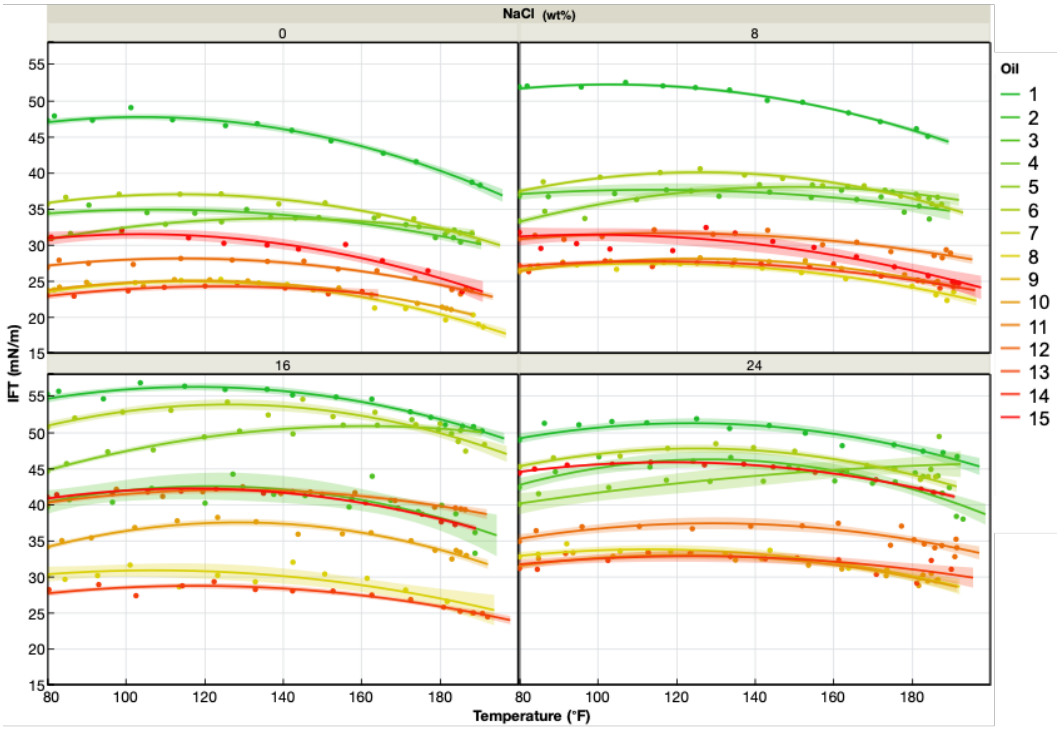

Figure 26 - Summary of 800+ IFT measurements as a function of temperature from 15 oil samples used in this study. Upper left is 0% NaCl and lower right is 24% NaCl.

More than 800 IFT measurements were utilized for this study. A summary of the IFT data as a function of the system temperature for each oil and each salinity level is presented in Figure 26. The following section presents the two correlations derived from this database as shown in $IFT = a_0 + a_1 * S + a_2 * S^2 + a_3 * Ar + a_4 * Ar^2 + a_5 * R + a_6 * R^2 + IFT_{Salt-Corr} * NaCl$..... Equation **3** and $IFT = b_0 + b_1 * S + b_2 * S^2 + b_3 * Ar + b_4 * Ar^2 + b_5 * R + b_6 * R^2 + IFT_{Salt-Corr} * NaCl + IFT_{Temp-Corr} * T^*$ .....

Equation 5. The first correlation in $IFT = a_0 + a_1 * S + a_2 * S^2 + a_3 * Ar + a_4 * Ar^2 + a_5 * R + a_6 * R^2 + IFT_{Salt-Corr} * NaCl$…… Equation **3** only analyzes data obtained from IFT measured at room temperature (80° F). The second correlation in $IFT = b_0 + b_1 * S + b_2 * S^2 + b_3 * Ar + b_4 * Ar^2 + b_5 * R + b_6 * R^2 + IFT_{Salt-Corr} * NaCl + IFT_{Temp-Corr} * T^*$ …… Equation 5 includes the temperature effect. The effect of the SARA components and their interaction with the salinity to the oil/water IFT is covered in the first correlation. While the effect of the interaction between temperature and SARA components is covered in the second correlation.

Oil/Water IFT Correlation for Ambient Conditions

The IFT data measured at ambient conditions (80°F) were selected and analyzed. Asphaltenes were not included in this correlation due to the lack of asphaltenes content in the shale oil samples as was shown in Figure 10. The correlation between the saturates, aromatics, resins, and salinity are presented in $IFT = a_0 + a_1 * S + a_2 * S^2 + a_3 * Ar + a_4 * Ar^2 + a_5 * R + a_6 * R^2 + IFT_{Salt-Corr} * NaCl$…… Equation **3** and $IFT_{Salt-Corr} = a_7 + a_8 * S + a_9 * S^2 + a_{10} * Ar + a_{11} * Ar^2 + a_{12} * R + a_{13} * R^2$…… Equation **4**. The saturates, aromatics, resins, and salinity are in wt%. The coefficients for this correlation are presented in Table 5. Salinity is included in this correlation by the $IFT_{Salt-Corr} * NaCl$ term, at the end of $IFT = a_0 + a_1 * S + a_2 * S^2 + a_3 * Ar + a_4 * Ar^2 + a_5 * R + a_6 * R^2 + IFT_{Salt-Corr} * NaCl$…… Equation **3**. This term is normalized to the salinity level, meaning that when DI water is used, this term equals zero. The $IFT_{Salt-Corr}$ term is defined by $IFT_{Salt-Corr} = a_7 + a_8 * S + a_9 * S^2 + a_{10} *$

$Ar + a_{11} * Ar^2 + a_{12} * R + a_{13} * R^2$…… Equation **4**. This equation has the same form as $IFT = a_0 + a_1 * S + a_2 * S^2 + a_3 * Ar + a_4 * Ar^2 + a_5 * R + a_6 * R^2 + IFT_{Salt-Corr} * NaCl$…… Equation **3**, but with different coefficients. This allowed us to further investigate the interaction between the different oil components and salinity and its effect on the oil/water IFT. The correlation shows good accuracy in estimating the IFT value with an R^2 of 0.92, which is shown in Figure 27. It is important to reiterate that this correlation is constructed with crude oil samples coming from shale oil reservoirs. Therefore, ideally, this correlation should only be used for estimating IFT value of shale crude oil with no asphaltenes. These oils are generally lighter and have a lower acid number (often zero) than conventional reservoir oils with the exception of sample 15 which is the 28°API oil.

$IFT = a_0 + a_1 * S + a_2 * S^2 + a_3 * Ar + a_4 * Ar^2 + a_5 * R + a_6 * R^2 + IFT_{Salt-Corr} * NaCl$…… Equation 3

Where,

$IFT_{Salt-Corr} = a_7 + a_8 * S + a_9 * S^2 + a_{10} * Ar + a_{11} * Ar^2 + a_{12} * R + a_{13} * R^2$…… Equation 4

Table 5 - Table of coefficients for equation 3 and equation 4.

S	:	Saturates content (in wt%)			
Ar	:	Aromatics content (in wt%)			
R	:	Resins content (in wt%)			
NaCl	:	Salt concentration (in decimals)			
a_0	:	-203.9266	a_7	:	-55.5764
a_1	:	-13.5899	a_8	:	-2.0608
a_2	:	15.8265	a_9	:	2.6088
a_3	:	14.3806	a_{10}	:	3.0346
a_4	:	-15.2289	a_{11}	:	-3.1883
a_5	:	31.0052	a_{12}	:	3.8941
a_6	:	-130.5776	a_{13}	:	-15.3946

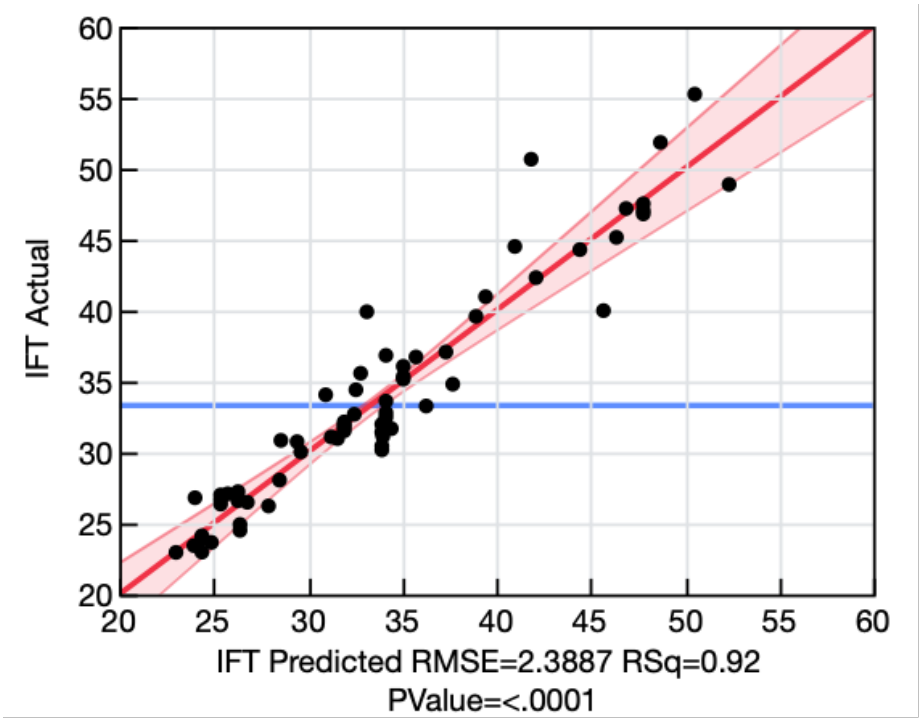

Figure 27 - Model fit for equation 3 and 4, oil/water IFT at various salinity for room temperature.

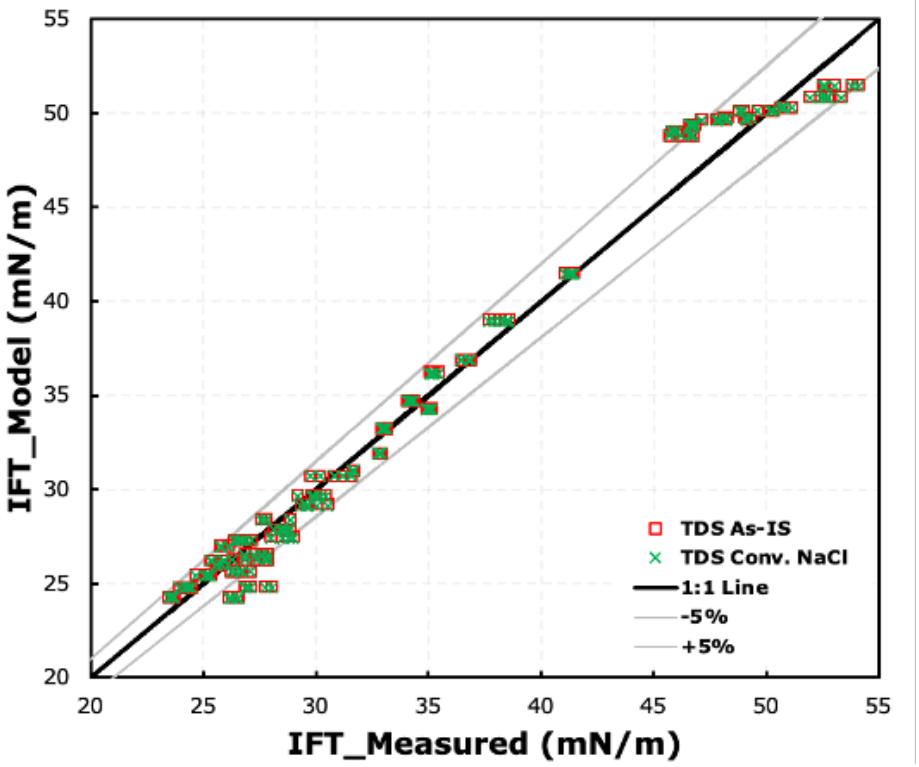

Figure 28 - Model fit for IFT calculation of the nine synthetic brines included in this study to demonstrate the applicability of the IFT correlation with natural produced brine.

The brine used in constructing the correlation contained only sodium chloride. Application to natural produced brine with divalent salt ions was tested by first converting the TDS to NaCl-equivalent TDS, using the VSM. This application was tested by comparing the calculated IFT to the IFT measured for the nine natural brine values included in the study. The model fit is presented in Figure 28. $IFT = a_0 + a_1 * S + a_2 * S^2 + a_3 * Ar + a_4 * Ar^2 + a_5 * R + a_6 * R^2 + IFT_{Salt-Corr} * NaCl$…… Equation **3** and $IFT_{Salt-Corr} = a_7 + a_8 * S + a_9 * S^2 + a_{10} * Ar + a_{11} * Ar^2 + a_{12} * R + a_{13} * R^2$…… Equation **4** correctly predict the IFT values within 5% of the measured IFT. However, the accuracy degrades at higher IFT value (>50 mN/m) due to the limited samples with IFT values larger than 50 mN/m. Figure 28 also compares the IFT calculated from two TDS's. The red squares represent the IFT values calculated from TDS directly, without conversion to NaCl-equivalent. The green crosses are the IFT values from NaCl-equivalent TDS as determined from the VSM. The IFT values from the two TDS's are surprisingly similar. These results can be explained by the salt composition of the produced water from the shale reservoirs which mainly contains up to 95% sodium chloride. Multiple authors have showed the impact of salt valences or salt ion types on the oil/water IFT. However, this study shows that, on actual divalent-monovalent salt ratio, the difference caused by the salt type is overshadowed by the dominant NaCl concentration.

Oil/Water IFT Correlation for Elevated Temperature

$IFT = a_0 + a_1 * S + a_2 * S^2 + a_3 * Ar + a_4 * Ar^2 + a_5 * R + a_6 * R^2 + IFT_{Salt-Corr} * NaCl$…… Equation **3** and $IFTSalt-Corr = a_7 + a_8 * S + a_9 * S^2 + a_{10} * Ar + a_{11} * Ar^2 + a_{12} * R + a_{13} * R^2$…… Equation **4** were expanded to account for the temperature effect on the oil/water IFT. This was performed by adding a similar correction factor term, like the $IFT_{Salt-Corr} * NaCl$ term, to account for the effect of temperature. The final correlation is presented in $IFT = b_0 + b_1 * S + b_2 * S^2 + b_3 * Ar + b_4 * Ar^2 + b_5 * R + b_6 * R^2 + IFT_{Salt-Corr} * NaCl + IFT_{Temp-Corr} * T^*$ …… Equation 5, $IFTSalt-Corr = b_7 + b_8 * S + b_9 * S^2 + b_{10} * Ar + b_{11} * Ar^2 + b_{12} * R + b_{13} * R^2$ …… Equation 6, $IFTTemp-Corr = b_{14} + b_{15} * S + b_{16} * S^2 + b_{17} * Ar + b_{18} * Ar^2 + b_{19} * R + b_{20} * R^2$ …… Equation 7, and $T* = {T^2}/{1000}$ …… Equation 8, with the coefficients listed in Table 6. The units for the saturates, aromatics, resins, and salinity are in wt%, and the temperature is in °F. The temperature term is purposely constructed in the same way as the salt correction factor: $IFT_{Temp-Corr} * T^*$. The temperature, however, is scaled with $T* = {T^2}/{1000}$ …… Equation 8. Model fit for the correlation is presented in Figure 29. Although the correlation has a good R2 value of 0.88, the fit is not as good as the first version presented above. This indicates that, when the temperature of the system is increased, there are other variables than saturates, aromatics, resins, and salinity, controlling the oil/water IFT. Similar to the previous correlation, this equation should only be used with low asphaltenes crude oils characteristic of unconventional reservoirs.

$$IFT = b_0 + b_1 * S + b_2 * S^2 + b_3 * Ar + b_4 * Ar^2 + b_5 * R + b_6 * R^2 + IFT_{Salt-Corr} * NaCl + IFT_{Temp-Corr} * T^* \quad \text{..... Equation 5}$$

Where,

$$IFT_{Salt-Corr} = b_7 + b_8 * S + b_9 * S^2 + b_{10} * Ar + b_{11} * Ar^2 + b_{12} * R + b_{13} * R^2 \quad \text{..... Equation 6}$$

$$IFT_{Temp-Corr} = b_{14} + b_{15} * S + b_{16} * S^2 + b_{17} * Ar + b_{18} * Ar^2 + b_{19} * R + b_{20} * R^2 \quad \text{..... Equation 7}$$

$$T^* = {}^{T^2}/_{1000} \quad \text{..... Equation 8}$$

Table 6 - Table of coefficients for equation 5, 6, 7, and 8.

S	:	Saturates content (in wt%)					
Ar	:	Aromatics content (in wt%)					
R	:	Resins content (in wt%)					
NaCl	:	Salt concentration, converted to NaCl equivalent (in decimals)					
T	:	Temperature (in °F)					
b_0	:	-670.2722	b_7	:	-31.6371	b_{14}	:	-28.3031
b_1	:	-17.4914	b_8	:	-1.8941	b_{15}	:	-0.8214
b_2	:	24.3852	b_9	:	2.2044	b_{16}	:	1.0984
b_3	:	26.9441	b_{10}	:	2.4192	b_{17}	:	1.3232
b_4	:	-25.3124	b_{11}	:	-2.7064	b_{18}	:	-1.3381
b_5	:	46.4821	b_{12}	:	3.1408	b_{19}	:	1.7061
b_6	:	-176.9055	b_{13}	:	-13.1649	b_{20}	:	-6.6729

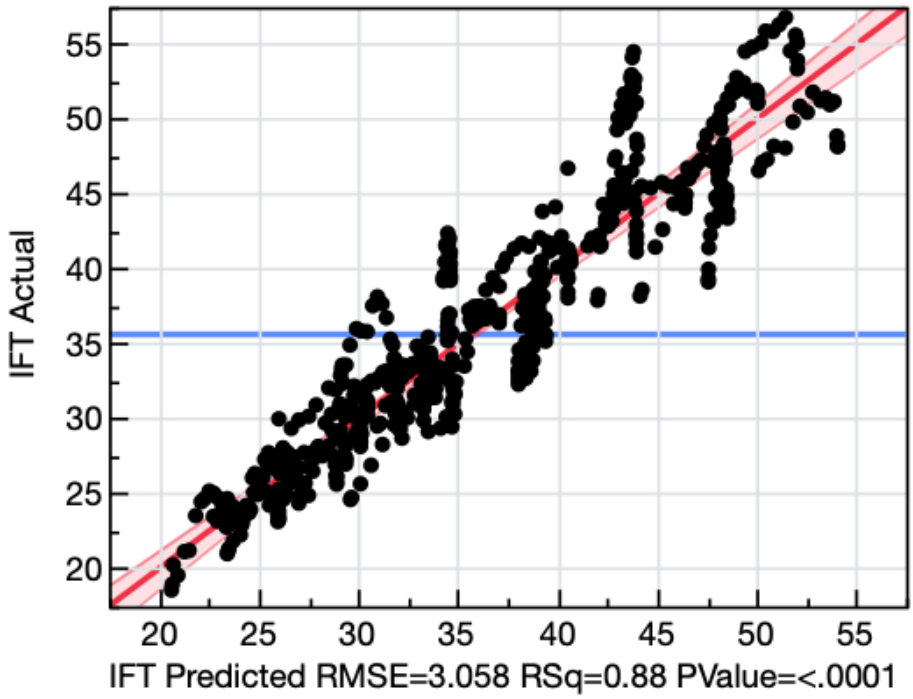

Figure 29 - Model fit for Equatio 4, Equation 5, Equiation 6, and Equation 7, oil/water IFT for variable salinity and temperature.

Effect of Saturates, Aromatics, and Resins Content to The Oil/Water IFT

This study includes oil samples with Saturate content ranging from 34% to 91%, aromatics ranging from 4% to 49%, and resins ranging from 4% to 15%. The effect of each component to the oil/water IFT are presented in Figure 30. Only data obtained at ambient conditions are included. The data are grouped in rows with different salinity level for the aqueous phase.

Generally, Figure 30 shows that a higher Saturate content increases the IFT. While a higher aromatics and resins content, decreases the IFT. Sample 15 is the heaviest oil included in this study which comes from the shallower section of the Eagle Ford shale reservoir and is shown in the red circles in Figure 29. Sample 15 has the lowest concentration of saturates and the highest concentration aromatics and resins points (the

datapoints are highlighted by the red circle from sample 15), The weakness of SARA separation procedure is highlighted with this oil. SARA method separates the crude oil based on the polarity of the solvent used, regardless of the molecular weight of the hydrocarbon molecule. It is believed that the saturates from oil #15 consists of longer and heavier paraffins, which causes higher IFT, as discussed in the Introduction section (Zeppieri et al. 2001). Therefore, the graph shows higher IFT at lower saturates content and higher aromatics-resins content.

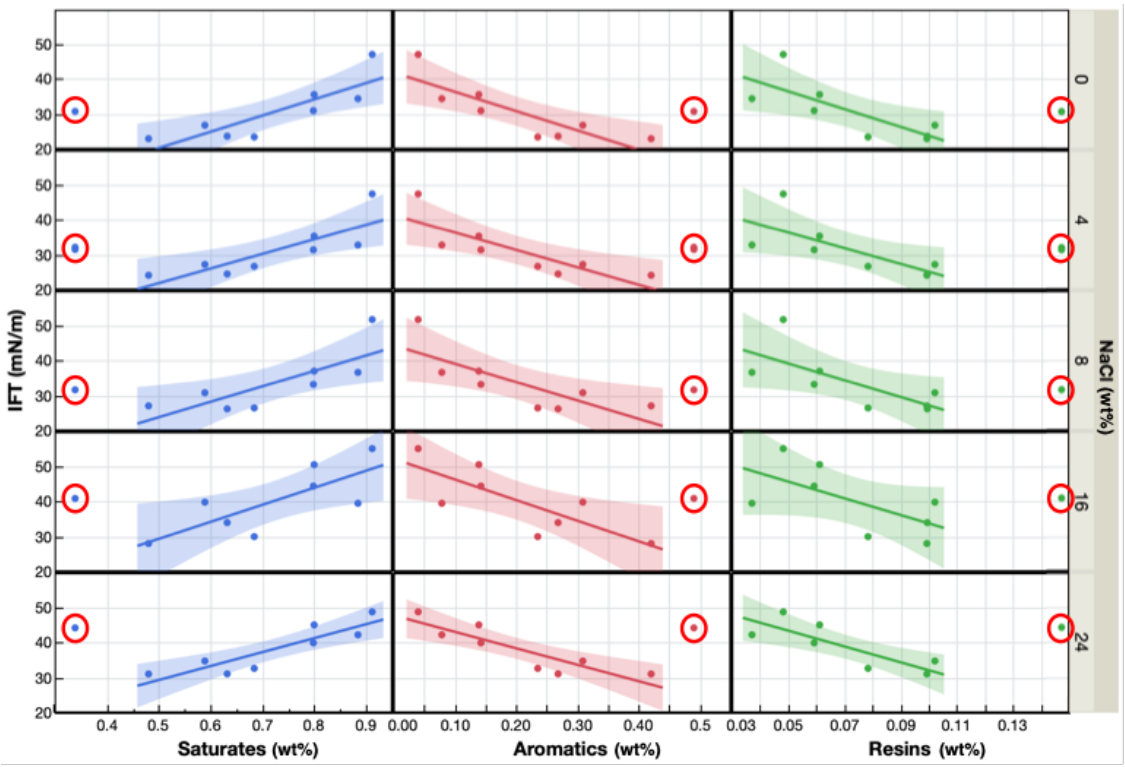

Figure 30 - The effect of saturates, aromatics, and resins content to the IFT at various salinity level; salinity level goes from 0% to 24% from top-to-bottom row. Oil 15, indicated by red circles, is excluded from the trendline due to its asphaltene content and heavier saturates.

In the SARA classification, the polarity of each class increases from saturates to asphaltenes. Saturates are highly non-polar, as they are mainly composed of paraffinic hydrocarbon molecules. An oil with a higher saturate content is more non-polar, resulting in a positive correlation with the IFT. Aromatics and resins are, instead, composed of cyclic or ring-shaped hydrocarbon molecules. With these shapes, the electrons are often disproportionately distributed, inducing a polarity. Although this polarity level is still not as strong as the water molecule, it is still stronger than the Saturate class. It has been established that the existence of polar hydrocarbon molecules in crude oils, result in IFT reduction (Lashkarbolooki and Ayatollahi 2018). However, in the majority of the available publications, the studies are performed using oil samples produced from conventional reservoirs which have a high asphaltene content. For these oils, the amphiphilic properties of the asphaltenes dominate the surface-active interactions overshadowing, or even cancelling, the amphiphilic effect of the aromatics and resins. In this study, using asphaltene-free shale crude oil samples it has been proven that the aromatics and the resins have the capability of reducing the IFT created by the saturates component of the crude oil.

The data presented in Figure 30 also shows the effect of salinity on IFT. Increasing the brine salinity, reduces the slope of the IFT reduction caused by the increase of aromatics and resins content. This indicates interaction between the oil components and the salinity. Salinity effect will be discussed in the next section.

Effect of Salinity to the Oil/Water IFT

Salinity levels ranging from 0% to 24% were included in this study. Figure 31 presents the IFT data obtained at ambient conditions. The colors represent the different crude oils used in this study. Positive correlation between IFT and salinity is well-documented in the literature and is observed in this study as well. Moeini et al. provided a very detailed explanation of the mechanism behind the "salting-out" process which is responsible for this positive correlation (Moeini et al. 2014).

The individual effect of oil components and salinity on the oil/water IFT has been discussed in the previous section. The following section are going to investigate the combined effect of the two variables to the oil/water IFT.

To investigate the effect of two variables simultaneously, the terms $IFT_{Salt-Corr} * NaCl$, obtained from the IFT data from nine natural brines are used. Figure 32 presents the $IFT_{Salt-Corr} * NaCl$ values on the y-axis, and the saturates, aromatics, and resins contents on the x-axis. The different colors represent the salinity level of the nine natural brines, with green being the lowest salinity brine, and red being the highest. It has been established that salinity increases the oil/water IFT. Therefore, it is expected that $IFT_{Salt-Corr} * NaCl$ value will always be positive indicating the IFT always increases as the salinity is increased as shown in Figure 30. The $IFT_{Salt-Corr} * NaCl$ term also shows an increasing trend with increasing brine salinity.

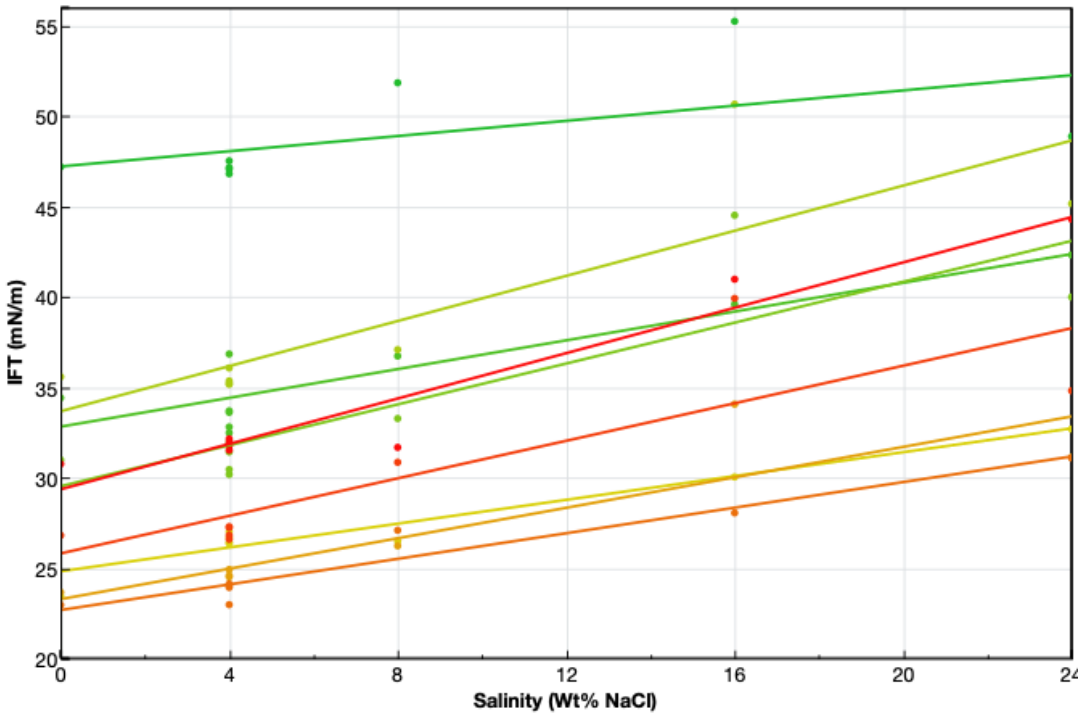

Figure 31 - The effect of salinity to oil/water IFT.

Looking into each of the three columns in Figure 31, increasing saturate content decreases the value of the salt correction factor. Increasing the aromatic and the resin content increases the value of the correction factor. In other words, crude oils with higher saturates content require less correction factor from the salinity effect. While oils with a higher aromatic and resin content need a larger salt correction factor to "calibrate" the IFT value. This observation indicates the independence of IFT generated by the saturate component to the salinity of the aqueous phase. On the other hand, the IFT generated by the aromatic and resin components is highly dependent on brine salinity. It is also important to note a fanning out behavior on the aromatic and resin columns, indicating a stronger salinity effect at higher aromatic and resin content. In the previous section, it was mentioned that aromatics and resins actually reduce the IFT created by the saturate

component. Therefore, it can be concluded that the magnitude of IFT reduction by the aromatic and resin components, decreases with increasing brine salinity.

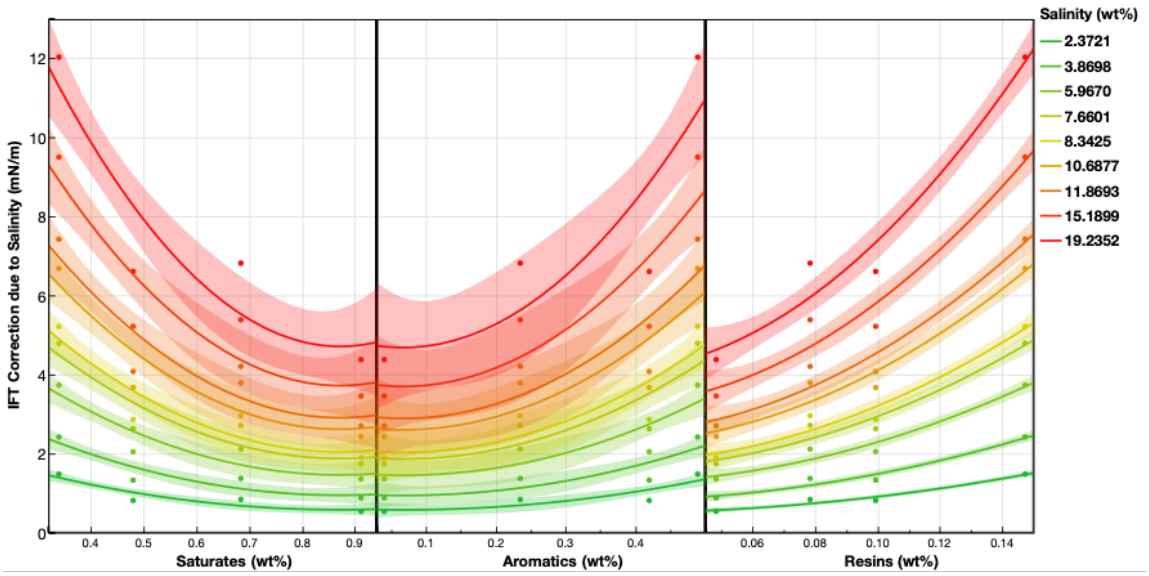

Figure 32 - The effect of saturates, aromatics, and resins content to the salinity correction term of in Equation 2 and Equation 3.

Figure 33 summarizes the effect of the oil components, salinity, and their interaction on the oil/water IFT. The oil/water IFT can be explained by the polarity contrast of the oil components and brine. Two components with similar polarity levels are soluble in one another, while components with contrasting polarity are not. When the polarity difference between two phases, i.e., crude oil and brine increases, the IFT between them increases. In an oil/brine system, the oil is the non-polar phase and brine is the polar phase. In the oil phase, the saturates are the main source of non-polarity, while the aromatics and the resins cause the crude oil to be slightly polar. Meanwhile, in the brine phase, the addition of salt

increases the polarity. The four components contribute to the IFT in the following ways: regardless of the brine salinity, the saturates contribute to the initial high IFT of oil and water (green arrows in Figure 33). Aromatics and resins act as a bridge between the saturates and the aqueous phase, reducing the IFT, due to their slight polarity (red, blue, and black arrows respectively in Figure 33). However, increasing the brine salinity results in the decrease of the IFT reduction by the aromatics and resins (smaller red and blue bar on the right figure of Figure 33). This is a result of increase in polarity contrast between the brine, the aromatics, and resins which as explained before, increase the IFT between the two phases.

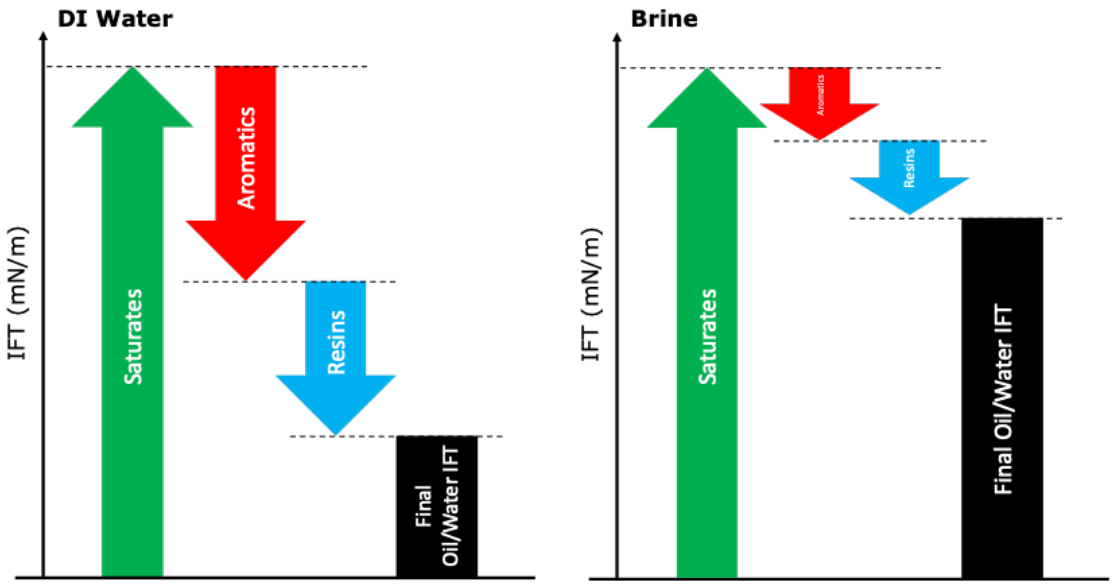

Figure 33 - IFT mechanism for crude oil containing saturates, aromatics, and resins content.

Effect of Temperature to the Oil/Water IFT

IFT data are presented in Figure 26 as a function of temperature. The data with 0%, 8%, 16%, and 24% salinity concentration are presented in each box respectively, starting from the top left corner and moving clockwise. The general observed trend shows a decrease of IFT when the temperature increases. However, this trend is only observed for temperatures above 120°F, with relatively constant trend observed below this temperature. It is important to note, however, that the IFT change caused by the temperature range from 0 to 195 in this study is less than 10% in most cases. The IFT reduction behavior at higher temperature can be explained by the increase of the kinetic energy of the two phases. This results in an increase in the system entropy, and an increase in the solubility between the two phases. However, this effect should be observable at any temperature range. The cause of the delayed response (IFT reduction only occurs above 120°F) with temperature, is currently undetermined. It is hypothesized that a complex interaction between the saturates, aromatics, resins, and system temperature, is the reason for this delayed temperature response.

In order to gauge the interaction between the oil components and the temperature, the IFT data presented in Figure 26 are normalized to the IFT value at 80°F. The normalized IFT values are plotted on the y-axis against the saturates, aromatics, and resins component on the x-axis, and grouped by rows based on the brine salinity. IFT data from low temperature (79° to 93° F), are averaged into Figure 34, while data from high temperatures, (181° to 193° F), are averaged into Figure 35.

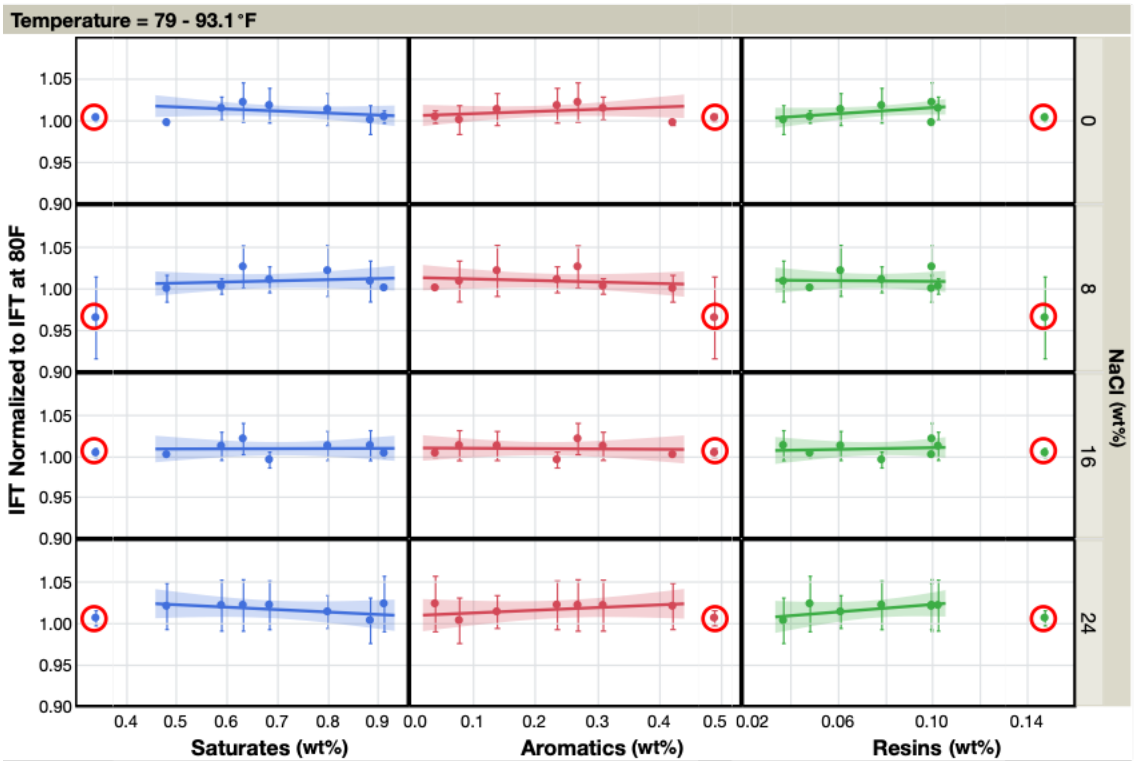

Figure 34 - The effect of saturates, aromatics, and resins to IFT change due to temperature. Data shown are averages of data from temperature of 79oF to 93oF. Rows are grouped by salinity level, top-to-bottom: 0%, 8%, 16%, and 24%. Oil 15 is excluded from the trendline as well due to its asphaltene content and heavier saturates.

At low temperatures and zero salinity (first row of Figure 34), the flat line indicates that the composition of the oil does not influence the change of IFT due to temperature. The datapoints of Oil#15 are excluded from the trendline. As was mentioned before, this data is considered as an outlier in this study since sample #15 does contain measurable asphaltene content. On the same graph, a flat behavior trend line is still observed when the salinity is increased to 8%, 16%, and 24%.

At higher temperature range, the IFT decreases (Figure 35). This is shown by most of the points located below the 1.00 line on the y-axis. Increasing salinity reduces the temperature driven decreasing IFT effect; IFT values at 24% salinity are closer to 1.00

compared to the data at lower salinity. Like the observation on the low temperature data, there is no significant evidence of interaction between the oil composition and the temperature that affects the IFT on the high temperature data.

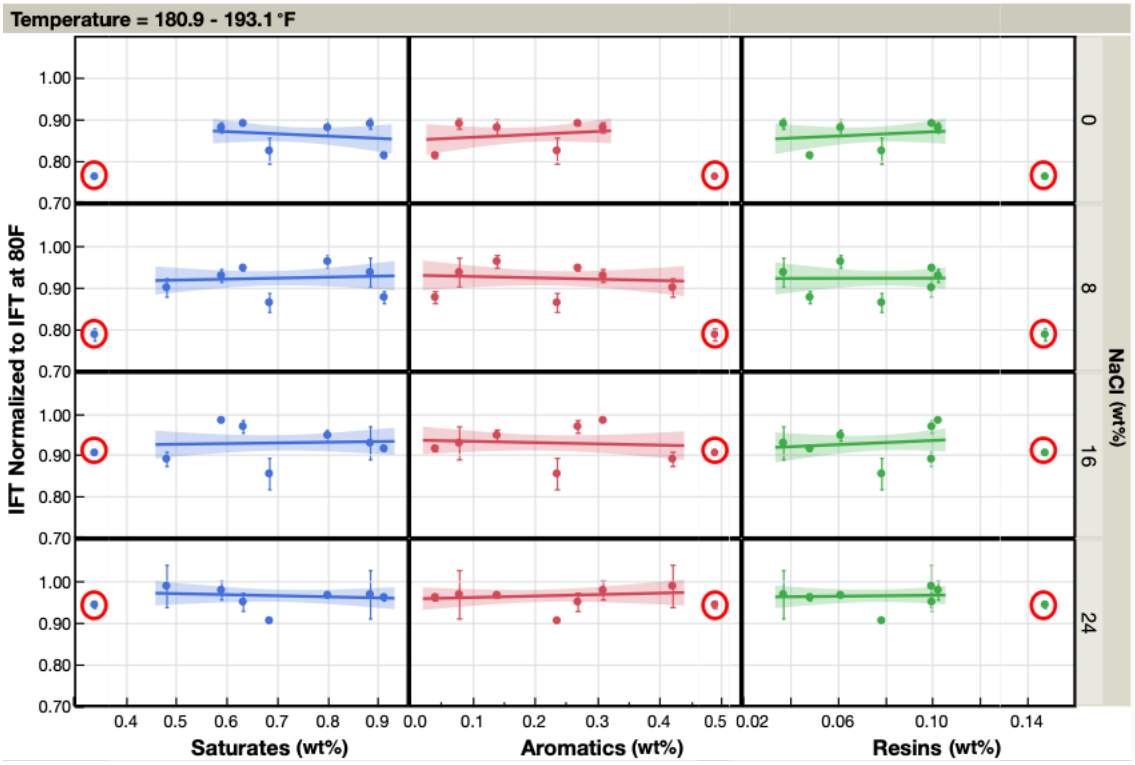

Figure 35 - The effect of saturates, aromatics, and resins to IFT change due to temperature. Data shown are averages of data from temperature of 181°F to 193°F. Rows are grouped by salinity level, top-to-bottom: 0%, 8%, 16%, and 24%. Oil 15 is excluded from the trendline as well due to its asphaltene content and heavier saturates.

In general, for an oil/brine system, increasing the temperature reduces the polarity contrast between the two phases. As explained before, higher temperatures result in higher system entropy, increasing the solubility of the two phases. Greater temperature allows aromatics and resins to further reduce the IFT. This behavior is observed in Figure 35,

where a lower IFT is observed at higher Aromatic and Resin content. However, similar to the trend observed in the previous section with regard to the discussion of salinity effects, increasing the salinity weakens the ability of the aromatics and the resins to lower the IFT at higher temperatures. At 24% salinity, the temperature effect is completely overshadowed by the salinity effect, as shown on the last row of Figure 35, where the trends are virtually flat.

Summary

Oil/water interfacial tension can be explained by examining the polarity of each phase, and the effect that the oil components, salinity, and temperature have on the polarity contrast of the two phases. Saturates are the non-polar components of the oil phase and have a larger influence on the oil/water IFT, at least for shale crude oils. Crude oils with larger Saturate concentration generally show greater IFT values. Aromatics and Resins are the two slightly polar components of crude oil. Crude oils containing more of these components tend to have lower IFT values. Aromatics and resins could be interpreted as a bridge between the saturates and brine. When the salinity of the brine-phase is increased, the aqueous-phase becomes strongly polar. Saturates, on the other hand, already have contrasting polarity, even with 0% salinity, and are not affected by the increase in salinity. However, aromatics and resins are slightly soluble at 0% salinity, and are affected by the increase in the brine salinity: a higher brine salinity results in more polar brine. As a result, the IFT increases for larger salinities, when the crude oil contains large amounts of aromatics and resins. When the temperature of the system is increased, the polarity

contrast between the oil and brine phase decreases. As a result, at higher temperatures, aromatics and resins become more proficient in reducing the oil/water IFT. However, the temperature effect is thwarted by the salinity effect. Ultimately, at higher salinities, the temperature has a smaller impact on the IFT.

CHAPTER V

LOWER 48 SHALE RESERVOIRS OIL/BRINE/ROCK INTERACTION

More than 1,100 contact angle data were acquired. In the following section, the data is dissected by the five control variables: aging time, rock composition, oil composition, brine composition, and the brine pre-soak process. The experimental variables are the magnitude of the wettability, represented by the contact angle, and the rate to reach a stable wettability, referred to as the stable aging time. It was hypothesized that the experimental variables are also influenced by interactions between the five control variables, which complicates the analysis. Therefore, the contact angle is often presented in the graph with multiple control variables presented at once. The stable aging time is determined through Tukey's analysis.

This section starts with the determination of optimum aging time to reach a stable wettability condition. Then the effect of rock mineralogy, oil composition, and brine salinity are discussed in separate parts. And finally, the effect of the brine pre-soak process on the rock wettability is presented.

Optimum Aging Time

The aging process was observed to render the rock surface oil-wet. In this part of the study, the optimum aging time to achieve a stable wettability condition was investigated. The stable aging time was first established by averaging the contact angle data based on the aging time. Multiple rock, oil, and brine were included in the mean contact angle

average value of each aging time. Then, Tukey analysis, which is an ANOVA test designed to perform more statistically accurate comparisons for more than one-pair of datasets, was conducted on these average means. This method is useful to determine minimum aging time as nine aging times were compared. The result of the analysis is presented in Table 7 with the graphical representation presented in Figure 36.

In this analysis, 775 contact angle datapoints were included. This dataset includes all seven rock samples, all six crude oil samples and all seven brine samples. The aging times are presented in rows. Aging times connected by the same letter (A, B, C, D, or E) are those aging times with wettability that are not significantly different one to another, i.e., the mean difference is not significantly larger than the combined variance of the two datasets. Zero days of aging resulted in a water-wet rock surface (mean contact angle of 24°, presented on the last row of Table 7), and aging the surface rendered it oil-wet. Aging the rock surface for a week already resulted in an oil-wet surface (contact angle of 105°, the second-to-last row of Table 7). However, the oil-wetness was still developing as aging the surface to 14-, 21-, 28-, and 35-days resulted in stronger oil-wetness with a mean contact angle of 105°, 109° 116°, 117°, and 135°, respectively. When the rock surface was aged for longer than 35 days, all the mean data for an aging time longer and equal than 35 days were connected, meaning that there was no statistically significant difference between the mean data of 35-, 42-, 49-, and 56-days of aging. From this, it can be concluded that a stable wettability condition is achieved after 35 days. This conclusion serves as a general guideline that fits the range of rock, oil, and brine included in this study.

Table 7 - Tukey analysis to determine minimum aging time for stable wettability condition (CI=95%).

Aging Time (Days)						Mean
49	A					137.96974
42	A					136.35000
35	A					135.05300
56	A	B	C	D		119.20000
28		B				117.69361
21		B	C			116.80078
14			C	D		109.07929
7				D		105.04490
0					E	24.10370

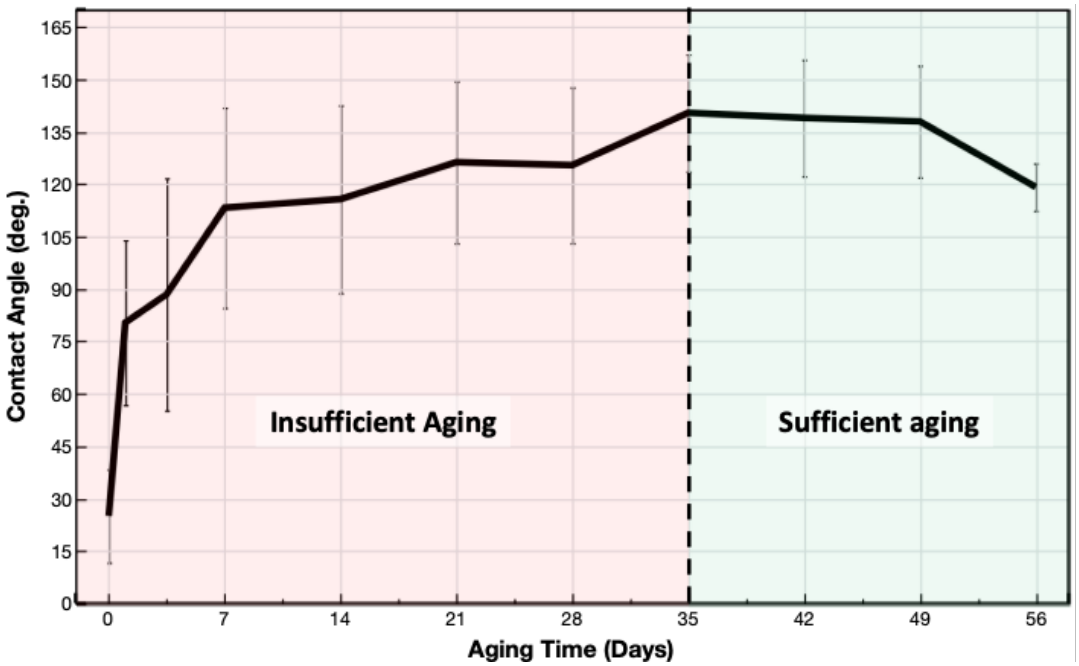

Figure 36 - Wettability evaluation throughout 0 – 56 days of aging time for all six crude oil samples and seven rock samples.

Rock Composition Effect on Wettability

In this section, the effect of the rock composition on the surface wettability is investigated. The contact angle data were grouped by their mineral compositions and

averaged. This grouping and averaging method meant that measurements from multiple crude oil samples were included in one data point. The result from all measurements performed with brine sample T (DI water) is presented in Figure 37. The figure is constructed using 380 datapoints. Consisting of three rock samples (A, B, and C) and four crude oil samples (1, 3, 4, and 5). The contact angle is presented as the y-axis. The x-axis represents the composition of four different rock minerals, represented in four columns: quartz, calcite, dolomite, and clay (left-to-right). The contact angle data were also grouped by their aging time, and the groupings are presented based on colors with the aging time increasing from green to red.

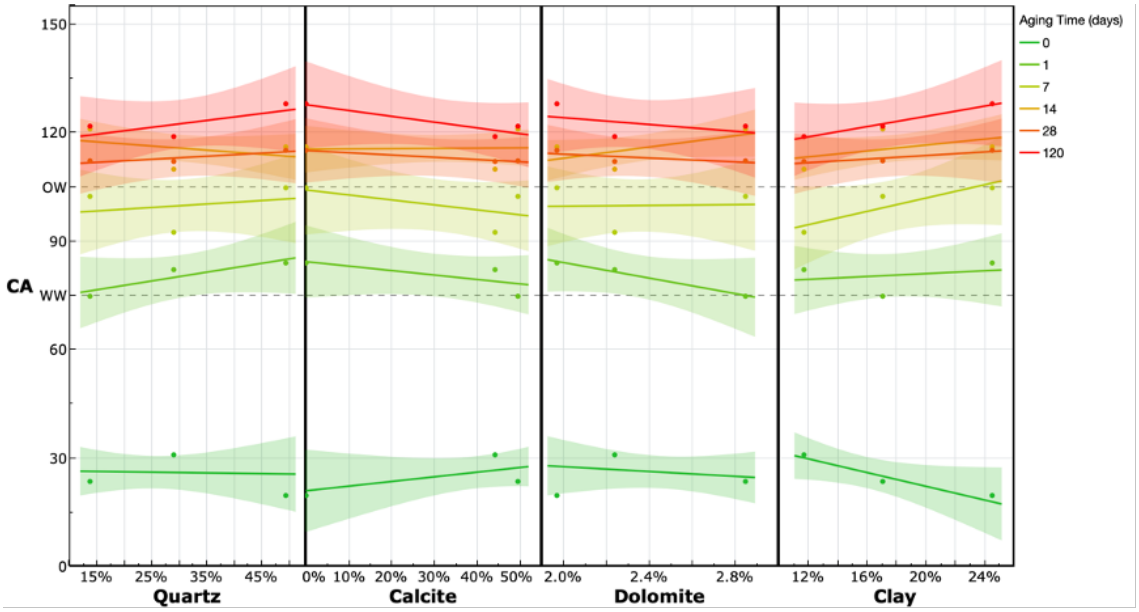

Figure 37 - The effect of quartz, calcite, dolomite, and clay content on the surface wettability after a duration of aging for samples measured in brine T (DI water). Colors represent the length of the aging duration, green-to-red: zero to 120 days of aging.

The creation of oil-wetness due to the aging process is observed from the graph with the position of the red data points significantly higher than the green. Before aging, there was no significant relationship observed between the contact angle and the quartz. On the other hand, a positive trend was observed on the calcite content, and a negative correlation was observed on the dolomite and clay composition in the rock. After the rock was aged, a positive correlation was observed between the contact angle and the quartz and the clay content. In comparison, both calcite and dolomite composition exhibited a negative trend. These observations are contrary to the established understanding that carbonates are more oil-wet than quartz. These results were not skewed by the oil composition since each datapoint presented in Figure 4 was an average value from four different crude oil samples.

It is hypothesized that the positive relationship between the oil-wetness and the carbonate composition available in the literature is driven by the asphaltene content and the acid number of the crude oil used in the study 13, 18, 25. Organic acids found in heavier conventional reservoir crude oil samples are known to easily bond to the free calcium atom on the surface of carbonate rock. The adsorbed organic acid then provides an anchor for the other crude oil component to bond to the surface, creating an oil-wet surface. It has been established in our previous publication that shale crude oil samples have virtually zero asphaltene content and zero acid number. The absence of these important components of the conventional crude oil-carbonate interaction resulted in the absence of a positive trend between the surface oil-wetness and the carbonate composition.

In our previous publication, it was established that aromatics and resins, in the absence of asphaltene, act as a bridge between the non-polar saturates component to the

water molecule. It is hypothesized that a similar explanation can be used to explain the behavior observed in this study. In the case of surface wetness, the aromatics and resins are bridging the non-polar components of the crude oil to the rock surface. The polarity of the rock surface is controlled by its mineralogy. Rock samples with a higher concentration of carbonates will become more polar due to the free calcium atom on its surface, while higher quartz composition results in a surface with less polarity. Carbonate rocks which are highly polar would result in the inability of the aromatics and resins to bond to its surface, resulting in the failure to create an oil-wet surface. Hence the observed negative trend between carbonate content and oil-wetness. Quartz and clay, on the other hand, have less polarity than carbonates and allows for a better bond of aromatics and resins to its surface. This results in a more oil-wet surface, as observed on the positive relationship between the quartz content and the oil-wetness.

The remaining of the oil/water/rock systems were added to Figure 37 and presented in Figure 38. This figure is constructed with 775 contact angle datapoints that includes all seven rock samples, all six crude oil samples and all seven brine samples. It is important to note that some degree of skewness is observed due to the partial factorial test matrix. For example, rock samples with dolomite content (rock F and G) were only measured in combination with oil 4 (the third heaviest oil) and brine Z (the brine with the highest TDS). The positive relationship between the surface oil-wetness and the quartz content was enhanced in this dataset. Similarly, the negative relationship to calcite content was also observed to increase. On the other hand, the dolomite content exhibited a positive trend, while the clay composition presented a negative trend.

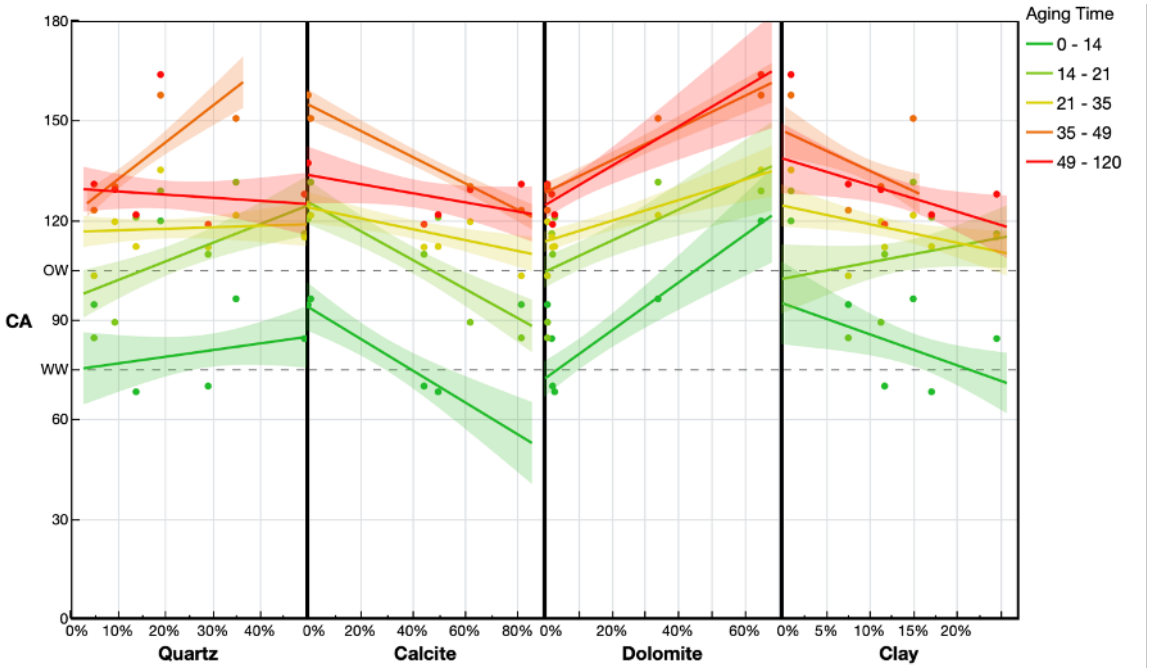

Figure 38 - The effect of quartz, calcite, dolomite, and clay content on the surface wettability after a duration of aging. Colors represent the length of the aging duration, green-to-red: zero to 120 days of aging.

In general, the trends observed in Figure 37 were repeated in Figure 38 except for dolomite and clay. It is hypothesized that the reversal in results for the dolomite was caused by the oil and the salinity. High dolomite content was observed only on rock F and G. These rocks were only measured with brine Z (32% TDS brine) and oil 4, which had high aromatic and resin content. These oil and brine combinations resulted in a strong oil-wetness and skewed the dolomite results to be more oil-wet. However, the difference between Figure 37 and Figure 38 highlighted an important observation that in the range of oil, rock, and brine properties included in this study, the rock composition had a diminutive effect on the surface wettability.

Also, the optimum aging time for stable wettability for each rock sample was also analyzed. Tukey's analysis was performed after the results were grouped by rock samples. The summary of the optimum aging time is presented in the left graph of Figure 39. The optimum aging data was then plotted against the calcite, dolomite, and quartz content on the x-axis, the right graph of Figure 39. From the right graph, it can be concluded that there was no significant trend observed between the rock composition to the optimum aging time. The independence of optimum aging time to rock mineralogy enforced the idea that in shale oil/water/rock systems, the rock mineralogy plays a minimum role in determining the rock surface wettability.

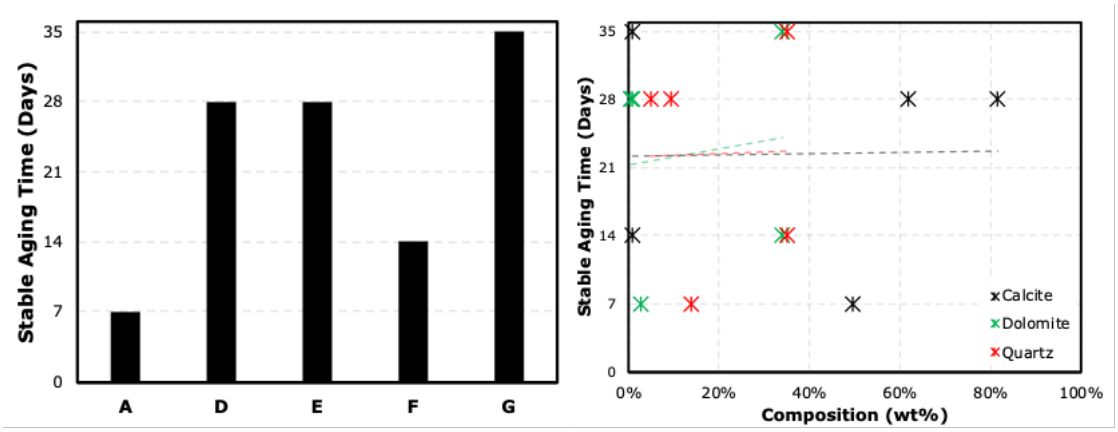

Figure 39 - Aging time required to establish stable and consistent wettability for the six reservoir rock samples (left). Values were obtained from Tukey analysis with contact angle data grouped by rocks. The stable aging time is plotted against the calcite, dolomite, and quartz content (right).

Oil Composition Effect on Wettability

The effect of saturates, aromatics, resins, and asphaltenes content on the rock surface wettability was investigated. Contact angle data for all measurements performed with

brine T (DI water) were grouped by their oil composition. The data are plotted against the saturate, aromatic, resin, and asphaltene composition on the x-axis in Figure 40. The dataset for this figure 380 datapoints from three rock samples (A, B, and C) and four crude oil samples (1, 3, 4, and 5). Similar to the previous figures, the datapoints were also grouped by their aging time, with the grouping presented in different colors. Increasing aging time is presented by the shift from green to red. In comparison to the analysis on the effect of rock mineralogy (presented in Figure 37), the trends observed in Figure 40 were significantly stronger; the gradients of the trendlines were larger than those in Figure 37. At the zero-day aging time, higher saturates content resulted in a more oil-wet surface. On the other hand, higher aromatic, resin, and asphaltene composition in the crude oil rendered the surface to be less oil-wet. After the rock surface was aged, the trend reversed with the saturates content decreased the oil-wetness of the rock surface while increasing aromatics, resins, and asphaltenes content improved the oil-wetness of the surface.

It was previously hypothesized that the rock composition does not play a significant role in determining the rock surface wettability. The fact that the trend line gradients in Figure 40 were larger than those in Figure 37 confirmed the hypothesis that in the shale oil/brine/rock system, the oil composition is the dominant factor in the surface wettability.

The trend of data points at zero days aging time was observed to be the inverse of the aged rock samples data. It was believed that this behavior was caused by the measurement artifact. Due to the water-wetness of the surface, a larger drop volume was needed to detach the drop from the needle and attach it to the surface. The minimum drop volume required for the detachment is a function of density; lower oil density implies smaller drop

volume and vice versa. Heterogenous drop volume skewed the contact angle reading with larger volume creating a smaller contact angle or less oil-wet. This measurement artifact did not exist on aged rock samples as aged rocks had an affinity to the oil, which allowed for easier oil drop placement on the surface.

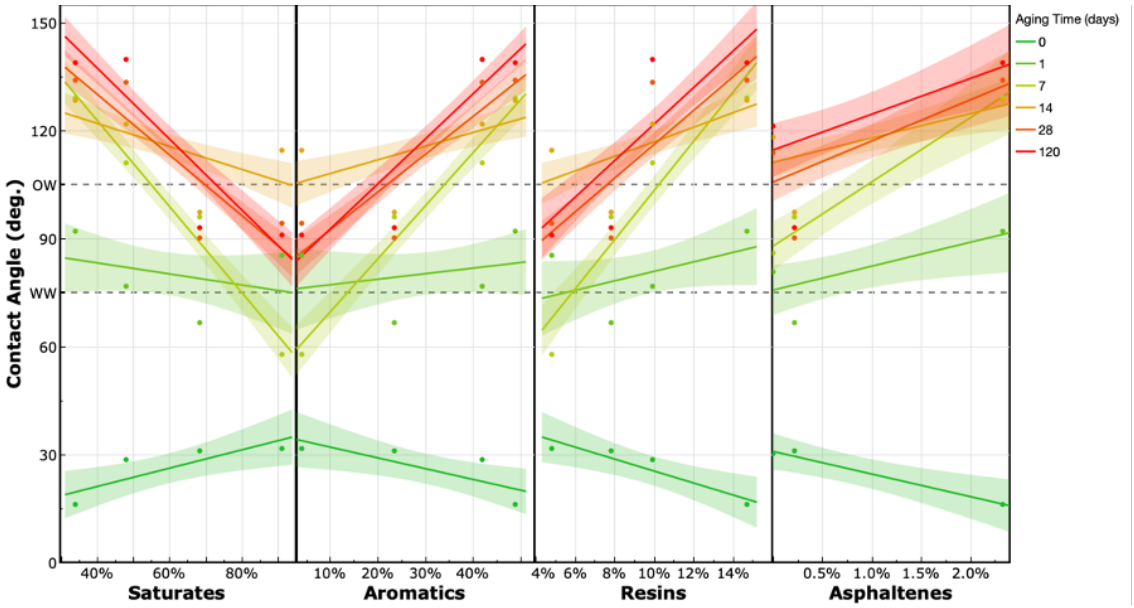

Figure 40 - The effect of saturates, aromatics, resins, and asphaltenes content on the surface wettability after a duration of aging for samples measured in brine T (DI water). Colors represent the length of the aging duration, green-to-red: zero to 120 days of aging.

The trend observed between the contact angle and the four oil components confirmed the applicability of mutual solubility theory to explain wetting behavior on shale oil/water/rock system. Higher aromatic, resin, and asphaltene content resulted in more crude oil components being initially adsorbed on the rock surface. The initial layer of adsorbed crude oil components then provided additional adsorption sites for the remainder of the oil components, i.e., the non-polar saturates. Crude oil with lower aromatic, resin,

and asphaltene and higher saturate composition lacked the essential initial oil adsorption on the rock surface. Hence, the more water-wet surface is created on these crude oil samples. It is important to note that these high-saturate crude oils still possess the capability to render the surface oil-wet, only to a lesser degree.

Additionally, a significant change in trend gradient was observed at different aging times. At the longer aging time, it was observed that the relationship between the oil composition and the oil-wetness became stronger; steeper trendlines were observed on all four columns in Figure 40 when the aging time was increased. This behavior implied that the adsorption process of the aromatics and resins is strongly influenced by the aging time. Therefore, it is essential to give enough time for the aging process (aging the rock until equal to or more than the optimum aging time) before any further wettability-related experiments. Prematurely aged rock surface would result in a misleading water-wet surface that would strongly affect wettability-related or surfactant study.

Like the previous part, the remaining of the oil/water/rock combinations were added to Figure 40 and presented in Figure 41. This figure contains 775 contact angle datapoints from all seven rock samples, all six crude oil samples and all seven brine samples. The trendline between the contact angle and saturates, aromatics, resins, and asphaltenes observed in Figure 40 were maintained. Unlike the trend reversal observed when investigating the effect of rock mineralogy in Figure 37 and Figure 38. This observation confirmed the dominant effect of the oil composition over the rock mineralogy on the wettability. However, some degree of gradient change from the trendline was still

observed. This change was believed to be driven by the brine salinity which will be discussed in the next part.

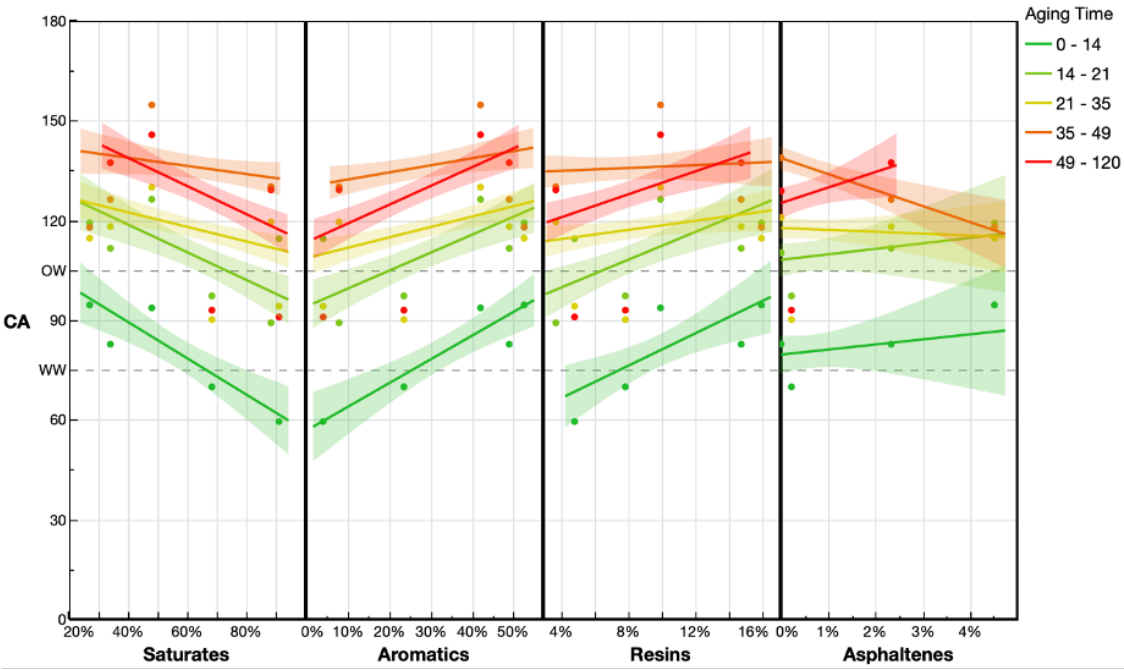

Figure 41 - The effect of saturates, aromatics, resins, and asphaltenes content on the surface wettability after a duration of aging. Colors represent the length of the aging duration, green-to-red: zero to 120 days of aging.

The effect of oil composition on the optimum aging time was also investigated. Multiple Tukey's analyses were performed on the contact angle data points, which were grouped by their crude oil components beforehand. The summary of the optimum aging time for each of the six crude oil samples is presented in the left graph of Figure 42. The data then were plotted against the content of saturates, aromatics, and resins, the right graph of Figure 42. In comparison to the effect of rock composition on the optimum aging time presented in the right graph of Figure 6, the trend in the right graph of Figure 42 was

more dominant. This observation served as another evidence of the hypothesis that the surface wettability is a greater function of the oil composition than rock composition in a shale oil/water/rock system. Larger saturates content increased the required aging time to reach a stable wettability condition, while the presence of more aromatics and resins reduced the time for aging. It was also observed that resins reduced the optimum aging time more than aromatics, which was indicated by the steeper trendline on resins when compared to aromatics.

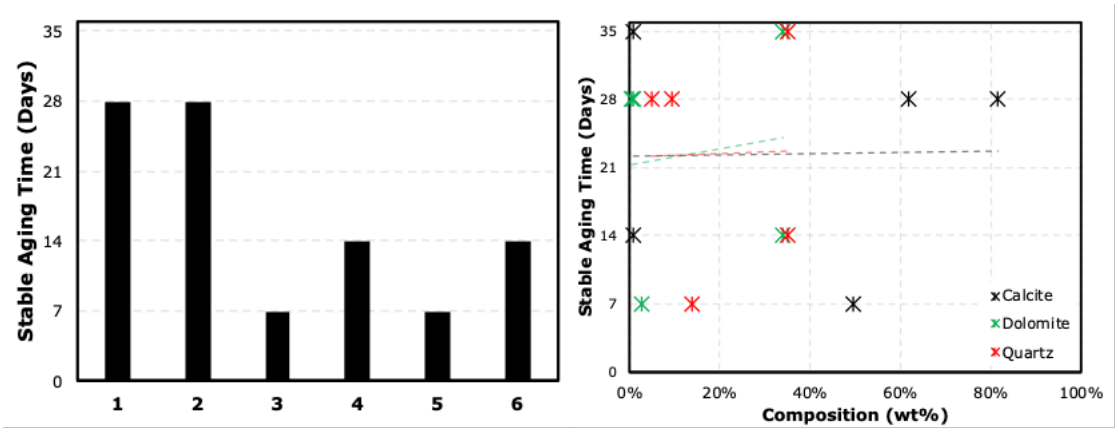

Figure 42 - Aging time required to establish stable and consistent wettability for the six crude oil samples (left). Values were obtained from Tukey analysis with contact angle data grouped by crude oil. The stable aging time is plotted against the saturates, aromatics, and resins content (right).

The relationship between the crude oil components and the optimum aging time allowed for an insight into the kinetics of the adsorption that renders oil-wetness on the rock surface. A higher concentration of aromatics and resins in the crude oil allows for faster oil adsorption on the rock surface, hence the shorter time needed to reach stable wettability conditions. Additionally, higher Resins composition shortens the optimum

aging time more than the aromatics, which implies that resins in the crude oil causes the greatest oil-wet tendency of a rock surface.

Combined Rock Mineralogy and Oil Composition Effect on Rock Wettability

The effect of both rock mineralogy and oil composition on the rock surface wettability was investigated. To evaluate this, the contact angle data with 7-, 14-, and 28-days aging time was plotted in Figure 43 against the saturate, aromatic, and resin composition. However, instead of their aging time, the different colors represented the quartz composition as described in the legend. This figure contains 400 datapoints with data from three rock samples (A, B, and C), four crude oil samples (1, 3, 4, and 5), and brine T. Generally, the trends between the contact angle and the three crude oil components were improved at higher quartz content. The gradient of the positive trend to the composition of aromatics and resins was observed to be larger at higher quartz content. Similarly, the negative gradient on the saturate content was also observed to be stronger at higher quartz composition.

In the previous section, a hypothesis of aromatic/resin interaction with the quartz mineral was presented as the main mechanism behind the rendering of surface oil-wetness on shale oil/brine/rock systems. From Figure 43, when both aromatic/resin concentration in the crude oil and the quartz content in the rock was increased, the surface became more oil-wet. Additionally, the individual effect of aromatic/resin concentration on surface oil-wetness was also enhanced when the rock contained more quartz as described earlier. These observations indicated that the aromatic/resin components had a higher affinity to

the quartz mineral. The aromatics and resins were adsorbed on the quartz mineral of the surface and created the oil-wet surface, which reaffirmed the hypothesis.

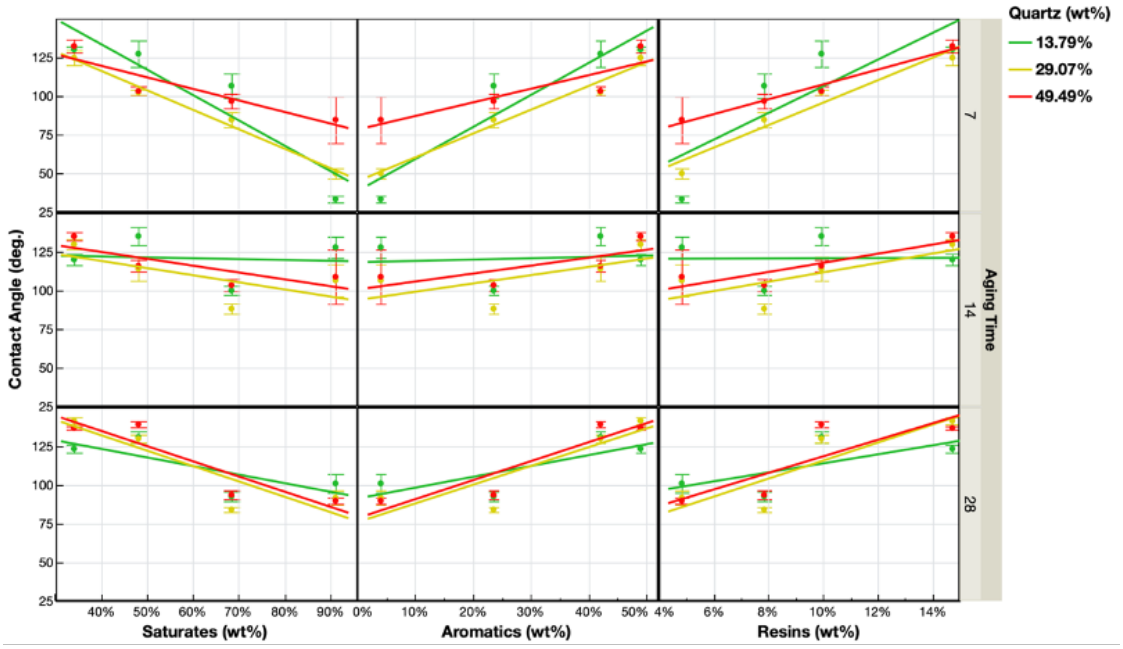

Figure 43 - The effect of saturates, aromatics, and resins composition at various quartz content on the contact angle. This figure was constructed to investigate the interaction between the oil composition and the rock mineralogy to the rock surface wettability.

Crude oil sample 5 contains a measurable amount of asphaltene and acid. It is well-established that crude oil with this composition has higher affinity to calcite-rich surface, rendering it more oil-wet. A mechanism of quartz-dominated oil wetness for shale system was proposed in the paragraph above. However, it was also observed that for crude oil 5, the oil-wetness is driven by the calcite content of the rock. This behavior was only observed with this sample. Additionally, this finding also enforces the statement that crude oil is the dominant factor in determining the oil-wetness of the shale system.

Salinity Effect on Rock Wettability

The effect of salinity on the surface wettability was investigated. The contact angle data was plotted against the brine salinity (TDS in ppm), Figure 44. In this figure 775 datapoints were included, containing all rock, oil, and brine samples presented in the methodology section. A positive trend between the surface oil-wetness to the brine salinity was observed. Similar to previous graphs, the data points were grouped by their aging time, which is presented in colors. Unlike the surface oil-wetness vs. oil composition trend in Figure 40 and Figure 41, the trendline gradient in Figure 44 for all aging time was similar. This observation indicated the absence of interaction between the brine salinity and the aging time.

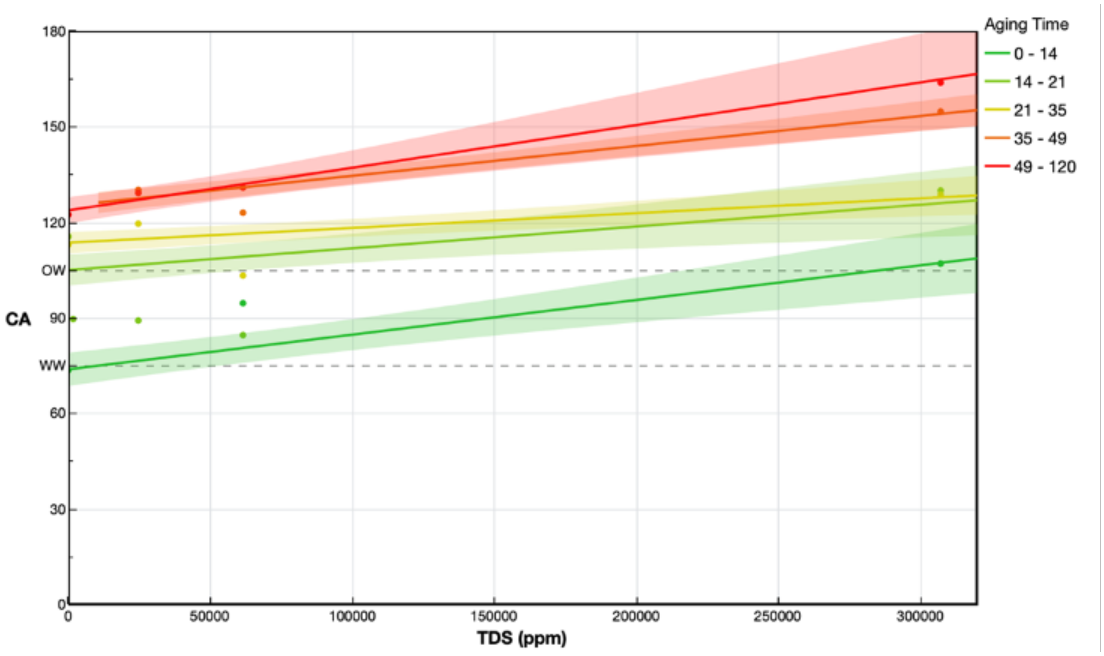

Figure 44 - Effect of brine salinity on the surface wettability. Colors represent the length of the aging duration, green-to-red: zero to 120 days of aging.

The presence of salt in the aqueous phase increased the polarity of the water when compared to DI water. In an oil/water system, this polarity increment increased oil/water IFT, as has been shown in our previous publication. In an oil/water/rock system, the increase of the brine polarity would cause the oil to be greater repelled by the aqueous-phase, resulting in the oil to be more attached to the oil-wet rock surface. Hence, the stronger oil-wetness at higher brine is observed in Figure 44.

Brine salinity was also observed to alter the optimum aging time. The result from Tukey's analysis on the comparison of aging time under different brine salinity is presented in Figure 45. A longer aging time required to achieve stable wettability conditions was observed in higher brine TDS. With brine T (DI water), the optimum aging time was 14 days. While when using brine Z, which has more than 300000 ppm TDS, the optimum aging time was more than doubled to 35 days.

In this study, the aged rock was not in contact with the brine until during the contact angle measurement. This means that at higher salinity, re-assembling of the adsorbed oil layer still occurs at a longer aging time. In our previous work on the interaction of the oil components and the brine salt ions, it was discovered that the increase of the brine salinity reduced the polarity of the aromatic and the resin components; at higher brine salinity, these two components lose their ability to reduce the oil/water IFT rendered by the saturates. In the earlier section of this work, it was also established that crude oils with higher non-polar saturates content required a longer aging time to reach stable wettability conditions. Based on these two observations, it was hypothesized that the re-assembling process of the adsorbed oil layer observed in this section occurred due to the reduction of

the polarity of the aromatics and resins in the presence of the brine. As a result, additional adsorption of both components on the rock occurred as they were repelled from the oil/water interface due to the high salinity level. This process kept occurring through-out the earlier aging time, which caused the contact angle to continue increasing. At the later aging time, the amount of aromatics and resins adsorbed on the rock surface hit the maximum. This resulted in the consistent contact angle reading even when the rock was aged longer, or in other words, a stable wettability condition was achieved.

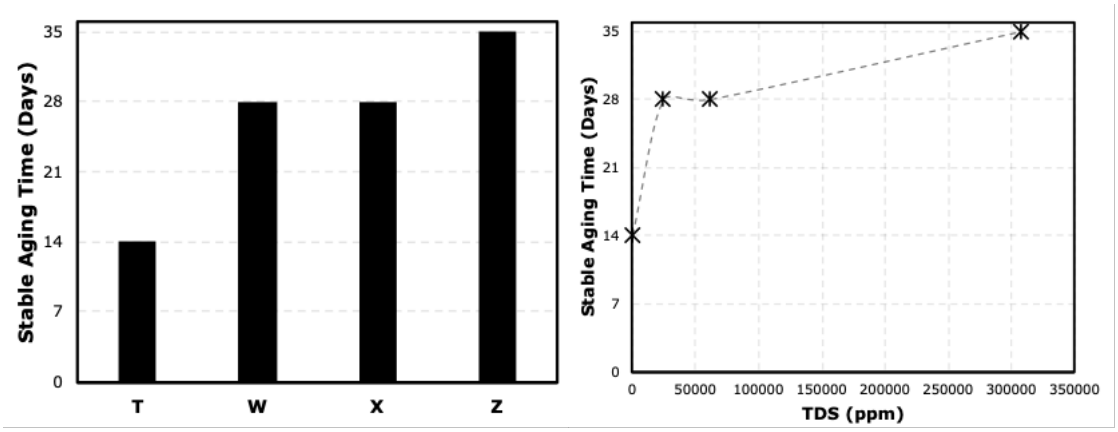

Figure 45 - Aging time required to establish stable and consistent wettability for the four brines (left). Values were obtained from Tukey analysis with contact angle data grouped by brine. The stable aging time is plotted against the TDS (right).

Simulating Reservoir Deposition Process: Brine Pre-Soak

The results from the rock samples that were subjected to the Brine Pre-Soak process are presented next. The first analysis performed was to investigate whether the additional step changes the rock wettability. Figure 46 presents the contact angle data evolution from zero- to 56-days of aging time for both samples with (red) and without the pre-soak (blue).

All 1,100+ contact angle data are included in this graph. Before aging in oil, samples that were pre-soaked were more oil-wet; datapoints at zero-days of aging shows the blue-line below the red-line. Surprisingly, throughout aging, rock samples with pre-soak were more oil-wet. Student's t-Test was also performed comparing the two groups of samples and shows that rock samples with pre-soak were more oil-wet with a significance level of 95%.

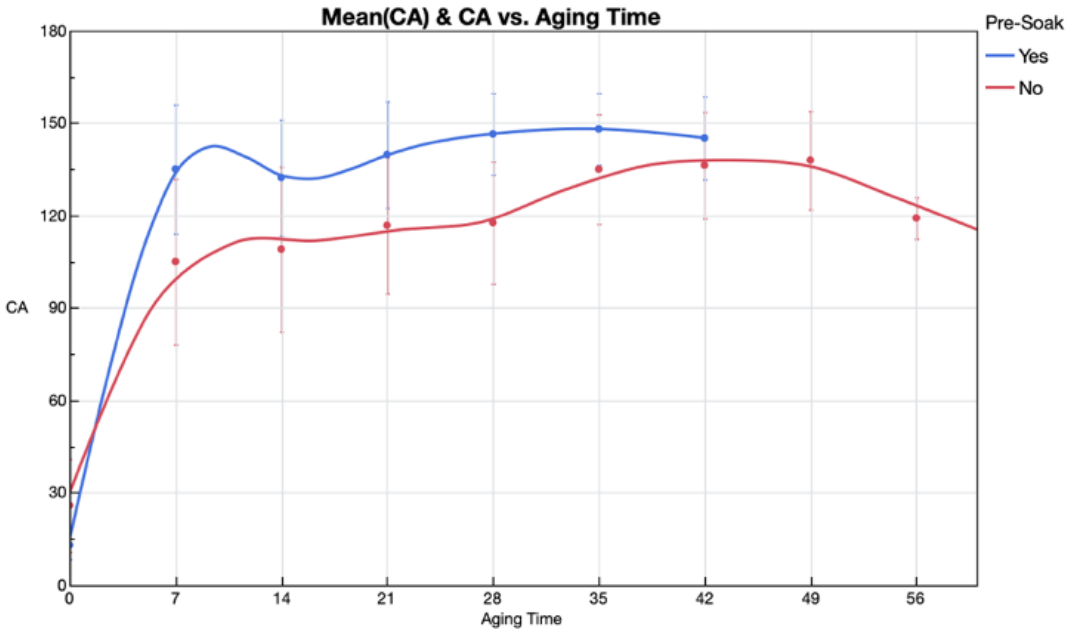

Figure 46 - Evolution of the wettability throughout the aging duration for samples with pre-soak (blue) and without (red).

Further investigation into the results presented in Figure 46 indicated that the pre-soak process amplifies the trends of the contact angle due to the oil components in Figure 40 and rock mineralogy reported in Figure 37. For example, a higher aromatic and resin content resulted in a more oil-wet surface, as presented in the previous section. However, increasing the aromatic and resin content to the same extent on the pre-soaked rock surface

resulted in a larger increase in oil-wetness. It is hypothesized that the ions present in the brine allowed for more adsorption sites for the crude oil components to adsorb. However, further investigation by varying the salt ion content in the brine must be performed to prove this hypothesis. Nevertheless, this result showed that even though the rock surface was pre-wetted or pre-soaked in its respective brine, the rock surface remained oil-wet after the aging process. The rock surface was even more oil-wet when it was pre-soaked before the aging process.

Table 8 - Tukey analysis to determine a minimum aging time for stable wettability for samples with pre-soak (CI=95%).

Aging Time (Days)					Mean
35	A				148.12429
28	A				146.48980
42	A	B			145.17727
21	A	B	C		139.81111
7		B	C		135.08649
14			C		132.34554
0				D	24.21915

Tukey's analysis to determine the optimum aging time was performed on the pre-soaked data. The optimum aging time was reduced from 35-days for samples without pre-soak to 21-days, as shown in

Table 8. However, upon further investigation, under some range of rock mineralogy, crude oil composition, and brine TDS, the optimum aging time for samples with pre-soak was longer than those without. Rocks with higher carbonates-to-quartz ratios were

observed to lead to a longer optimum aging time when pre-soaked (left figure of Figure 47). Crude oil with a higher aromatic and resin content was also observed to require extended optimum aging time when the rock samples were pre-soaked (middle figure of Figure 47). Higher brine salinity, on the other hand, was observed to reduce the optimum aging time for pre-soaked samples (right figure of Figure 47).

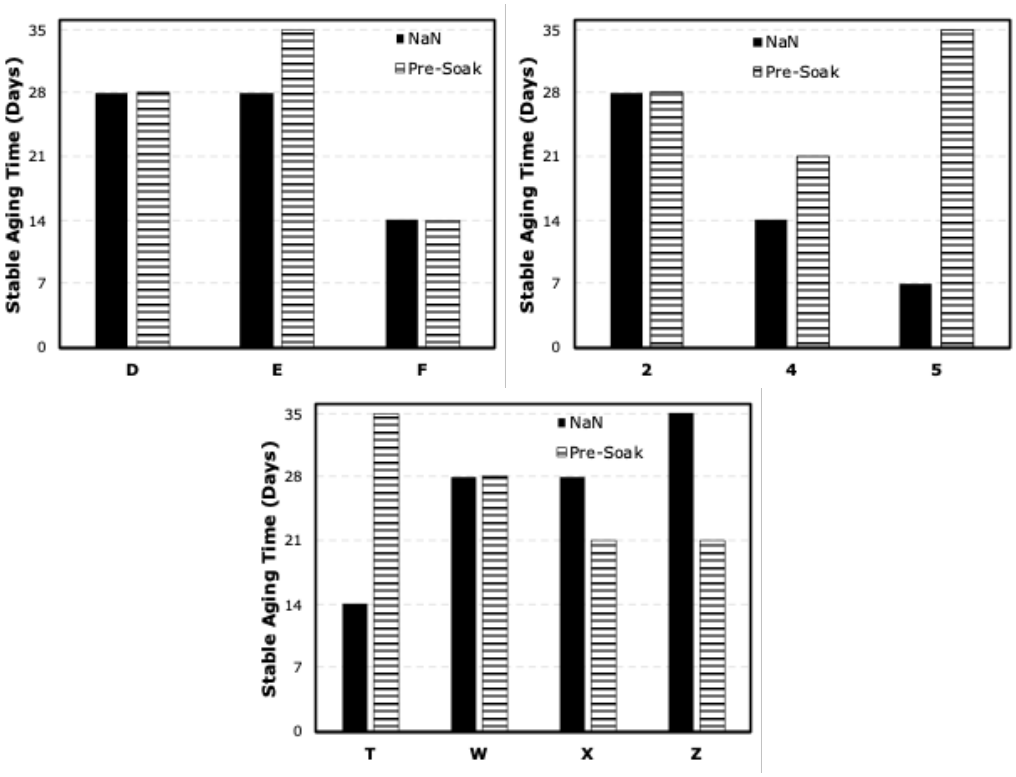

Figure 47 - Comparisons of aging time required to reach stable wettability for samples without and with pre-soak. Left graph was generated by averaging on the reservoir rock samples. Middle graph was generated by averaging on the crude oil samples. Right graph was generated by averaging on the brine.

Summary

In this study, the surface wettability of shale oil/brine/rock systems was investigated by analyzing two experimental variables: the final wettability and the aging time required to reach stable wettability. The first variable determined the magnitude of the wettability, and the second one determined the kinetics. Five control variables were included to have a better understanding of the mechanism behind oil-wetness: aging time, rock mineralogy, oil composition, brine TDS, and brine pre-soak.

In this study, shale systems from both the deeper and the shallower section of the Eagle Ford, Wolfcamp (carbonate rich and silica rich facies), and Bakken were tested. All shale oil/brine/rock systems investigated in the course of this work are oil-wet. The contact angle measured through the water phase averages above 110o after sufficient aging time.

It was observed that rock mineralogy played a minimal role in determining surface wettability. To some extent, higher quartz content resulted in stronger oil-wetness. Whereas higher carbonate content rendered the surface less oil-wet. This behavior is the opposite of what previous studies have shown. It is hypothesized that the absence of asphaltene and organic acid in the shale crude oil was the reason behind this observation; most wettability studies in the literature were performed on conventional reservoir systems with high asphaltene and organic acid content.

The oil composition strongly determined the level of oil-wetness of a shale oil/brine/rock system. Higher aromatic and resin content rendered the surface more oil-wet, while higher saturates resulted in a less oil-wet surface. It is hypothesized that the aromatic and resin components of the crude oil acted as a bridge for the saturate components to attach to the rock surface. In conjunction with the more oil-wet surface

observed on the quartz-rich rock, this strongly implies that the aromatics and resins have a greater affinity to quartz compared to carbonates. The proposed mechanism behind the oil-wetting of a shale system is encapsulated in Figure 48. The cartoon shows that the aromatics and resins of the crude oil are adsorbed more on the quartz-rich surface. The adsorbed aromatics and resins then serve as adsorption sites for the saturate components of the crude oil. As a result, more oil is adsorbed on the quartz-rich surface, rendering the surface more oil-wet. On the other hand, a carbonate-rich surface has a significant polarity contrast to the shale crude oil due to the absence of asphaltenes and organic acids in shale crude oil. Therefore, less adsorption of oil occurs, and a less oil-wet surface is created.

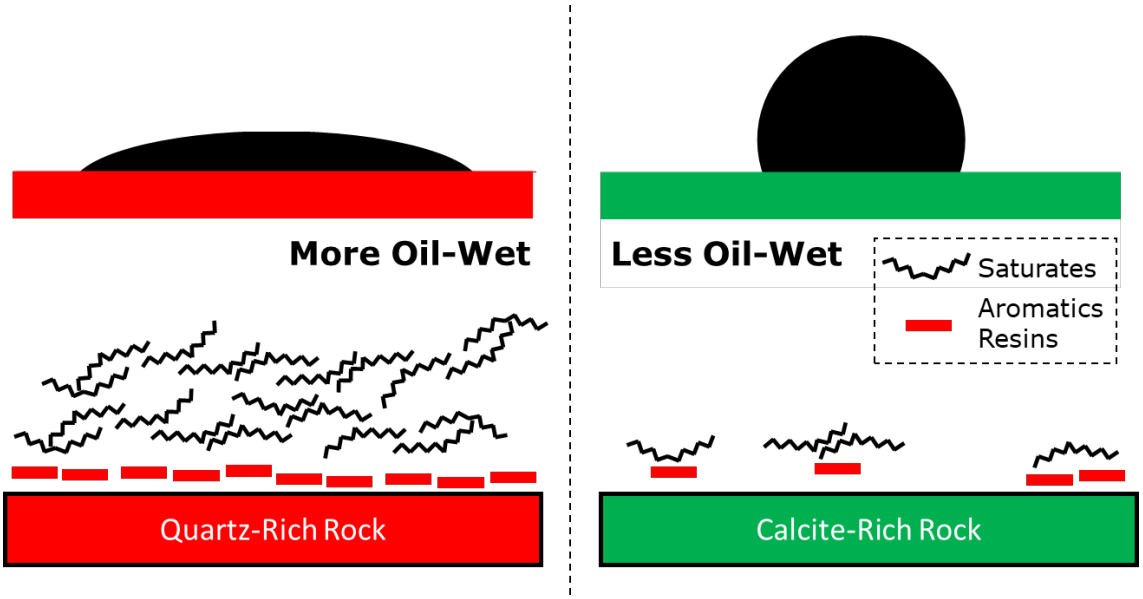

Figure 48 - Oil-wetting mechanism for shale oil reservoir oil/brine/rock system.

Higher brine salinity renders the rock surface more oil-wet. It is hypothesized that the increasing polarity of the aqueous phase forces the aromatics and resins away from the

oil/water interface, increasing their adsorption on the rock surface. This results in a more oil-wet surface as was observed for all contact angle experiments.

Generally, a minimum aging time of 35-days was required to achieve a stable surface wettability where the contact angle no longer changes. This number was derived by performing Tukey's analysis on various aging times and this analysis allows determination of the earliest aging time for which there was no significant change observed in contact angle with a significance level of 95%. Under certain conditions, the 35-day rule could be reduced, i.e., when the crude oil contains more aromatics and resins thereby forcing these components to partition to the surface faster. At higher TDS, the reassembling process of the adsorbed layer at the rock surface occurs whereas when the brine TDS is low it doesn't occur thus requiring lower amount of time to reach a stable wetting condition.

The final observation relates to pre-soaking the sample in brine before aging in crude oil. A rock surface that was pre-soaked in its respective brine maintained its oil-wetness after aging in its corresponding oil. This result is important as it showed that the shale surface maintains its oil-wetness even when it is pre-wetted with brine.

CHAPTER VI

NONIONIC SURFACTANT CLOUD POINT AND ITS COMPARISON TO LOWER 48 SHALE RESERVOIRS TEMPERATURE

Around 250 cloud point data were accumulated in this study. In this section, we will start with single nonionic surfactant system, specifically looking at the effect of EO group length of the surfactant to its cloud point. Then, the effect of the aqueous-phase salinity and its ionic composition are discussed next. To close the single surfactant system, the effect of the hydrophobic structure of the surfactant as well as how concentration is affecting the cloud point is covered. Next, the co-surfactant system is investigated, starting with the proof of concept. Then, to optimize the co-surfactant method, the effect of the ionic surfactant's hydrophobic and hydrophilic structure on the magnitude of the cloud point increase is discussed. And lastly, the effect of brine salinity on the efficacy of the co-surfactant method is investigated.

Extending EO Group Length Increases the Cloud Point, Up to A Point

Nonionic surfactants achieve their hydrophilicity through the ethoxylation process of an alkyl alcohol chain. The number of EO group attached is known to determine the hydrophilicity of the surfactant; more EO group results in stronger hydrophilicity. With hydrophilicity directly corresponding to the solubility of the surfactant, a similar trend should be observed between the number of EO groups and cloud point. Figure 5 presents the relationship between cloud point and the EO number of the four types of nonionics

included in this study at brine salinity ranging from fresh water to 24% NaCl. It is important to note that tailgroup and brine salinity also affect the cloud point, however the positive trend of cloud point to EO is still observed across the board.

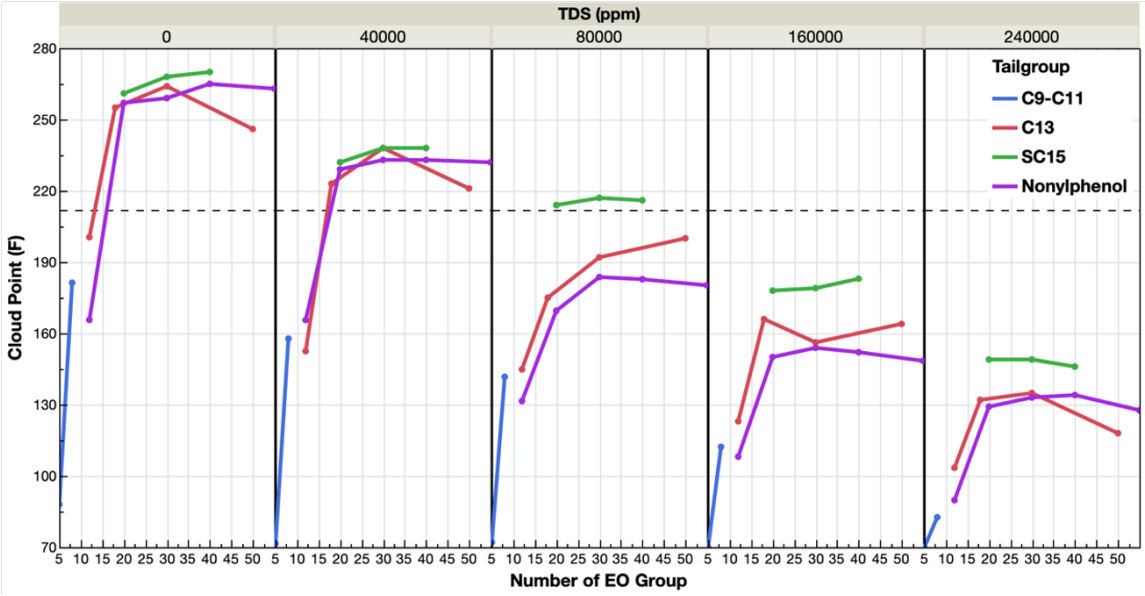

Figure 49 - EO length shows positive effect to the cloud point with plateau observed. Data are grouped by salinity in columns, left-to-right is 0 to 24 wt% NaCl concentration. Tail groups are represented by the color of the line.

Nonionic surfactants achieve their hydrophilicity through the ethoxylation process of an alkyl alcohol chain. The number of EO group attached is known to determine the hydrophilicity of the surfactant; more EO group results in stronger hydrophilicity. With hydrophilicity directly corresponding to the solubility of the surfactant, a similar trend should be observed between the number of EO groups and cloud point. Figure 49 presents the relationship between cloud point and the EO number of the four types of nonionic surfactants included in this study at brine salinity ranging from fresh water to 24% NaCl.

It is important to note that tailgroup and brine salinity also affect the cloud point, however the positive trend of cloud point to EO is still observed across the board.

An optimum number of EO is also observed around 20 EOs. Below 20, adding more EO group to the surfactant significantly improves its cloud point. While above 20, the addition does not result in substantial increase of the cloud point. In some cases, increasing the EO number above 20 could actually reduce the cloud point of the surfactant. Case in point, nonylphenol surfactants at brine salinity above 8% NaCl and tridecanol surfactants at brine salinity of 24% NaCl. This behavior is hypothesized to be caused by size of the extended EO group. As the temperature of the system is increased to reach the cloud point, the EO group loses its hydrophilicity due to the diminishing of the hydrogen bond. At higher temperature, a surfactant with 30 to 55 EO groups now has a large molecule that is hydrophobic; the previously hydrophilic EO groups are now hydrophobic due to the vanishing of hydrogen bond. This large molecule then induces more phase separation of the surfactant from the aqueous-phase. As a result, a lower cloud point is observed.

Aqueous-Phase Salinity Decreases the Cloud Point

From Figure 49, the brine salinity plays an important role in determining the cloud point of the nonionic surfactant. To investigate this further, the same database now is plotted differently in Figure 6. Increasing the brine salinity is observed to reduce the surfactant cloud point, unaffected by the tailgroup structure and the length of the EO group that the surfactant has. This result is expected as adding salt ion in the aqueous-phase reduces the availability of the water molecule to interact with the EO group of the

surfactant; salt ions attract water molecules with their ionic interaction, this interaction is stronger than hydrogen bond that occurs between EO groups and water molecule.

In Figure 50, the color represents the number of EO group of the surfactant. As discussed before, adding more EO improves cloud point. With the improvement ceases after 20 EOs, as the data are now stacked on top of each other. This observation confirms the optimum EO number argument that was brought up previously. On this maximum cloud point dataset, a trend of cloud point decrease of 4.8° F for each 1 wt% NaCl salinity increment is observed by putting a linear correlation on the dataset. This trend includes all three tailgroup (C13, SC15, and Nonylphenol).

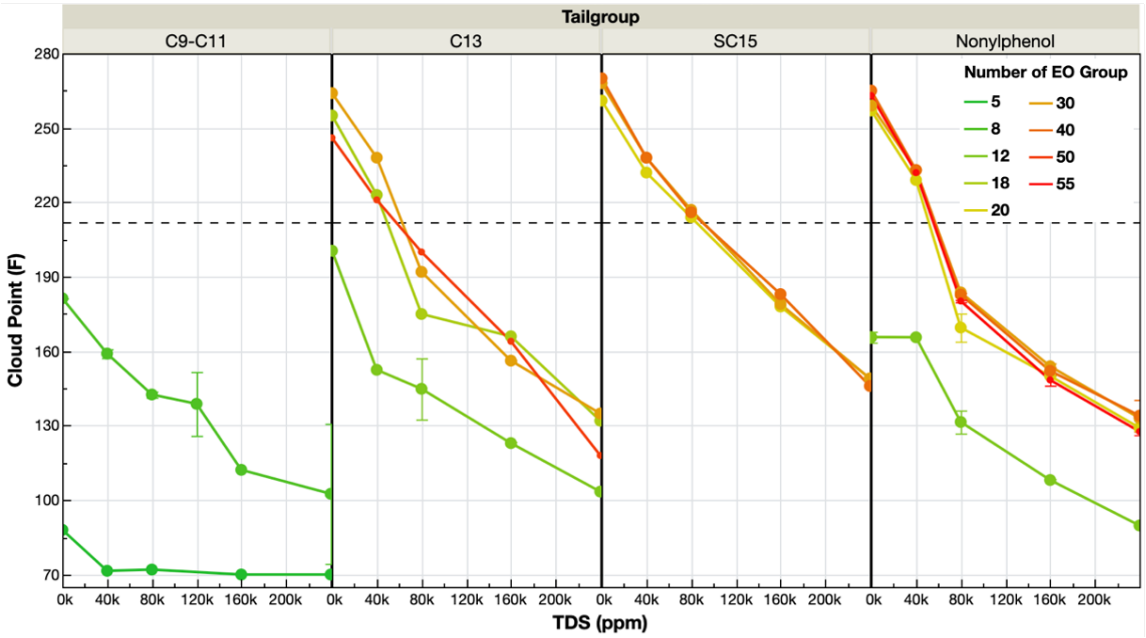

Figure 50 - Salinity shows negative effect on the cloud point. Data are grouped by tail group in columns. Color represents the different EO group length on the headgroup.

This study only incorporates sodium chloride to increase the salinity of the aqueous phase. With most reservoir produced water containing salt ions other than sodium and chloride, it is imperative to investigate the effect of salt ion composition on cloud point. Figure 51 presents the cloud point comparison of surfactant TD-18 and TD-30 in four types of aqueous-phase, DI, 8% CaCl2, 8% NaCl, and 8% reservoir brine (EF-L1). Replacing all the sodium chloride salt with calcium chloride results in higher cloud point of both surfactants. Heavier cations have larger nucleus, resulting in higher charge density. Calcium is heavier when compared to sodium, resulting in its smaller hydrodynamic radius. With smaller hydrodynamic radius, higher surfactant solubility is obtained which is observed in the data as higher cloud point.

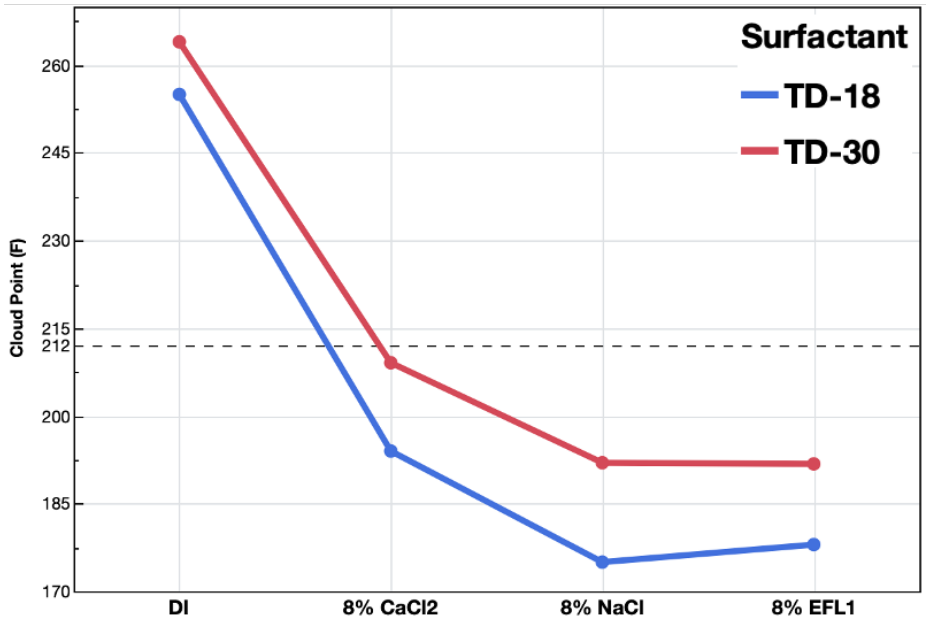

Figure 51 - Compared to sodium chloride, calcium chloride on the same concentration gives higher cloud point. This is due to the smaller ionic radius of calcium ion in water. With a mixed salt ion (EFL1), the cloud point of surfactant TD-18 falls in-between the sodium chloride and the calcium chloride.

For an actual produced water, brine with higher valences salt ion composition of higher than 10% is highly unlikely to be obtained (cite IFT paper). Brine EF-L1 is included to investigate the effect of salt ion to cloud point with representative salt ion composition. The salt ion composition of this brine is composed of 95% NaCl. From Figure 6, the cloud point of the surfactant TD-30 is like its cloud point with 8% NaCl. While for surfactant TD-18 with brine EF-L1, the cloud point is higher than with 8% NaCl but still lower than with 8% CaCl2. This result shows that replacing some sodium chloride with a higher valences salt cation could be a solution to improve the surfactant cloud point. However, it might only be beneficial with shorter EO surfactant (TD-18 compared to TD-30).

Tail group Structure Affects the Cloud Point

Surfactant solubility in the aqueous phase, aside being controlled by its hydrophilic part, is known to be a function of its hydrophobic tailgroup. A heavier hydrophobic tail would cause the surfactant to be less-soluble in water, which can be observed as lower cloud point in this study. In the previous discussion, this effect was observed. To investigate further, the database was screened to only C13, SC15, and Nonylphenol surfactants with 30 EO groups. Their cloud points are presented in Figure 52.

On all salinity levels, tailgroup SC15 has the highest cloud point, followed by C13, and lastly nonylphenol. Nonylphenol is expected to have the lowest cloud point as it has, not only 19 hydrocarbon chain length, but also a ring structure in its tailgroup. However, SC15 was not expected to have the highest cloud point as C13 should have higher cloud point since it has the shortest hydrocarbon chain on its tailgroup; C13 has 13 while SC15

has 15. It is hypothesized that with the SC15 surfactant being a secondary alcohol ethoxylate, its hydrodynamic radius might be smaller than those of primary alcohol C13. A smaller hydrodynamic radius would result in higher solubility in the aqueous phase, which is observed as a higher cloud point. Selecting a shorter hydrophobic tailgroup could help improve the surfactant cloud point. Additionally, moving from primary alcohol to secondary alcohol could also increase the surfactant cloud point. However, it is hypothesized that each tailgroup would have a compatibility factor to the reservoir crude oil which should be considered before deciding to switch the surfactant tailgroup to improve the cloud point performance of the surfactant.

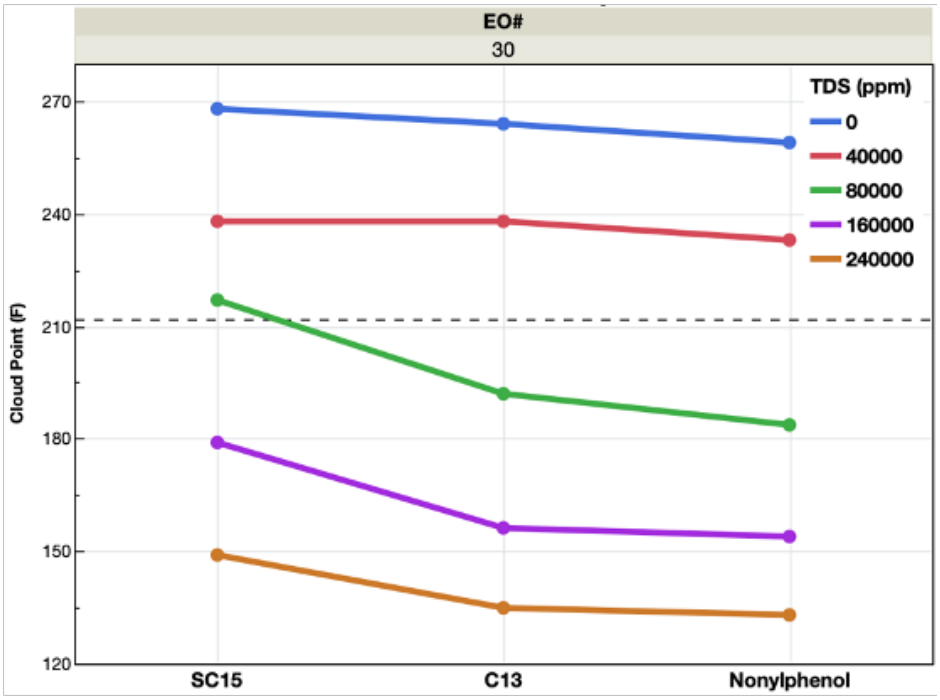

Figure 52 - The structure of the surfactant tail group affects the cloud point. Heavier hydrophobic tail group like the nonylphenol generally has lower cloud point. Interestingly, secondary alcohol with 15 carbon atoms has higher cloud point than linear tridecanol. Data are grouped by salinity, blue-to-red is 0 to 24 wt% NaCl.

Cloud Point Is Not Observed at Surfactant Concentration Lower than the CMC

Cloud point and micellization are both driven by the reduction of nonionic surfactants' hydrophilicity, either due to an increase in temperature or an increase in salinity. Therefore, surfactant concentration might have an influence on the surfactant cloud point. Figure 53 compares the cloud point of surfactant TD-18 and TD-30 with fresh water and 24% NaCl brine at 0.01 wt% and 0.2 wt%.

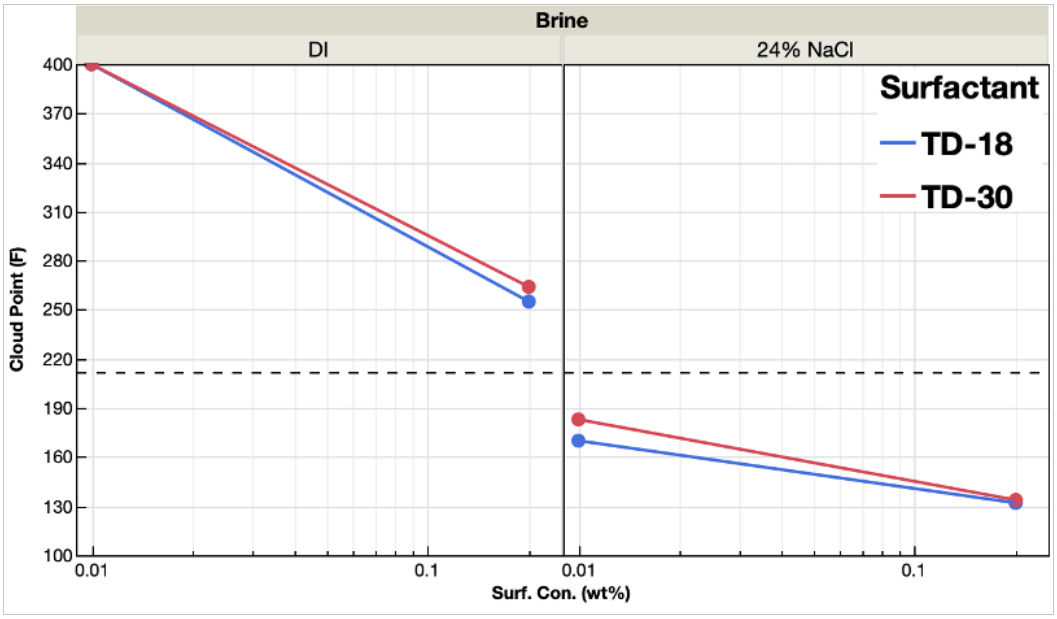

Figure 53 - Cloud point is not observed when the surfactant concentration is below the CMC. In the left column (0 wt% salinity), surfactant concentration of 0.01 wt% results in clear solution up until 400° F. While in the right column (24 wt% salinity), cloud point is still observed at 0.01 wt%. It is important to note that the CMC is lower at 24 wt% salinity than 0 wt%.

In the freshwater column, cloud point was not observed at 0.01 wt% surfactant concentration, even at a temperature of 400° F. While at 0.2 wt% cloud point was reached at 255° F and 264° F for surfactant TD-18 and TD-30 respectively. At 0.01 wt% both

surfactants are below their CMC. It is then can be concluded that the phase separation of nonionic surfactant and the aqueous phase occurs only when the surfactant concentration is above its CMC. It is hypothesized that below the CMC, surfactant molecules are still suspended in the aqueous phase as monomers due to the low amount of surfactant molecules in the system. Even though the hydrophilic part of the surfactant already loses its ability to bond with the water molecule, the high system temperature allows for the suspension due to the increased dispersion.

On the other hand, cloud point is observed on both surfactants at 0.01 wt% with 24% NaCl brine. Increasing salt ion content reduces the surfactant CMC. With 24% NaCl, surfactant concentration of 0.01 wt% is already above its CMC which explains the observed cloud point. It is also important to note that with this brine, the cloud point of the surfactant is higher when the surfactant concentration is reduced.

Mixing Ionic Co-Surfactant Improves the Cloud Point

The range of reservoir temperature for Lower 48 shale ranges from 155° to 325° F. From Figure 49, there is a significant portion of the nonionic surfactant whose cloud point falls well below this range. To enable nonionic surfactant application within this temperature range, the cloud point of the nonionic surfactants must be improved. One method to improve the cloud point is to blend ionic surfactants with the nonionics, referred as co-surfactant system in this manuscript. Figure 54 presents a summary of the cloud point of the co-surfactant systems included in this study. Nonionic surfactants TD-30, 15-S-30, and NP-30 at 0.2 wt% loading were used as the base surfactant, their data are

presented as blue, red, and green bars respectively. Two cationic surfactants, C12TAC and C18TAC, as well as three anionic surfactants, SDS, S-2, and S-3B were added separately at 0.1 wt% loading as the ionic stabilizer (presented on the x-axis). Each co-surfactants system was tested with DI (left column) and 8% NaCl (right column).

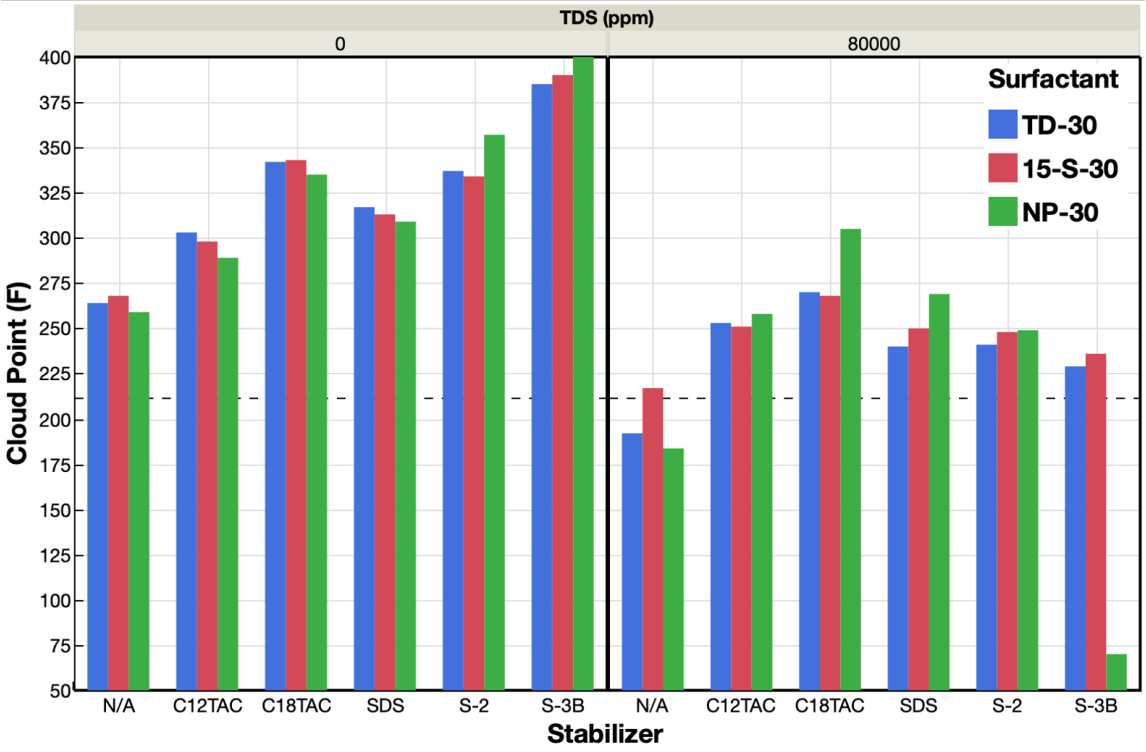

Figure 54 - The addition of ionic surfactant as co-surfactant (plotted on the x-axis) improves the cloud point of nonionic surfactants. Both cationic and anionic surfactants can be used as stabilizer.

Compared to the single surfactant (labeled as N/A on the x-axis), co-surfactant system has higher cloud point with all nonionic surfactants tested at all salinity levels. With the only exception of co-surfactant system NP-30 and S-3B at 8% NaCl brine where the solution is already turbid at room temperature. At 0% salinity, all ionic surfactants that

were added improved the cloud point of all three nonionic surfactants to above 300° F. Allowing for the extension of the nonionic surfactant application to high-temperature shale reservoir such as the deeper interval of the Eagle Ford and the Middle Bakken/Three Forks. The cloud point improvement ranges from 30° on NP-30/C12TAC co-surfactants to 141° on NP-30/S-3B co-surfactants. With higher brine salinity, the improvement ranges diminish to 19° on 15-S-30/S-3B co-surfactants to 121.3° on NP-30/C18TAC co-surfactants. A consistent trend is also observed between increasing hydrophobicity of the ionic stabilizer and the magnitude of the cloud point improvement. The effect of the structure of the ionic stabilizer will be discussed in the following section.

Adding ionic stabilizer to nonionic surfactant improves the cloud point due to the interaction between the hydrophobic tail of the main surfactant and the stabilizer. With both hydrophobic tailgroups being non-polar, Van der Waals interaction between the two tails exists. The bond between the two tails is hypothesized to be in the form of stacked hydrocarbon tails instead of an end-to-end tail. This is because in this configuration, the free energy of the system would be at its lowest state as the hydrodynamic radius of the nonionic-ionic "micelle" is in its smallest magnitude. With this new configuration, the hydrophilicity of the surfactant system which is initially only supported by the EO group is now also reinforced by ionic interaction between the hydrophilic ionic headgroup of the ionic surfactant. As a result, the cloud point of the nonionic surfactant is now increased.

From Figure 54, the cloud point improvement from this method is still susceptible to higher brine salinity. As a matter of fact, due to the nature of the ionic bond between the hydrophilic tail of the ionic stabilizer and the water molecule, it is hypothesized that the

co-surfactant system is more prone to salting-out. A more detailed discussion on the effect of brine salinity on the cloud point performance of the co-surfactant system will be covered in the last section of this work.

The ability to improve the single surfactant cloud point presented above must be applied with caution. It is true that staying below the surfactant cloud point in the reservoir is preferable to avoid phase separation. However, increasing the surfactant cloud point excessively to achieve this criterion should be avoided. Surfactant molecule can only perform its interfacial mechanism when it is able to positions itself on the polar/non-polar interface. Excessively increasing the cloud point through ionic stabilizer addition also means that the surfactant hydrophilicity is increased unreasonably. This would allow the surfactant molecule to comfortably remain in the aqueous phase, preventing it from positioning itself at the interface, highly likely resulting in the degradation of surfactant performance.

Increasing the Hydrophobicity of the Tailgroup of Both Nonionic and Ionic Stabilizer Surfactants Results in Higher Cloud Point Increment.

To investigate the efficacy of the co-surfactant system on improving cloud point, the cloud point increment is plotted against the three different tailgroup of the main nonionic surfactant in Figure 55. The difference between the cloud point of the co-surfactant system and the base case single surfactant system of each respective nonionic surfactant is defined as the cloud point increase. The nonionic tailgroup is ordered from the least hydrophobic to the most, based on the cloud point data of their single surfactant system; lower cloud

point implies stronger hydrophobicity and vice versa. With the exception of cationic stabilizer at 0% brine salinity, a positive trend between the CP increase and the hydrophobicity of the nonionic surfactant is observed. The co-surfactant system is more effective in increasing cloud point on a more hydrophobic nonionic surfactant. A more hydrophobic nonionic surfactant allows for more Van der Waals interaction sites for the ionic stabilizer hydrophobic tailgroup to bond. This causes the hydrophobic tailgroup stack to be more compact, reducing the hydrodynamic radius, and ultimately results in better cloud point improvement.

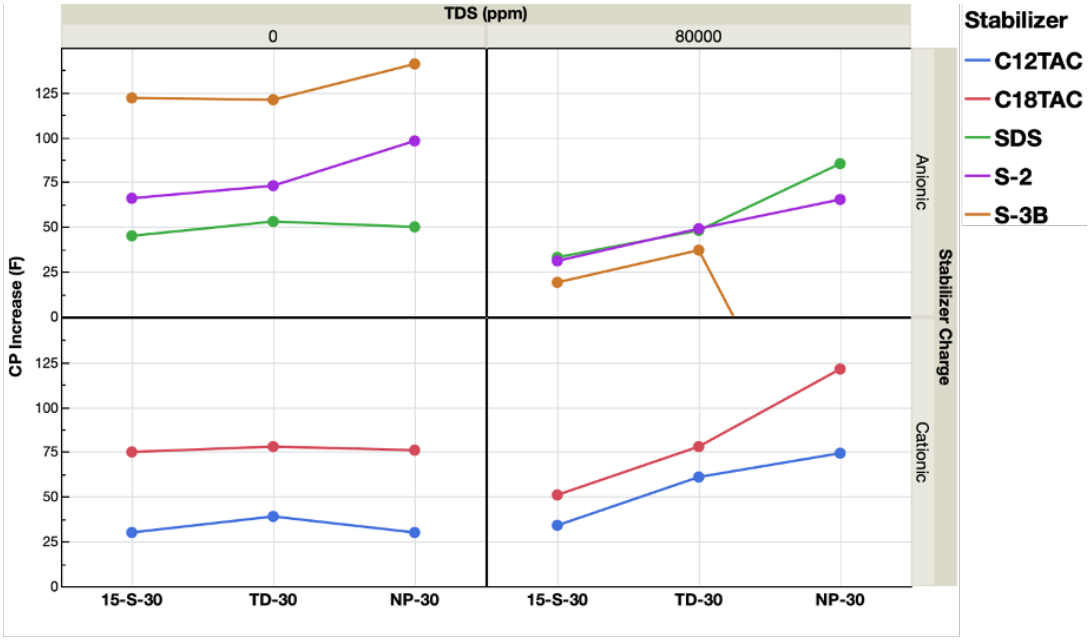

Figure 55 - The increment of cloud point from the single surfactant system plotted against the different tailgroup of the main nonionic surfactant. Co-surfactant system is more effective on a more hydrophobic nonionic surfactant.

Under the same explanation, a more hydrophobic tailgroup of the ionic stabilizer should also improve the efficacy of the co-surfactant system in improving the cloud point. Figure 56 plots the cloud point increase against the length of the hydrophobic tail of the ionic stabilizer. Similar to the observation in Figure 55, positive trend of cloud point improvement and the length of the ionic stabilizer hydrophobe is observed. This observation holds true apart from surfactant NP-30 with anionic stabilizer in 8% NaCl brine. The positive trend observed in Figure 56 confirms the proposed hydrophobic-hydrophobic interaction mechanism of co-surfactant cloud point improvement. Understanding this mechanism is essential as it allows for the specific customization of the co-surfactant method. Customization of the co-surfactant system to match the target reservoir can be done by modifying the hydrophobicity of either the nonionic surfactant or the ionic stabilizer. By doing this, essentially a full range of cloud point to match the Lower 48 shale reservoir temperature could be achieved.

It is important to note however that it is possible to over-saturate the co-surfactant system. In Figure 56, nonionic surfactant NP-30 reaches the maximum cloud point with anionic co-surfactant that has 12 hydrocarbon chain length. Increasing the length above 12 results in lower cloud point. With 22 hydrocarbon chain length, the co-surfactant system becomes insoluble even at room temperature. For this NP-30 nonionic surfactant and brine combination, choosing cationic stabilizer would be a better option.

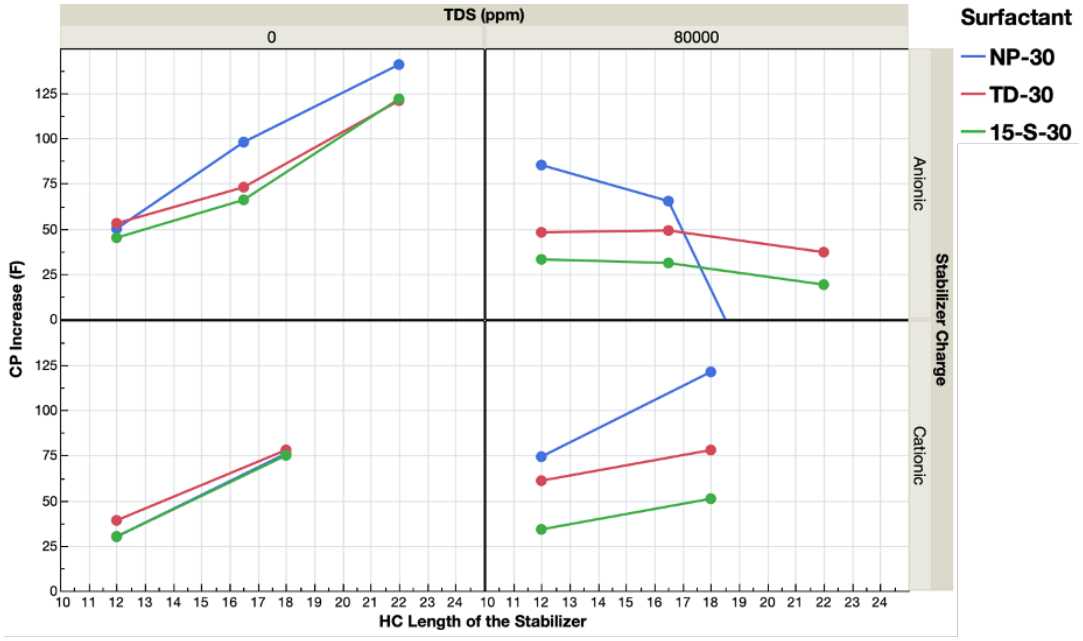

Figure 56 - The cloud point of the co-surfactant system is plotted against the hydrocarbon tail length of the ionic surfactant. The data are grouped by the brine salinity (column) and by the ionic surfactant charge (row). Longer hydrocarbon chain improves the cloud point of the co-surfactant system. However, with surfactant NP-30, 8% NaCl brine, and anionic co-surfactant, an optimum length of 12 is observed.

Co-Surfactant System Increases Cloud Point of Higher Salinity Brine More Than Fresh Water

Higher brine salinity results in lower co-surfactant system cloud point as presented in Figure 54. It is important to note that the cloud point of a single nonionic surfactant system is also reduced, as shown in Figure 49. Therefore, it is possible that the cloud point improvement by the co-surfactant system is larger when the brine salinity is at a higher level. To investigate this hypothesis, the magnitude of cloud point increment by the co-surfactant system is plotted against the brine TDS in Figure 57.

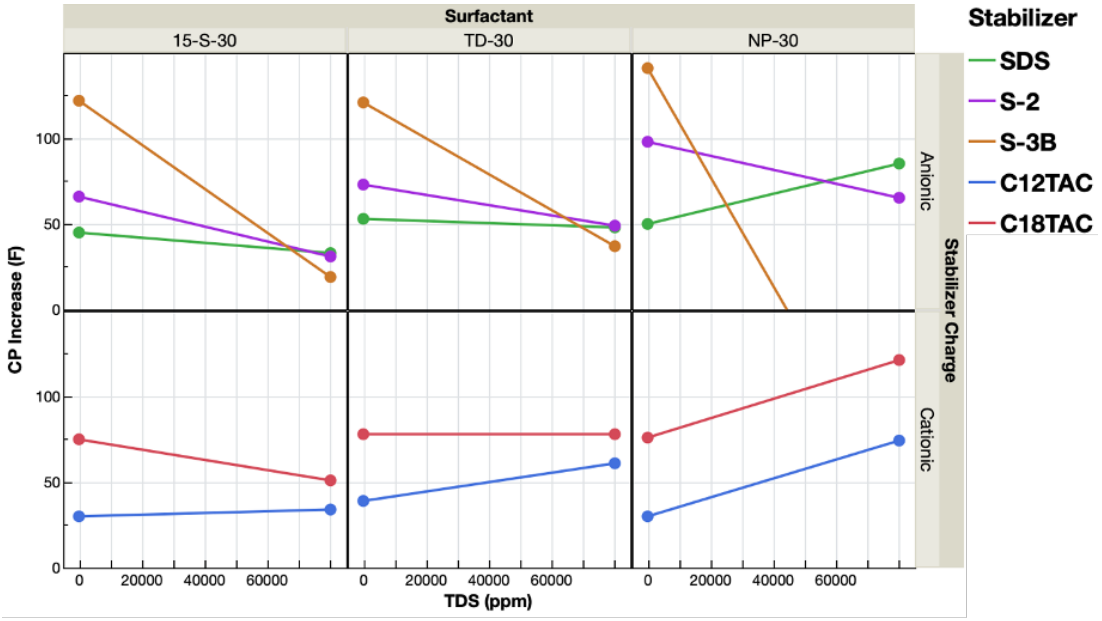

Figure 57 - The cloud point increase of the co-surfactant system is plotted against salinity of the aqueous phase. Data are grouped with the nonionic surfactants on the columns, the charge of their stabilizer on the rows, and the stabilizer as presented in the legend. With the anionic stabilizers, increasing the brine TDS generally reduces the efficacy of the stabilizer to increase the cloud point. While for cationic stabilizers, increasing the brine TDS generally improves the cloud point increase.

The top row of Figure 57 contains all the cloud point data of anionic co-surfactants system. Increasing the brine TDS on this system results in lowering the co-surfactant system efficacy in increasing the cloud point. This observation holds true for all the three nonionics and three anionic stabilizer combinations, except for the NP-30 and SDS co-surfactants which shows positive trend with salinity. It is also interesting to note that at 0% salinity, the ascending order of the cloud point increment performance is SDS, S-2, and S-3B (green, purple, and orange). While at 8% salinity, the order is inversed (orange, purple, and green).

On the bottom row, all cloud point data of the cationic co-surfactant systems are presented. Going from the least to the most hydrophobic nonionic surfactant (left-to-right

column), increasingly positive trendlines are observed on both cationic stabilizers used in this study. Negative correlation between cloud point increment and brine salinity observed in 15-S-30/C18TAC system becomes flat on the TD-30/C18TAC and finally positive on the NP-30/C18TAC. Likewise, the C12TAC cationic stabilizer starts with flat trendline on its 15-S-30 combination. Then turns more positive with TD-30 and NP-30.

Increasing the salinity of the aqueous phase reduces the ability of water to dissolve the anionic stabilizer which results in the lower cloud point at higher brine TDS observed on the anionic co-surfactant systems. The same trend is not observed on the cationic stabilizer due to the higher charge density of the cationic stabilizer. Larger charge density attracts the electron to occupy smaller volume in water, causing the cationic stabilizer to possess smaller hydrodynamic radius than the anionic stabilizer. The presence of salt ion at the higher TDS condition is hypothesized to enhance this hydrodynamic radius compression phenomenon. As a result, the efficacy of cationic co-surfactant systems to improve the cloud point is amplified at higher brine salinity. In addition, sufficient hydrophobic-hydrophobic interaction discussed in the previous section is also essential for this synergistic behavior to occur. From Figure 57, increasing the hydrophobicity of the nonionic surfactants improves the co-surfactant efficacy to improve the cloud point. As discussed in the previous section, strong hydrophobic-hydrophobic interaction between the nonionic and the ionic stabilizer results in a more compact hydrophobic structure to be dissolved in water by the hydrophilic part of the co-surfactant systems. The conjunction of the hydrodynamic radius compression by the cationic stabilizer and the compaction of the hydrophobic structure culminates in the synergistic effect of cloud point

improvement on cationic co-surfactant systems, suitable for cationic co-surfactant systems for higher brine salinity conditions. To confirm this result, the cloud point data is plotted in Figure 58. Anionic co-surfactants (blue) show slightly better performance in improving the cloud point for lower brine salinity. While at higher brine salinity of 8% NaCl, cationic co-surfactants (red) provide a better cloud point improvement.

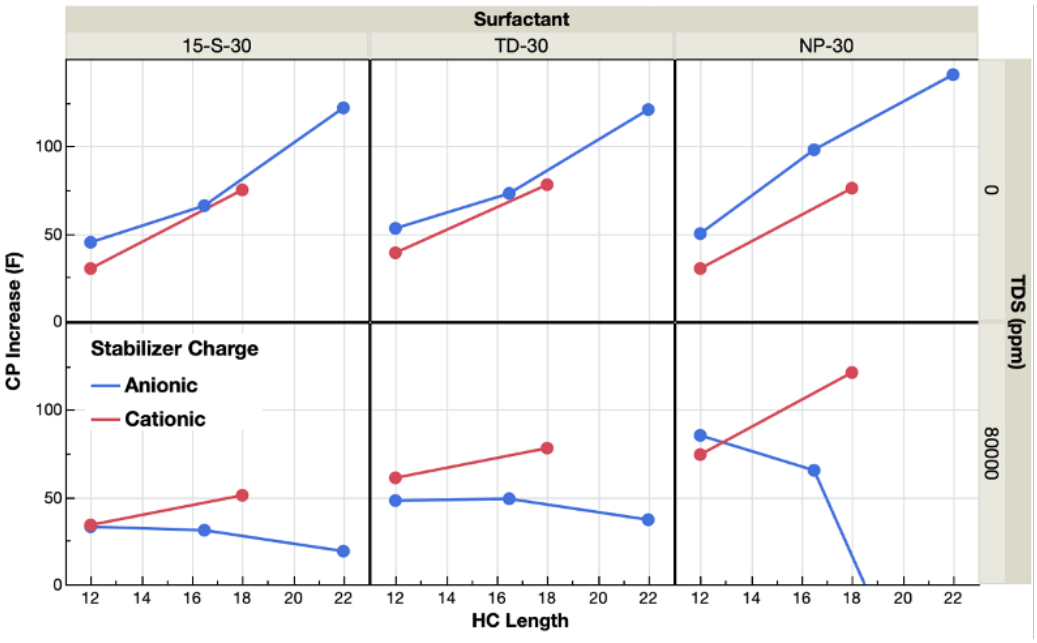

Figure 58 - Cloud point improvement comparison between anionic (blue) and cationic (red) stabilizer.

CHAPTER VII

SURFACTANT STRUCTURE EFFECT TO OIL/WATER IFT

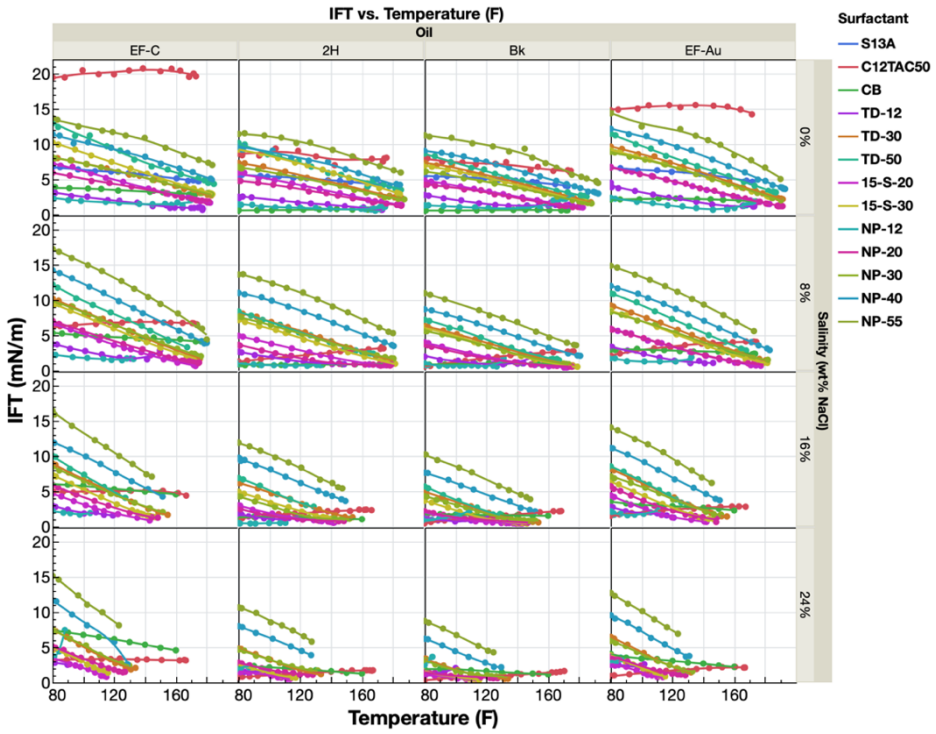

Figure 59 - IFT database constructed from this study.

More than 2,900 IFT values were measured. All IFT datapoints are plotted against temperature and shown in Figure 59. In this chapter, the data will be dissected based on the oil, salinity, temperature, and surfactant used to investigate the effect of each of the listed variables to the surfactant efficacy in reducing the oil/water IFT. Interaction between variables is expected, and already recorded in the literature, to exist. To investigate this interaction, the IFT data will be normalized based on the variables in question. Additionally, data modelling, several novel transformations, and graphical analysis will

be performed. These normalization, modelling, transformation, and graphical analysis will be covered in the first section of this chapter.

Introduction to Variables and Graphs

From Chapter IV (page 72), it was presented that the IFT of oil and water without surfactant in the system is strongly affected by the salinity and temperature of the system. From the literature, the IFT reduction performance of surfactant is also reported to be affected by the salinity and temperature. Since both initial IFT and IFT after surfactant are a function of salinity and temperature, this study employs normalization of the IFT after surfactant to the base IFT at each corresponding salinity and temperature to investigate the effect of surfactant to IFT reduction. This is deemed necessary to ensure an apple-to-apple comparison.

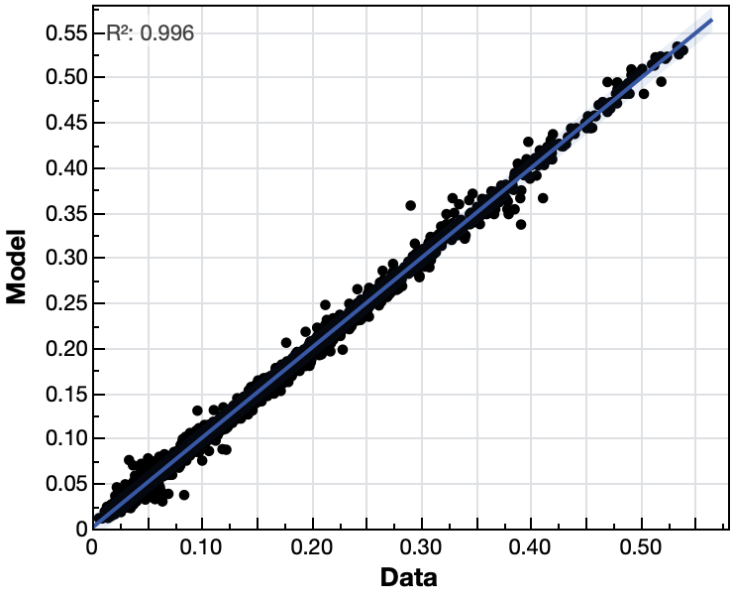

Figure 60 – Model fit for the IFT Probit 2P model.

The normalization method however brings another problem. The IFT database presented in Figure 59 are obtained from laboratory measurements. Although salinity can be replicated over and over across different crude oils and different surfactants, it is rare that the measurement can be performed at the exact temperature. To accommodate for this variability, the IFT datapoints are modeled using Probit 2P model $\left(IFT = \Phi\left(\frac{T-a}{b}\right)\right)$ for each surfactant, salinity, and crude oil (model fit is shown in Figure 60). Then, another database is created using the model equation with consistent temperature points from 70°F to 200°F at 10° increment applied. This method results in IFT database with consistent temperature points, allowing for a more straight-forward normalization.

The next section of this chapter will investigate the distribution of the base IFT of the crude oils used in this study. This is important since the surfactant IFT will be presented in terms of normalized IFT, IFT normalized to the base IFT of each respective salinity and temperature condition. Then, on the section following that, the effect of headgroup structure to the IFT reduction performance is investigated. Following that, the effect of tailgroup structure is studied. Then, the effect of EO group length of nonionic surfactants is explored. Up to this point, all crude oils are still represented by its name. With the effect of headgroup and tailgroup structure understood, the next step is to quantify the crude oil characteristic to investigate further the interaction between surfactant structure and the crude oil and its effect to the IFT reduction performance of the surfactant. The crude oil characteristic is quantified by $\boldsymbol{R_{oil}}$,

$R_{oil} = \frac{L_{C<10}{}^{*}}{L_{C\geq 10}{}^{*} + C^{*}}$..... Equation **2**

where with the $\boldsymbol{R_{oil}}$ value, each crude oil is represented by a single number. The interaction between tailgroup and crude oil is inquired next using this value. Followed by the interaction between the headgroup and the crude oil.

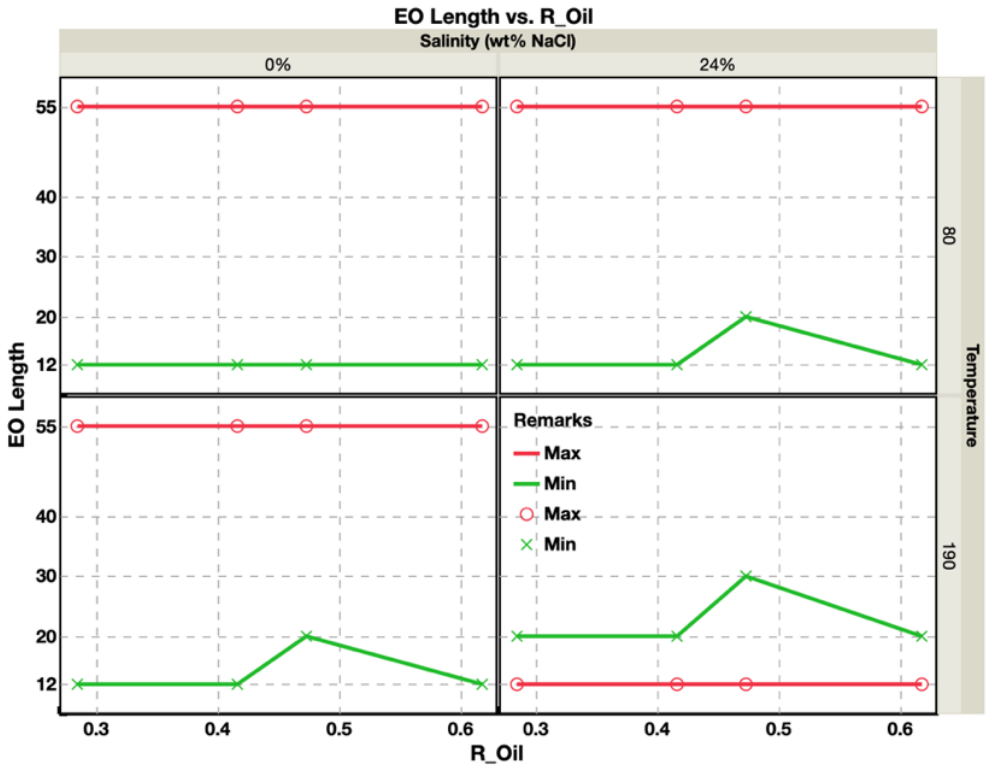

Figure 61 – An example of surfactant headgroup and $\boldsymbol{R_{oil}}$ optimization graph.

In the last two sections, a new type of graph is employed. This graph is created to provide a comprehensive look into the effect of surfactant structure, crude oil, salinity, and temperature. In this plot, the surfactant headgroup or tailgroup is plotted on the y-axis, against the crude oil R_{oil} value on the x-axis. Then the data are grouped by salinity in columns and by temperature in rows. In each box, the tailgroup/headgroup structure that

provides either the lowest (green) or the highest (red) normalized IFT, or in other words, the largest (green) or the smallest (red) IFT reduction is presented. This figure is constructed to better optimize surfactant structure to achieve the best compatibility to the vast character of crude oil presented in this study. Compatibility is analyzed from the performance of the surfactant in lowering the IFT. An example of this graph is provided in Figure 61.

Oil/Water IFT Without Surfactant

Out of fifteen crude oils included in the earlier part of this study, four are selected to be used with surfactants. The crude oils selected are EF-C (Oil 1), 2H (Oil 7), Bk (Oil 14), and EF-Au (Oil 15). These crude oils are chosen to provide crude oil properties ranges that is inclusive of the range of crude oil produced by Lower 48 shale reservoirs. Crude oil EF-C is acquired from the condensate part of the Eagle Ford shale reservoir. It is the lightest crude oil in this study and the lightest crude oil that is produced by Lower 48 shale. On the other extreme, crude oil EF-Au comes from the black oil window of the Eagle Ford shale reservoir. It is the heaviest crude oil in this study and among the heaviest crude oil found in Lower 48 shale. In between the two extremes there are crude oil 2H from the Wolfcamp and crude oil Bk from the Middle Bakken. These two crude oils are intermediated between crude oil EF-C and EF-Au in terms of density and composition.

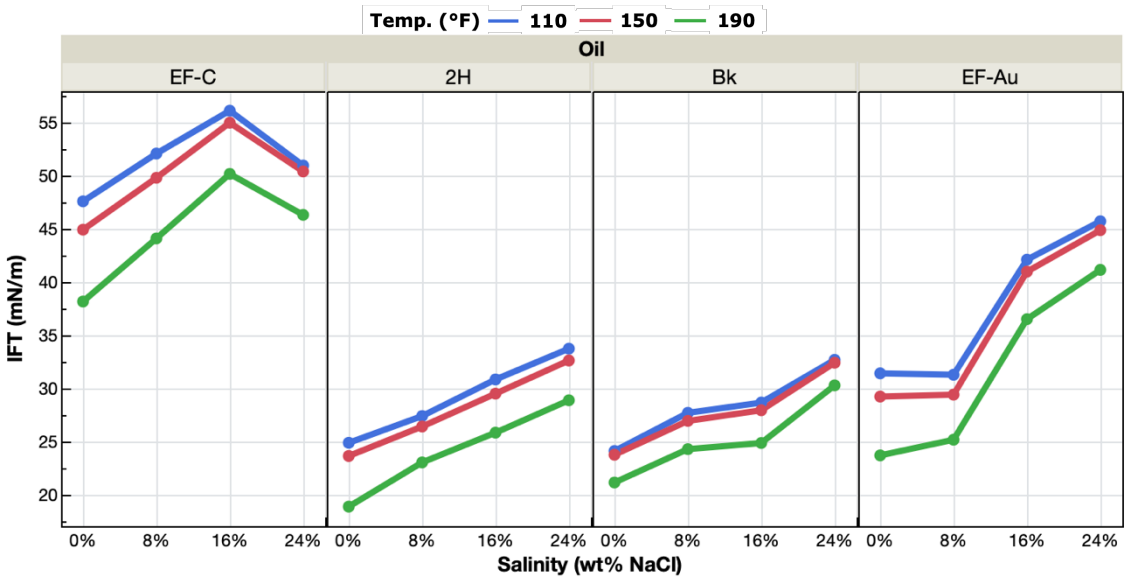

Figure 62 – Base case IFT of the four crude oils included in this chapter, plotted vs salinity.

The IFT of the four crude oils are presented in Figure 62. The data are plotted against salinity. The four crude oils are presented in the different columns. The data at different temperature are displayed as different color, blue to green represents increase in temperature. The IFT of the four crude oils are diverse, ranging from the 20 to 50 mN/m at the same temperature and salinity condition. The lighter crude oil is dominated by Saturates, which is highly non-polar, and as a result this oil has higher IFT. Crude oil EF-Au has the second highest IFT value behind EF-C. This oil does contain some amount of Aromatics and Resins that should reduce IFT value. However, it is also dominated by long linear hydrocarbon chains that have high IFT values with water. The lowest IFT is observed with crude oil 2H and Bk. Their low IFT values are driven by their composition with less Saturates, more Aromatics, and less heavy linear and aromatic chains. Observing how oil composition affects the initial IFT of the crude oil, even before surfactant molecule

is introduced, shows that surfactant structure interaction with the oil composition exists, and it would affect the IFT reduction of the surfactant.

The IFT in Figure 62 also contains the effect of salinity and temperature. The effect of these two variables on the base case IFT has been investigated in detail in Chapter IV (Page 72). Higher salinity leads to higher oil/water IFT due to the increase of the polarity of the aqueous-phase. Higher temperature lowers the IFT due to the increased interaction between the crude oil and the water molecule that allows for better bonds between the two moieties.

Headgroup Structure Effect to IFT Reduction

To analyze the effect of surfactant headgroup to IFT reduction, normalized IFT data are plotted against the headgroup structure in Figure 63. Five surfactants from the 16 included are selected for the figure since they have similar tailgroup but different headgroup structure. Five headgroup structures are included, sulfate, trimethyl ammonium, betaine, 12 EOs, and 30 EOs. The charge of these headgroups is anionic, cationic, zwitterionic, nonionic, and nonionic respectively. The headgroups are presented in this order on the x-axis. The sulfate headgroup data is only available at 0% salinity due to the poor solubility in the aqueous-phase once the salinity is increased. Only data measured with oil EF-C are shown. The data are grouped by salinity in columns. Each color represents different temperature, listed in the legend.

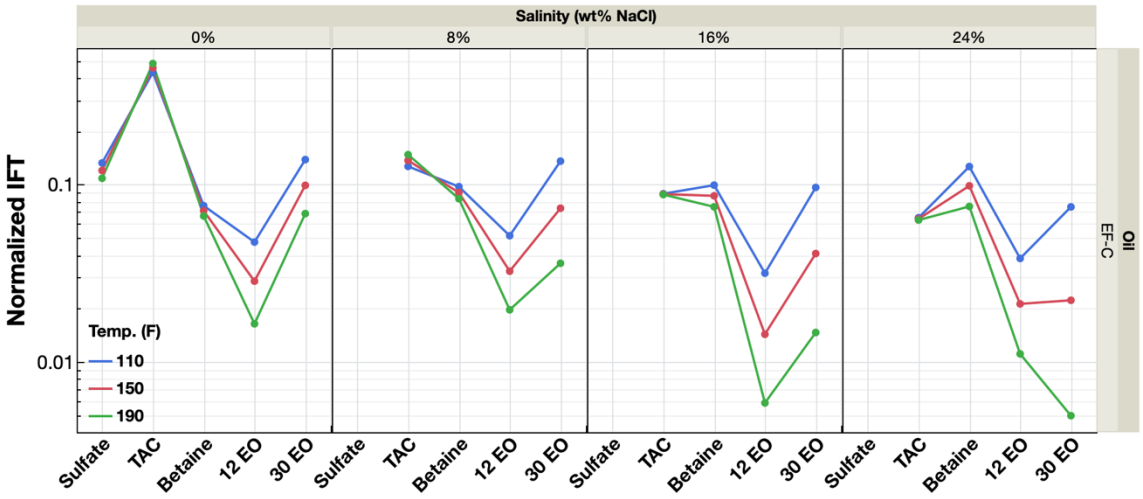

Figure 63 – Normalized IFT of C12 tailgroup surfactant vs headgroup.

First, observe the top-left box where the data for oil EF-C and 0% salinity are presented. Cationic headgroup (TAC) has the lowest IFT reduction with no more than 55% IFT reduced at all temperatures, while all other headgroup have at least 90% IFT reduction. The lowest normalized IFT is given by the 12 EO headgroup. The effect of temperature is significant on this nonionic headgroup with 95% IFT reduction increased to more than 99% when the temperature is increased from 110°F to 190°F. Similar temperature effect is observed on the other nonionic headgroup, the 30 EO headgroup. However, the IFT reduction with this headgroup is significantly less when compared to the 12 EO. The betaine headgroup does not show a strong temperature effect. As a matter of fact, all the ionic headgroups are less affected by temperature when compared to the nonionic headgroups.

The cationic headgroup has the highest normalized IFT value due to the high solubility of the trimethyl ammonium ion in water. As a cation, the high proton density in its nucleus compresses its electron cloud which reduces its hydrodynamic radius when dissolved in

water. With smaller hydrodynamic radius, this headgroup occupies less space in the aqueous-phase which allows for better solubility. With higher solubility, surfactant molecules prefer to be in the aqueous-phase and do not partition to the interface. As a result, less IFT reduction occurs. On the other hand, anionic sulfate headgroups have lower proton density in its core. Thus, the opposite phenomenon occurs; larger hydrodynamic radius and lower solubility in the aqueous-phase. This results in greater IFT reduction than the cationic headgroup. For the anionic surfactant, this also results in poor solubility, evidenced by the inability of the surfactant to be completely dissolved at a salinity higher than 0%. It is also important to note that this surfactant also has propoxy group that could also affect the solubility of the surfactant.

The nonionic headgroup is comprised of a group of ethylene oxides (EO). Ethylene oxide bonds with the water molecule via hydrogen bonding. Compared to the ionic headgroup which bonds with the water molecule through ionic bonding, the hydrogen bond is weaker. As a result, a nonionic headgroup has lower solubility in water than the ionic headgroup. This is reflected in the IFT reduction of the nonionic surfactant that is lower than the ionic since lower solubility causes more surfactant molecule to partition to the oil/water interface. Adding more EO groups increases the strength of the hydrogen bond. This is evidenced by the higher normalized IFT values for nonionic surfactant with 30 EO compared to 12 EO. However, the IFT reduction is still larger compared to the ionic headgroups, even with 30 EO groups. Another dominant characteristic of the EO group is decreasing hydrophilicity with increasing temperature. Hydrogen bonds loses their bond strength at higher temperature. As mentioned earlier, the EO group bonds with

water molecules through hydrogen bonding. Therefore, higher temperatures would reduce the interaction between the EO group and the water molecules which results in less hydrophilicity. This behavior is displayed by the deviation of the three lines in the top-left box in Figure 63. Increasing the temperature (blue to green) results in larger IFT reduction.

Comparing from the four boxes in Figure 63allows for the investigation of the interaction of headgroup and salinity. Higher salinity increases the IFT reduction of all headgroups except the betaine. This behavior is expected due to the fact that the addition of salt ion into the aqueous-phase reduces the availability of water molecules for the surfactant headgroup to bond with. Since the hydrophilicity mechanism between the EO headgroup and trimethyl ammonium headgroup are different, the sensitivity of these headgroups to the salinity is different as well. The normalized IFT of TAC and 30 EO headgroup are plotted against salinity in Figure 64 to investigate further. The nonionic headgroup is generally more sensitive to salinity than the cationic headgroup as evidenced by the stronger gradient in Figure 64. Additionally, the gradient of the TAC headgroup becomes less at higher salinity. While for the nonionic, the gradient becomes greater. From the same figure, increasing the temperature accentuates the effect of salinity to normalized IFT on 30 EO headgroup surfactants. On the other hand, for the trimethyl ammonium chloride headgroup, increasing the temperature reduces the effect of salinity to normalized IFT. This interaction of salinity, temperature, and headgroup and its effect on the IFT reduction of the nonionic headgroup is also visible in the original Figure 63. At higher salinity, the trendline of the two nonionic headgroups diverge more.

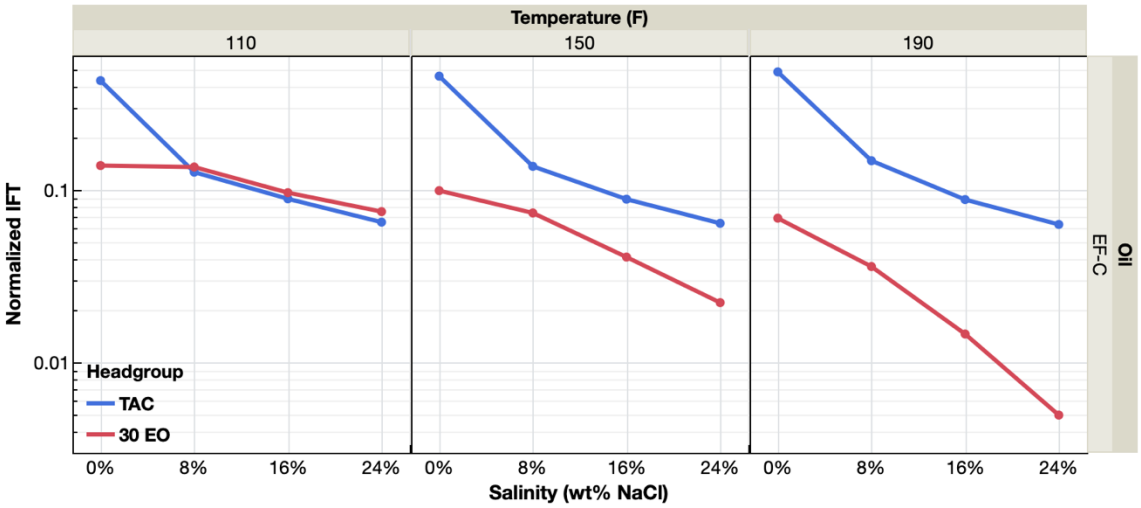

Figure 64 - Normalized IFT of C12 surfactant with TAC and 30EO headgroup vs salinity for oil EF-C.

To further investigate the interaction of temperature and headgroup, IFT data is plotted in Figure 65. Normalized IFT as a function of temperature is presented. The data is grouped by salinity in columns. The different headgroups are presented in colors. Only data from oil EF-C is presented. All headgroups except cationic TAC show negative trend with temperature. At 0% salinity, the cationic headgroup has significantly higher normalized IFT. Increasing the salinity reduces the normalized IFT value to be in the average of other headgroup's value. Additionally, salinity increase also reduces the positive gradient of the TAC headgroup to temperature. At 24% salinity, the trend is virtually flat. The strong hydrophilicity of the TAC headgroup has been covered previously. The trend observed in Figure 65 confirms the theory. Furthermore, the trend also suggests that cationic headgroup is ineffective in low salinity and high temperature system due to its low surface activity and the corresponding condition. The TAC headgroup is more suitable for high salinity reservoir system.

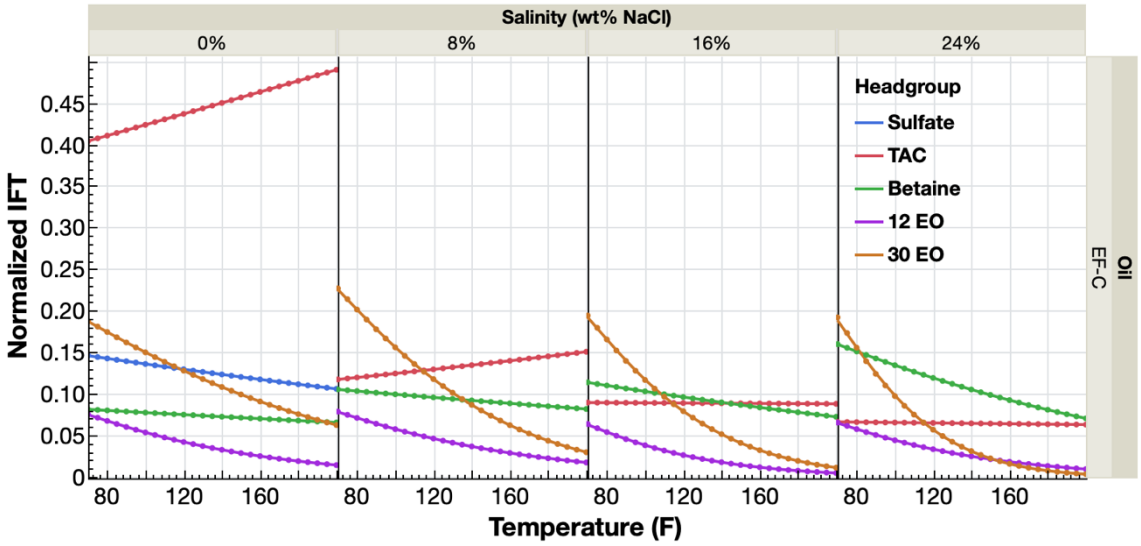

Figure 65 – Effect of temperature to normalized IFT for C12 surfactant.

The two nonionic headgroups are more sensitive to temperature compared to the ionic headgroups, thus confirming that hydrogen bonding from EO groups has higher sensitivity to temperature when compared to ionic bonds. At ambient temperature, 30 EO groups start with high normalized IFT value. Although that the 30 EO group line never intersects the 12 EO group at any salinity and temperature condition, it is also observed to have steeper slope with temperature. More EO groups results in more hydrogen bonding reduction when temperature is increased, causing the 30 EO groups to have the steepest trend with temperature as shown in Figure 65. The trend observed on the nonionic headgroups suggest that its surface activity is enhanced at higher temperature, suggesting it is suitable for higher temperature applications. However, the nonionic headgroup also has upper temperature limit (cloud point) where it completely loses its hydrophilicity.

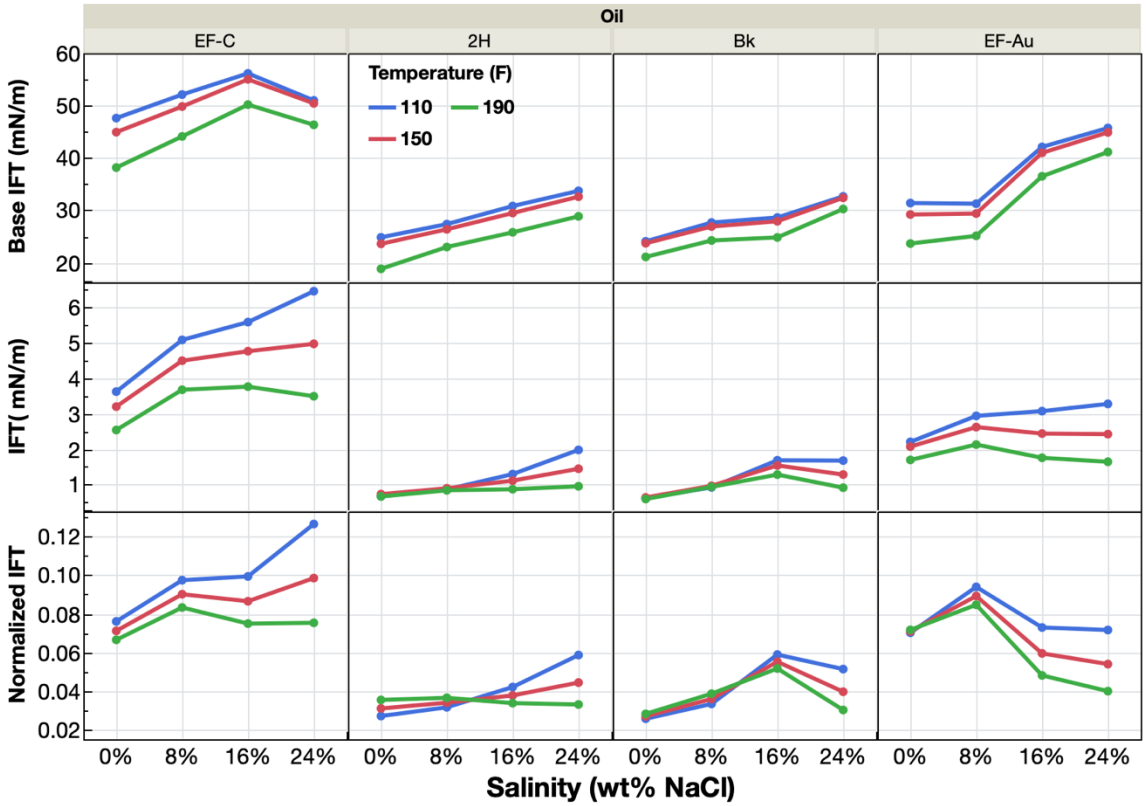

Figure 66 – Base case IFT, IFT, and normalized IFT of C12 surfactant with betaine headgroup vs salinity.

In this graph, salinity increases the normalized IFT value of the zwitterionic headgroup. This behavior is observed up to 24% with oil EF-C and 2H, up to 16% with oil Bk, and up to 8% with oil EF-Au. On the other hand, increasing the system temperature decreases the normalized IFT value. With the exception of oil 2H and oil Bk at 0% and 8% salinity, it is hypothesized that this behavior is solely driven by the base IFT. As can be seen, the base case IFT is strongly driven by the salinity with positive trend observed between the two variables. Temperature on the other hand reduces the IFT of the base case. Zwitterionic headgroup's IFT follows the same trend and shows that its ability to reduce the IFT is relatively unaffected by the salinity (change through 24 wt% salinity

change is no larger than two times, an insignificant change when compared to other headgroups). Temperature also has trivial effect to the IFT reduction performance of this zwitterionic headgroup. But since the base case IFT changes with salinity and temperature and is the denominator to calculate the normalized IFT value, the normalized IFT value is altered as well with change in salinity and temperature. More evidence of this behavior is the fact that the betaine is an ionic compound with ionic bonding facilitating its hydrophilicity. Temperature should promote ionic bonds which should result in increasing the value of normalized IFT. However, in Figure 66, temperature reduces the normalized IFT. This trend occurs since at higher temperature, the base case IFT decreases with increasing temperature.

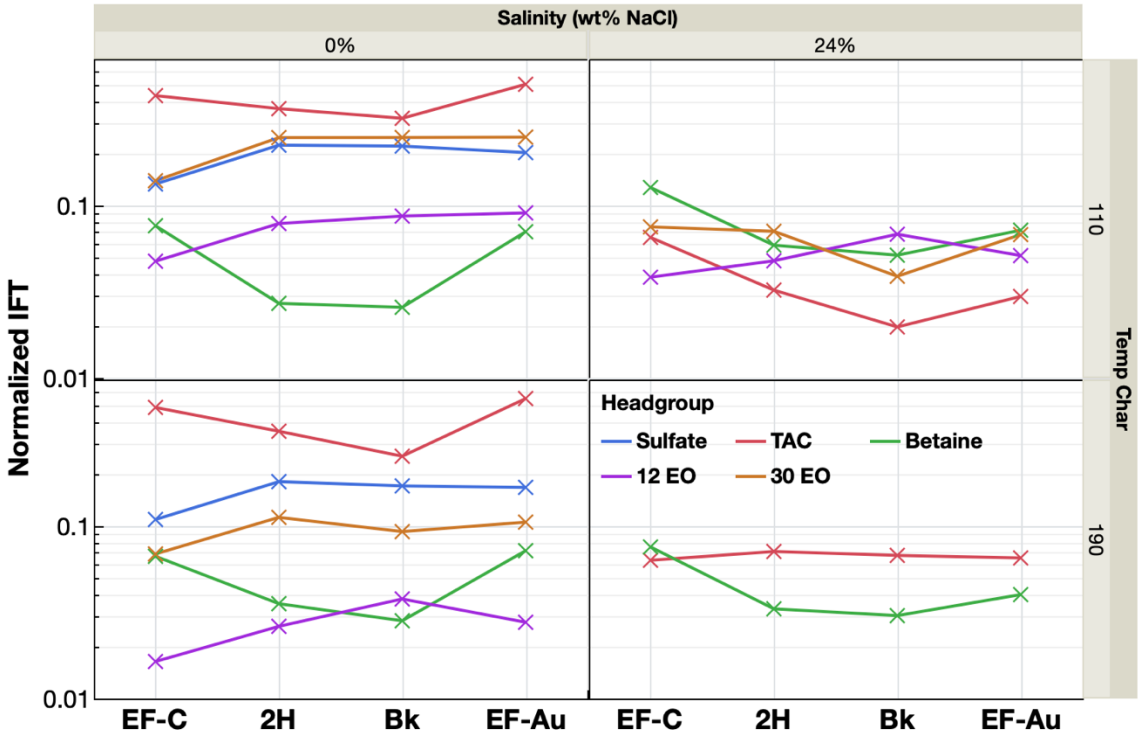

Figure 67 –Crude oil and headgroup interaction plot of normalized IFT.

To investigate for interaction between headgroup and the crude oil, the IFT data are plotted in Figure 67. Normalized IFT is plotted against the four crude oil samples. The data is grouped by salinity and temperature in rows and columns respectively. The headgroups are presented in different colors. Each box represents a different salinity and temperature condition and thus would have different normalized IFT. The interaction is inspected by looking at whether parallel or intersecting lines are observed in each box. Except for the cationic TAC and the zwitterionic betaine headgroups, no interaction is observed between the crude oil and headgroup. It is hypothesized that the presence of positively charged molecule results in the interaction between the headgroup and the crude oil; positively charged molecules are present only in these two headgroups. It seems these two headgroups are most compatible with crude oil 2H and Bk. Further research on the relationship between positively charged headgroups and crude oil with balanced Saturates and Aromatics composition must be performed to understand the precise mechanism behind this trend.

To summarize, there are several key observations on how the headgroup of the surfactant affects its IFT reduction performance:

1) salinity improves the IFT reduction of both nonionic and ionic headgroups. Nonionic headgroups exhibit higher sensitivity to salinity compared to ionic headgroups.
2) higher temperature improves the IFT reduction of nonionic headgroup while lowering the IFT reduction of the ionic headgroup.
3) zwitterionic is relatively unaffected by both salinity and temperature compared to all other headgroups.

4) the performance of different surfactant headgroups is also affected by the oleic-phase characteristic. For cases where hydrophobic bond between the tailgroup and the oleic-phase is not favorable, the surfactant headgroup could be replaced to those with less hydrophilicity to enforce the surfactant molecule partitioning to the interface. And finally, some form of compatibility to produce lower normalized IFT value between positively-charged headgroup molecule and crude oil with balanced Saturates and Aromatics composition is also observed.

The Effect of Tailgroup Interaction with Crude Oil and Salinity to IFT Reduction

Normalized IFT data is plotted against surfactant type in Figure 68. In the figure, data are grouped by salinity in columns. The left-to-right column is 0% to 24% NaCl. Three surfactants are included in this graph: 15-S-30, NP-30, and TD-30. Since the goal is to investigate the effect of surfactant tailgroup structure, the headgroups are kept constant by only including surfactants with 30 EO groups. The four lines represent different oils used in the study as described in the legend.

On the 0% salinity data, lowest normalized IFT values are given by the EF-C oil. From the SARA composition, EF-C oil is composed mainly of saturates thus resulting in the most non-polar crude oil in this group. Since the lowest free energy is created when surfactant molecules are at the interface of polar and non-polar phases, the interface of water and EF-C would be the ideal location, hence creating the lowest normalized IFT. The other three crude oils have similar IFT reduction with TD tailgroup and similar

reduction with oil Bk and EF-Au with 15-S tailgroup. Interestingly, oil 2H shows incompatibility with the tailgroup 15-S.

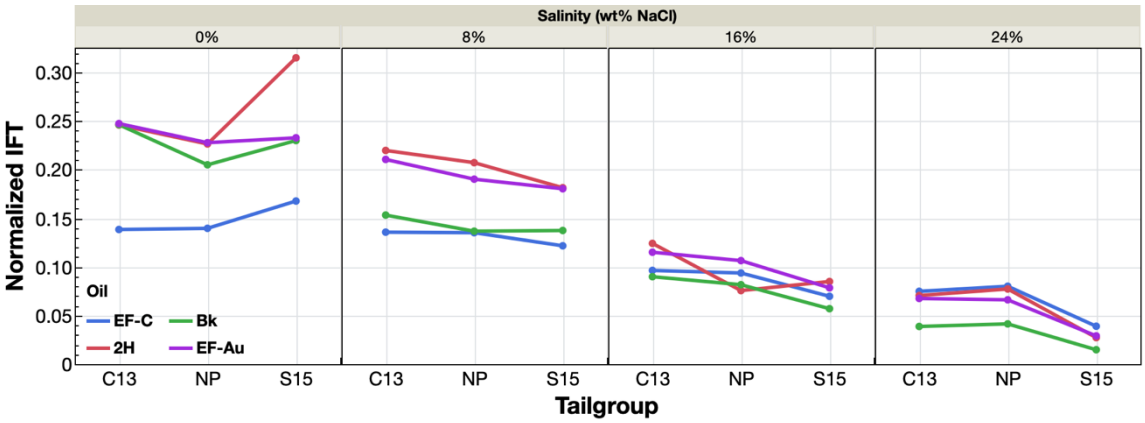

Figure 68 – Normalized IFT vs 30EO nonionic surfactant tailgroup, grouped by oil, 110°F.

Tailgroup 15-S contains a longer hydrocarbon chain than C13 which should make it a more hydrophobic molecule thus producing a lower normalized IFT value. However, with lighter oil like EF-C and 2H, the normalized IFT values from tailgroup 15-S are higher than C13. This can be observed as negative trend lines at 0% salinity. However, the trend changes with increasing salinity. At higher salinity, most of the data exhibits a positive trend which means that tailgroup 15-S actually lowers IFT the most on all four oils. From here it can be concluded that tailgroup 15-S is unique in that it becomes the most hydrophobic only when salinity is increased. Tailgroup 15-S is a secondary alcohol. It is hypothesized that the angle between the two branches of alkane is smaller at 0% salinity. This results in higher water solubility and higher hydrophilicity. At higher salinity, salt ions occupy the space between the two branches and force the two branches to be more

linear. As a result, the tailgroup becomes more hydrophobic which causes tailgroup 15-S to be more effective at reducing IFT at higher salinity conditions.

In Figure 68, the salinity of the system increases from left to right. All lines shift down when the salinity is increased. This behavior is driven by the salting out process. With increasing salinity, the hydrophobic tailgroup causes the surfactant tailgroup to be pushed out of the aqueous-phase due to the reduction in water solubility. As a result, more surfactant molecules partition to the interface and greater IFT reduction occurs. It is also important to note that as salinity increases, higher IFT value between the crude oil and the brine, without surfactant are observed. Since the variable plotted is normalized IFT, the figure already incorporates this change. And the salting out effect overcomes the increase of base case IFT since all lines shift down.

With closer inspection of Figure 68, some interaction between salinity and crude oil EF-C is observed. At lower salinity values, crude oil EF-C has the greatest IFT reduction; blue lines are the lowest line at 0% and 8% salinity. When the salinity is increased to 16% and 24%, crude oil EF-C no longer has the greatest IFT reduction. It is observed that crude oil Bk has the greatest IFT reduction. This phenomenon could be caused by two mechanisms. First, micellization is significantly enhanced at higher salinity. More micelles translates into less surfactant molecules partitioning to the interface, resulting in less IFT reduction. Second, as surfactant becomes less soluble in water, surfactant molecules can partition into the oleic-phase. More molecules transported to the oleic-phase means less molecules at the interface to reduce the IFT. Either one of the two

mechanisms is possible. More data, specifically looking at trends with temperature, will narrow down which mechanism is predominant.

The initial objective of plotting Figure 68 is to investigate the interaction between surfactant tailgroups and the crude oil. Some analysis into the interaction has been described previously. However, another method to analyze such interactions will be described. The easiest way to examine for interaction in this graph is to check for intersection between the four lines. Since the four oils are characteristically different, the four lines are located at different places on the y-axis. Intersecting lines implies that with a particular oil and tailgroup combination, IFT reduction is particularly high or low, showing that a specific interaction between the two variables exist. Parallel lines on the other hand, show that all tailgroups reduce IFT consistently from one oil to another.

The most pronounced intersection can be observed with crude oil 2H. At 16% salinity, crude oil 2H (red line) shows lowest IFT when tailgroup NP is used. While on the same condition, it shows the highest IFT compared to the other crude oil with the other tailgroups. This behavior indicates some compatibility between the crude oil and the NP tailgroup. From the GC composition, crude oil 2H has the highest composition of ring structures, like the NP tailgroup. This could explain the compatibility between the two variables.

A similar plot is generated with data at a higher temperature of 150° F as shown in Figure 69. It is observed that higher temperature results in greater IFT reduction. This behavior is driven by the EO group of nonionic surfactants. EO molecules loses the ability to maintain hydrogen bonds with water molecules at higher temperature, resulting in lower

hydrophilicity. Lower hydrophilicity implies more surfactant molecules leaves the bulk aqueous-phase and partitions at the interface, ultimately resulting in greater IFT reduction.

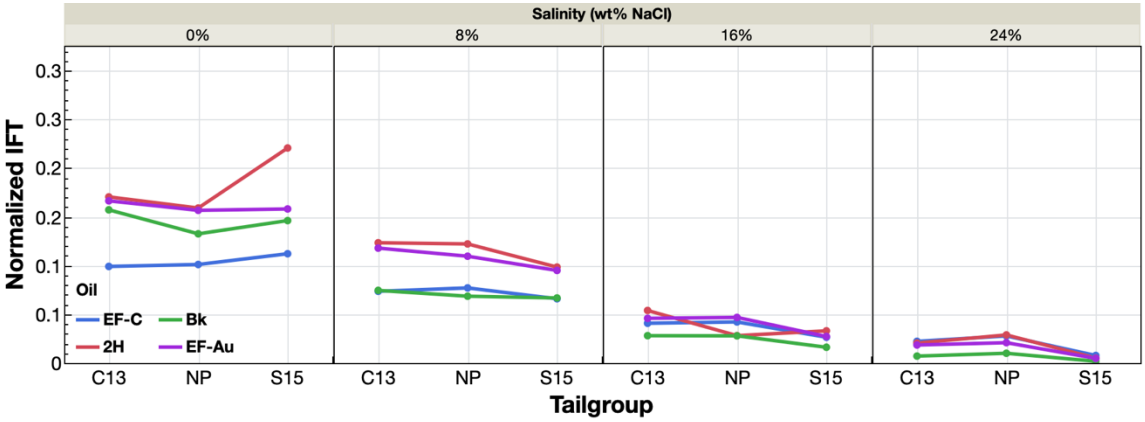

Figure 69 – Normalized IFT vs 30 EO nonionic surfactant tailgroups, grouped by oil, 150°F.

Trends observed at lower temperature are also observed at higher temperature. Tailgroup 15-S is still the least effective at reducing IFT at 0% salinity. Crude oil EF-C is still the crude oil with the greatest IFT reduction at 0% salinity. However, crude oil EF-C no longer shows the greatest IFT reduction when the salinity is increased to 16% at lower temperature. At higher temperature, the shift occurs at lower salinity. It is observed in Figure 68 and Figure 69 that crude oil Bk is the crude oil with the greatest IFT reduction at 8% salinity instead of 16%. Previously, the mechanisms behind this shift were left to two possible explanations. Based on the trend observed with temperature, the mechanism can be narrowed down to transfer of surfactant to the oleic-phase, the second mechanism in the aforementioned discussion. EO groups are the hydrophilic part of a nonionic surfactant. As previously asserted, these groups lose hydrophilicity at higher temperature.

Micelle formation implies the creation of surfactant structure that is driven by the hydrophobic-hydrophobic interaction between surfactant molecules, covered by the hydrophilic headgroup on the outside layer. This structure can only be suspended in the aqueous-phase due to the hydrophilic part of the surfactant. If the surfactant loses its hydrophilicity, like nonionic surfactants at higher temperature, micelle formation is hindered. Therefore, the mechanism behind the upward shift of crude oil EF-C and 2H at higher salinity is caused by the partitioning of surfactant molecules to the oleic-phase.

The interaction between the surfactant tailgroup and brine salinity is investigated next. The data are grouped by oil in columns and the different line colors represent the brine salinity as shown in Figure 70.

As previously stated, higher salinity results in greater IFT reduction. From Fig. 70, it becomes apparent that salinity has stronger effect on crude oil 2H, Bk, and EF-Au. Larger reductions in Normalized IFT are observed when the salinity is increased (blue-to-red-to-green-to-purple) with crude oil other than EF-C. This behavior is driven by the polarity, or more appropriately the non-polarity, of the crude oil and its relation to surfactant partitioning. Crude oil 2H, Bk, and EF-Au are not as non-polar as EF-C due to the higher content of non-Saturate components. As a result, surfactant molecule becomes more soluble in the aqueous-phase instead of partitioning to the interface. When salinity is increased, surfactant molecules favor the interface which results in greater IFT reduction. Unlike the other three crude oils, with crude oil EF-C and its stronger non-polarity, surfactant molecules are already at the interface even at lower salinity. Therefore, less IFT change occurs at the same amount of salinity increment compared to the other crude oils.

Unfortunately, this behavior applies to all tailgroups, meaning that optimization through tailgroup for crude oil EF-C is not possible. However, surfactant optimization for less non-polar crude oil can be achieved by increasing the system salinity.

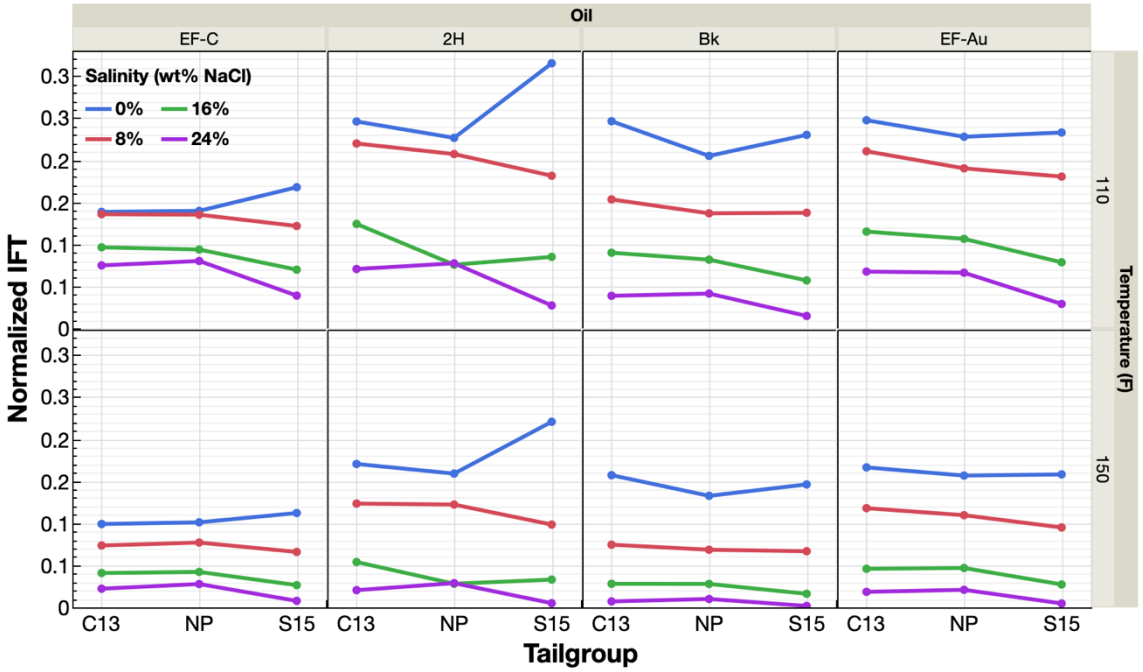

Figure 70 – Normalized IFT vs 30EO nonionic surfactant tailgroup, grouped by salinity.

Plotting the data in these graphs also accentuates the interaction of tailgroup 15-S with salinity. Salinity increment results in greater IFT reduction from this tailgroup and this trend is consistently observed on all crude oils and at all temperatures. The normalized IFT value of the 15-S tailgroup is always the highest value compared to the two other tailgroup structuresat lower salinity. As the salinity is increased, the normalized IFT value gradually lowers to be the lowest value of the three tested tailgroups at above 16% salinity.

This clearly shows the increasing efficacy of tailgroup 15-S when applied at higher salinity.

The Effect of EO Length Interaction with Crude Oil and Salinity to IFT Reduction

In this section, the interaction between the length of the EO group and the crude oil is investigated. The data used are from the NP surfactants which has a range of EO lengths from 12 to 55. Normalized IFT variables are utilized once again here on the y-axis, plotted against the EO length on the x-axis as shown in Figure 71. In this figure, IFT data at 110°F are presented, grouped by the salinity level in columns, and by crude oil as observed in the colored lines.

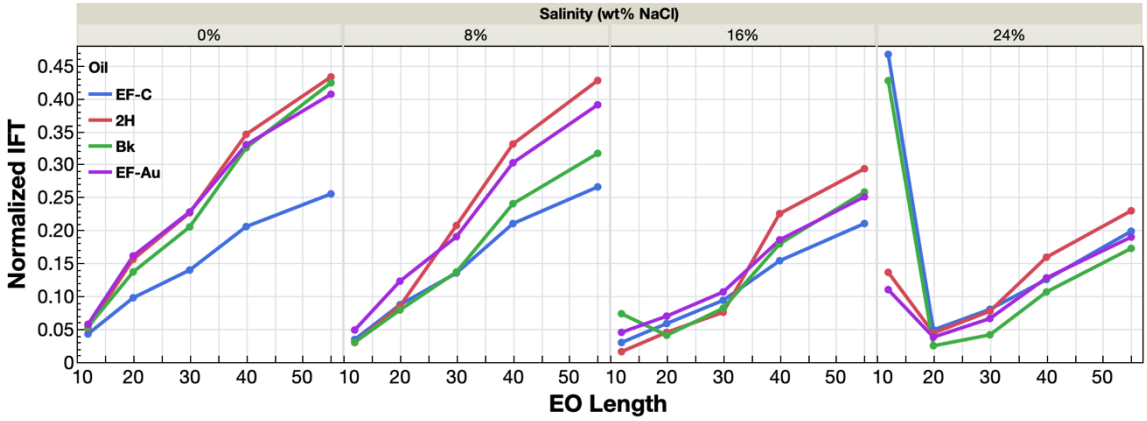

Figure 71 – Normalized IFT vs EO Length of NP surfactants, grouped by crude oil, 110°F.

A positive trend between normalized IFT and EO group length is observed as expected. From the description in the previous section, a longer EO group increases the surfactant solubility in the aqueous phase which decreases the amount of surfactant

molecules at the interface. However, the trend does not apply with 12 EO group at higher salinity level. This behavior has also been explained previously and attributed to the cloud point proximity of the NP-12 surfactants at the respective temperature.

At 0% salinity, all crude oils except for EF-C fall virtually on the same line that is greater than observed for EF-C. The explanation behind this behavior has been covered in the previous section. Increasing the brine salinity results in observed interaction between crude oil and EO group. With higher salinity, increased IFT reduction is observed with crude oil 2H and Bk with shorter EO groups than the normalized IFT value of crude oils EF-C's. With crude oil Bk, the intersection begins at an EO group of 20 at 8% salinity, starts at 30 at 16% salinity, and falls below EF-C for all EO lengths at 24% salinity. This behavior is similar in nature to the interaction observed between surfactant tailgroups and crude oil in the previous section. Greater IFT reduction occurs when more surfactant molecules are present at the interface. The only difference being that previously the surfactant is driven to the interface based on the tail group structure, whereas now it is driven by the headgroup structure. With shorter EO groups, the surfactant is less hydrophilic which causes the surfactant to partition to the interface more. The effect is enhanced with higher salinity since both shorter EO and higher salinity causes the surfactant to be less hydrophilic.

Crude oil 2H shows an intriguing trend. With shorter EO groups, it has the largest IFT reduction. With longer EO group however, the IFT reduction for this crude oil is the lowest. This behavior is in essence describing an interaction between EO length and crude oil and is significantly affecting the surfactant performance by reducing IFT. The

mechanism behind this is still the effect of EO group length in relation to the hydrophilicity of the surfactant. However, it appears that the effect is accentuated for crude oil 2H. This phenomenon indicates that longer EO group (longer than 30) might not be suitable for application in reservoir that contains crude oil like 2H.

Figure 71 is repeated in Figure 72 with data at a temperature of 150°F. In the two figures higher temperature results in larger IFT reduction; the y-axis limit is smaller at higher temperature. This behavior is driven by the properties of nonionic surfactants. Having EO groups as its hydrophilic headgroup causes the hydrophilicity of the surfactant to decrease at higher temperature. As a result, more surfactant partitions to the surface and a lower IFT is observed.

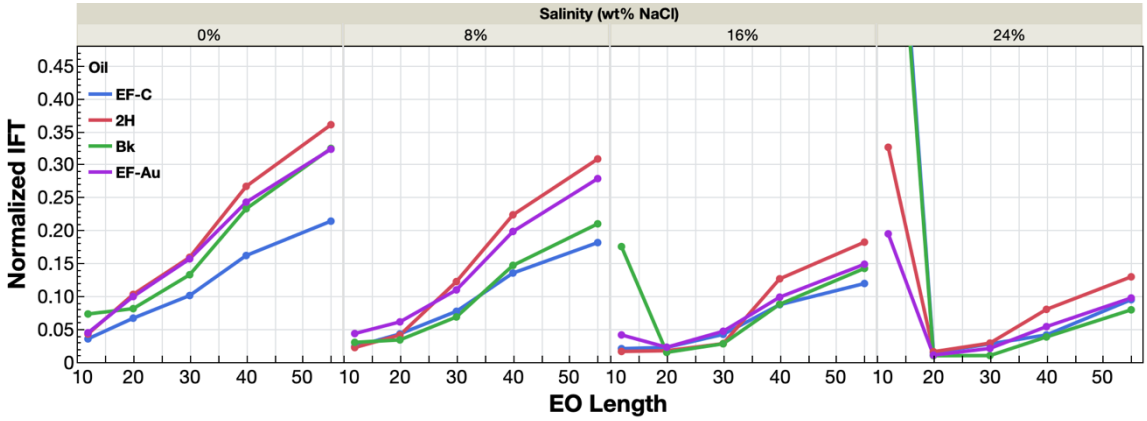

Figure 72 – Normalized IFT vs EO Length of NP surfactants, grouped by crude oil, 150°F.

With the two graphs at higher temperature, the trend deviation onset at 12 EO groups occurs earlier at lower salinity and with a greater change. This behavior is also driven by the temperature effect on the EO group hydrophilicity. Since both temperature and salinity

negatively affecting the hydrophilicity of the EO group, the combination of high temperature and high salinity results in significant reduction of EO group hydrophilicity.

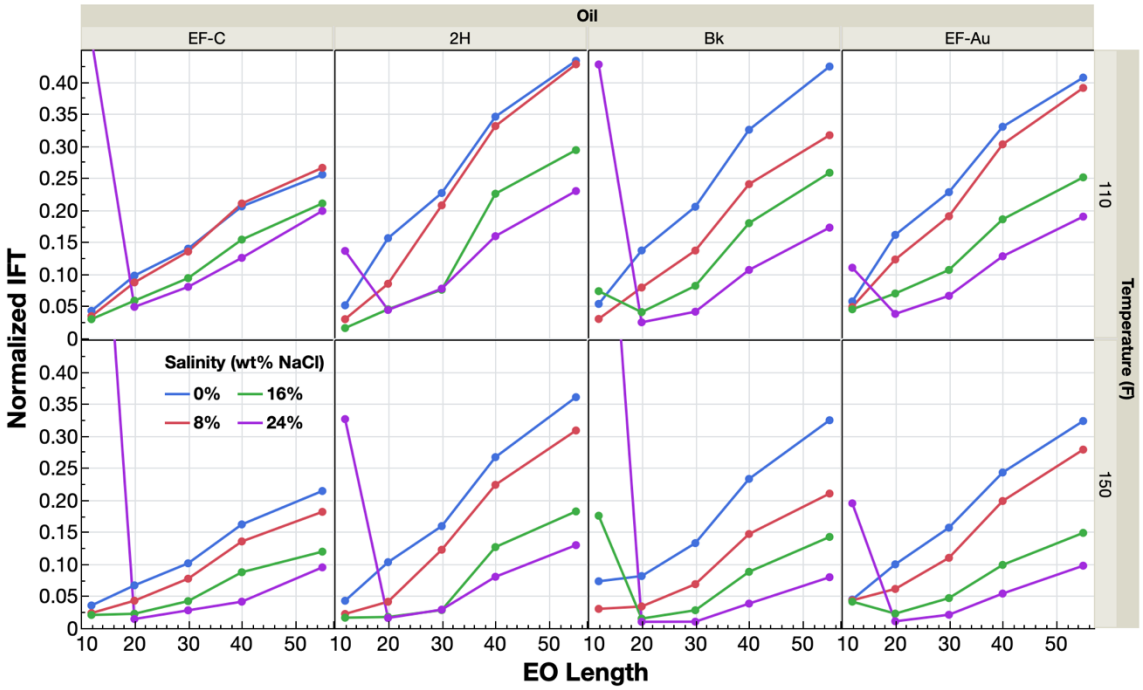

Figure 73 – Normalized IFT vs EO Length of NP surfactants, grouped by salinity, 110°F, 150°F, 190°F.

The interaction between EO length and salinity is discussed next. The graphs are presented in Figure 73. From the figures, parallel lines are observed instead of intersecting lines which indicates interaction between EO length and salinity does not exist. Increasing salinity lowers the IFT of the system. But all graphs show that all lines are parallel one to another which indicates that EO length and salinity do not interact. Except for the case of 12 EO, which was previously discussed. Higher temperature lowers the magnitude of normalized IFT with parallelism maintained between the curves. This behavior means that

salinity, with a constant tail group, affects the EO group of the surfactant in a consistent manner from one crude oil to another and from one temperature to another.

Optimum Nonionic Surfactant Tailgroup Structure for Lower 48 Shale

In this section, hydrophobic-hydrophobic interaction between the surfactant tailgroup and crude oil is scrutinized further. A new term, $\boldsymbol{R_{oil}}$, represents the crude oil characteristic with a single number. This term is derived from the composition of each oil from gas chromatography. Hydrocarbon chains in each crude oil are grouped to: linear hydrocarbons with less than and equal to 10 carbon atoms, linear hydrocarbons with more than 10 carbon atoms, and cyclic hydrocarbons. The term $\boldsymbol{R_{oil}}$ is calculated by taking the ratio of the short linear hydrocarbons to the sum of long linear and cyclic hydrocarbons as shown in $R_{oil} = \frac{L_{C<10}{}^{*}}{L_{C\geq 10}{}^{*}+C^{*}}$..... Equation **2**. The formula is constructed to represent the polarity of the crude oil. Short linear hydrocarbons are strongly non-polar and it is used as the numerator of the equation. Both long linear and cyclic hydrocarbons are more polarizable compared to short linear hydrocarbons. Therefore, it is utilized as the denominator of the $\boldsymbol{R_{oil}}$ term. A larger $\boldsymbol{R_{oil}}$ value means the crude oil is highly non-polar, while lower $\boldsymbol{R_{oil}}$ value means the crude oil is less non-polar.

Nonionic surfactants with 30EO are selected since there are three tailgroup structures that has a 30EO headgroup: C13, secondary C15, and nonylphenol. The tailgroup is plotted against the $\boldsymbol{R_{oil}}$ in Figure 74. These tailgroups are ordered by the number of carbon atoms they contain: 13, 15, and 19 respectively. The data at different salinity and temperature are presented in columns and rows respectively. Salinity increases from the

left to right columns. Temperature increases from the top to the bottom row. In each box, a single line represents the combination of tailgroup structure and $\boldsymbol{R_{oil}}$ that provides the lowest normalized IFT at each respective salinity and temperature. For example, tailgroup NP gives the greatest IFT reduction on less polar crude oils (smaller $\boldsymbol{R_{oil}}$ value) while tailgroup TD has the best compatibility for strongly non-polar crude oil in the top-left box, while tailgroup 15-S has the best compatibility to all crude oils in the bottom-right plot.

At zero salinity and low temperature (top-left box), the linear tail group is more compatible with the more non-polar crude oil. Reducing the non-polarity of the crude oil results in a shift of the compatible tailgroup to the longer and more complex tailgroup. The NP tailgroup contains more carbon atoms and more importantly, includes a cyclic structure. It can be observed that strongly non-polar oil does not have the strongest hydrophobic-hydrophobic bond with this tailgroup structure. As a matter of fact, this statement holds true for all fifteen salinity and temperature conditions: increasing salinity and temperature results in the secondary linear C15 tail group providing the highest IFT reduction. From the previous section, it was hypothesized that the secondary C15 tailgroup maintains its linear shape at higher salinity resulting in longer hydrocarbon chain when compared to the linear C13. Therefore, it can be concluded that highly non-polar crude oils have the highest compatibility with linear hydrocarbon tailgroups. Longer linear hydrocarbon chain tailgroups improves the hydrophobic-hydrophobic bond to the oil molecule, enhancing the compatibility to produce the lowest IFT value.

The NP tailgroup is more compatible to less non-polar oils as presented in the top-left box of Figure 74; tailgroup NP has the lowest normalized IFT at lower $\boldsymbol{R_{oil}}$ value. The NP

tailgroup while heavier also contains cyclic hydrocarbons. With the composition of cyclic hydrocarbon as one of the denominators of the $\boldsymbol{R_{oil}}$ equation, it is hypothesized that this tailgroup would have better compatibility with crude oil with lower $\boldsymbol{R_{oil}}$ value. This is supported by the compatibility of tailgroup NP with the two crude oils with 0.4 to 0.5 $\boldsymbol{R_{oil}}$ value. These two crude oils have higher content of cyclic hydrocarbon compared to the other two crude oils with the highest and lowest $\boldsymbol{R_{oil}}$ value. As a result, tailgroup NP has the best compatibility with these crude oils in the range of salinity and temperature tested; tailgroup NP is compatible with the two intermediate crude oils at all temperatures and from 0% and 16% salinity is also compatible up until 120°F at 8% salinity. Tailgroup NP is compatible with a high $\boldsymbol{R_{oil}}$ value only at 0% salinity because this crude oil is composed more of long linear hydrocarbon than cyclic hydrocarbon. At any other salinity and temperature condition, secondary C15 is more compatible with this oil. Therefore, it can be concluded that tailgroup NP should be used for crude oils with high content of cyclic hydrocarbons due to the compatibility between the ring structures that exist in both the tailgroup and in the crude oil.

The behavior of the 15S tailgroup for changing salinity has been covered in the previous section. Increasing the salinity results in the shift of the hydrocarbon chain conformance into a more linear shape from a V-shaped. In Figure 74, the most compatible tailgroup changes from linear C13 to NP to 15S at low salinity and low temperature. While at higher salinity and temperature, moving to the right columns and the bottom rows, the most compatible tailgroup structures for all ranges of $\boldsymbol{R_{oil}}$ shifts to 15S. This behavior is believed to be driven by the 15S conformance change mentioned earlier. However, the

specific reason for the deviation of the cyclic-hydrocarbon-rich crude oil from the NP tailgroup to the 15S is not fully understood. One hypothesis is that the polarizable nature of the cyclic structure is enhanced at higher salinity and temperature, resulting in less hydrophobic-hydrophobic bond to the surfactant tailgroup. Further investigation is necessary to confirm this hypothesis. Nevertheless, it can be concluded that with the surfactant headgroup being equal, the secondary C15 tailgroup structure should be used for systems at high temperature and high salinity.

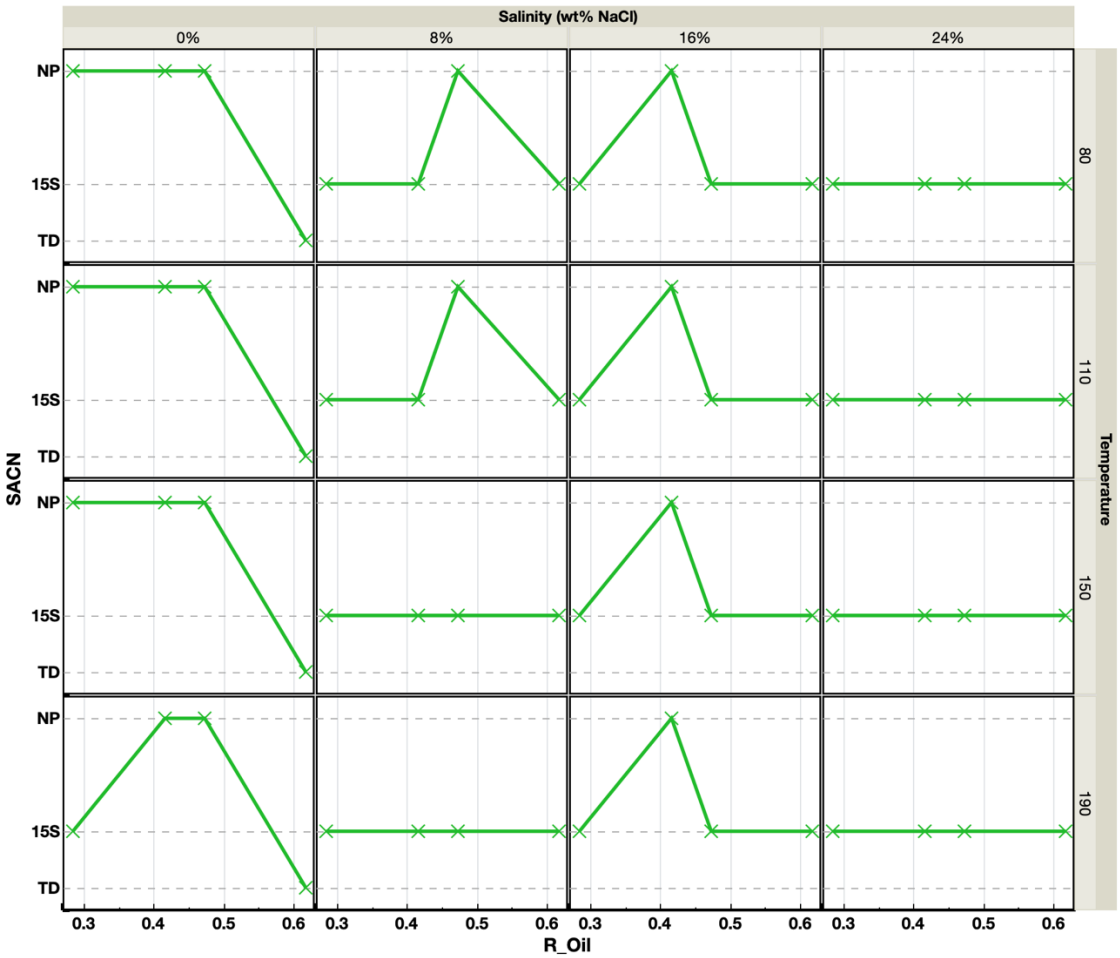

Figure 74 – Optimum tailgroup structure for Lower 48 shale crude oil.

The discussion above regarding the compatibility of secondary C15 brings up an important detail. As observed in Figure 74, the most compatible tailgroup structure varies not just with different $\boldsymbol{R_{oil}}$ values, but also with changing salinity and temperature. The headgroup structure of the surfactants are kept constant in the data presented in the figure. Clearly there is an interaction between the system salinity and temperature to the tailgroup of the surfactant. Most of the equations found in the literature to define the state of the surfactant in an oil/brine system (e.g. HLD, NAC, etc.) does not incorporate this interaction. In this study, crude oil characteristics, surfactant structure, salinity, and temperature are utilized as separate independent variables without accommodating the interaction between each variable. Constructing a new equation to embody the complex interaction between the system condition and surfactant structure would require a significantly larger database. However, a new surfactant equation-of-state still needs to be assembled in further research.

Optimum EO Length of Ethoxylated Nonylphenol Surfactants for Lower 48 Shale

In this section, the effect of EO group length is scrutinized further. Surfactants with the NP tailgroup are selected with EO ranges from 12 to 55. Figure 74 is recreated into Figure 75 with the EO length replacing the SACN on the y-axis. In addition to the minimum normalized IFT value, the maximum normalized IFT value is also included. The EO length that reduces IFT the most is presented in green and the EO length that reduces IFT the least is presented in red.

The EO length controls the partition of the surfactant to the interface. With the tailgroup structure held constant, the surfactant partitions to the interface in a more consistent manner with increasing salinity and temperature. This has been covered in the previous section. As a result, 12 EO would have the lowest IFT and 55 EO would have the largest IFT. These are observed in most of the plots in Figure 75 until 16% salinity and 150°F.

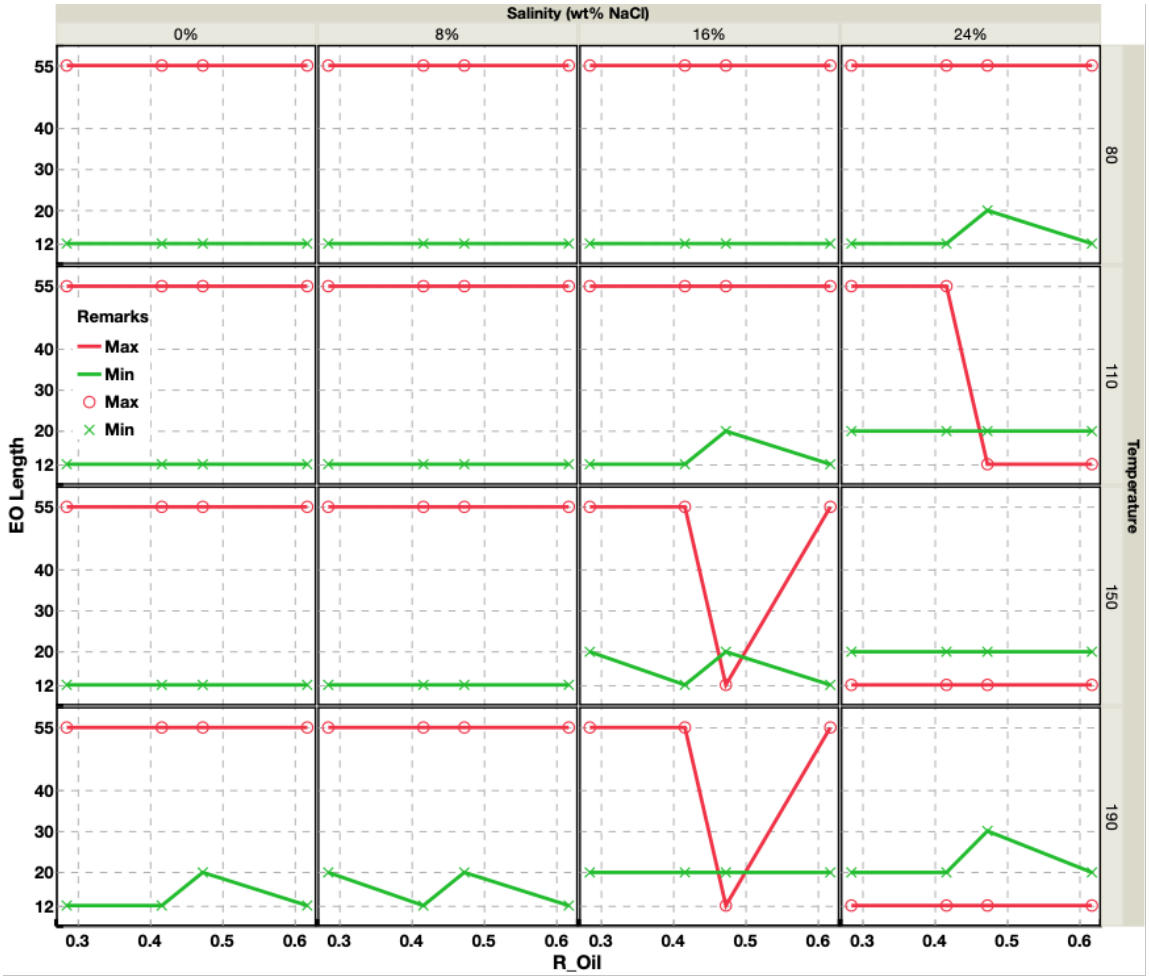

Figure 75 – Optimum EO length for NP surfactants determined for Lower 48 shale crude oil.

Figure 75 also presents the EO length that results in the least IFT reduction which is labeled in red. Headgroup 55 EO has a maximum at almost all salinities, temperatures, and $\boldsymbol{R_{oil}}$ values. Longer EO groups result in the surfactant being more hydrophilic, thereby reducing partitioning to the interface and ultimately decreasing IFT reduction. However, headgroup 12 EO is observed to replace 55 EO as the maxima at high salinity and high temperature. This behavior is driven by the cloud point of the shorter EO headgroup. Once the cloud point is surpassed, the surfactant loses its amphiphilic nature. As a result, the IFT reduction is now lacking and at some conditions could be less than the IFT reduction of 55 EO headgroups. Therefore, it is important to be aware of surfactant cloud point at the system salinity and its relation to system temperature. Applying EO groups that are too short, with a cloud point far below the reservoir temperature, may result in an ineffective surfactant system.

CHAPTER VIII

SURFACTANT STRUCTURE EFFECT TO WETTABILITY

More than 3,000 contact angle data are included in this study. The base wettability of unconventional reservoir system is investigated first along with the effect of variation of each phase. Then the wettability alteration performance of individual surfactant is analyzed. In this section, the effect of crude oil characteristics, system salinity, temperature, and rock mineralogy on surfactant performance in altering wettability are also investigated. Surfactant NP-12, NP-30, NP-55, TD-30, 15-S-30, C12TAC, C18TAC, S-2, and CG-50 are included in this section. Then, the interaction between the EO length of the surfactant to the variation of oil, brine, and temperature are explored. And finally, the same exercise is repeated on the tailgroup structure of the nonionic surfactant.

Wettability Alteration Data Processing

Due to the nature of the measurements often contact angle data is not recorded at the exact temperature for each of the surfactant, crude oil, rock, and brine combination tested. Using the data as-is would significantly complicate the analysis. Therefore, curve fitting of contact angle vs temperature is performed on each of the combinations tested. Then using the curve fit, a new contact angle vs temperature plot is constructed at the desired temperature. The five-coefficients biexponential function is used and the fit is presented in Figure 76 with 0.99 R^2 value.

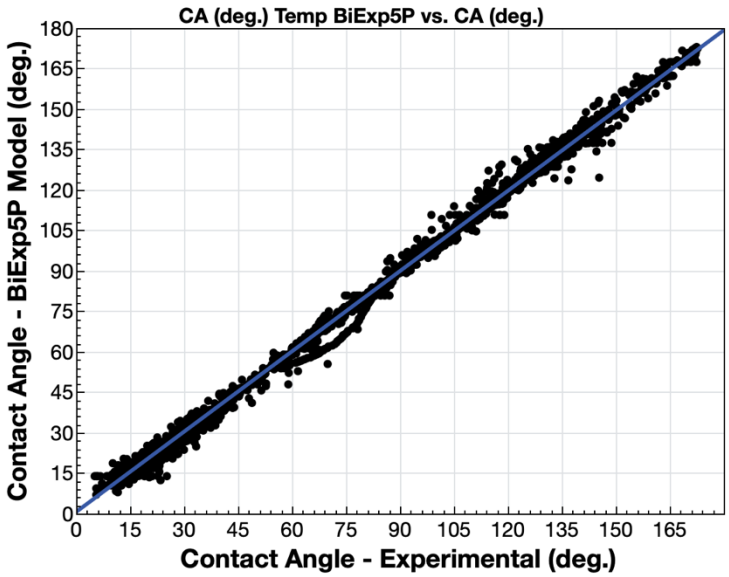

Figure 76 - Contact angle data fit using five-coefficients biexponential function.

Base Wettability of Shale

The base wettability of the system investigated in this study is presented in Figure 77. A more detailed work on the wettability of domestic unconventional reservoir system is available in our previous publication (Saputra et al. 2022) . In the left-hand plot of Figure 77, contact angle data of crude oil EF-C, 2H, Bk, and EF-Au on the calcite-rich reservoir samples are presented. The left-hand plot in Figure 77 contains data measured at 0% salinity and the righthand plot contains 8% salinity data. These four crude oil samples are oil-wet on calcite-rich rock surface with different degree of oil-wetness. At lower salinity, the oil-wetness decreases in order of EF-Au, 2H, Bk, and EF-C. All crude oil except for crude oil EF-Au shows minimal effect of temperature on the wettability. Even for crude oil EF-Au, the contact angle only changes by 20° for temperature change of 160°F.

At higher salinity condition (left box of the right figure of Figure 77), all four crudes are still at oil-wet conditions. Increasing salinity results in increasing oil-wetness, this is observed with crude oil EF-C and Bk. While for crude oil EF-Au and 2H the samples are observed to be more water-wet but still in the oil-wet region (CA > 105). Similar to the lower salinity condition, temperature is also observed to have minimal effect on sample wettability.

In Figure 77, the effect of mineralogy to the base wettability is highlighted. With the same crude oil and salinity, changing the rock mineralogy from carbonaceous to siliceous results in increasing oil-wetness. This result confirms our previous finding (Saputra et al. 2022).

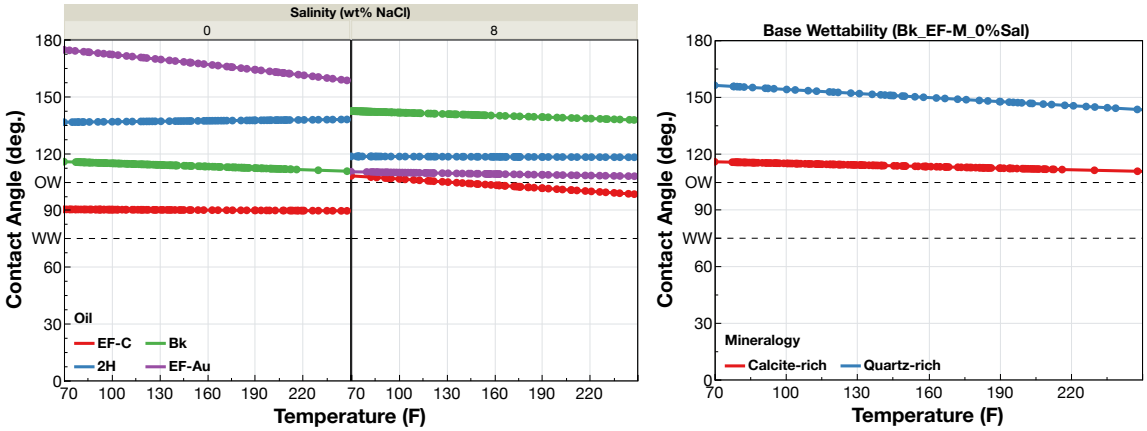

Figure 77 - Base wettability on calcite-rich mineralogy that highlights the effect of temperature, crude oil, and salinity (left) and base wettability of oil Bk that focuses on the effect of mineralogy to the wettability (right).

Surfactant Wettability Alteration Performance: Effect of Oil, Salinity, Temperature, and Mineralogy

In this section, the effect of crude oil, salinity, temperature, and mineralogy on wettability alteration of each surfactant is investigated. Nonylphenol ethoxylated surfactant family is presented first with EO groups of 12, 30, and 55. Then, the nonionic tailgroup is changed to linear tridecanol and secondary pentadecanol while keeping the EO length consistent at 30. Once the effect of the system conditions on wettability of nonionic surfactants is covered, the effect on wettability alteration of ionic surfactants is analyzed. Cationic surfactants C12TAC and C18TAC are included, keeping the headgroup trimethyl ammonium constant with two hydrocarbon chain lengths.

Nonionic Surfactant: Nonylphenol Ethoxylate Family

The wettability alteration of surfactant on four different crude oils is presented in the top-left of Figure 78. These contact angle data are compiled for calcite-rich mineralogy and 0% salinity. Four temperature levels are presented as different colors. This surfactant can render the surface water-wet (contact angle below 30°) on all crude oils tested except for the EF-Au crude oil, which is the heaviest crude oil with the highest content of polarizable crude oil components. From the base wettability section above, the EF-Au crude oil also results in the strongest oil-wet surface which results in a less water-wet condition for surfactant NP-12. The effect of salinity on the performance of surfactant NP-12 is presented in the top-right of Figure 78. Contact angle data are gathered from calcite-rich system at 70°F (left box) and 120°F (right box). The four crude oils are presented in

different colors. Increasing salinity to 8% reduces the ability of surfactant NP-12 to render the surface water-wet as observed by the positive trend between the contact angle vs. salinity. The temperature effect on the ability of surfactant NP-12 to render the surface water-wet is presented in the bottom-left of Figure 78. With crude oil EF-Au, surfactant NP-12 is observed to have less wettability alteration capability. At higher temperature, this surfactant can render a surface more water-wet with contact angle shifting from 100° to 80° as observed in the figure. On systems where this surfactant can render a water-wet surface (crude oil EF-C, 2H, and Bk), increasing temperature results in increase of contact angle value or reduction of water-wetness. The temperature effect observation is compiled from calcite-rich surfaces and 0% salinity. On the bottom-right of Figure 78, the effect of mineralogy to wettability alteration is presented. Surfactant NP-12 completely lose its wettability alteration capability when the mineralogy is shifted from calcite-rich to quartz-rich. A quartz-rich mineralogy is observed to have stronger oil-wet base wettability which makes it more difficult for the surfactant to alter the wettability of the surface.

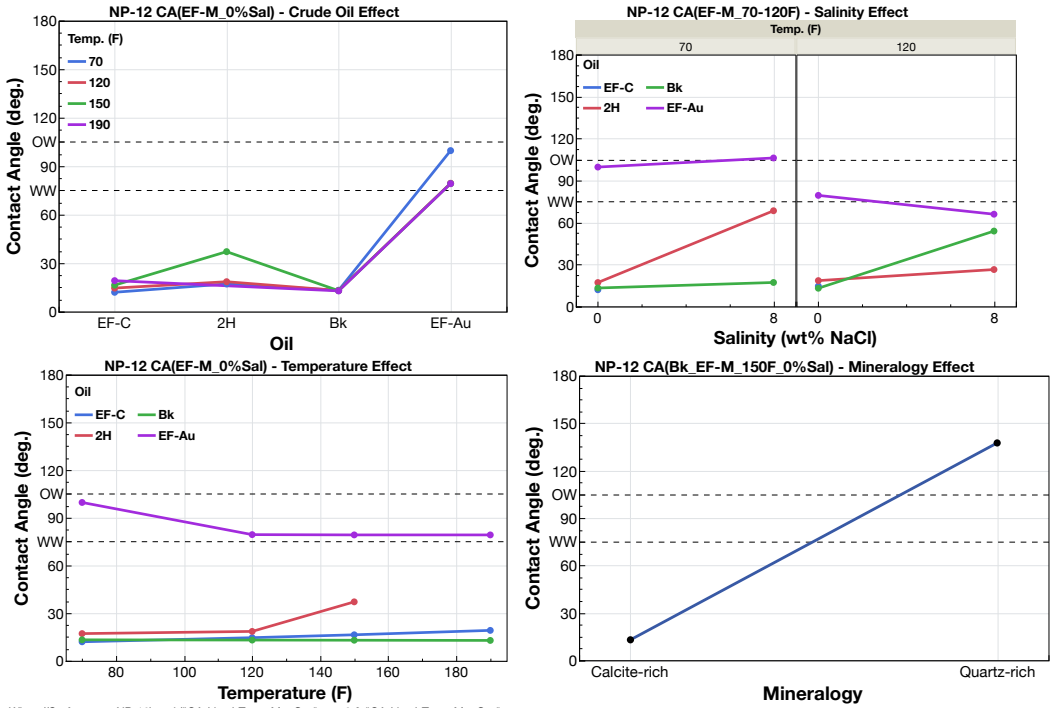

Figure 78 - Crude oil (top-left), salinity (top-right), temperature (bottom-left), and mineralogy (bottom-right) effect to wettability alteration of nonionic surfactant NP-12.

The next surfactant has the same tailgroup structure with the EO group length extended to 30 thus making it a more hydrophilic surfactant. The effect of having more EO groups will be investigated in the latter part of the study. In this section, the same exercise of analyzing the effect of the system condition as the previous surfactant is performed. On the top-left of Figure 79, the effect of crude oil on wettability alteration of NP-30 is presented. Unlike the previous surfactant, differences in wettability alteration from one crude oil to another is more prominent. With surfactant NP-12, crude oil EF-C, 2H, and Bk are all strongly water-wet with contact angle value less than 30°. With NP-30, water-wetting is only observed with crude oil EF-C and Bk. Even with these two crude oils, contact angle differences of up to 15° are observed with EF-C showing more water-

wetness. Crude oil 2H and EF-Au are not in the water-wet region with NP-30, but still less oil-wet when compared to the base case. Looking at the effect of salinity and temperature (top-right and bottom-left of Figure 79, both system variables show positive trend to the water-wetness of the rock surface with surfactant NP-30. Additionally, surfactant NP-30 is observed to be more sensitive to changes of these two system conditions when compared to NP-12. However, a different trend is observed with mineralogy. While changing the mineralogy from calcite-rich to quartz-rich still results in the reduction of the effectiveness of the surfactant in rendering the surface water-wet, the contact angle value change between the two mineralogies is less when compared to NP-12.

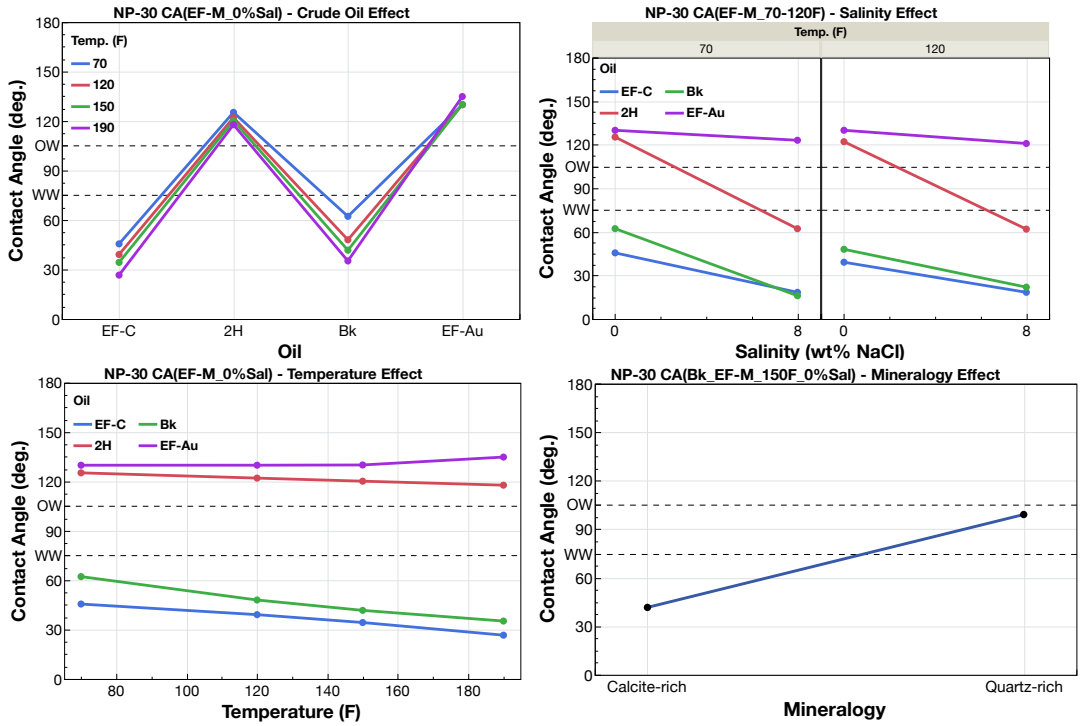

Figure 79 - Crude oil (top-left), salinity (top-right), temperature (bottom-left), and mineralogy (bottom-right) effect to wettability alteration of nonionic surfactant NP-30.

For the next surfactant, the nonylphenol ethoxylated surfactant is made more hydrophilic by extending the number of EO groups to 55. The effect of crude oil (top-left), salinity (top-right), temperature (bottom-left), and mineralogy (bottom-right) on wettability alteration of this surfactant is presented in Figure 80. Surfactant NP-55 can only render water-wetness on the system containing crude oil 2H. With crude oil EF-Au, a minimal change of contact angle is observed, whereas for crude oil EF-C and Bk, the surfactant renders the rock surface more oil-wet than the base case. At higher salinity, surfactant NP-55 renders the surface water-wet with crude oil EF-C while at lower salinity the surface oil-wetness was increased. With all crude oils, increasing the salinity of the system improves surfactant performance (top-right Figure 80). This trend is enhanced at higher temperature. However, changing only the temperature without increasing salinity does not result in major change of contact angle values (bottom-left Figure 80). Like the previous two surfactants, NP-55 loses its ability to render the surface water-wet when the mineralogy is shifted from calcite-rich to quartz-rich.

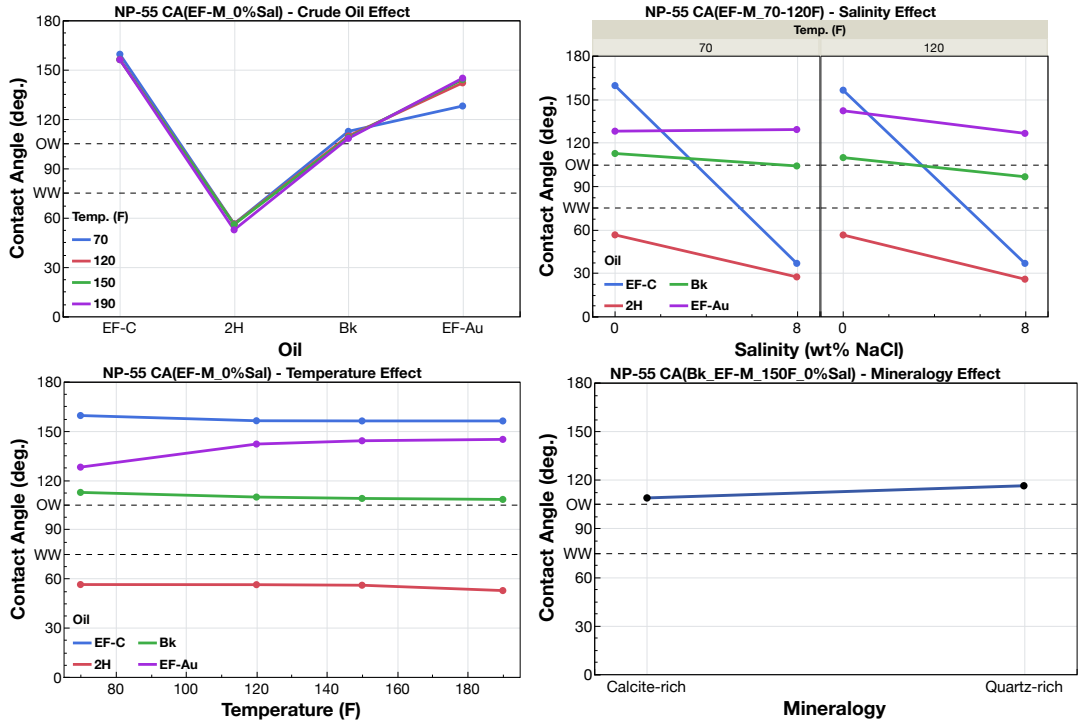

Figure 80 - Crude oil (top-left), salinity (top-right), temperature (bottom-left), and mineralogy (bottom-right) effect to wettability alteration of nonionic surfactant NP-55.

Nonionic Surfactant TD-30

Surfactant TD-30 has linear tridecanol as its tailgroup with 30 EO on the headgroup. Crude oil, salinity, and temperature effect on the wettability alteration performance of this surfactant is presented in Figure 81. TD-30 renders a strong water-wet condition only with crude oil EF-C. When applied on crude oil 2H and Bk, a water-wet condition is still observed but at a greater contact angle value (60° instead of <30°). Like NP-30, TD-30 is unable to render the surface water-wet with crude oil EF-Au. For the two crude oils (2H and EF-Au) where surfactant TD-30 does not alter wettability, increasing the salinity does improve the tendency to water-wetness. This is especially so when combined with a higher temperature application. Crude oil EF-Au, which has contact angle of more than 120° at

low temperature and low salinity with surfactant TD-30, has a contact angle of 60° when applied at higher temperature and salinity. On the other hand, for crude oil EF-C, where strong water-wetness is already achieved at lower salinity, increasing the salinity results in the reversal of the wetting effect to the more oil-wet region. Increasing temperature results in minimal change of contact angle value (bottom Figure 81). However, it is interesting to note that with crude oil EF-C the trend of contact angle and temperature is a positive trend. While for the other three crude oil, the trends are all negative. For crude oil EF-C, water-wetness is already observed for surfactant TD-30 at lower temperature and increasing the temperature further reduces the water-wetness. On the other hand, less water-wetness is observed for crude oil 2H, Bk, and EF-Au at lower temperature. Increasing the temperature for this system results in a stronger water-wet surface.

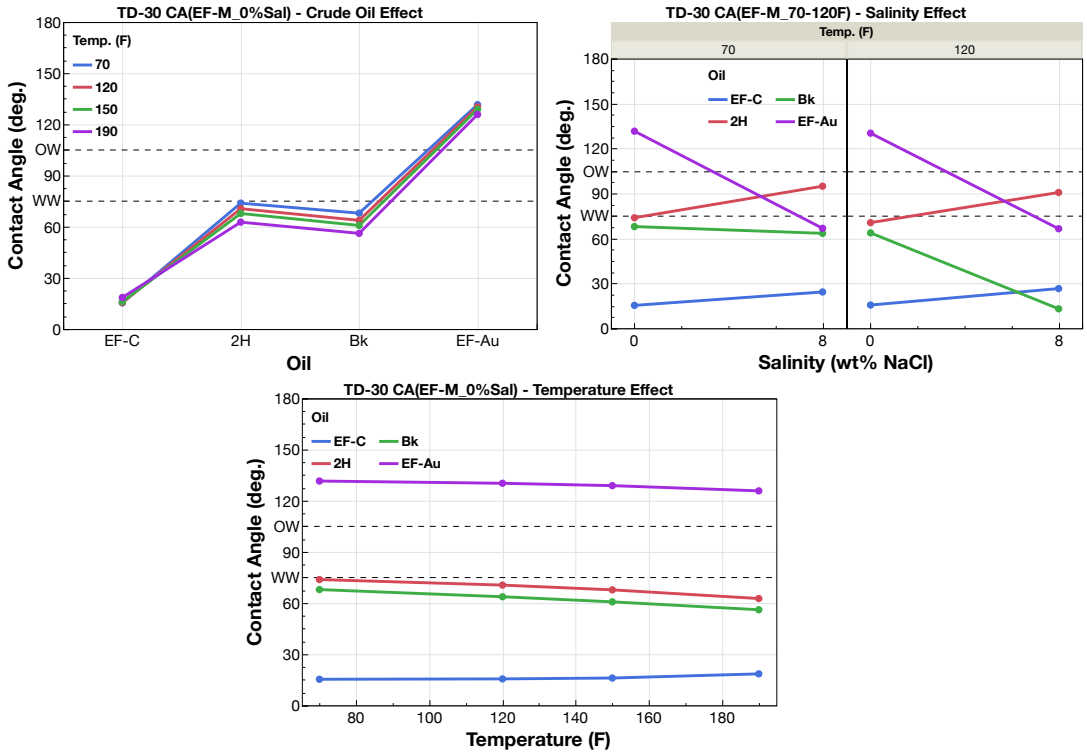

Figure 81 - Crude oil (top-left), salinity (top-right), and temperature (bottom) effect to wettability alteration of nonionic surfactant TD-30.

Nonionic Surfactant 15-S-30

For the last nonionic surfactant, a different tailgroup structure with 30 EO headgroup is analyzed. Surfactant 15-S-30 has pentadecanol as its tailgroup with the EO group sitting in the middle of the tailgroup chain instead of at the end, making it a secondary ethoxylated alcohol nonionic surfactant. The wettability measurement results of this surfactant to investigate the effect of crude oil, salinity, and temperature are provided in Figure 82. Surfactant 15-S-30 can only alter the wettability with a system containing crude oil Bk. For the other three crude oil systems used, the contact angle value, once the surfactant is applied, are all above 90°. For crude oil EF-C, the surfactant actually renders the surface more oil-wet similar to surfactant NP-55. Salinity increases results in better wettability

alteration for crude oil EF-C, 2H, and Bk. This behavior is observed in the previous chapter on surfactant IFT reduction where the secondary alcohol tailgroup results in stronger interfacial activity at higher salinity levels. Increasing the system salinity does not improve the wettability alteration on crude oil EF-Au system where the wettability of the system is more oil-wet with surfactant 15-S-30 at higher salinity level. Temperature increase results in improved water-wetness. In comparison with previous surfactants with the same 30 EO headgroup, surfactant 15-S-30 shows the greatest sensitivity to temperature.

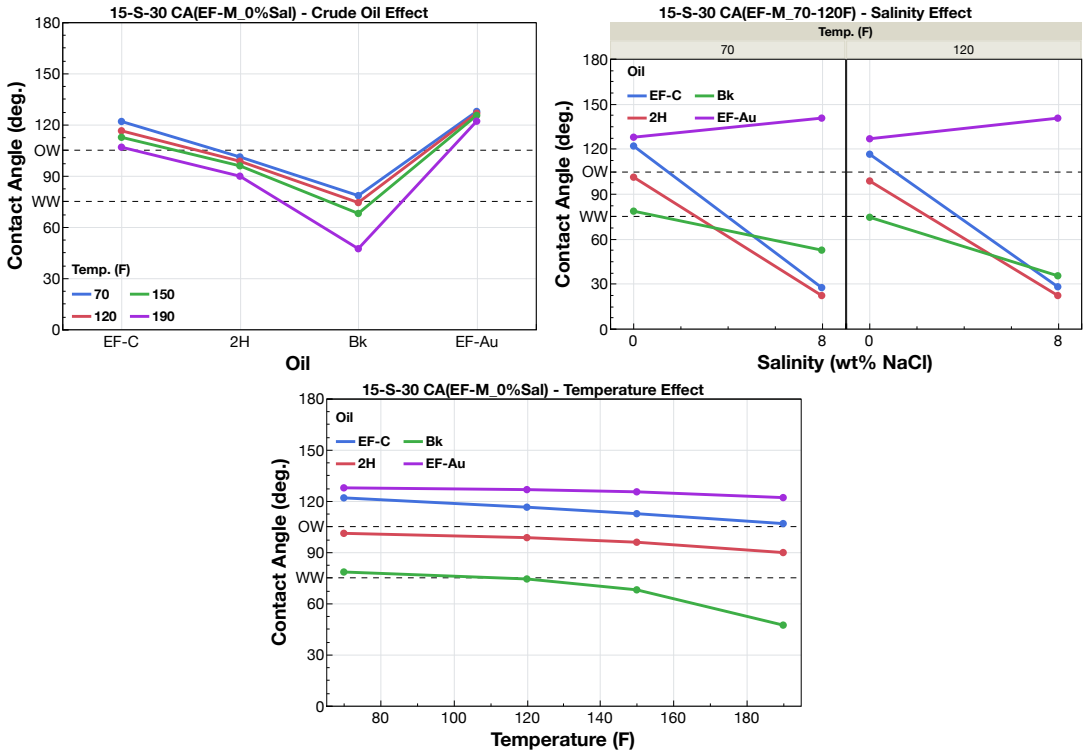

Figure 82 - Crude oil (top-left), salinity (top-right), and temperature (bottom) effect to wettability alteration of nonionic surfactant 15-S-30.

The five previous surfactants are all nonionic surfactants. In this section, the behavior of ionic surfactants at variable system conditions is investigated. Surfactant C12TAC has dodecane tailgroup with trimethylammonium as its headgroup. The effect of crude oil composition (top-left), salinity (top-right), temperature (bottom-left), and mineralogy (bottom-right) are presented in Figure 83. Reducing the non-polarity of the crude oil results in the degradation of the wettability alteration performance of the surfactant. This is observed as positive correlation between contact angle and crude oil. The four crude oils are plotted in descending order according to saturate content. Increasing the system salinity also improves the water-wetting properties of the surfactant, similar to the observation with nonionic surfactants. However, unlike the nonionic surfactants, increasing temperature results in reduction of wettability alteration for the cationic surfactant. The thermal stability is observed to be a problem for cationic surfactants where an initially water-wet condition at lower temperature could turn into oil-wet when the temperature is raised to 180°F. This is the opposite of the trend observed with nonionic surfactants where higher temperature generally leads to better wettability alteration. Mineralogy is observed to have minimal impact on surfactant performance.

Thermal stability is a problem for cationic surfactants. Having a cationic charge implies that the hydrophilicity of the surfactant is achieved by ionic bonds between the headgroup of the trimethylammonium head and the water molecule. Since the ionic bond strength has positive correlation with temperature, increasing the temperature would increases the surfactant solubility in water. This reduces the amount of surfactant molecules at the interface and ultimately reduces the wettability alteration potential of the

surfactant. Increasing the tailgroup hydrophobicity, increasing the system salinity, and increasing the surfactant concentration could reduce the thermal effect of surfactant hydrophilicity.

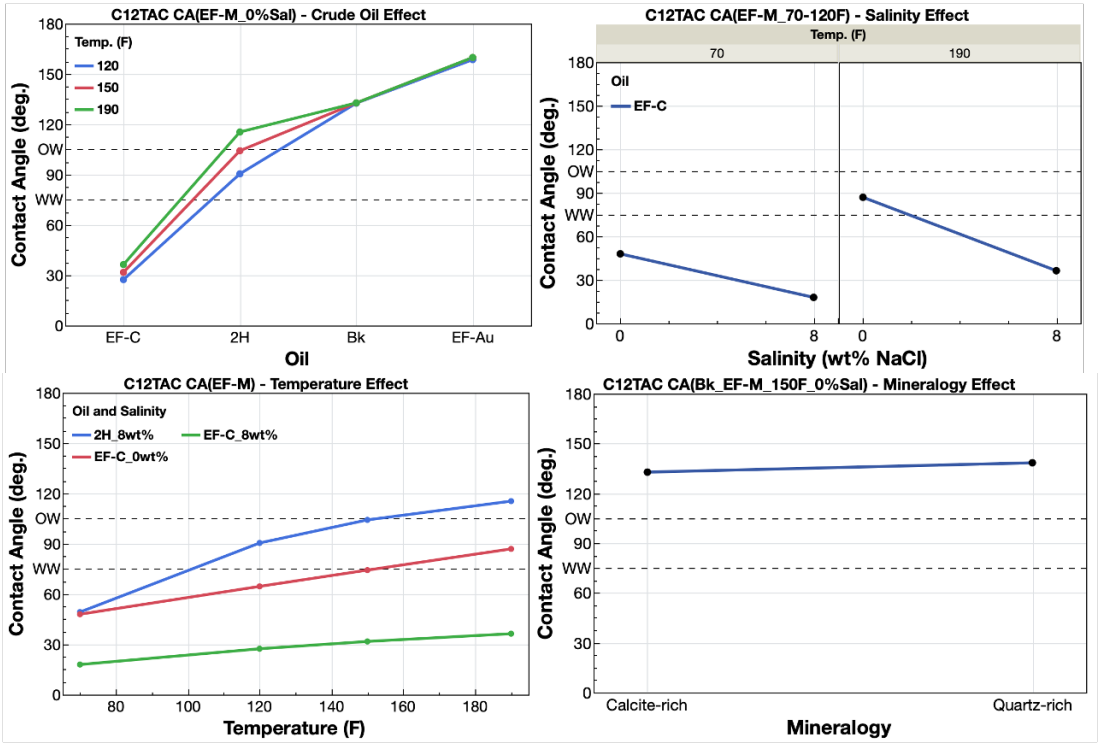

Figure 83 - Crude oil (top-left), salinity (top-right), temperature (bottom-left), and mineralogy (bottom-right) effect to wettability alteration of nonionic surfactant C12TAC.

The thermal stability of three cationic surfactants, C12TAC, C18TAC, and 1010 are presented in Figure 84. Surfactant C18TAC (green line) has significantly better thermal stability than C12TAC (red line). Where C12TAC shows a positive trend between contact angle and temperature from room temperature upward. Surfactant C18TAC maintains water-wetness to up to 250°F before the thermal effect is observed. Increasing the

tailgroup chain length from 12 to 16 reduces the thermal effect due to the stronger hydrophobic nature of the surfactant. Increasing the temperature still increases the surfactant hydrophilicity, however, the effect on wettability alteration is dampened since the tailgroup is longer. Further increasing the surfactant hydrophilicity results in a worse thermal stability problem. An example of this phenomenon is observed with cationic surfactant 1010. Compared to the other two cationic surfactants, this surfactant has 20 carbon atoms on its tailgroup. However, the headgroup is a dimethylammonium which has higher valence than the trimethylammonium. Higher valence results in stronger hydrophilicity of the surfactant. As a result, temperature increase results in an even stronger increase of surfactant hydrophilicity and is observed as stronger positive trend between contact angle and temperature (red line).

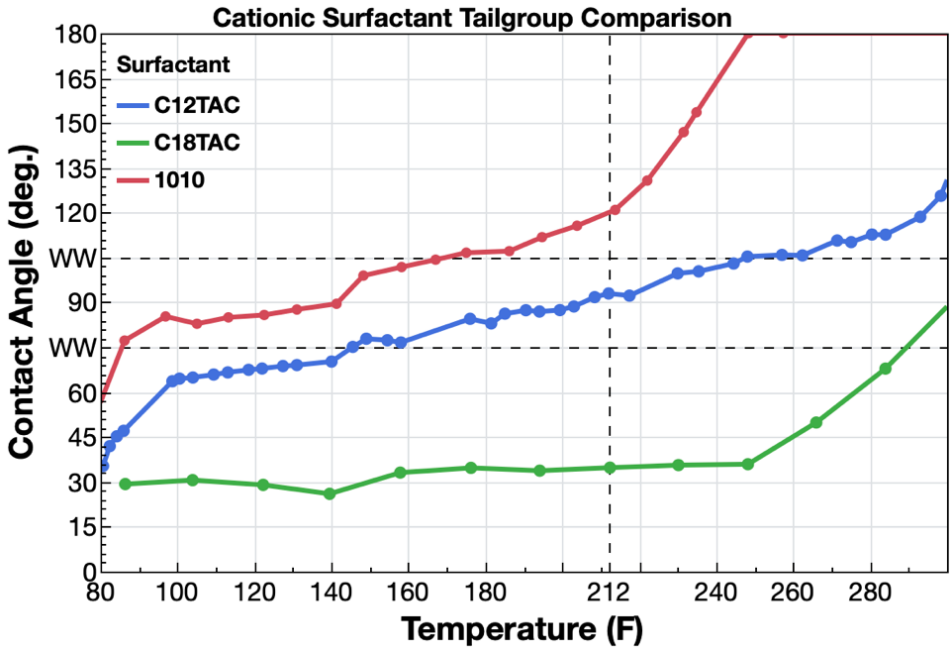

Figure 84 - Temperature effect on three cationic surfactants. Increasing temperature results in less water-wetness. Increasing the tailgroup chain length increases the water-wetting stability at higher temperature (C12TAC to C18TAC). While increasing the charge of the headgroup reduces the stability (C18TAC to 1010).

System salinity (left) and surfactant concentration (right) effect on the thermal stability of cationic surfactants is presented in Figure 85. Higher salinity improves the thermal stability of cationic surfactant C18TAC. Increasing the salinity (left figure) from 0.2 wt% (blue) to 1 wt% (red) results in the water-wet condition maintained up to 300°F from 250°F. Further increasing the salinity to 2 wt% (green) improves the initial water-wetness at lower temperature while still maintaining the thermal stability at higher temperature. Higher salt ion content in the aqueous-phase reduces the solubility of the surfactant molecule in water due to the salting-out process, driven by the dissolved salt ions. Applying higher surfactant concentration causes the same mechanism to occur since ionic surfactant is in some sense a salt ion. In the right figure of Figure 85, increasing the

1010 surfactant concentration from 0.2 wt% (blue) to 0.4 wt% (red) results in better thermal stability where water-wetness is maintained up to 260°F. Increasing the concentration more to 0.6 wt% (green), results in reversal of the thermal stability. The green line shows a larger contact angle value than the red, more oil-wet at 0.6 wt% than 0.4 wt%. This behavior is driven by the micellization process of the surfactant. Increasing the surfactant concentration causes the surfactant to be pushed closer to the critical micellization concentration (CMC). As this concentration is approached, the surfactant starts forming micelles, thus reducing the number of monomers in the system. Ultimately this results in a lower amount of surfactant at the interface the is able to alter the wettability of the surface and is reflected by the reversal of wetting to the more oil-wet.

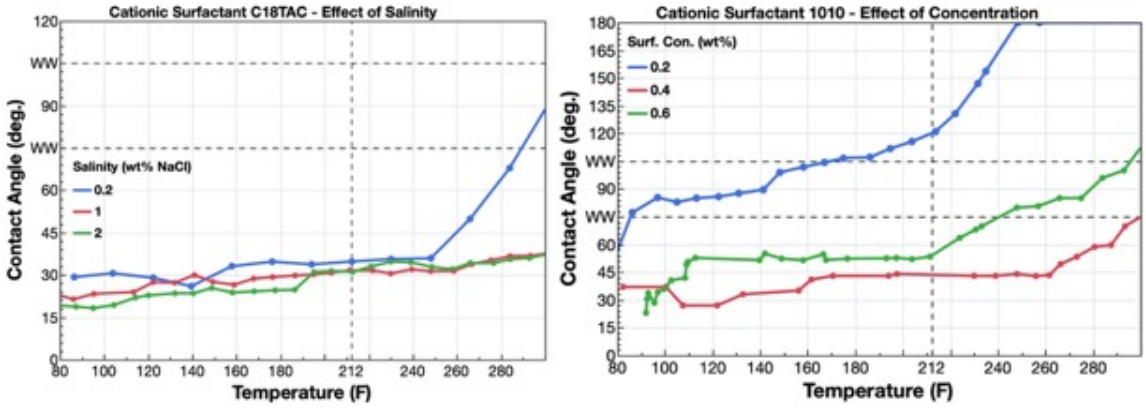

Figure 85 - Salinity (left) and concentration (right) effect on cationic surfactant C18TAC thermal stability. Higher salinity and higher surfactant concentration improve the thermal stability of the cationic surfactant to maintain water-wetting at higher temperature.

The Interaction of Surfactant EO Length with Crude Oil, Salinity, and Temperature

By looking at the surfactant behavior at varied conditions in the previous section, a second-degree interaction between the surfactant structure and the system conditions can be observed. For example, between the top-right of Figure 78 (NP-12) and the top-right of Figure 79 (NP-30) where contact angle decreases with increasing salinity for crude oil 2H for surfactant NP-12 while for surfactant NP-30 a positive trend between contact angle and salinity is observed. This indicates the effect of interaction between the number of EO groups and the salinity of the system to the wettability alteration performance. Another example is the trend difference between the top-left of Figure 79 (NP-30) and Figure 82 (15-S-30). The NP tailgroup on surfactant NP-30 is observed to render the surface water-wet with crude oil EF-C. On the other hand, the secondary C15 tailgroup is unable to alter wettability for the same crude oil which indicates another interaction second-degree interaction between the tailgroup structure of the surfactant and the crude oil characteristic that is affecting the wettability alteration process of the surfactant. The following section is dedicated to further investigate the surfactant structure and interaction with the system conditions and ultimately how it affects the final wettability state.

Nonionic Surfactant EO Length – Crude Oil Characteristic Interaction

Contact angle data is plotted against the number of EO groups in Figure 86. Data from measurements performed at 150°F and 0% salinity on calcite-rich mineralogy are presented. The four crude oils are presented as different colors. The effect of EO length to

wettability alteration was difficult to observe since surfactants were investigated separately. In this figure, positive trend is observed between the number of EO group and the contact angle value. Having more EO groups results in reduction of surfactant ability to render the surface water-wet. A similar result was observed in our previous publication on IFT reduction on unconventional brine/oil system (Saputra and Schechter 2021). Nonionic surfactants obtain their hydrophilicity through the hydrogen bond between the EO and the water molecule. Attaching more EO groups to the surfactant headgroup increases the hydrophilicity of the surfactant. When the surfactant is too hydrophilic, it has high water solubility and does not partition to the interface. Less surfactant at the interface results in less IFT reduction as reported in our previous work as well as less wettability alteration as observed in Figure 86. However, since the strength of the hydrogen bond is affected by the salinity and the temperature of the system, the behavior of wettability alteration as a function of the EO length could change when the system condition is changed. For example, while 30 EOs results in more oil-wetness in Figure 86, it could render water-wet surface once the salinity and temperature are changed. This phenomenon will be covered in the next section.

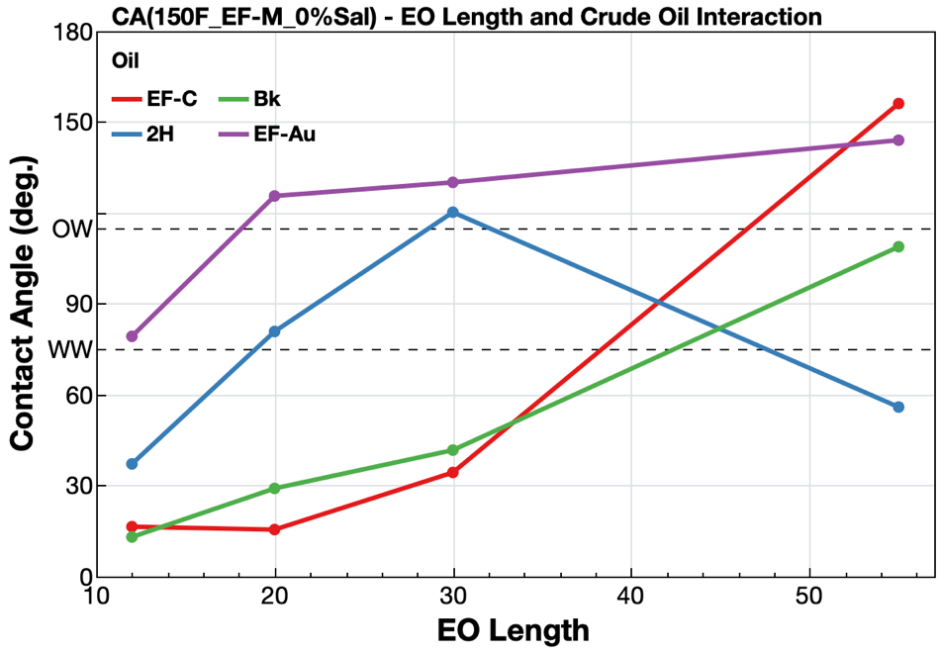

Figure 86 - The effect of EO group length and crude oil characteristic interaction to the wettability alteration of nonionic surfactants.

Figure 86 contains the data of the four crude oils. Generally, all for crude oils show positive trend of contact angle and EO length as described above. Crude oil with strong water-wetness at 12 EO (contact angle less than 30°) maintains water-wetness up until 30 EO with a gradual positive trend as the temperature is increased as observed with crude oil EF-C and Bk. For crude oil 2H and EF-Au where the contact angle with 12 EO is larger than 30°, a steeper positive trend between contact angle and EO length is observed up to 30 EO. Increasing the EO from 30 to 55 results in a more gradual trend for these two crude oils. The effect of the hydrophilicity of the EO group in relation to surfactant wettability alteration, and thus the changing gradient in the trendline in Figure 86 for different crude oils can be explained by the following: Water-wetting behavior observed with crude oil EF-C and Bk occurs due to the higher affinity of the surfactant to the interface. Aside from

the headgroup structure (number of EO groups), the tailgroup of the surfactant also plays a dominant role in determining the surfactant affinity to partition to the interface. For crude oil EF-C and Bk, the NP tailgroup shows good compatibility while it is less compatible for crude oil EF-Au and 2H. With good compatibility between the tailgroup and the crude oil, increasing the hydrophilicity of the surfactant through increasing EO length causes minimal effect as shown by the gradual change for the two compatible crude oils for an EO below 30. On the other hand, once the tailgroup and the crude oil is less compatible, the same EO change results in steeper change in contact angle value as observed with crude oil EF-Au and 2H. For the EO change above 30, the surfactant affinity to the interface is already lower even for crude oil EF-C and Bk. As a result, increasing the EO to 55 causes the contact angle to increase with a steeper trend. This mechanism indicates a compatibility factor between the crude oil characteristics and the surfactant tailgroup structure. This factor will be investigated in the latter part of this manuscript.

Surfactant EO Length – Salinity Interaction

Hydrogen bonding that causes hydrophilicity of nonionic surfactants is affected by the salinity of the system. Higher salinity results in less availability of water molecules for hydrogen bonding with EO molecules, thus resulting in lower hydrophilicity. Therefore, the interaction between EO and salinity could dominate the ability of nonionic surfactants to alter wettability. Contact angle data are plotted against EO length in Figure 87. The data is grouped by salinity in colors (blue is 0% and red is 8%) and by crude oil in columns. The blue lines in this graph are the same data presented in Figure 86.

In Figure 86, comparing the low (blue) and high (red) salinity data generally concludes to better wettability alteration performance of the surfactant when applied at higher salinity with red lines show lower contact angle value than blue lines. Higher salinity levels reduce the hydrophilicity of the surfactant, resulting in higher affinity of the surfactant at the interface. With more surfactant molecules positioning at the interface, more wettability alteration occurs which observed as lower contact angle values for the red lines in Figure 87. Although their hydrophilicity is driven by different mechanisms, the same observation is also presented in the left of Figure 85 which presents contact angle data of cationic surfactants. While one is driven by hydrogen bonding (nonionic surfactants) and the other is driven by ionic bonding, both mechanisms are negatively affected by salinity; the higher the content of salt ions in the system the less availability of water molecules for both hydrogen and ionic bonding to establish hydrophilicity. Consequently, stronger water-wetness is also observed at higher salinity for the ionic surfactants.

With these results, the question then becomes should surfactant be combined with the highest salinity available for each application in order to achieve the best wettability alteration performance? For nonionic surfactants, the upper limit of salinity exists due to the nature of the EO group. At high salinity levels, nonionic surfactants could completely lose hydrophilicity as the EO group is unable to form any bond with water molecules. This behavior is observed even in a simpler system containing only brine and the surfactant, known as the cloud point. At this state, the surfactant loses its amphiphilicity since it loses its hydrophilicity nature. With its surface-active properties subdued, the surfactant loses

its ability to alter wettability. In Figure 87, this behavior is observed. With crude oil EF-C and Bk, an EO length of 12 and 20 render the surface more oil-wet than an EO length of 30 at a higher salinity. At 0% salinity, an EO length 12 and 20 are already at their limit. Increasing the salinity to 8% results in the surfactant losing its hydrophilicity, its surface activity, and ultimately its ability to alter the wettability of the rock surface.

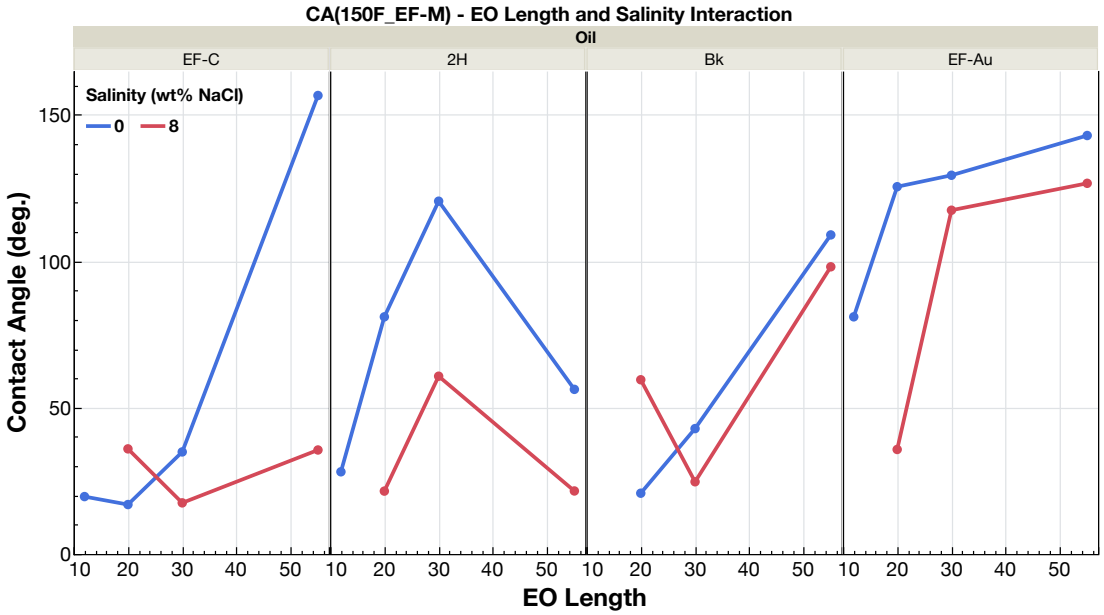

Figure 87 - The effect of EO group length and salinity interaction to the wettability alteration of nonionic surfactants.

The trend covered above is not observed on crude oil 2H and EF-Au. With these two crude oils, generally the trend between contact angle and EO length observed with the lower salinity is replicated at higher salinity, only at lower contact angle values. The difference between EO length and salinity interaction for crude oil 2H and EF-Au to crude oil EF-C and Bk is caused by the same mechanism that drives the gradient difference in

Figure 86. When applied to crude oil EF-C and Bk at lower salinity, the surfactant already reaches its limit at 12 and 20 EO as observed by the contact angle value lower than 30°. While at the same salinity level and EO length, the surfactant has not reached the limit with crude oil EF-Au and 2H as shown by the more oil-wet contact angle data. Increasing the salinity for the case of EF-C and Bk results in the suppression of the surfactant hydrophilicity as explained before. However, when salinity is increased on crude oil EF-Au and 2H, the surfactant is pushed closer to the limit of amphiphilicity which results in better wettability alteration. Increasing the salinity more than 8% would cause the same wettability reversal to oil-wet as observed with the other crude oils. For crude oil 2H, the amphiphilicity limit is observed since the contact angle value for 12 and 20 EO at 8% salinity is the same value.

This mechanism indicates that the ability of the surfactant to alter wettability is optimum when the surfactant reaches its amphiphilicity limit. The amphiphilicity limit is driven not just by the surfactant structure, but also the interaction of the surfactant structure with the total system. This is not limited to hydrophilic headgroup interaction with the brine and tailgroup interaction with the crude oil separately, but also the combination of both interactions. The surfactant amphiphilicity limit for a surfactant structure at a salinity level could be different when applied to a different crude oil. For system combinations containing good compatibility between the tailgroup of the surfactant, the amphiphilicity limit is achieved at a lower salinity level. However, when the system combination has lower compatibility, the salinity level where the amphiphilicity limit is achieved is higher.

Surfactant EO Length – Temperature Interaction

In addition to salinity, the strength of the hydrogen bond between the EO group and the water molecule is also affected by temperature. Hydrogen bonds loses strength when the system temperature is increased resulting in the reduction of nonionic surfactant hydrophilicity at higher temperature. When the surfactant is below its amphiphilicity limit, this reduction would result in the improvement of surfactant amphiphilicity since more surfactant molecules would position at the interface. On the other hand, when conditions exceed the amphiphilicity limit, this reduction would result in the surfactant losing its amphiphilicity.

Contact angle data are plotted against the EO length in Figure 88. For this analysis, the data are presented for 0% salinity and a calcite-rich system. Different temperatures are presented by color and different crude oils are grouped in columns. Generally, higher temperature results in lower contact angle; the color from high to low contact angle value is red, orange, green, and purple respectively. This trend confirms the theory that for nonionic surfactants, higher temperature results in better wettability alteration performance. It is important to note that this trend is the opposite of the trend observed with cationic surfactants where surfactant loses its wettability alteration capability when the temperature is increased (Figure 84). This difference is driven by the different mechanism of hydrophilicity of the two surfactants. Hydrogen bonds with nonionic surfactant loses the ability to bond with water at increased temperature, whereas ionic bonds increase in strength at higher temperature. Since bond strength with water determines the hydrophilicity and ultimately the surfactant amphiphilicity, increasing

temperature results in better nonionic surfactant wettability alteration and worse ionic surfactant performance.

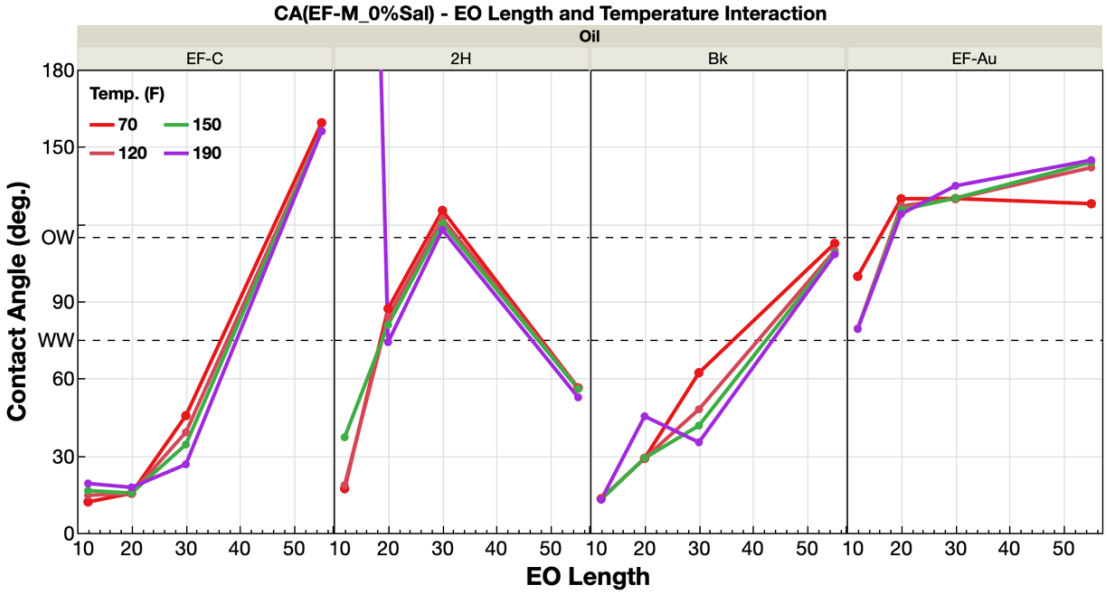

Figure 88 - The effect of EO group length and temperature interaction to the wettability alteration of nonionic surfactants.

The data plotted in Figure 88 shows minimal interaction between EO length and temperature. Compared to the interaction with salinity, presented in Figure 87, the difference between lines is minimal. This implies that the effect of EO length to the wettability alteration performance of the surfactant is dominated by the salinity level of the system rather than the system temperature.

The Interaction of Surfactant Tailgroup Structure with Oil, Salinity, and Temperature

The surfactant ability to alter system wettability is driven not only by the headgroup structure and its interaction with the system condition, but also by the tailgroup structure and presumably its interaction with the condition of the system. In this section, these interactions are presented.

Surfactant Tailgroup – Crude Oil Characteristic Interaction

Contact angle data are plotted against the number of carbon atoms in the surfactant tailgroup are presented in Figure 89. Tridecanol ethoxylated, secondary pentadecanol, and nonylphenol are represented by 13, 15, and 19 respectively. The data is measured at 150°F, 0% salinity, and calcite-rich mineralogy. All three surfactants included have 30 EO in their headgroup. The relation between wettability alteration and the surfactant tailgroup when the data Is grouped by the crude oil is not 192traightt forward as its relationship with the number of EO groups as shown in Figure 86. This indicates the dominant effect for wettability alteration is the interaction between crude oil characteristics and the surfactant tailgroup structure.

With crude oil EF-C and Bk, the 15-S tailgroup has the worst wettability alteration performance. This is due to its unique interaction with the system salinity. At low salinity, the secondary functional group causes the surfactant to have higher hydrophilicity which reduces the amount of surfactant on the interface to perform interfacial activity. This behavior was observed in cloud point (Chapter VI) and interfacial tension (Chapter VII)

data as well as in the case of wettability alteration as observed in Figure 89. Based on this mechanism the performance of tailgroup 15-S could be improved by increasing the system salinity. This will be covered in the next section.

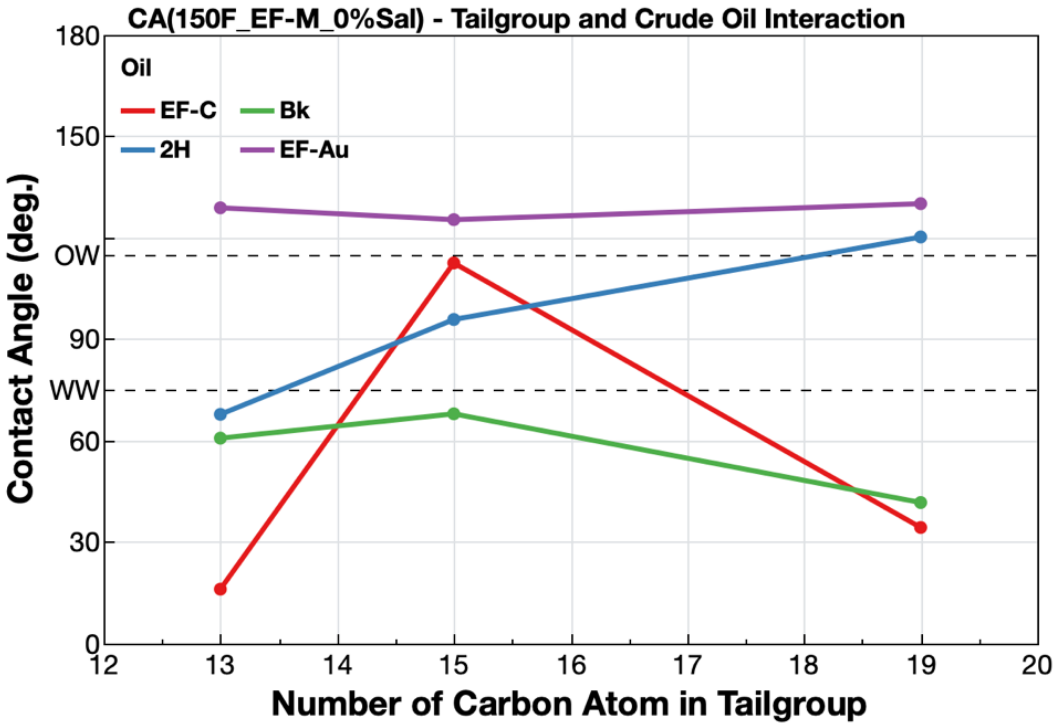

Figure 89 - The effect of tailgroup structure and crude oil characteristic interaction to surfactant wettability alteration.

For crude oil EF-C, tridecanol shows the most water-wetness. While for crude oil Bk, the lowest contact angle value is achieved by the nonylphenol tailgroup. Crude oil EF-C is composed of mostly Saturates while crude oil Bk is dominated by Aromatics. The tridecanol tailgroup is a linear saturated hydrocarbon chain that matches with the Saturate content of crude oil EF-C. Similarly, the nonylphenol tailgroup contains a hydrocarbon

ring that has similar structure to the Aromatics of crude oil Bk. A similar observation is observed with crude oil 2H. This crude oil contains more Saturates than Aromatics. Both its Saturate and Aromatic content are between those of EF-C and Bk. From the trend (blue line), the tridecanol tailgroup shows the best wettability alteration performance which is driven by the compatibility of the Saturates-dominated crude oil composition with the linear hydrocarbon tailgroup. The contact angle value of this crude oil is higher than EF-C and Bk due to the stronger oil-wetness of the base case as presented in Figure 77. Therefore, it can be concluded that wettability alteration of the surfactant can be optimized by matching the tailgroup structure of the surfactant to the dominant crude oil hydrocarbon content. Future studies to investigate whether mixing the linear and cyclic structure, i.e., adding tridecanol ethoxylated and nonylphenol ethoxylated together, could improve the compatibility of the surfactant to the crude oil should be pursued.

Surfactant Tailgroup – Salinity Interaction

In the previous section, the 15-S tailgroup indicated some degree of interaction with the system salinity that affects its performance in wettability alteration. The contact angle data presented in Figure 89 is presented again in Figure 90. This time the data is grouped by salinity in colors and by crude oil in columns. Tailgroup 15-S is observed to be affected the most by the increase of salinity. Poor wettability alteration observed at lower salinity significantly changes when the salinity is increased. Aside from crude oil EF-Au, this tailgroup renders strong water-wetness with contact angle values less than 30° at 8% salinity. This observation confirms the results previously observed in cloud point and IFT

measurements and that this particular tailgroup must be applied at high salinity in order to achieve impactful interfacial activity, Chapter VI and Chapter VII.

A different interaction with salinity is observed with the linear C13 tailgroup. From Figure 90, salinity increase results in less wettability alteration with crude oil containing more Saturates than Aromatics. On the other hand, the linear tailgroup provides better wettability alteration at higher salinity when applied on crude oil with an Aromatic content higher than the Saturates. This behavior is not observed for IFT reduction of this tailgroup when applied on the same four crude oils. Salinity increase results in lower IFT or more IFT reduction on all four crude oils without any reversal observed. However, it is important to note that the change in IFT reduction due to salinity differs from one crude oil to another. Crude oil with higher saturate content (EF-C) is less affected by salinity than heavier crude oil. From the trend observed in the wettability alteration and IFT reduction, there are two things that can be concluded. First, IFT reduction occurs at almost 100% certainty when surfactant is added to a system containing oil and water. Changes in the system condition could increase the amount of IFT reduction, i.e., salinity increases, higher temperature for nonionic surfactants, lower temperature for ionic surfactants, and crude oil with a higher Saturate content. The only reversal of IFT reduction occurs with nonionic surfactant when applied at a temperature higher than its cloud point. Second, to the contrary, wettability alteration occurs in a specific range of system conditions, a window at an optimum condition. Below the optimum condition, minimal wettability alteration is observed. Pushing the system condition to the optimum window results in a stronger water-wet condition. However, unlike IFT reduction, pushing the system

condition further than the optimum window results in reduced surfactant performance. An example of this behavior is with the C13 tailgroup where initially at lower salinity and with a more non-polar crude oil, strong water-wetness is observed and increasing the salinity further results in less wettability alteration. This indicates the system is already at its optimum for wettability alteration at low salinity and by increasing the salinity further, the system condition is pushed above its optimum window. On the other hand, poor wettability alteration observed with low salinity and less non-polar crude oil is transformed into strong water-wetness when the system is pushed to higher salinity. This means that at low salinity, the system condition is below its optimum window for wettability alteration. Pushing the salinity to a higher value drives the system condition to an optimum condition for wettability alteration.

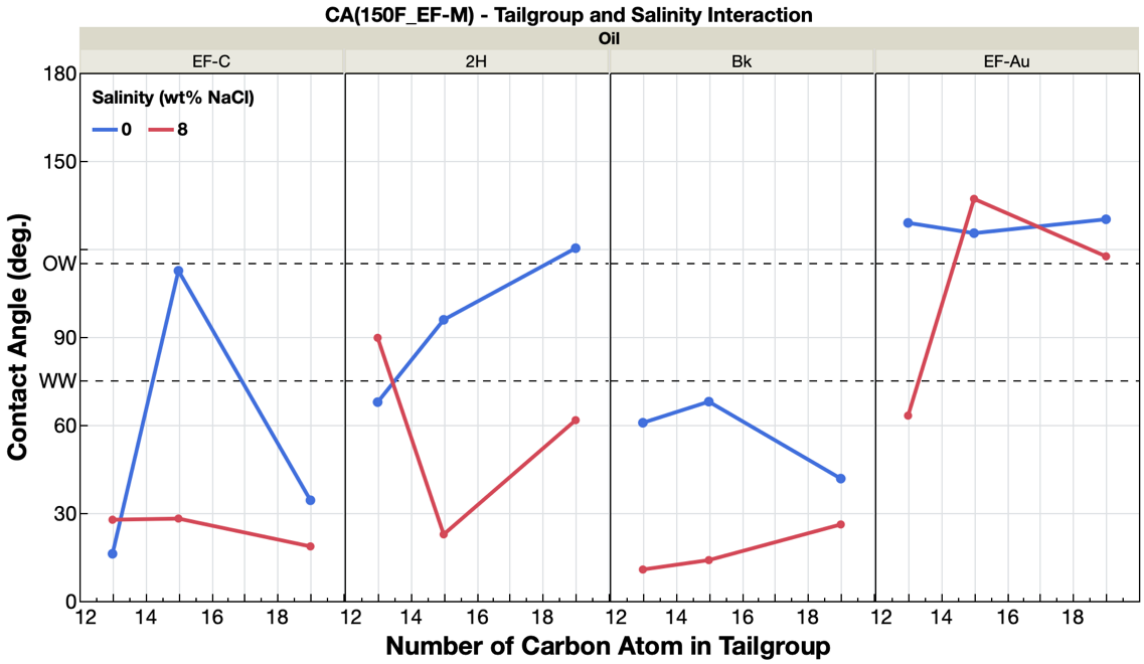

Figure 90 - The effect of tailgroup structure and salinity interaction to surfactant wettability alteration.

The trend observed with the linear C13 tailgroup does not apply to the nonylphenol tailgroup. Salinity increases results in better wettability alteration for the nonylphenol tailgroup for all four crude oils. The changes in contact angle value due to salinity for this tailgroup is observed to be a function of the crude oil. The largest change is observed on crude oil 2H while similar level of changes is observed with crude oil EF-C, Bk, and EF-Au.

Surfactant Tailgroup – Temperature Interaction

The last tailgroup interaction to be analyzed is performed with the system temperature. Contact angle vs tailgroup structure is now grouped by temperature in color and crude oil in columns as observed in Figure 91. Data from 0% salinity and calcite-rich mineralogy are presented. Unlike other system parameters, crude oil and salinity, minimal interaction between the tailgroup and the system temperature is observed. This is observed as generally parallel lines in Figure 16. Therefore, it can be concluded that the temperature of the system is unimportant when selecting the structure of the tailgroup for wettability alteration applications.

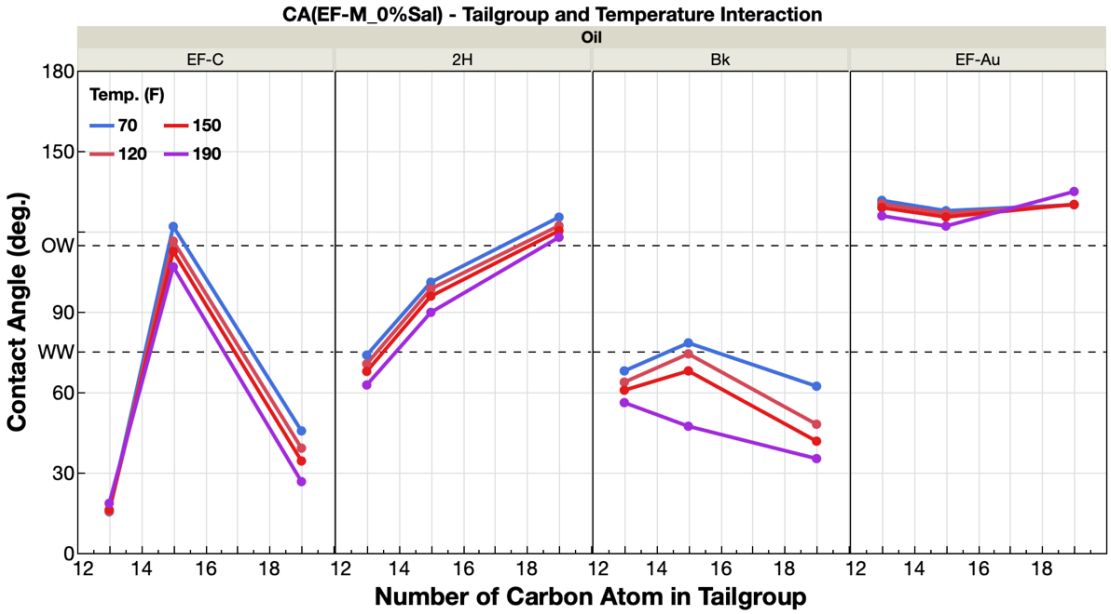

Figure 91 - The effect of tailgroup structure and temperature interaction to surfactant wettability alteration.

CHAPTER IX

SPONTANEOUS IMBIBITION OF BASE CASE WITHOUT SURFACTANT

The system combinations investigated to this point include brine, crude oil, and rock via IFT and contact angle. One last variable is yet to be investigated and that is the influence of these parameter on flow through porous media of the rock. This chapter presents the analysis of the most complex system combinations in this study that contains brine, crude oil, rock, and flow in porous media phase. As mentioned previously, this system combination is analyzed through spontaneous imbibition experiments with combinations of temperature, salinity, crude oil, and surfactant structure. Trends from spontaneous imbibition recovery factor are presented in this section. Initially, the base case without surfactant is presented. The effect of crude oil composition, rock mineralogy, brine salinity, temperature, and interactions between variables are scrutinized. The recovery factors are correlated back to trends observed in the base IFT and base wettability to explore the reasoning behind the observed data, as well as to confirm the theory explored previously. This chapter is divided into three parts. The first part looks at the effect of crude oil composition and rock mineralogy to base recovery. The second part investigates the effect of brine salinity and finally, the effect of temperature is presented.

The Effect of Crude Oil on the Base Recovery

Figure 92 shows the final recovery factor of base scenarios on four crude oils and two lithologies. With carbonaceous rock (left figure), crude oil EF-C has the highest recovery, followed by EF-Au, 2H, and finally crude oil Bk. However, the opposite order is observed when siliceous system (right figure) is applied. On siliceous lithology, crude oil 2H has the highest recovery factor, followed by Bk, EF-Au, and EF-C. This trend is intriguing as it shows the dominant effect of crude oil/rock interaction to the imbibition profile. It is important to note that the effect of crude oil composition, rock mineralogy, and their interaction to the rock surface wettability (measured by contact angle) is investigated already in Chapter V. In the chapter, it was observed that the aromatic content of the crude oil and quartz content of the rock surface interacts and their interaction results in stronger oil-wetness for the crude oil/rock system. This trend is reflected in Fig. 92 as shown by the inversion in the maximum recovery factor order for the two mineralogies.

It is also important to note that, while spontaneous imbibition depends on the wettability, it is also strongly affected by various other mechanisms. Therefore, it is expected that the trend observed in the wettability study of this work will not easily translate to imbibition results. Additionally, contact angle data presented in previous chapters are measured on sidewall core samples where the imbibition experiments that will be presented are performed on outcrop samples. This could be a source of uncertainty when correlating the wettability result from contact angle measurement to the oil recovery from the imbibition experiments. One example here is the maximum recovery factor of the two mineralogies. From the figure it can be observed that the maximum recovery factor

range of the carbonaceous rock is below 15%. While for the quartz-rich mineralogy, the range is in the 50%. From these two results, one could make a conclusion that the siliceous rock is more water-wet than the calcite-rich rock. However, these two rocks have significant permeability difference. The carbonaceous rock is an Indiana Limestone outcrop with 2 md permeability and the siliceous rock is Scioto outcrop with 0.001 md permeability which is three orders of magnitude difference. The permeability difference is driven by the pore throat size difference. These two pore throat dimensions are directly related to the capillary pressure that drives spontaneous imbibition. The difference in recovery factor range is an example of the complex mechanisms and interactions that are involved in the spontaneous imbibition process. It is hypothesized that the difference between the two recovery factors range is strongly driven by the permeability and pore radius difference. Further analysis on the crude oil characteristics in the next part of this section would provide more evidence of this hypothesis.

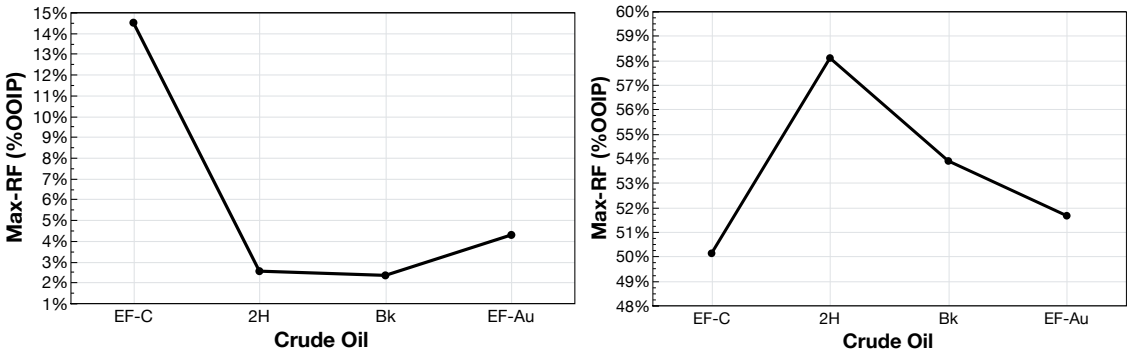

Figure 92 - Final recovery factor for base case of the four crude oils at 0% salinity, calcite-rich on the left and quartz-rich on the right.

It is intriguing that the three orders of magnitude difference of the permeability could heavily impact the recovery from spontaneous imbibition, overshadowing the effect of wettability. Furthermore, per the definition of capillary pressure from the Young-Laplace equation, oil-wet samples should have zero oil production from a spontaneous imbibition process since the capillary pressure is negative. The result in this study does not agree with this statement. It is important to note that studies in the 2000s by Zhou et al. (Zhou et al. 2000) have shown positive trend observed between oil-wetness and oil recovery from core plugs. With the result observed here as well as confirmation from previous studies, the application of wettability term to the Young-Laplace equation should be updated. In the current definition, applying wettability through a cosine function of the contact angle results in the negative capillary pressure on an oil-wet system. Perhaps applying the cosine to the half of the contact angle value ($P_c = \frac{\sigma \cos^{\theta}/_{2}}{2r}$ ……Equation **9**) could alleviate this problem. With this transformation, oil-wet system would still have lower recovery factor than a more water-wet system. But the resulting capillary pressure would still be positive, allowing oil to be produced which is more representative of the results observed in laboratory experiments.

$P_c = \frac{\sigma \cos^{\theta}/_{2}}{2r}$ ……Equation 9

Figure 93 plots the maximum recovery factor data with two other crude oil characterization parameters in addition to the IFT. However, these two parameters, Saturates to Aromatics and Resins ratio and the linear to cyclic hydrocarbon ratio, do not correlate to the recovery factor as well as the IFT which is unlike the wettability section

of this study, where these parameters correlate well to the system wettability. It is hypothesized that in a tortuous system such as a core plug, the interaction between the crude oil components become more complicated than a linear relationship contained in the two parameters presented. From the IFT section of this study, it was observed that the crude oil/water IFT is also driven by the crude oil components and their interaction. The advantage of IFT values is that it contains all the complex interaction between the crude oil components that is not captured in a linear relationship. Additionally, the crude oil component interaction also influences how easy the fluid flows in terms of viscous flow. Therefore, in Figure 93, IFT shows better trend to the maximum recovery factor values than the two other crude oil components.

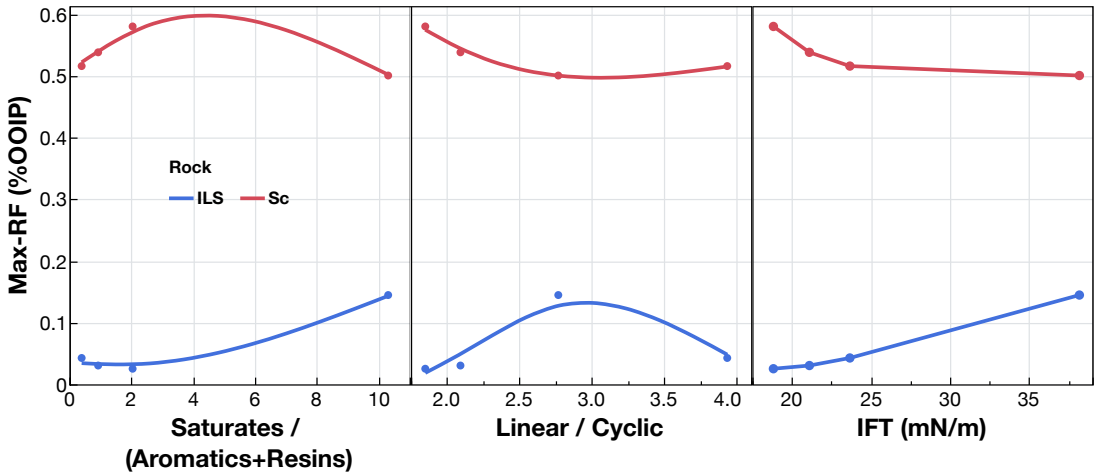

Figure 93 - Base recovery plotted against three crude oil characterization parameters.

This study has the main goal of surfactant application in shale crude oil/brine/rock system. As a groundwork, the behavior of the base condition where no surfactant is used

is also studied. The idea is to investigate what part of rock mineralogies and crude oil composition cause a system to be oil-wet. Then that information is used to devise a surfactant structure that addresses the corresponding components. Later, even the base condition is found to be complex. In the upcoming section on spontaneous imbibition involving surfactants, the results obtained as well as the analysis will be presented in terms of normalized improvement to the base case of each crude oil/brine/rock system. This is done to incorporate the complex interaction observed in the base scenario without the need to explicitly define these interactions, thus allowing for a more accurate surfactant analysis since an explicit definition of these interactions is not available.

Salinity Effect to Base Recovery

Salinity is observed to strongly affect the interaction between crude oil and water as well as the interaction of crude oil, water, and rock surface. Base spontaneous imbibition cases with four salinity levels are presented in this study. Salinity levels from 0% to 24% in an 8% increment are investigated with crude oil EF-C and Bk on both siliceous and carbonaceous mineralogies. as presented in Figure 94. The left graph contains all data from calcite-rich core plug and the data from the quartz-rich plug are presented in the right graph. Crude oil EF-C is represented by the blue lines and the red lines represent crude oil Bk in both graphs.

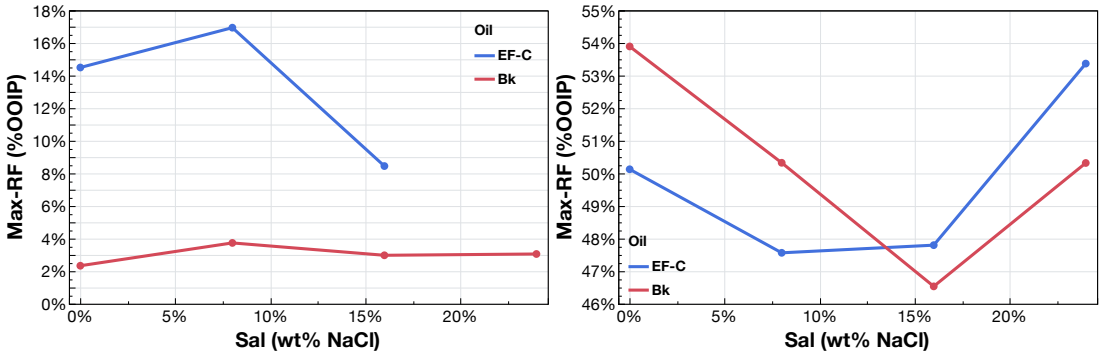

Figure 94 - Final recovery factor of crude oil EF-C and Bk at a range of salinity. Left is limestone, right is quartz-rich core.

On calcite-rich rock, salinity is not observed to significantly affect the base recovery on crude oil Bk for salinity higher than 8 wt%. From the graph increasing the salinity from 0% to 8% results in increase of recovery factor from 2.5% to 4% OOIP. Further salinity increases to 16% to 24% results in base recovery of around 3% OOIP. With crude oil EF-C, a similar increase of base recovery is also observed for salinity increase from 0% to 8%. Interestingly, it is then followed by the same decrease of recovery factor value once the salinity is increased further to 16%. The opposite trend for the siliceous rock is observed as increasing salinity reduces the base recovery. At a given salinity level, specific to the crude oil, the trend reverses. In that case, increasing salinity results in the base recovery being greater. The inversion point is at 16% for crude oil Bk and at 12.5% for crude oil EF-C.

From the base wettability and the base IFT section of this study, it was concluded that salinity increase generally results in more oil-wet system and higher IFT value. These two variables are important contributors to the spontaneous imbibition mechanism. Therefore, the change of base recovery due to salinity change as described before is expected. To

further analyze the trend between recovery factor and salinity, the data is processed into Figure 95. In incorporating two types of core plug and two crude oils it is important to realize that the base recovery of each rock/crude oil combination is different. Therefore, to analyze the effect of salinity change, a normalization to the base recovery value at 0% salinity should be performed. This normalization is presented in Figure 95.

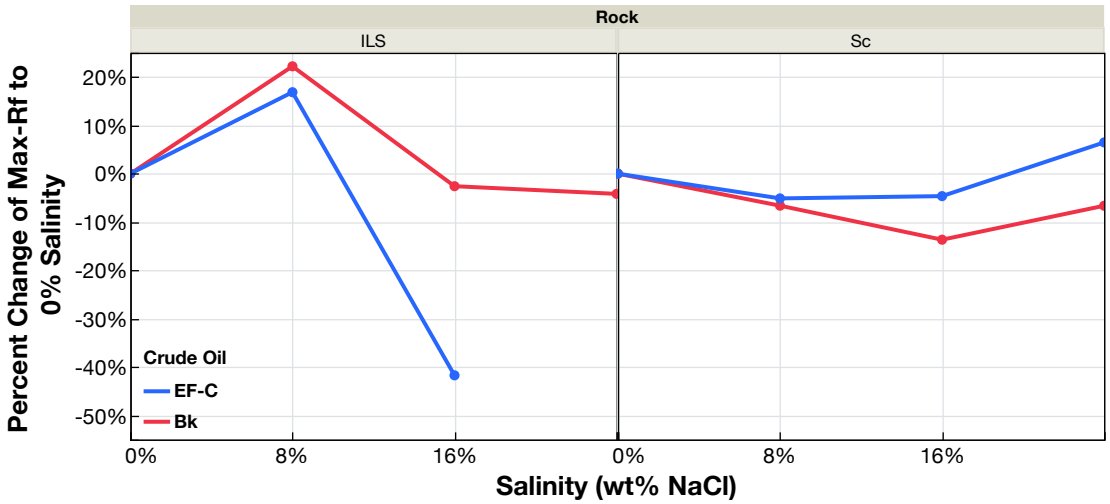

Figure 95 - Percent change of recovery factor to the base recovery at 0% salinity as a function of the brine salinity.

The base recovery data are normalized to 0% salinity at each rock/crude oil combination, thus resulting in the plot of the 0% salinity to be at zero. The recovery increase observed on the limestone sample with salinity increase from 0% to 8% is still observed in the figure. However, this salinity increase affects crude oil Bk (red line) more than crude oil EF-C (blue line). The quadratic curve on recovery versus salinity on the quartz-rich rock is still captured. Like the limestone, the salinity change in the quartz-rich rock affects crude oil Bk more than crude oil EF-C. From the base IFT section of this

study, it was observed that salinity change affects the IFT of crude oil that contains more Aromatics and Resins. It is hypothesized the same process is also observed here. Crude oil Bk contains more Aromatics and Resins than crude oil EF-C. From the section above, it was also noticed that the base recovery is in good agreement with the crude oil IFT. Therefore, the mechanism behind the change of base recovery due to salinity is driven mostly by the change of IFT due to changing salinity. As a matter of fact, the trend between Figure 31 and Figure 95 agrees. In Figure 95, higher IFT causes higher base recovery for the limestone samples. In Figure 31, higher salinity results in higher IFT which also causes the base recovery to increase for the limestone samples. For siliceous rock, higher IFT results in lower recovery as shown in Figure 95. In Figure 31, higher salinity results in higher IFT which also results in lower recovery.

It is important to note that the previously observed trend applies only for the first half of the salinity scan. On both rocks, the second half of the salinity scan shows an inverse trend between base recovery and salinity. Initially, a positive and negative trend was observed between base recovery and salinity on the limestones and quartz-rich respectively. At a higher level of salinity, the trend is inversed to negative for the carbonate samples and positive for the siliceous samples. As previously outlined, salinity does not only change IFT, but also wettability. It is hypothesized that wettability change due to changing salinity causes the trend to be inverted. Figure 95 shows IFT has a different trend for oil-wet and water-wet systems. At lower salinity level, limestone is water-wet and IFT has a positive trend to recovery. At higher salinity level, the wettability shifts to oil-wet resulting in the change of the IFT trend where higher IFT results in lower recovery.

The shift described in the paragraph above can be clearly seen in Figure 96. The base recovery is plotted against the crude oil characterization parameters. The lines represent the salinity level. For the limestone, a salinity increase (green to light green to orange to red) reduces the gradient of the line. On the siliceous rock, the gradient of the trendline also becomes flatter at higher salinity and reverses from a negative to a positive trend when the salinity is increased further (comparing light green and orange line). This systematic slope change due to the salinity level is a strong indication of wettability shift throughout the salinity sweep.

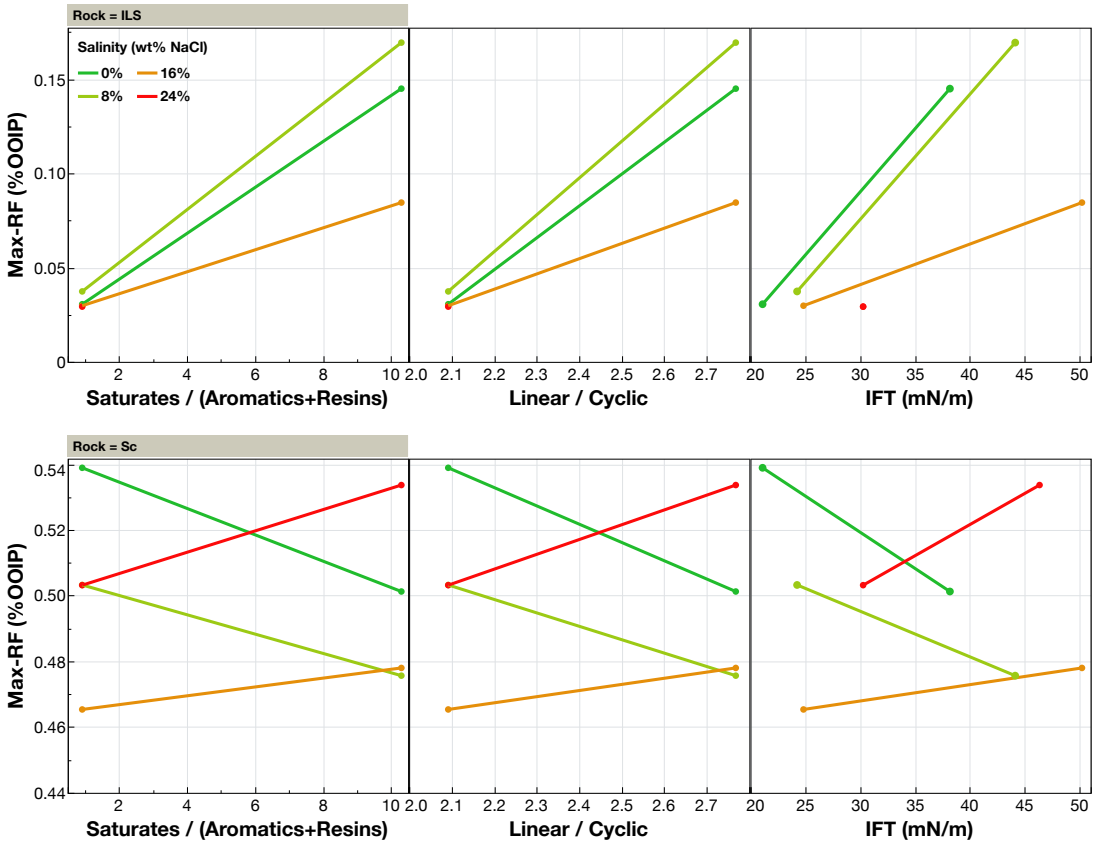

Figure 96 - Interaction between crude oil characterization parameters and brine salinity and its effect to the base recovery.

Temperature Effect to Base Recovery

One final important variable on base case spontaneous imbibition is temperature. Figure 97 presents the base recovery data of crude oil EF-Au in siliceous rock and crude oil 2H in carbonaceous rock at different temperatures. A positive trend is observed as higher temperature results in higher base recovery. Higher temperature results in lower viscosity and weaker bond between the crude oil components and the rock surface, therefore, allowing for easier oil production out of a porous media which is shown in the trends observed in Figure 97.

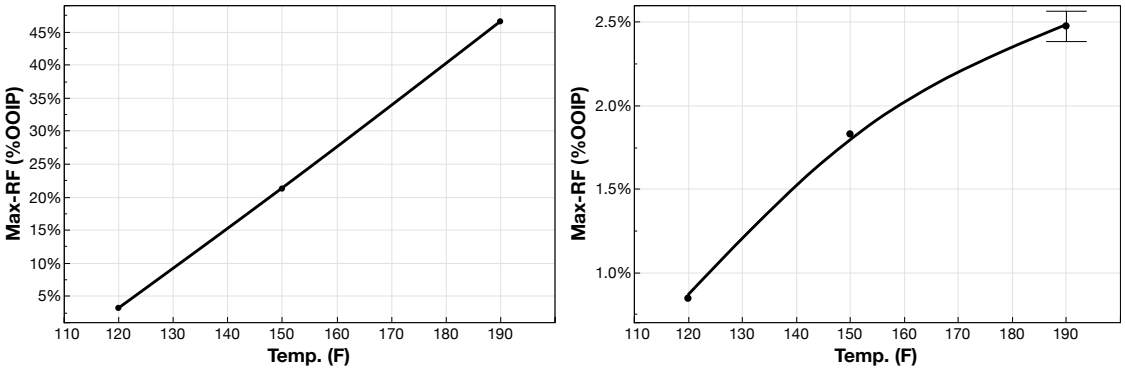

Figure 97 - Effect of temperature to base recovery, left is crude oil EF-Au in quartz-rich rock and right is crude oil 2H in carbonate-rich rock.

CHAPTER X

OPTIMIZING TAILGROUP AND HEADGROUP STRUCTURE OF SURFACTANT FOR SASI APPLICATION ON LOWER 48 SHALE

There are more than 85 imbibition experiments performed for this study. Eight different surfactants with one base case are tested on four crude oils, two rock lithologies, and four brine salinity levels. The test matrix is not full factorial. The surfactant/crude oil/rock/brine systems are selected to investigate the following:

- Effect of crude oil composition, salinity, rock lithology, and comparison to the base imbibition experiments,
- Effect of surfactant on imbibition recovery factor and the imbibition rate,
- Crude oil composition and surfactant tailgroup compatibility on the imbibition profile
- How salinity and rock lithology are affecting the compatibility described above,
- The optimum headgroup configuration for nonionic surfactants (number of EO group) from imbibition recovery perspective,
- The effect of crude oil composition to the optimum headgroup structure, and
- The behavior of cationic surfactants on various salinity levels and its effect on the imbibition profile

The first bullet is already covered in the preceding chapter This chapter is focused more on the analysis of imbibition profile with the presence of surfactant in the system.

Spontaneous Imbibition Recovery Data, General Observations

Imbibition results performed on the calcite-rich rock are presented in Figure 98. The results are presented for recovery factor (volume of oil produced, normalized to the total oil originally in the core plug) vs imbibition time. As shown in the previous chapter, the baseline recovery with no surfactant differs with different crude oil and salinity. To better display the data, the recovery curves are compiled in boxes with each plot showing the data for different crude oil and salinity combinations. For example, the top-left box contains imbibition data from crude oil 2H with 0% salinity as the title of the box suggests. The same plot is repeated in Figure 99, this time containing all imbibition data performed on the siliceous core plugs. In both figures, the black lines and dots represent the base imbibition cases where surfactant is not introduced into the system. While the different colors represent cases with surfactant added, with the surfactant name presented in the legend. It can be seen that in most cases, surfactant results in higher recovery factors compared to base the case, this demonstrating the advantages of introducing surfactant to improve imbibition recovery. However, two important observations must be presented. First, although most surfactant cases improve the oil production, the level of improvement varies from one surfactant to another. More importantly, it varies from one crude oil/rock/brine system to another system. A more detailed analysis must be performed in assessing surfactant performance, by incorporating the difference in the base recovery of each crude oil/rock/brine system combination. Second, there exist cases where surfactant is detrimental to the oil recovery from the imbibition mechanism. Only 7 out of the 87 imbibition experiments performed showed lower recovery compared to the base case. This

phenomenon should be investigated thoroughly to avoid the application of surfactants that would reduce recovery in an actual field case.

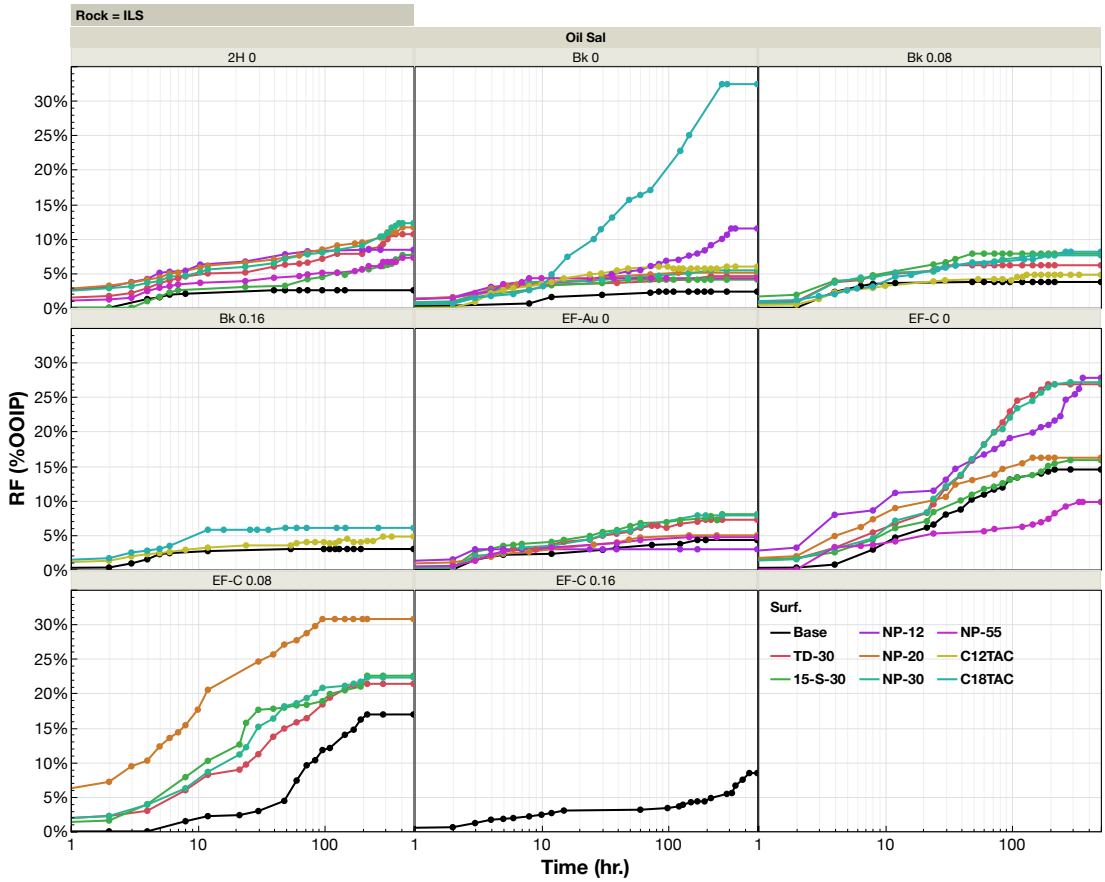

Figure 98 – Imbibition recovery factor data of all experiments performed on carbonaceous mineralogy.

The most obvious difference between systems in this study is the difference between the two rocks tested. Comparing Figure 98 and Figure 99, it is observed that the ILS core plugs have recovery factors of below 25% for the majority of the tests, whereas the Sc sandstone core plugs have recovery factors in the 50% range. The transport of surfactant molecule to the pores of the core plugs is driven by the base imbibition. Where water-

phase is initially brough into the core plug along with the surfactant molecule. With the base recovery of the Sc core plugs in the 50% range, that means that more surfactant molecule is available in the core plug with these core plugs compared to the ILS core plugs.

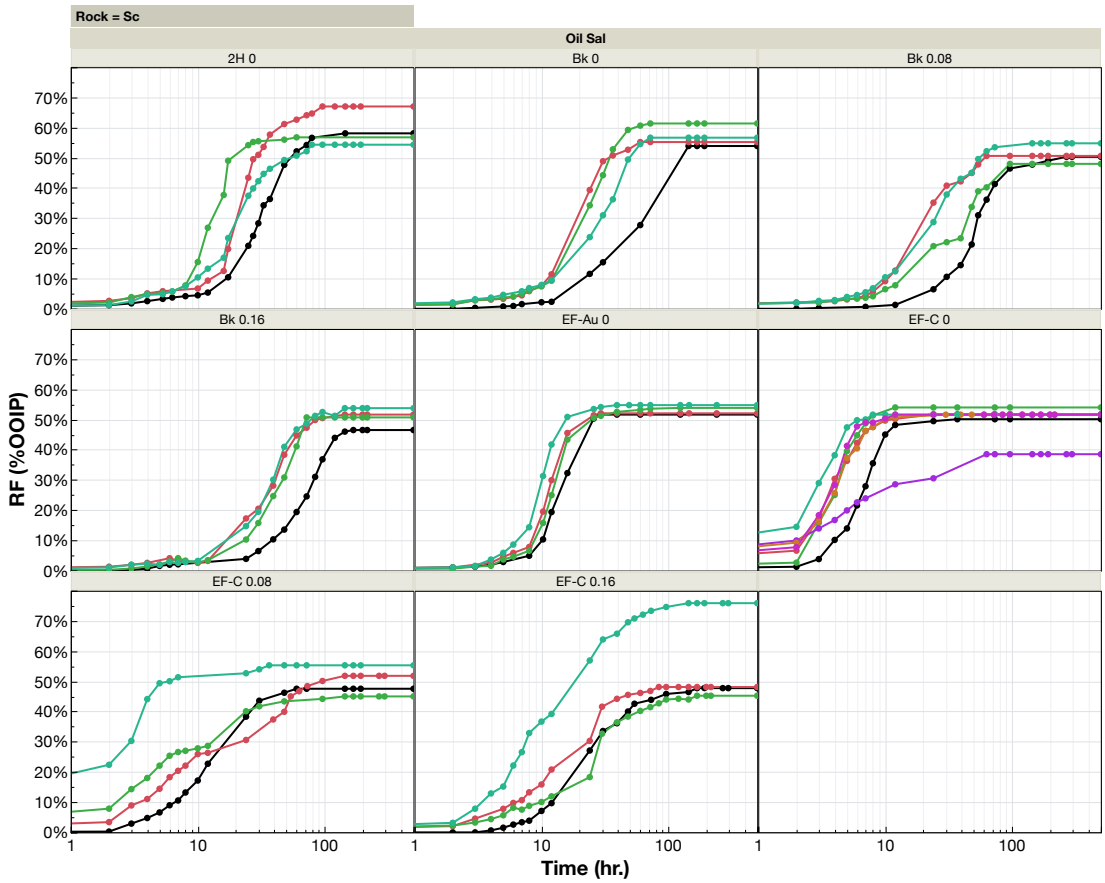

Figure 99 - Imbibition recovery factor data of all experiments performed on siliceous mineralogy.

More surfactants would ideally result in better improvement of the imbibition profile. Figure 100 is plotted to investigate this behavior. The improvement of final recovery factor of all surfactant cases from the final recovery of the base case of each corresponding crude

oil/brine/rock system is normalized to the final base recovery. The normalized recovery factor is plotted as recovery improvement on the y-axis against the final base recovery on the x-axis. The data incorporates all crude oil/rock/brine combinations. A negative trend is observed where less improvement of recovery is observed with higher value of base recovery. Meaning that the theory described above is not directly applicable. There are two possible reasons for this trend.

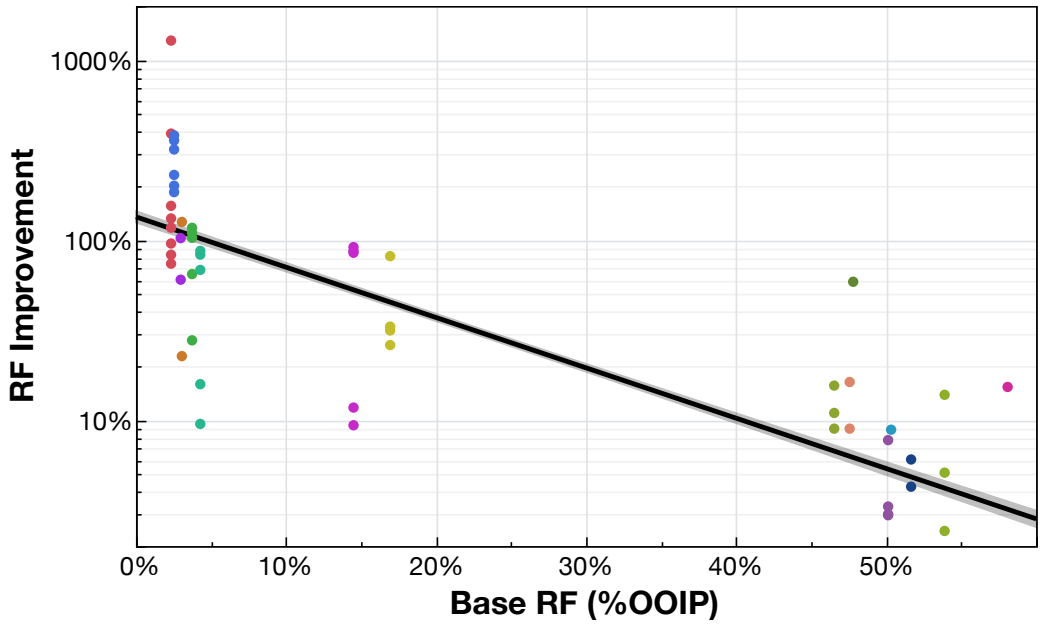

Figure 100 – Improvement of recovery by surfactant cases from the base recovery plotted against the base recovery to show the negative trend between the improvement and the base recovery.

First, the higher base recovery values come from the quartz-rich rock. From the wettability alteration portion of this work, it was presented that less wettability alteration to the water-wet condition is observed with the quartz-rich mineralogy. This behavior would result in lower efficacy of the surfactant which will be reflected by the lower

improvement of recovery, which falls in line to the trend observed in Figure 100. Second, the imbibition process involves multi-phase flow in porous media where the water-phase imbibes into the core sample and displaces the oil-phase out of the core. This means relative permeability is also an important factor to consider. Higher base recovery means the water saturation would be higher. Higher water saturation causes the oil relative permeability to be lower, hindering the flow of oil out of the core plug. This could be another reason why the recovery improvement for higher base recovery is lower. It is also important to note that surfactant could alter the relative permeability of a multi-phase system through the reduction of the IFT between the two phases implying that IFT could reduce the detrimental effect of relative permeability.

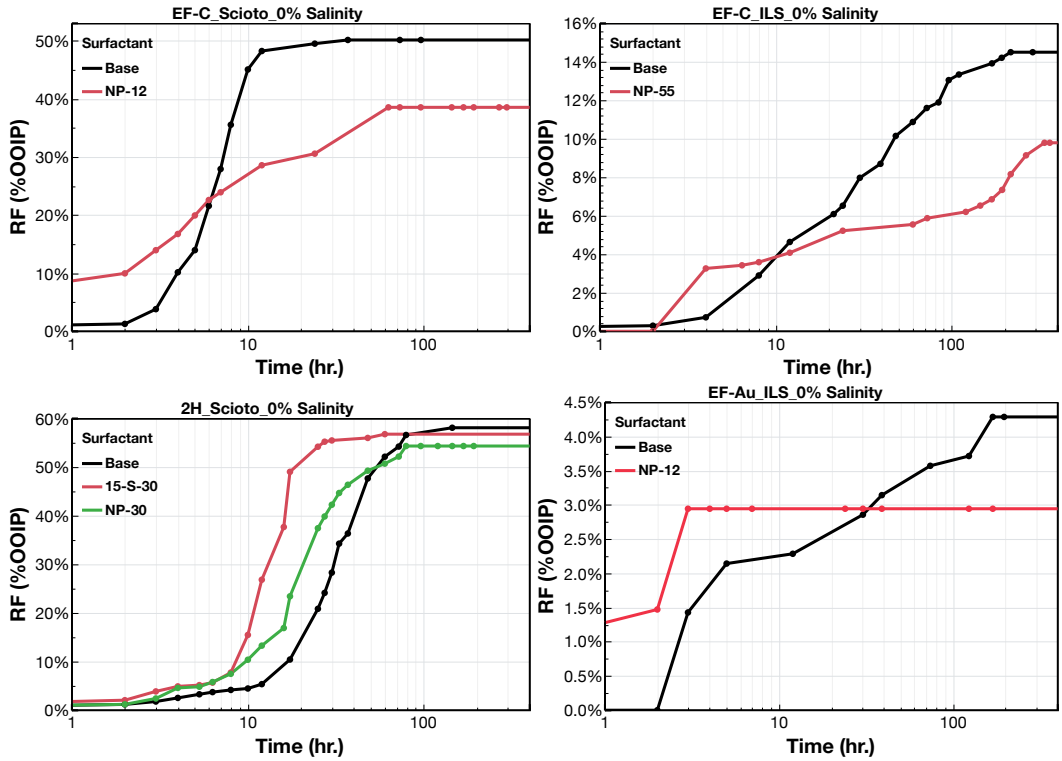

Figure 101 – Cases showing the detrimental effect of incompatible surfactants on the imbibition experiments. Top-left is from crude oil EF-C on siliceous, top-right is from crude oil EF-C on carbonaceous, bottom-left is from crude oil 2H on siliceous, and bottom-right is from crude oil EF-Au and carbonaceous mineralogy. All with 0% salinity.

As mentioned above, while most of the surfactant cases show recovery improvement when compared to the base case, there are cases where less recovery is observed when surfactants are applied. These cases are presented in Figure 101. The top-left figure shows the detrimental effect of surfactant NP-12 when applied on crude oil EF-C with a siliceous mineralogy at 0% salinity. The base case shows recovery of 50% and the addition of surfactant NP-12 reduces the recovery factor to 39%. The top-right figure shows the detrimental effect of surfactant NP-55 on the crude oil EF-C, a carbonate-rich rock at 0% salinity. The base recovery of 14.5% is reduced to 10%, more than 30% reduction in recovery factor. The bottom-left figure presents the detrimental effect of surfactant 15-S-

30 and NP-30 when applied to crude oil 2H with siliceous mineralogy at 0% salinity. Initially, the base recovery is close to 58%. With the addition of surfactant, the final recovery is reduced to 56% and 54% for 15-S-30 and NP-30 respectively. Finally, the detrimental effect of surfactant NP-12 when applied with crude oil EF-Au in a carbonate-rich sample at 0% salinity is presented in the bottom-right figure. The recovery is reduced from 4.3% to 2.9% by the surfactant. The reasoning behind this effect is still unknown. Both surfactants NP-12 and NP-55 are observed to have poor wettability alteration performance. The former due to the low cloud point, and the latter due to the strong hydrophilicity of the surfactant. This however does not explain why surfactant 15-S-30 and NP-30 are also on the lists of the surfactant that reduces the recovery. It is important to also note that the same surfactants found to be detrimental in Figure 101 also performs extremely well when applied to a different crude oil/rock/brine system. This ultimately proves that the surfactant itself is not damaging, only if it is applied to the wrong system.

From Figure 101, it can also be seen that all surfactant cases initially have better recovery compared to the base cases. In all the graphs, the red and green lines which represent surfactant cases are always higher than the blue lines at initial time. At later time, the blue lines start to take over and finally results in higher final recovery. This implies that these surfactants only reduce the final recovery, not the production of oil during the early time of the imbibition process. This observation also shows that surfactant improves the rate of recovery, in addition to the magnitude of the recovery.

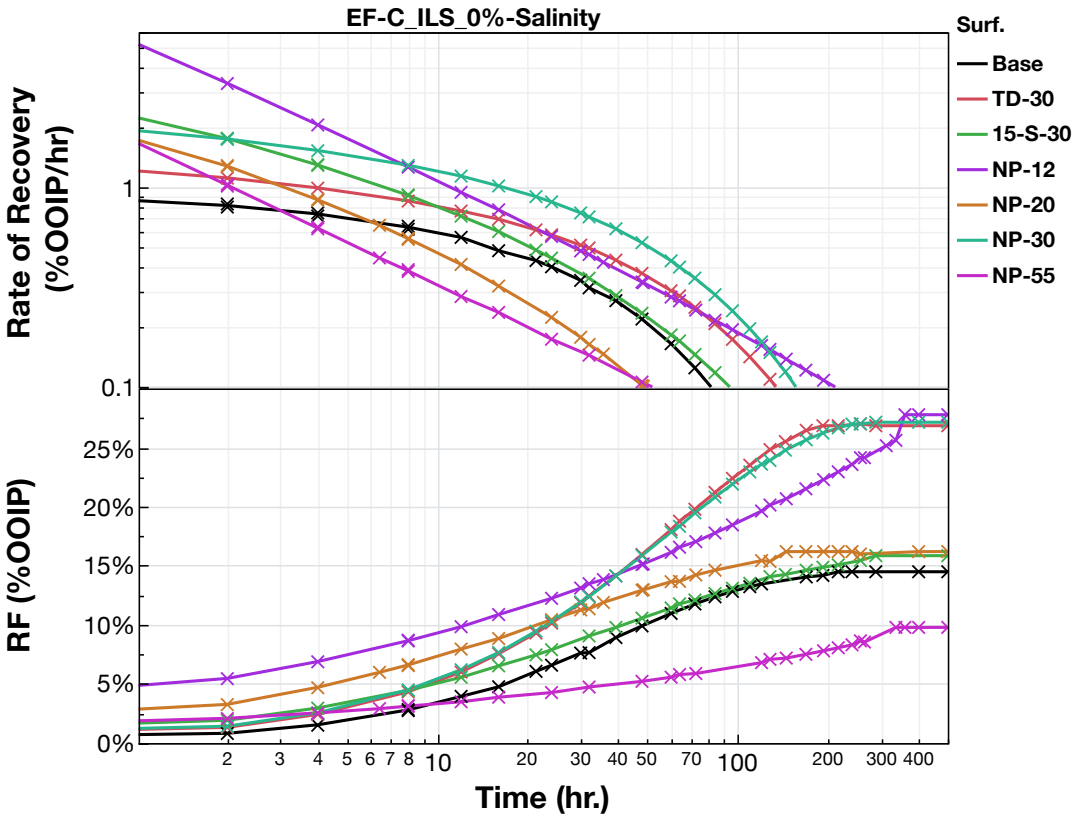

Figure 102 - Analysis of rate of recovery on crude oil EF-C, limestone mineralogy, and 0% salinity. The top box shows the rate of recovery which is calculated by taking the first derivative of recovery factor vs time (the bottom box).

The rate of recovery can be obtained by taking the first derivative of the imbibition recovery curve. This will give the rate in the unit of %OOIP/hour. By applying this derivative, the effect of surfactant to the rate of recovery can be explicitly presented. The imbibition data from five surfactants, TD-30, 15-S-30, NP-12, NP-20, NP-30, and NP-55, performed on crude oil EF-C, carbonate-rich rock, and 0% salinity system are selected to explore this derivative method. The typical recovery factor curves of these imbibition experiments are presented in the bottom row of Figure 102. In the plots, the black lines represent the base case, and all other colors represent an experiment with surfactant. The

first derivative is plotted against time on the top row of the figure. Here it shows that the rate of recovery is improved by surfactant in all cases. For the case of NP-55 where the surfactant is detrimental to recovery, the initial rate of recovery is higher which then slows down to lower than the base case. The rate of recovery for a pure imbibition case is driven by the magnitude of the capillary force where larger capillary pressure results in faster transfer of oil and water.

Tailgroup and Crude Oil Composition Compatibility

As presented in the previous section of this study, the various shale reservoirs in the Lower 48 produces a wide range of crude oil. The easiest way to distinguish, using API gravity, shows a range of 28° to 55° API. However, crude oil is composed of a wide range of hydrocarbon molecules. From SARA and GC, it has been observed that each of the crude oils produced from each shale reservoirs are composed of different compositions of hydrocarbon components. This heterogeneity of crude oil is hypothesized to affect the performance of different surfactant molecules. Specifically, when interacting with the tailgroup of the surfactant which directly interacts with the crude oil. For example, a crude oil containing more aromatics or hydrocarbons with cyclic molecules may interact stronger with surfactants also containing a cyclic structure on the tailgroup. In this study, this behavior is referred to as surfactant tailgroup and crude oil composition compatibility factor

To investigate the compatibility factor, several spontaneous imbibition data from Figure 98 and Figure 99 are selected. Better comparison of tailgroup structure is performed

by selecting surfactants with the same headgroup structure. In this study, surfactant TD-30, 15-S-30, and NP-30 are selected. These surfactants have 30 EO groups as their headgroup with primary tridecanol, secondary pentadecanol, and nonyphenol as the tailgroup respectively.

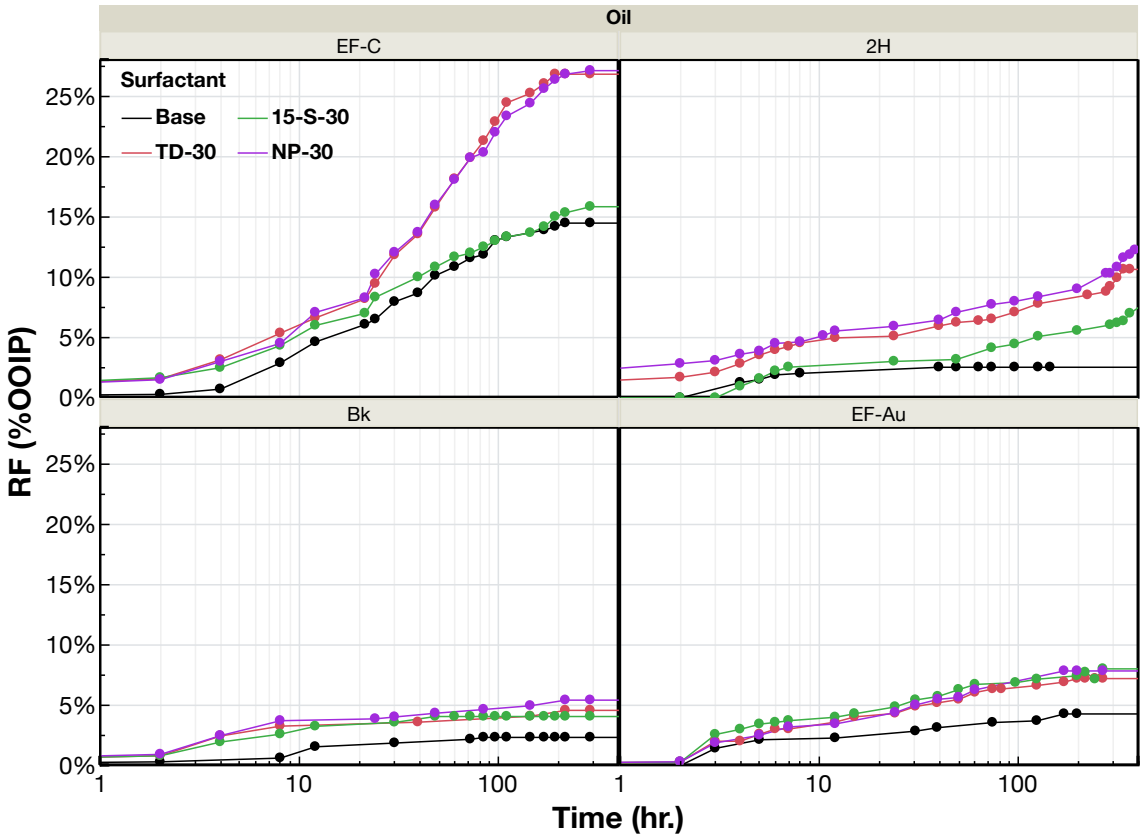

Figure 103 - Imbibition recovery factor data of the three tailgroup, primary alcohol, secondary alcohol, and nonylphenol. Performed on the carbonate-rich mineralogy on crude oil EF-C (top-left), 2H (top-right), Bk (bottom-left), and EF-Au (bottom-right).

The imbibition recovery factors from these three surfactants along with the base case on the four crude oils are presented in Figure 103 for carbonate-rich rock and in Figure 104 for quartz-rich rock. In most cases, the production of oil from core plugs submerged

in surfactant solution is greater than the base case. There are two exceptions, surfactant 15-S-30 and NP-30 on quartz-rich sample saturated with crude oil 2H. These two cases are in the top-right box of Figure 104, are shown as the green and purple lines respectively. It is important to note that these two surfactants, like all negative cases presented before, have faster and higher recovery factor during early time.

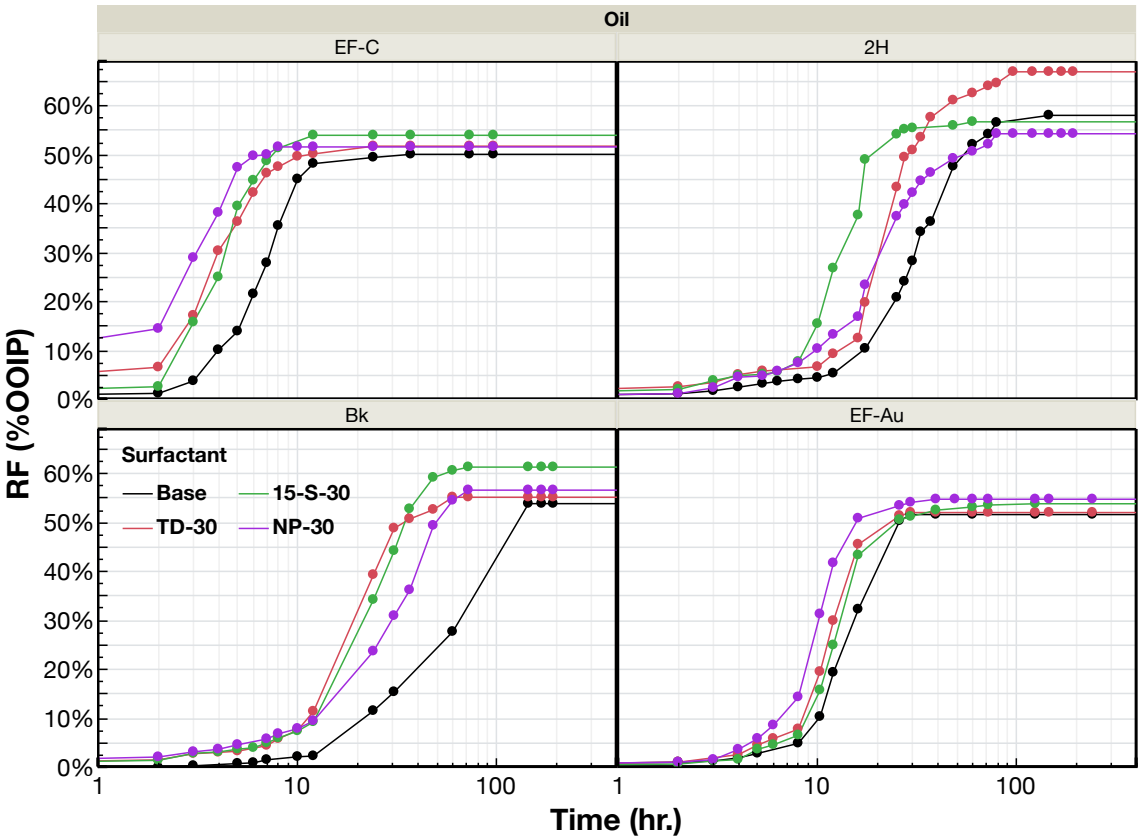

Figure 104 - Imbibition recovery factor data of the three tailgroup performed on the quartz-rich mineralogy on crude oil EF-C (top-left), 2H (top-right), Bk (bottom-left), and EF-Au (bottom-right).

On the calcite-rich mineralogy, all surfactants (green, red, and purple lines) improve the oil recovery compared to the base case (black lines). The extent of improvement differs

from surfactants and systems. The imbibition result using crude oil EF-C is presented in the top-left box. The base case results in a 14% recovery factor. Adding the secondary alcohol surfactant increases the production to 16%. Nonylphenol and primary alcohol tails increase the production to greater than 26%, almost doubling the base production. For crude oil 2H (top-right), the base recovery is less than EF-C with only 2% recovery. With this crude oil, the secondary alcohol tailgroup is relatively more effective as it improves the recovery to 8%, quadrupling the base recovery. It is still the least effective tailgroup in comparison to the other two tailgroups. Nonylphenol tailgroup produces the best recovery improvement at 12%, followed by the primary alcohol tailgroup at 10%. Improving the recovery by the factor of 6 and 5 respectively. For crude oil Bk (bottom-left), the base recovery is similar to crude oil 2H at 2%. Just like the two previous crude oils, the secondary alcohol tailgroup is the poorest performing surfactant with 4% recovery. The nonylphenol and primary alcohol tailgroup produces more at 6% and 4.5% respectively. However, it is important to note that with crude oil Bk, the difference in performance between the three tailgroup is closer and the overall improvement of recovery from surfactant is the lowest compared to the other crude oils. Finally, the imbibition results from crude oil EF-Au are presented in the bottom-right figure. The base recovery of this oil is 4%. All three tailgroups improve the recovery to a similar level of approximately 8%, thus doubling the recovery. The secondary alcohol tailgroup is the best performing tailgroup, followed by the nonylphenol, and then the primary alcohol. The imbibition results presented here show strong evidence of tailgroup/crude oil compatibility

which results in significant difference in recovery between different tailgroup and crude oil combinations.

Compatibility is also observed for the quartz-rich mineralogy. In the top-left box of Figure 104, the imbibition results performed with crude oil EF-C are presented. As mentioned before, the base recovery of the siliceous rock is larger and the level of improvement by surfactant on this mineralogy is less than the limestone. The base recovery of crude oil EF-C is 50%. Nonylphenol and primary alcohol tailgroups show similar recovery improvement to 52%, while the secondary alcohol tailgroup increases recovery to 55%. This is an interesting result as this tailgroup provided the least recovery improvement on the limestone mineralogy but in this mineralogy, it performs the best compared to the other two tailgroups. With crude oil 2H, the base recovery is higher than EF-C at 58%. The primary alcohol tailgroup improved recovery to 67%. While both secondary alcohol and nonylphenol tailgroups reduce recovery to 55% and 57% respectively. As a comparison, on the calcite-rich mineralogy, the primary alcohol tailgroup produces less than the nonylphenol tailgroup and the secondary alcohol tailgroup produces the least. The recovery trend changes on the siliceous mineralogy to primary, secondary, and nonylphenol tailgroup in descending order. The recovery factors of crude oil Bk are presented in the bottom-left box of Figure 104. The base recovery sits at 54%. The secondary alcohol tailgroup improves the recovery the most to 62%, followed by the nonylphenol at 58% and the primary alcohol at 55%. The secondary alcohol tailgroup that performs poorly on the carbonaceous mineralogy is now the best tailgroup on the siliceous mineralogy. Finally, results from crude oil EF-Au on the quartz-rich mineralogy are

presented in the bottom-right box of Figure 104. Compared to the three previous crude oils, minimal improvement from the surfactant is observed. The base recovery is 52%. The primary alcohol tailgroup does not improve the recovery. The secondary tailgroup increases the recovery to 54% and the nonylphenol tailgroup improves the recovery to 55%.

A summary of the surfactant performance is presented in Figure 105. In these figures, the recovery factor from each surfactant is normalized to the base recovery factor. Generally, lighter crude oil prefers the nonylphenol tailgroup on the calcite-rich mineralogy. While the heaviest crude oil, EF-Au, has the highest production when the nonylphenol tailgroup is used. On the siliceous mineralogy, the trend is less consistent. The secondary alcohol tailgroup shows the best performance with crude oil EF-C and crude oil Bk, while crude oil 2H has greatest recovery improvement with the primary alcohol tailgroup. And the EF-Au crude oil performs best with the nonylphenol tailgroup. These results highlight the importance of tailgroup/crude oil compatibility. However, it also shows that the compatibility is also a strong function of the rock mineralogy.

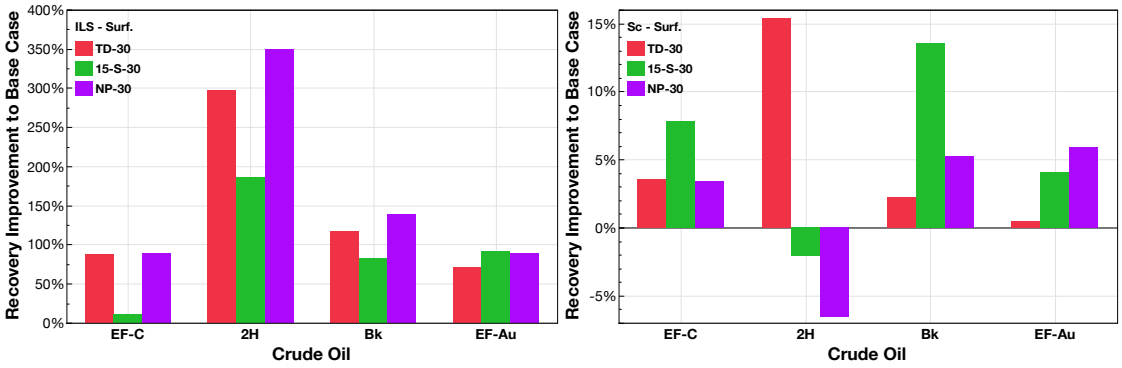

Figure 105 – Summary of recovery improvement of the three tailgroup structures on all crude oil and mineralogy combinations.

Figure 106 compiles the imbibition data into rankings. The three tailgroups are ranked based on their recovery factor with each crude oil and mineralogy combination. The tailgroup with the highest recovery is given the first rank. The ranking is plotted against the crude oil, and the plot is grouped by mineralogy. With limestone, as mentioned previously, nonylphenol provides the highest recovery for all crude oils except EF-Au. It is postulated that the high content of long linear hydrocarbons in crude oil EF-Au causes this trend. It was expected that the high aromatic content in crude oil EF-Au would result in the nonylphenol to be the most compatible. The reasoning behind this discrepancy is still not understood. This discrepancy also only occurs with limestone. For the quartz-rich mineralogy, the nonylphenol tailgroup is now the most compatible with the EF-Au crude oil as it has the highest ranking as shown in the right plot of Figure 106. All trends observed in the limestone on the remainder of the crude oils also change. For this mineralogy, the secondary alcohol tailgroup is now performing well on crude oil EF-C

and Bk. The primary alcohol tailgroup performs better with lighter crude oil, 2H and EF-C, but performs worse with a heavier crude oil like Bk and EF-Au (observed on the negative trend of the red line). On the other hand, the nonylphenol is more compatible with heavier crude oils as shown by the positive trend of the purple line. The trend with the quartz-rich rock is more in line to the observations observed in this study from cloud point, IFT, and wettability point of view.

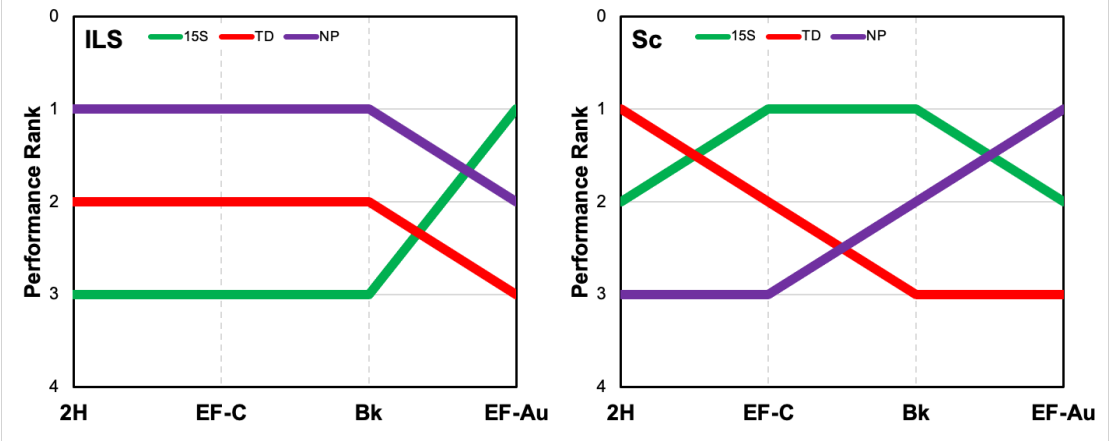

Figure 106 – Performance ranking analysis for the crude oil/tailgroup compatibility study.

Initially, the imbibition experiments were designed to only investigate compatibility between crude oil composition and surfactant tailgroup. As shown above, this compatibility is also dictated by mineralogy. The system salinity also strongly controls the compatibility as will be discussed in this section. This behavior was suspected early in the cloud point section of this study. At low salinity, the secondary alcohol tailgroup has the highest cloud point compared to other tailgroups. Once the salinity is increased, the IFT reduction of this tailgroup improves and is lower than the nonylphenol and primary

alcohol. This means that the hydrophobicity of the tailgroup of the surfactant is also controlled by salinity. Since the tailgroup interacts with the crude oil, this could result in the change of compatibility by salinity.

Figure 107 presents the recovery data of imbibition performed with crude oil EF-C and Bk on the limestone mineralogy. Like the previous section the base case, TD-30, 15-S-30, and NP-30 are selected since the tailgroup effect is the focus. The data from the siliceous mineralogy is presented on Figure 108. In each of these figures, the first column presents data of imbibition performed at 0% salinity. The middle column shows data at 8% salinity and the right column presents the data at 16% salinity.

Several changes can be observed when comparing the imbibition profile of calcite-rich mineralogy between 0% and 8% (Figure 107). With crude oil EF-C, the performance difference between surfactants is minimized when the salinity is increased to 8%. For crude oil Bk, the difference between surfactants is similar to low salinity. But the improvement of recovery by surfactant when compared to the base case is improved at higher salinity. With both crude oil EF-C and Bk at lower salinity, tailgroup nonylphenol produces the most oil, followed by the primary alcohol and finally the secondary alcohol. When the salinity is increased, the secondary alcohol tailgroup is now the best performing tailgroup. The nonylphenol tailgroup is the second best and the primary alcohol tailgroup is the worst performing. Previously it was mentioned how the hydrophobicity of the secondary alcohol tailgroup is improved by salinity as observed from IFT measurements. Increased salinity provides the best condition for this tailgroup to produce oil by

imbibition for both crude oils. It is suspected that a more hydrophobic tailgroup provides better recovery factor on the limestone mineralogy.

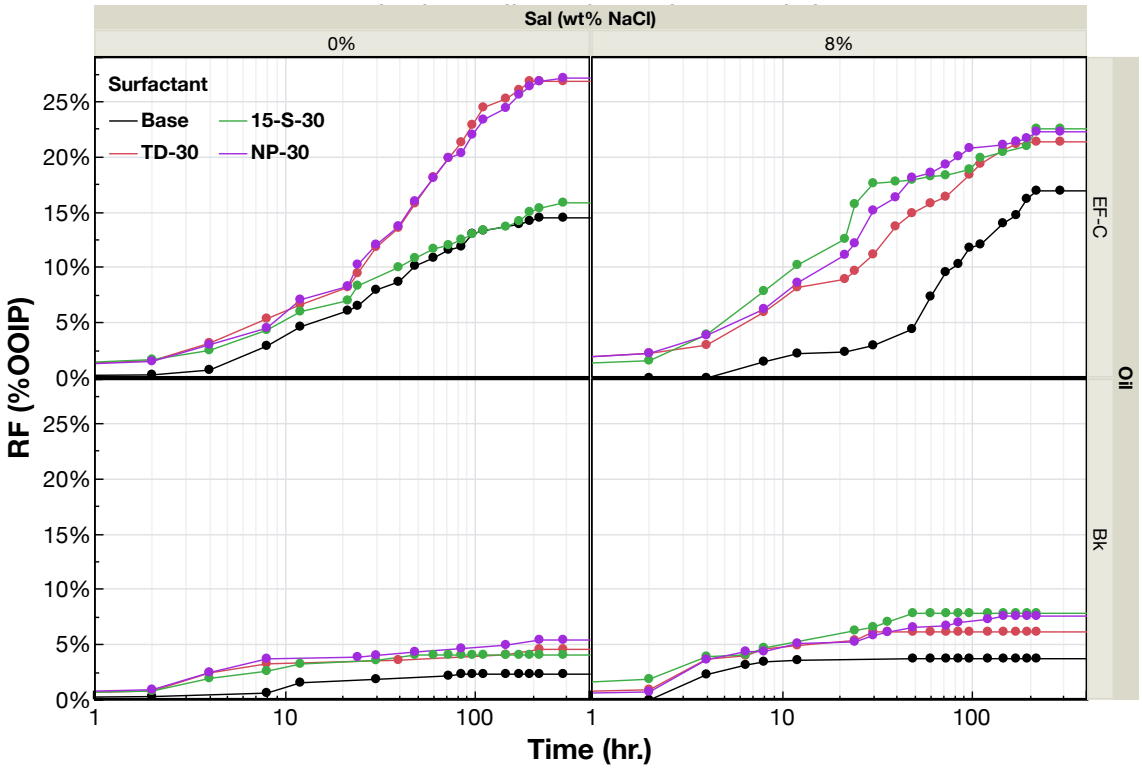

Figure 107 - Imbibition recovery factor data of the three tailgroups structures performed on the carbonaceous mineralogy on crude oil EF-C (top) and Bk (bottom). The main analysis is the effect of salinity to the compatibility. Columns contain salinity data from 0% and 8%.

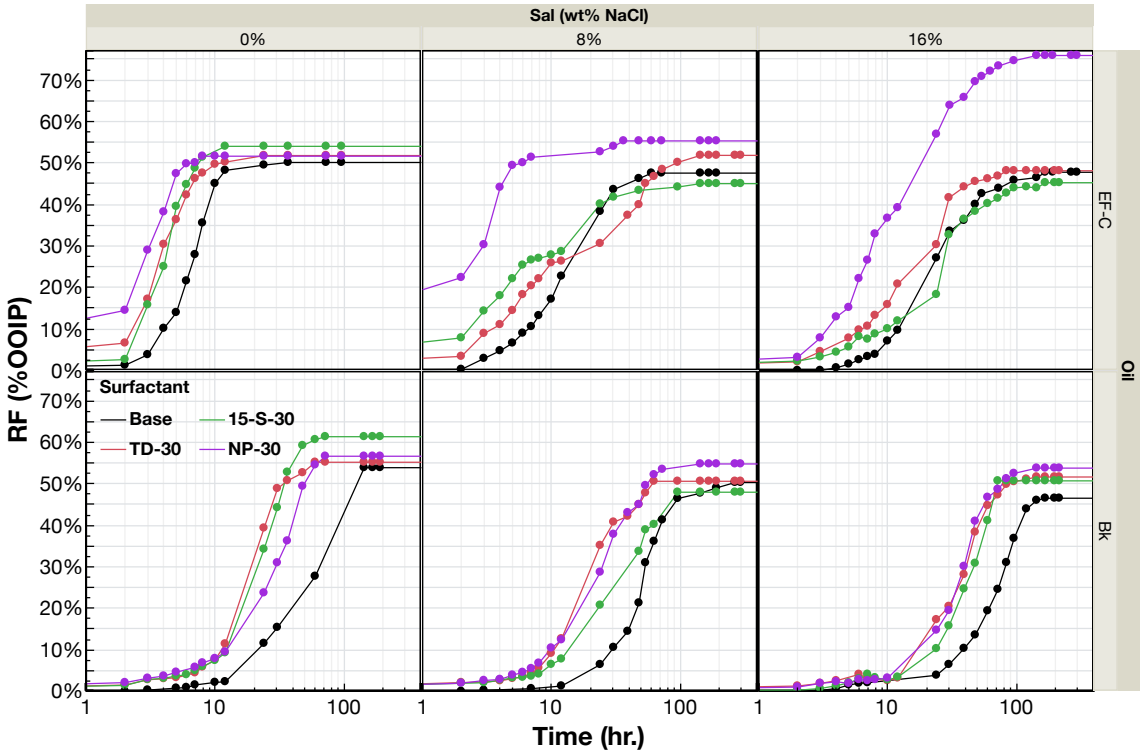

Figure 108 - Imbibition recovery factor data of the three tailgroups structures performed on the siliceous mineralogy on crude oil EF-C (top) and Bk (bottom). The main analysis is the effect of salinity to the compatibility. Columns contain salinity data from 0%, 8%, and 16% from left to right.

For the quartz-rich mineralogy (Figure 108), a higher salinity improves the performance of the surfactant with both crude oils as the recovery improvement with surfactants is greater at higher salinity. However, the opposite trend regarding the secondary alcohol tailgroup is observed. At 0% salinity, this tailgroup has the highest recovery improvement for both crude oils. Unlike the carbonaceous mineralogy, salinity increase actually reduces the efficacy of this tailgroup. With crude oil EF-C, the recovery improvement by the secondary alcohol tailgroup becomes lower when the salinity is increased from 8% to 16%. A similar observation is observed with crude oil Bk. Although the recovery factor is the same when the salinity is increased from 8% to 16%, the

secondary alcohol tailgroup is still the worst performing surfactant when compared to the other tailgroups.

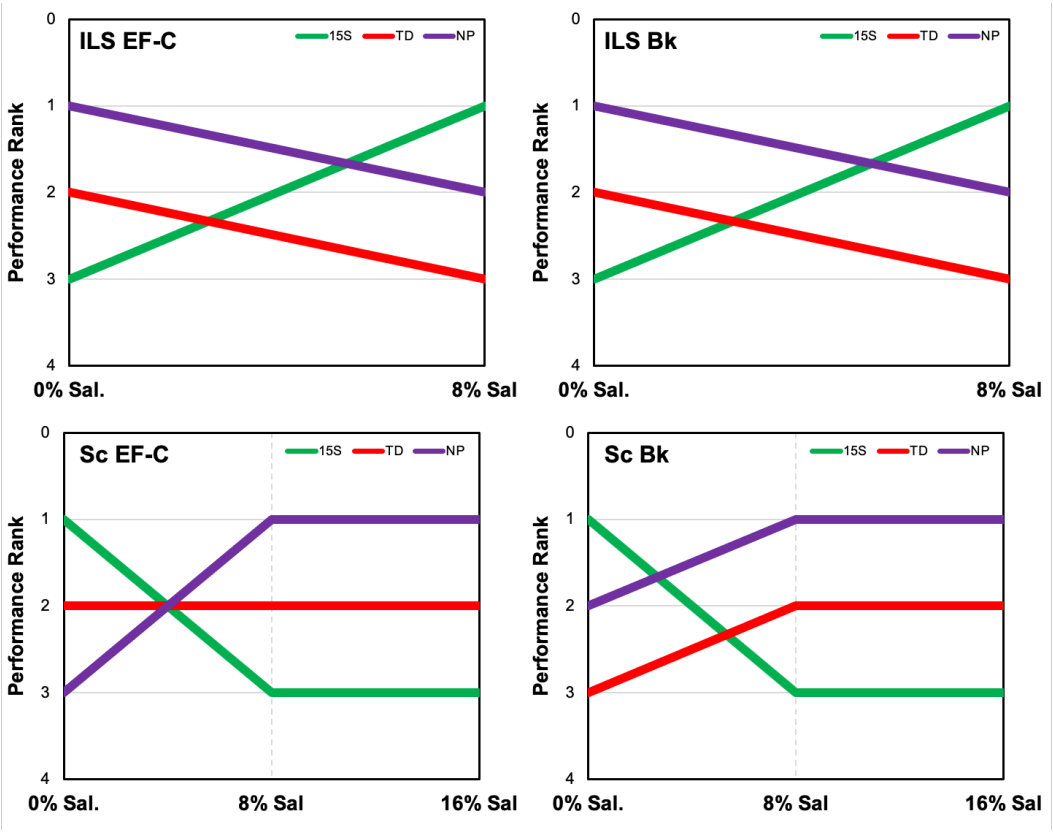

Figure 109 – Performance ranking analysis to investigate the effect of salinity to the crude oil/tailgroup compatibility. The two plots on top show data of carbonaceous mineralogy and the two bottom shows siliceous. The two left plots and the two right plots contain data with crude oil EF-C and crude oil Bk respectively.

To better present this salinity-driven compatibility shift, the same performance rank analysis as previously shown is applied to the results shown in Figure 107 and Figure 108. This analysis is presented in Figure 109. Here, the performance rank based on imbibition is plotted against salinity. Data from EF-C on carbonate-rich, Bk on carbonate-rich, EF-C

on siliceous, and Bk on siliceous are presented in clockwise order. A consistent shift is observed on both crude oils. For the limestone lithology, a more hydrophobic tailgroup is preferred as secondary alcohol tailgroup at 8% salinity provides the best recovery factor. Meanwhile, on the quartz-rich sample, a less hydrophobic tailgroup is preferred. This is demonstrated by the secondary alcohol tailgroup at higher salinity becoming the poorest performing surfactant when compared to the other tailgroups.

Headgroup Structure Effect: Finding Optimum EO Number

The next step is to investigate the effect of headgroup on imbibition. To perform this analysis, imbibition results from the nonylphenol tailgroup family are selected. In this tailgroup family, a range of EO groups from 12 to 55 are included. An analysis of the headgroup effect can only be performed while keeping the tailgroup structure constant.

The imbibition data are presented in Figure 110. The top-left box contains data from crude oil EF-C, top-right is with crude oil 2H, bottom-left is with crude oil Bk, and bottom-right is with crude oil EF-Au. Only imbibition performed on the limestone mineralogy is available. In each box, the number of EO's is represented by color. Black is base case, or the base case, red is 12 EO, green is 20 EO, purple is 30 EO, and yellow is 55 EO. With crude oil EF-C, all number of EO groups improves the recovery from the base recovery except for 55 EO. The base recovery is at 14%. The highest recovery comes from 12 EO with 28%, followed by 30 EO at 27%, 20 EO at 16%, and finally 55 EO with lower recovery than base case at 10%. Crude oil 2H shows a lower base recovery at close to 5%. The highest recovery factor is given by 30 EO at 12% but closely followed by 20 EO at

11%. Nonylphenol with 12 EO groups produces less at 8% and 55 EO is the least with 7%. With crude oil Bk, the best improvement with the nonylphenol surfactants is observed. The base recovery of this crude oil is at 2%. The production is improved to almost six times to 12% with the 12 EO groups. The surfactant with 30 EO tailgroup produces close to 6%. While 20 EO groups and 55 EO groups produce 5% and 4% respectively. Finally on the heaviest crude oil, EF-Au, the base recovery is 4%. The headgroup with 30 EO produces the highest recovery at 8%. This is followed by 20 and 55 EO groups with 5% recovery. And headgroup of 12 EO produces less than the base case with 3% recovery.

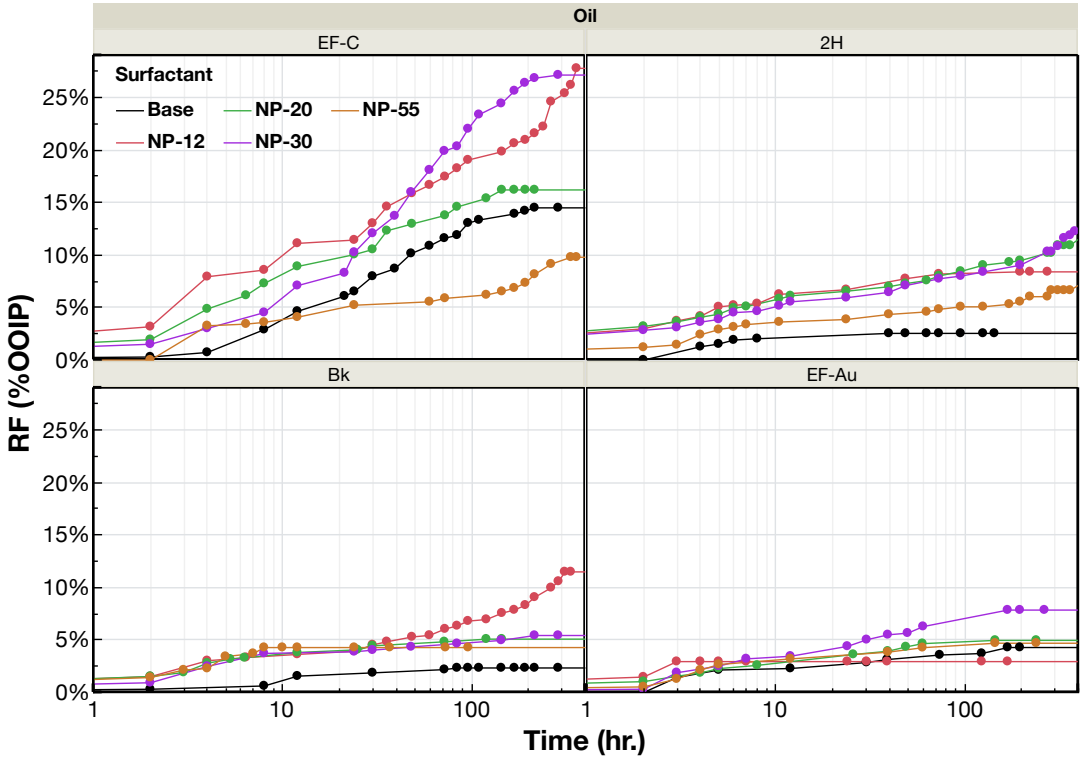

Figure 110 – Imbibition data of the four headgroup structures (12, 20, 30, and 55 EO) along with the base recovery. Experiments are performed on limestone at 0% salinity. Crude oil EF-C (top-left), 2H (top-right), Bk (bottom-left), and EF-Au (bottom-right) are used.

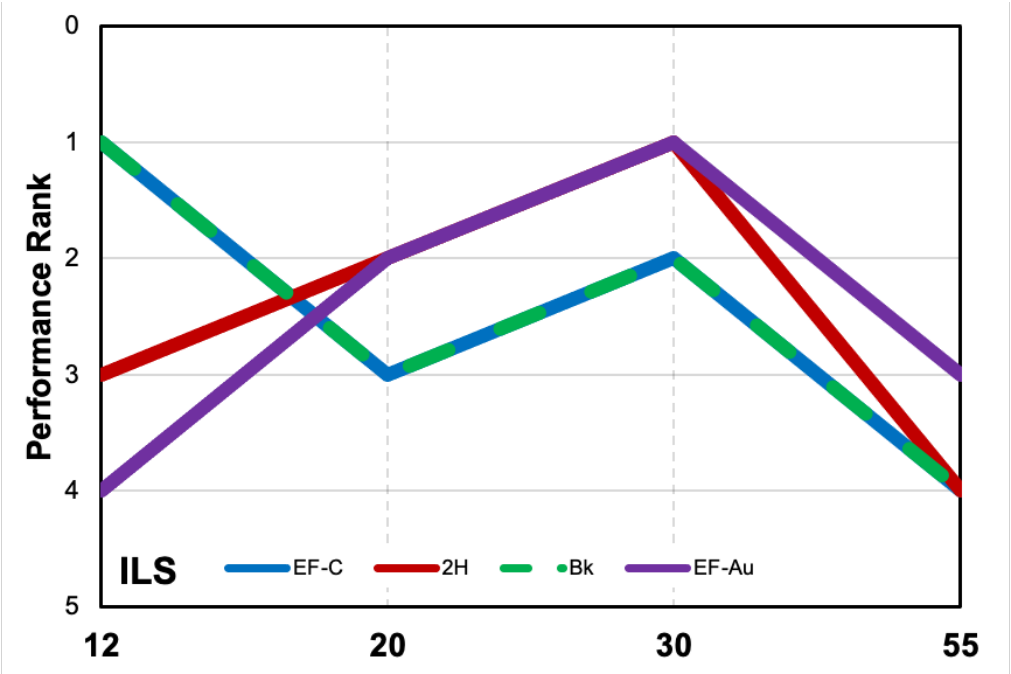

Figure 111 – Performance ranking analysis on the effect of the count of EO group on the headgroup.

The performance ranking analysis applied to this section is presented in Figure 111. The number of headgroups, plotted on the x-axis, is ranked (y-axis) based on their recovery factor from the imbibition process. Ranking for crude oil EF-C (blue) and crude oil Bk (green) is the same. In general, there are two EO groups that show the best recovery, 12 and 30. Crude oil EF-C and Bk have the highest recovery with the nonylphenol tailgroup with 12 EO. Crude oil 2H and EF-Au have the highest recovery with the 30 EO group. Unlike the tailgroup/crude oil compatibility, the performance ranking in this case does not vary in consistent manner between crude oils. Although that there are two groups of crude oils with two different optimum EO lengths, the 12 EO group actually has 30 EO as their second rank. This result is expected since there is minimal interaction between the headgroup of the surfactant and the crude oil unlike the tailgroup which directly interacts

with the crude oil. A balanced hydrophobic and hydrophilic state of the surfactant is required for the surfactant to perform optimally. For the case of the nonylphenol tailgroup, 30 EO on the headgroup provides the best amphiphilicity for the surfactant to produce more oil from the imbibition process.

The better performance of 12 EO groups with crude oil EF-C and Bk with 30 EO groups is intriguing. Ideally, going too far of the balance condition (30 EO) would cause the surfactant to be either too hydrophobic (lower EO) or too hydrophilic (higher EO). This behavior is observed on crude oil 2H and EF-Au, but not on the other two crude oils. The imbibition profile from Figure 110 is reconfigured into Figure 112. In this figure, the recovery factor is plotted against the number of EO groups. Each box contains different crude oils, EF-C, 2H, Bk, and EF-Au, in clockwise direction. In each box, the data are grouped in lines and colors by the experimental time. It is observed that green to yellow to red is moving from early in the experiment to later time in the experiment. From the figure, it is shown that recovery from the 12 EO groups is the fastest compared to all other tailgroups. With the shorter EO group, recovery improvement occurs immediately at the early time. This is believed to be caused by the smaller size of the 12 EO group surfactant, allowing for faster movement into the porous media. At later time, the 30 EO groups slowly increase production. And finally for the case of crude oil 2H and EF-Au, 30 EO surpasses 12 EO and shows the highest recovery. For the case of crude oil EF-C and Bk, this mechanism does not occur. Although the 30 EO headgroup gradually increases recovery to greater than 20 and 55 EO headgroups, the 12 EO headgroup also maintains its recovery increment. It is hypothesized that crude oil EF-C and Bk has the ability to

contain the surfactant molecule in the crude oil. This occurs with the 12 EO headgroup since it is the most hydrophobic surfactant when compared to the rest of the surfactants. Surfactant molecules transferring to the crude oil could improve the recovery by expanding the crude oil and provide an emulsification benefit.

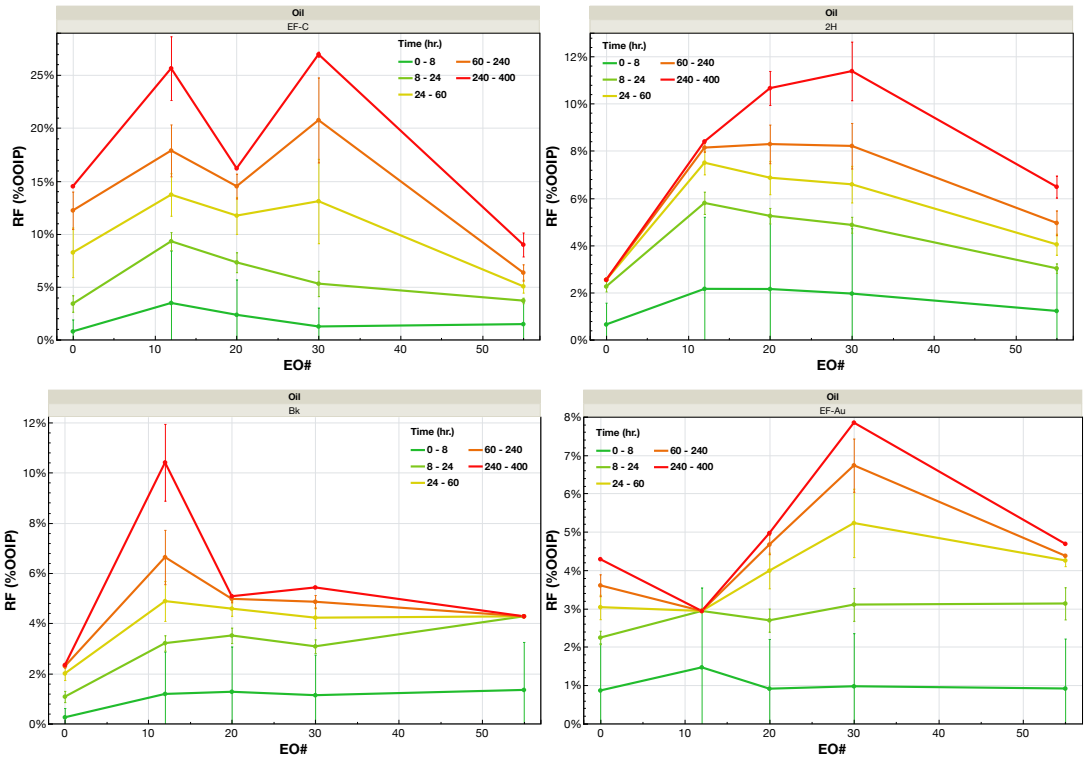

Figure 112 – The imbibition data of the four headgroups. The recovery factor is plotted against the number of EO groups, and the data are grouped by experimental time. Green to yellow to red is moving from early to later time.

An additional analysis is performed by investigating the net adhesion of the four surfactants assessed in the section. The net adhesion tension term of the four different headgroups is plotted in Figure 113 against the EO group length. The data are grouped by

colors and lines. The net adhesion tension term represents the capillary force of the surfactant to produce oil. Higher values indicate greater capillary forces, resulting in more oil produced. Therefore, higher net adhesion tension should result in higher recovery factor. The crude oil in Figure 113 is presented with the same color-coding as Figure 111. For crude oil 2H and EF-Au, 30 EO shows the best recovery improvement. However, in Figure 113, 30 EO shows the second lowest net adhesion tension with crude oil EF-Au and the lowest net adhesion tension with crude oil 2H. The highest net adhesion tension with crude oil 2H is with 55 EO and for crude oil EF-Au with 12 EO. This contradicts the recovery improvement ranking presented in Figure 111 where 55 EO with crude oil 2H actually has the lowest recovery and 12 EO on crude oil 2H also has the lowest recovery. With crude oil EF-C, the highest net adhesion tension is obtained with 30 EO while the highest recovery is with 12 EO. The correlation between net adhesion tension and recovery agrees for crude oil Bk. The net adhesion tension for 12 EO is the highest and the recovery with 12 EO is also the highest. The order of EO group agrees in the two figures, 12, 30, 20, and 55 EO. The erratic behavior here shows that capillary is not the only mechanism working in the application of surfactant to improve oil recovery.

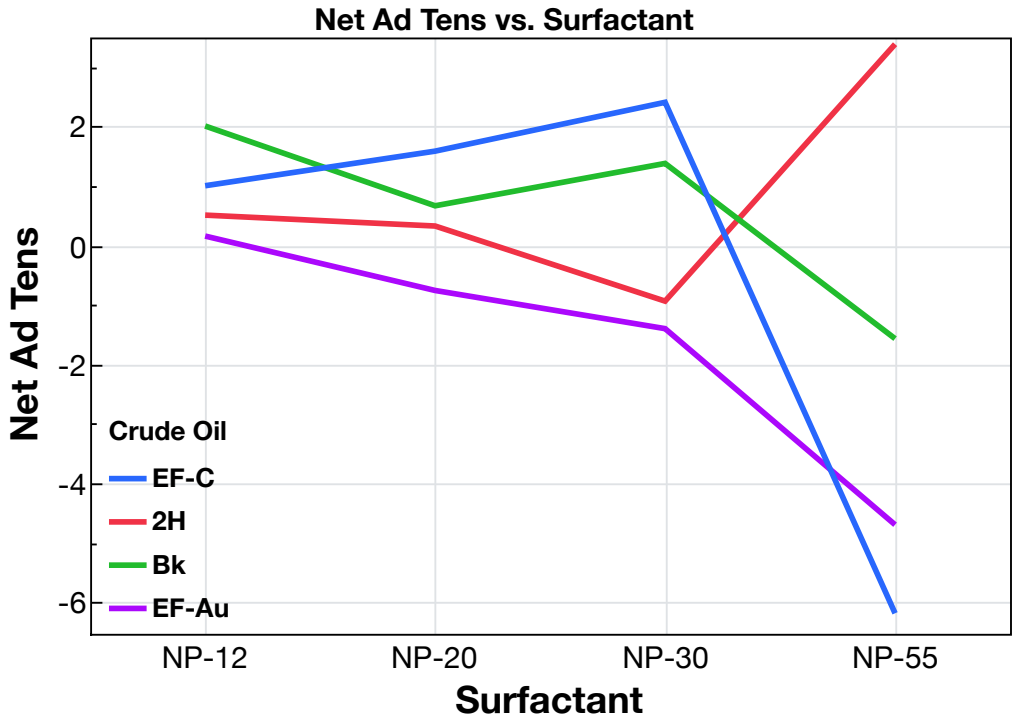

Figure 113 – Net adhesion tension values for four headgroup configurations on the four crude oils.

The Imbibition Profile of Cationic Surfactants

The two previous sections show the results of spontaneous imbibition results performed with nonionic surfactants. In this section, the behavior of cationic surfactants for imbibition experiments is presented. Two cationic surfactants are investigated, C12TAC and C18TAC. Both surfactants have trimethyl ammonium as their headgroup structure. Surfactant C12TAC has a dodecyl group as the tailgroup. While C18TAC has an octadecyl tailgroup. Imbibition is performed on the carbonaceous core plug with crude oil Bk. Four levels of salinity are tested, from 0% to 24% at 8% increments. The crude oil, mineralogy, and salinity are selected in order to apply the study to the high salinity brine of the Williston basin.

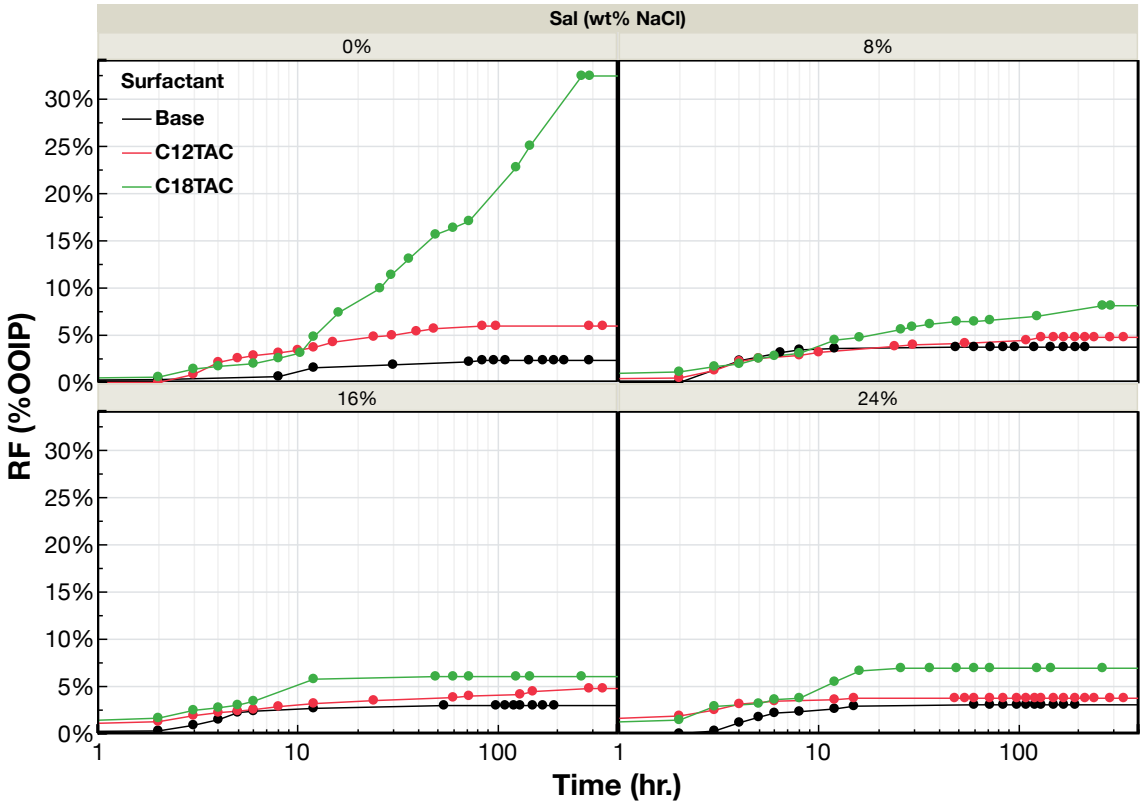

Figure 114 – Imbibition data for cationic surfactants. Experiments are performed with crude oil Bk on the limestone rock. Four levels of salinity from 0% to 24% at 8% increment is tested.

The imbibition results are presented in Figure 114. Black, red, and green represent the base, C12TAC, and C18TAC respectively. The salinity levels are 0%, 8%, 16%, and 24% in clockwise direction. Both cationic surfactants provide recovery improvement from the base case at all salinity levels granted that the degree of improvement from the base case varies with salinity. This will be discussed later. At all salinity levels, the cationic surfactant with the longer tailgroup shows the highest recovery. The C18TAC surfactant, represented by green lines, always has higher recovery compared to the red lines which represents the C12TAC. The cationic headgroup has the lowest IFT reduction due to the high degree of hydrophilicity, driven by the ionic bond between the surfactant and the

water molecules. This means that this headgroup causes the surfactant molecule to remain in the aqueous-phase, reducing surface activity. By increasing the length of the hydrocarbon chain on the tailgroup, the total hydrophilicity of the surfactant is reduced thus allowing the surfactant to be more surface active. This is represented in the imbibition results that show superior performance of the C18TAC surfactant when compared to C12TAC. This result also agrees with a previous study performed where the focus was development of surfactants for ultra-high temperature shale reservoirs.

To better analyze the recovery data presented in Figure 114, the final recovery for imbibition is compiled into Figure 115. This figure plots the final recovery factor as well as the recovery improvement (final recovery normalized to the final recovery of the base case at each salinity level) against the salinity. Here it can be clearly seen that the surfactant performance decreases with increasing salinity. At 0% salinity, C18TAC improves the recovery by more than an order of magnitude while C12TAC more than doubles recovery. At 8% salinity, the improvement drops to 100% and 10% respectively. Increasing the salinity to 16% and 24%, the recovery does not change. However, when normalized to the base recovery, the improvement increases slightly with C18TAC. With C12TAC, the improvement increases from 40% at 16% salinity and then decreases to less than 10% at 24% salinity. The cationic headgroup is shown to be strongly hydrophilic and causes the surfactant to be less effective. One way to decrease the hydrophilicity is to increase salinity, since the headgroup of the surfactant will have to compete with the salt ions to capture a free water molecule. Therefore, it is expected that cationic surfactant would provide better performance at higher salinity. The result shown in Figure 115 does

not support this theorem as the recovery improvement from both cationic surfactants becomes lower with increasing salinity. This discrepancy could be driven by multiple reasons. First, higher salinity reduces the CMC of the surfactant. This could cause the de-micellization to be slower thereby restricting surfactant partitioning at the interface. Second, once soluble in water, the cationic surfactant is in essence a pair of salt ions. The trimethyl ammonium could easily bond with the chloride ion in the solution thus reducing the amphiphilicity of the surfactant. In order to improve the surface activity of the surfactant, another method should be pursued other than increasing the salinity of the system. Since C18TAC shows better improvement than C12TAC, a longer tailgroup should be selected in applying cationic surfactants as a method to reduce the total hydrophilicity of the surfactant thus allowing the surfactant to be more surface active to improve the oil recovery.

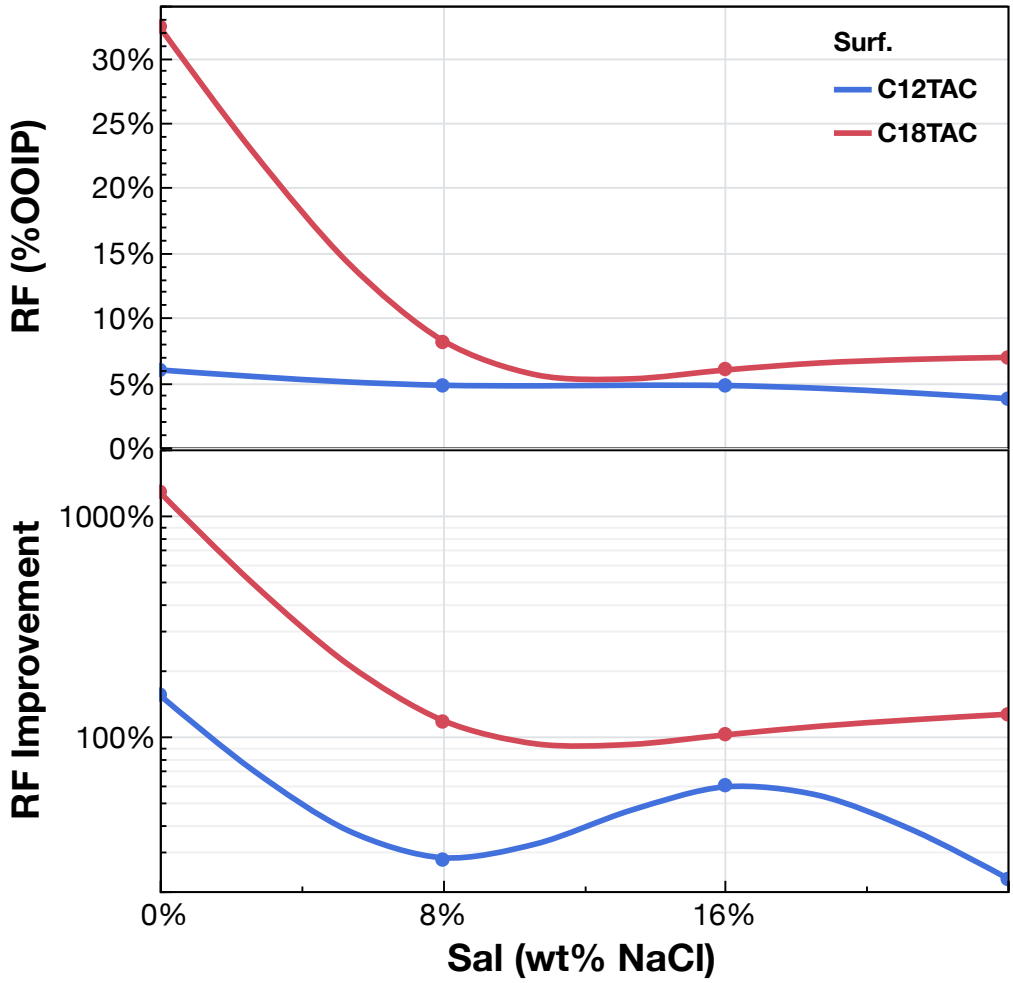

Figure 115 – Recovery factor (top) and recovery improvement (bottom) of the two cationic surfactants tested plotted against the system salinity.

CHAPTER XI

CONCLUSIONS

This study covers a vast area of surfactant/crude oil/brine/rock interaction. Just the base case analysis, when the surfactant is not included, is already an extensive study with large numbers of variables and interaction between variables. Adding surfactant into the mix complicates this further since the surfactant molecule interacts with each of the variables and also with the interaction between variables. Due to the relatively young age and the fast nature of shale development, this type of study is still very rare in the literature. This highlights the importance of carrying out this kind of comprehensive study. To make the study more manageable, it is divided in parts. Starting from where the system is simple and gets more complicated by chapter with the addition of more phases. The study starts with a system containing crude oil and brine to a system containing surfactant, crude oil, brine, smooth rock surfaces, and porous media. This is spread over seven chapters in this thesis. The conclusions are presented below, grouped by how the study is divided in chapters.

Chapter IV, Lower 48 Shale Reservoirs Oil/Brine Interaction

- Shale crude oil samples presented in this study have virtually zero asphaltene content, zero acid number, and zero basic number. The only exception is from the heavier crude oil produced in the shallower section of the Eagle Ford. This is in contrast to the crude oil recovered from conventional reservoirs where asphaltene components are often

found. The explanation for this could be from the relatively higher temperature of unconventional reservoirs. Unconventional reservoirs are mostly the source rock of conventional reservoirs, meaning that it would be deeper and hence the higher temperature.

- A novel SARA-based oil/water IFT correlation for shale crude oil is presented with excellent accuracy at ambient condition. The correlation can be used at high temperatures with reduced accuracy.
- Saturates increase the oil/water IFT due to their extreme non-polarity, while aromatics and resins decrease the IFT due to their polarizable nature.
- Salinity increases the polarity of the aqueous-phase, causing the aromatic and resin components to lose their polarizable properties. As a result, the oil/water IFT is increased when the crude oil contains aromatic and resin components.
- The presence of divalent ions in produced brine does not significantly affect the oil/water IFT thus the Variable Sinclair Method is not necessary to obtain accurate prediction of IFT for the produced brines where 95% of the ions are NaCl.
- Temperature decreases the oil/water IFT by reducing the polarity contrast between the oil/water phases. This interaction only occurs at low salinity. At high salinity, the aqueous-phase contains substantial amounts of salt ions that results in significant polarity, thus the temperature effect is virtually absent.

- Shale oil/brine/rock systems in all reservoirs and even the multiple facies in each reservoir investigated (Wolfcamp, Eagle Ford, Three Forks and Middle Bakken) were observed to be oil-wet with contact angles averaging above 110° after sufficient aging time.
- Pre-soaking the samples with brine expedites the rate of oil wetting during the aging process and increases the ultimate degree of oil wettability as determined by contact angle measurements.
- Rock with higher quartz content (>50%) created a more oil-wet surface with no effect on the optimum aging time. Oil with a higher concentration of aromatics and resins rendered the surface more oil-wet and reduced the optimum aging time. These two crude oil components were major drivers of the creation of an oil-wet surface on the shale oil/brine/rock systems investigated.
- Shale crude oil is observed to be non-asphaltic. The effect is observed in this base wettability chapter. Currently available wettability studies mainly revolves around the theory of asphaltenes and organic acid adsorption on the calcite surface. Due to the difference between conventional and unconventional crude oil characteristics, this theory is not applicable as shown in the previous conclusion.
- Brine with higher salinity resulted in stronger oil-wetness and increased the time required to achieve stable aging. Higher brine salinity resulted in an aqueous phase with stronger polarity, which forces the aromatic and resin components of the crude oil to be more adsorbed on the rock surface.

- Oil composition and brine TDS affected the surface wettability to a greater degree compared to the rock mineralogy.
- The aromatic and resin components of the crude oil were observed to form stronger bonds with the quartz minerals associated with the rock which resulted in more oil-wetness.

Chapter VI, Nonionic Surfactant Cloud Point and Its Comparison to Lower 48 Shale Reservoirs Temperature

- Increasing the length of surfactant EO groups increases the CPT. However, it was demonstrated that an optimum number of EO groups exists and is observed to be in the 20-30 EO groups range. Increasing the EO groups further does not substantially improve the CPT.
- Lower CPT is observed with longer tailgroups since longer hydrocarbon chains are more hydrophobic. However, the nature of the ethoxylation process, e.g., primary, or secondary, also determines the surfactant hydrophobicity. In this study, the secondary alcohol ethoxylate has higher CPT than primary alcohol with shorter carbon number at lower salinity condition.
- Lower CPT is observed at higher brine salinity. As a rule-of-thumb, CPT decreases by ~4.8° F for each 1 wt% NaCl increase in the brine salinity.
- CPT is not observed when the surfactant concentration is below its CMC at its respective salinity.

- Mixing nonionic surfactants with an ionic surfactant increases the CPT. With this co-surfactant system, the CPT ranges from 250° to 400° F at 0% brine salinity and 225° to 325°F at 8 wt% NaCl.
- Increasing the hydrophobicity of both the primary nonionic surfactant and the ionic stabilizer increases the CPT. However, a solubility limit is observed when mixing nonylphenol nonionic surfactant and C22-C24 IOS anionic stabilizer.
- Higher brine salinity results in a decrease of the CPT for the co-surfactant system using anionic stabilizer.
- Cationic stabilizer shows increased CPT performance at higher brine salinity; it was observed that the CPT for 8 wt% NaCl salinity is greater than at 0% salinity.

Chapter VII, Surfactant Structure Effect to Oil/Water IFT

- Higher base oil/water IFT results in larger IFT reduction by surfactant molecules. This is due to the stronger hydrophobicity of the higher IFT crude oils which allows for better bonding with the surfactant tailgroups.
- With the same tailgroup, ionic headgroups have less IFT reduction due to its stronger hydrophilicity.
- From the cloud point chapter, nonionic surfactant loses its ability to be dissolved in water when the temperature is increased. When placed in a system containing both oil and water, this effect is translated into greater IFT reduction at higher temperature for these nonionic surfactants. Higher temperature reduces the strength of the hydrogen

bond between EO groups and water molecules which pushes more surfactant molecule to the oil/water interface.

- The hydrophilicity of ionic surfactant is in the form of an ionic bond between the headgroup and the water molecule. The ionic bond has an opposite effect with temperature where its strength is improved at higher temperature. This results in less surfactant molecules at the interface. Therefore, the IFT reduction is further minimized at higher temperature.
- Increasing salinity results in greater IFT reduction for both ionic and nonionic headgroups. This is due to the reduced solubility in water of both types of surfactant headgroups at higher salinity. This results in more surfactant partitioning at the interface. With the same tailgroup structure, the nonionic surfactants are more sensitive to salinity.
- Nonionic headgroups with longer EO groups are more sensitive to temperature compared to the shorter EO groups. The increase of IFT reduction is larger on longer EO groups when the temperature is increased.
- With constant tailgroup, reducing the length of the EO groups results in greater IFT reduction.
- The zwitterionic headgroup is relatively unaffected by salinity and temperature when compared to all other headgroup charge.
- Generally, the surfactant headgroup does not interact with the oleic phase. The only interaction observed is on a headgroup containing a positive charge and crude oil with a high content of cyclical hydrocarbon chains.

- Compatibility between the tailgroup structure and the crude oil composition is observed. Crude oil that contains more linear hydrocarbons based on GC measurement has its IFT reduced the greatest with shorter linear tailgroups. At the same system condition, crude oil with more cyclical and longer linear hydrocarbon chains showed greatest IFT reduction with the branched, aromatic tailgroups.
- At higher salinity and temperature, the greatest IFT reduction on all crude oils shifts to the secondary alcohol tailgroup. From the cloud point study, the same tailgroup structure is observed to have the highest CPT (least hydrophobicity) at lower salinity and the lowest CPT (most hydrophobicity) at higher salinity. This could be the explanation of the crude oil-tailgroup compatibility shift to the secondary alcohol at more extreme conditions.
- Salinity level alters the secondary C15 tailgroup. At 0% salinity, it has the least IFT reduction. At 8% salinity and above, it causes the greatest IFT reduction. This behavior is only observed on this tailgroup, no interaction between salinity and the other two tailgroups was observed.
- Shorter EO groups provides the largest IFT reduction. However, when the temperature and salinity become greater, shorter EO groups could potentially provide the lowest IFT reduction. When selecting the optimum EO group, the system condition (salinity and temperature) should be considered. Surfactant with 30 EO groups could provide larger IFT reduction than the same surfactant with 12 EO groups when the system has high salinity and temperature as observed in this study.

- Quartz-rich mineralogy is more oil-wet on the base case scenario, as shown in the previous chapter. This has a direct effect on the wettability alteration as surfactants are found to be less effective in rendering water-wetness on this mineralogy when compared to carbonaceous rock.
- Reducing the hydrophilicity of the surfactant, by increasing the system salinity and increasing the system temperature (for nonionic surfactants), improves the wettability alteration capability of the surfactant.
- Applying nonionic surfactant at temperatures above their cloud point results in the reversal of the wettability alteration, back into the oil-wet region.
- With consistent tailgroup and system conditions, longer EO groups results in lower wettability alteration. This is driven by the inhibition of surfactant transfer to the interface by the more hydrophilic, longer EO groups. Since shorter EO groups have a lower cloud point, the shorter EO length selection is limited due to the previous conclusion.
- Surfactant must have balanced hydrophilicity and hydrophobicity. Going further away from the optimum point, either to be more hydrophilic or more hydrophobic, decreases the wettability alteration capability of the surfactant.
- The balance is driven by the structure of the surfactant and more importantly the system condition, temperature, salinity, crude oil, and mineralogy. Each of these variables can push the surfactant out of balance in either direction. For example, surfactant with nonylphenol tailgroup and 12 EO as headgroup at 0% salinity and

120°F is already balanced. Increasing the salinity to 8% pushes the surfactant out of balance, to be more hydrophobic, and results in less water-wet conditions. Reducing the temperature to 70°F also removes the surfactant balance, making it more hydrophilic, and results in a more oil-wet condition.

- An indication of compatibility between the surfactant tailgroup structure and the crude oil composition is observed. Crude oil EF-C is dominated by saturated hydrocarbons, while crude oil Bk contains more aromatics than saturates. The linear tailgroup C13 alters wettability to more water-wet with crude oil EF-C. The nonylphenol tailgroup shows better wettability alteration on crude oil Bk.
- With the same headgroup configuration, tailgroup 15S (secondary alcohol) has the worst wettability alteration performance at low salinity. This tailgroup only renders water-wetness on crude oil Bk. Tailgroup 15S also renders the system containing crude oil EF-C to be more oil-wet than the base case. When the salinity is increased, the surfactant with a 15S tailgroup is able to render water-wetness on oil-wet system.
- With the same tailgroup structure, increasing the EO length reduces the water-wetness of the surfactant system. At higher salinity the same trend is observed, only that shorter EO would already be too close to its cloud point and the wettability alteration is reversed.
- Ionic surfactants are ultra-sensitive to temperature. Higher temperature results in the surfactant becoming more hydrophilic, reducing its wettability alteration capability. Increasing salinity and increasing the surfactant concentration alleviates the problem.

- Oil production from an imbibition process is a function of its crude oil, mineralogy, and the interaction between the two phases.
- From the base wettability chapter, shale systems are observed to be oil-wet. However, all base spontaneous imbibition data still has certain degree of oil recovery. It is important to note that based on the contact angle measurement, the oil-wetness observed is not a complete hydrophobic condition. Therefore, oil recovery should still exist. This result implores the need to review the wettability term of the Young-Laplace equation where any degree of oil-wetness results in negative capillary pressure that indicates zero oil production.
- The quartz-rich is presented as more oil-wet than the calcite-rich mineralogy. Therefore, the expected result is for it to have lower recovery factor. The opposite is observed in this study. This discrepancy is driven by the two orders of magnitude permeability difference between the two rock types.
- There is no clear trend between oil composition from either SARA or GC analysis to the recovery factor.
- It is observed that IFT has a definitive trend. On a more oil-wet mineralogy (quartz-rich), higher IFT results in lower recovery. While on a more water-wet mineralogy (calcite-rich), higher IFT results in higher recovery.
- On a more water-wet mineralogy (calcite-rich), an optimum salinity is observed where the recovery is the highest. On the other hand, the optimum point results in the lowest

recovery when applied on a more oil-wet rock. This trend is driven by the IFT change due to salinity change, further explained in Chapter IV.

- Temperature increase results in better recovery on the base imbibition, driven by lower viscosity of the phases and the weaker bond between the crude oil and the rock surface.

Chapter X, Optimizing Tailgroup and Headgroup Structure of Surfactant for SASI Application on Lower 48 Shale Reservoirs

- Surfactant improves oil recovery in most cases. In addition to final recovery, surfactant also improves the rate of recovery. Both magnitude and rate of recovery is improved by the surfactant immediately from time zero.
- There are two types of rate improvement observed. First, is the rate improvement that occurs from the beginning of the experiment (Type I), consistently until the end of the production. Second, is the rate improvement that only occurs at the early time of production (Type II). In the second case, the rate of recovery becomes lower than the base case at later time. The first case results in the improvement of the final recovery factor. While the second one actually reduces recovery where the final recovery for these surfactants are lower than the base case.
- Applying the wrong surfactant, like those that are present in Type II rate improvement, reduces the imbibition recovery. Reduction of recovery factor from the base case is observed when applying surfactant NP-12 to EF-C siliceous system, NP-55 to EF-C carbonaceous system, 15S-30 and NP-30 to 2H siliceous system, and NP-12 to EF-Au carbonaceous system.

- Surfactant is more effective in improving recovery factor of system with lower base recovery factor.
- On carbonaceous rock, more hydrophobic tailgroups produce more oil with the lighter crude oil, while the more hydrophilic tailgroup shows the best compatibility to the heavier crude oil.
- On siliceous rock, the opposite is observed. Lighter crude oil is produced more when a less hydrophilic tailgroup is used. And the more hydrophobic tailgroup shows greater improvement with the heavier crude oil.
- Salinity only affects the imbibition behavior of the 15S tailgroup. Salinity increase causes the 15S tailgroup to become more hydrophobic. On carbonaceous rock, this results in performance improvement. While on siliceous, this reduces surfactant performance. This result correlates to observations for cloud point. Higher salinity increases the hydrophobicity of this tailgroup.
- EO number of 30 is observed as the more optimum headgroup configuration for nonionic surfactants as it produces the highest recovery improvement. However, shorter EO groups with crude oil EF-C and Bk has the best performance. It is believed that this is driven by the increase of the surfactant solubility in the oleic-phase.
- For cationic surfactants, increasing the hydrophobicity of the tailgroup greatly improves the recovery by surfactant. At higher salinity, the surfactant performance is reduced due to the salting out of the surfactant and the increase in micellization of the surfactant.

- Capillarity, wettability alteration, and IFT reduction are not the only mechanism for SASI. As demonstrated, surfactants with strong wettability alteration and high net adhesion tension value increase oil recovery. But there are multiple cases where surfactant that shows poor wettability alteration and low net adhesion tension provides excellent recovery. It is hypothesized that this is driven by the increase in surfactant solubility in oil. Further research must be performed to investigate the other undiscovered mechanism of surfactant-driven recovery improvement, or reduction.
- The effect of porosity and permeability is not excluded from this study. As a result, the more porous calcite-rich rock that is less oil-wet produces more oil in the base scenario when compared to the more oil-wet quartz-rich rock but with lower porosity and permeability. The pore radius is suspected to be the cause of this discrepancy. Larger capillary pressure resulted by the smaller pore radius causes higher production, even at more oil-wet state, than the larger pore radius. The current dimensionless scaling method only normalized the recovery rate, not the magnitude of recovery. A new dimensionless scaling that does not only scale the x-axis (time), but also the y-axis (recovery factor), based on the wettability, IFT, porosity, and permeability must be developed.
- The calculation of the Young-Laplace equation includes the term of $cos(\theta)$ to represent wettability. With this convention, oil-wet samples with contact angle larger than 90° would have negative capillary pressure value. Negative capillary pressure value implies the complete blockage of the oil phase in the pore space when placed

under imbibition condition. In this study, it has shown multiple results where some oil is still produced out during the imbibition process with oil-wet sample. This implies that the oil phase is not completely blocked inside the pore space and highlights the discrepancy to the Young-Laplace capillary pressure equation. Systems with contact angle between 90°and 180° are system that is oil-wet, but not completely. Which is why oil is still produced from these systems. Therefore, a modification to the equation is proposed. The wettability term can be introduced in the form of $cos(\theta/_2)$. In this form, intermediate-wet systems would still have positive capillary pressure. Which is a better representation of results observed in the laboratory.

- The effect of temperature has been investigated in crude oil/brine, crude oi/brine/rock, surfactant/crude oil/brine, surfactant/crude oil/brine, and crude oil/brine/rock/porous media system. It has not been investigated in its effect to surfactant performance in imbibition process. This should be performed in future research since the Lower 48 shale reservoirs have a wide range of reservoir temperature.
- Nonionic surfactant with shorter EO group shows the best performance when applied at condition below its cloud point. Once the cloud point is exceeded, the performance drops completely. Longer EO groups have lower performance but have larger window of operation. Future research can be performed by mixing the two surfactants together to obtain the performance level of the shorter EO groups and the robustness of the longer EO groups.
- In the IFT with surfactant part of this study, interaction between headgroups containing positive charge and the crude oil is observed. Headgroup structure was not

expected to interact with the crude oil since it is the hydrophilic part of the surfactant and should only interact with the aqueous-phase. It is hypothesized that the presence of charged molecule in some of the crude oil results in this interaction. It seems these two headgroups are most compatible with crude oil 2H and Bk. Further research on the relationship between positively charged headgroup molecule and crude oil with balanced Saturates and Aromatics composition must be performed to understand the mechanism behind this trend.

- The partitioning of the surfactant molecule when introduced to the shale system is hypothesized to be a significant variable to the surfactant performance. Future research to confirm this hypothesis can be performed by measuring the surfactant content in the aqueous-phase, oleic-phase, and the rock when introduced to a specific system (crude oil, salinity, mineralogy, and temperature). The ratio between the surfactant content in the three phases then can be correlated to the performance of the surfactant to produce oil through imbibition mechanism.
- In the wettability alteration section of this study, compatibility between crude oil composition and the tailgroup structure is observed. Crude oil EF-C that is dominated by saturated hydrocarbon is turned more water-wet with linear C13 tailgroup. While crude oil Bk that has more aromatics content is more water-wet with the nonylphenol tailgroup. Future research can be performed by mixing the two surfactants to match the composition of the crude oil.

REFERENCES

Adel, Imad A., Tovar, Francisco D., Zhang, Fan et al. 2018. The Impact of MMP on Recovery Factor During CO2 – EOR in Unconventional Liquid Reservoirs. *Proc.,* SPE Annual Technical Conference and Exhibition. https://doi.org/10.2118/191752-MS.

Afra, Salar, Nasr-El-Din, Hisham A., and Samouei, H. 2019. Characterization of Iron Interaction with Viscoelastic Surfactant (VES)-Based Stimulation Fluid. Presented at the SPE Western Regional Meeting, San Jose, CA, USA. 2019/4/23/.

Akbarabadi, M., Saraji, S., and Piri, M. 2015a. Spontaneous Imbibition of Fracturing Fluid and Oil in Mudrock. *Proc.,* SPE/AAPG/SEG Unconventional Resources Technology Conference. https://doi.org/10.15530/URTEC-2015-2174372.

Akbarabadi, M., Saraji, S., and Piri, M. 2015b. Spontaneous Imbibition of Fracturing Fluid and Oil in Mudrock. Presented at the Unconventional Resources Technology Conference, San Antonio, Texas, USA. 2015/7/20/. https://doi.org/10.15530/URTEC-2015-2174372.

Akhlaghi, Naser, Riahi, Siavash, and Parvaneh, Ronak. 2021. Interfacial tension behavior of a nonionic surfactant in oil/water system; salinity, pH, temperature, and ionic strength effects. *Journal of Petroleum Science and Engineering* **198**: 108177. https://www.sciencedirect.com/science/article/pii/S0920410520312316.

Al-Maamari, Rashid S. H. and Buckley, Jill S. 2003. Asphaltene Precipitation and Alteration of Wetting: The Potential for Wettability Changes During Oil Production. *SPE Reservoir Evaluation & Engineering* **6** (04): 210-214. https://doi.org/10.2118/84938-PA.

Al-Sabagh, A. M., Nasser, N. M., Migahed, M. A. et al. 2011. Effect of chemical structure on the cloud point of some new non-ionic surfactants based on bisphenol in relation to their surface active properties. *Egyptian Journal of Petroleum* **20** (2): 59-66. https://www.sciencedirect.com/science/article/pii/S1110062111000079.

Al-Sahhaf, T., Elkamel, A., Suttar Ahmed, A. et al. 2005. The Influence of Temperature, Pressure, Salinity, and Surfactant Concentration on the Interfacial Tension of the N-Octane-Water System. *Chemical Engineering Communications* **192** (5): 667-684. https://doi.org/10.1080/009864490510644.

Alasiri, Hassan S., Sultan, Abdullah S., and Chapman, Walter G. 2019. Effect of Surfactant Headgroup, Salts, and Temperature on Interfacial Properties: Dissipative Particle Dynamics and Experiment for the Water/Octane/Surfactant System. *Energy & Fuels* **33** (7): 6678-6688. https://doi.org/10.1021/acs.energyfuels.9b01740.

Alharthy, Najeeb, Teklu, Tadesse, Kazemi, Hossein et al. 2015. Enhanced Oil Recovery in Liquid-Rich Shale Reservoirs: Laboratory to Field. *Proc.,* SPE Annual Technical Conference and Exhibition. https://doi.org/10.2118/175034-MS.

Alharthy, Najeeb, Teklu, Tadesse Weldu, Kazemi, Hossein et al. 2018. Enhanced Oil Recovery in Liquid-Rich Shale Reservoirs: Laboratory to Field. *SPE Reservoir Evaluation & Engineering* **21** (01): 137-159. https://doi.org/10.2118/175034-PA.

Alhashim, Hassan W., Zhang, Fan, Schechter, David S. et al. 2019. Investigation of the Effect of Pore Size Distribution on the Produced Oil from Surfactant-Assisted Spontaneous Imbibition in ULRs. *Proc.,* SPE Annual Technical Conference and Exhibition. https://doi.org/10.2118/195931-MS.

Alotaibi, M. B. and Nasr-El-Din, H. A. 2009. Salinity of Injection Water and Its Impact on Oil Recovery. Presented at the EUROPEC/EAGE Conference and Exhibition, Amsterdam, The Netherlands. 2009/1/1/. https://doi.org/10.2118/121569-MS.

Alvarez, J. O., Saputra, I. W., and Schechter, D. S. 2017a. The Impact of Surfactant Imbibition and Adsorption for Improving Oil Recovery in the Wolfcamp and Eagle Ford Reservoirs. *Proc.,* SPE Annual Technical Conference and Exhibition. https://doi.org/10.2118/187176-MS.

Alvarez, J. O., Saputra, I. W., and Schechter, D. S. 2018a. The Impact of Surfactant Imbibition and Adsorption for Improving Oil Recovery in the Wolfcamp and Eagle Ford Reservoirs. *SPE Journal* **23** (06): 2103-2117. https://doi.org/10.2118/187176-PA.

Alvarez, J. O. and Schechter, D. S. 2016a. Wettability Alteration and Spontaneous Imbibition in Unconventional Liquid Reservoirs by Surfactant Additives. *SPE Reservoir Evaluation & Engineering* **20** (01): 107-117. https://doi.org/10.2118/177057-PA.

Alvarez, J. O., Tovar, F. D., and Schechter, D. S. 2017. Improving Oil Recovery in Unconventional Liquid Reservoirs by Soaking-Flowback Production Schedule with Surfactant Additives. *Proc.,* SPE Liquids-Rich Basins Conference - North America. https://doi.org/10.2118/187483-MS.

Alvarez, J. O., Tovar, F. D., and Schechter, D. S. 2018. Improving Oil Recovery in the Wolfcamp Reservoir by Soaking/Flowback Production Schedule With Surfactant Additives. *SPE Reservoir Evaluation & Engineering* **21** (04): 1083-1096. https://doi.org/10.2118/187483-PA.

Alvarez, Johannes O., Saputra, I. W. R., and Schechter, David S. 2018b. The Impact of Surfactant Imbibition and Adsorption for Improving Oil Recovery in the Wolfcamp and Eagle Ford Reservoirs. *SPE Journal* **23** (06): 2103-2117. https://doi.org/10.2118/187176-PA.

Alvarez, Johannes O., Saputra, I. Wayan Rakananda, and Schechter, David S. 2017b. Potential of Improving Oil Recovery with Surfactant Additives to Completion Fluids for the Bakken. *Energy & Fuels* **31** (6): 5982-5994. https://doi.org/10.1021/acs.energyfuels.7b00573.

Alvarez, Johannes O. and Schechter, D. S. 2016b. Wettability, Oil and Rock Characterization of the Most Important Unconventional Liquid Reservoirs in the United States and the Impact on Oil Recovery. In *Unconventional Resources Technology Conference, San Antonio, Texas, 1-3 August 2016*, 2997-3017. SEG Global Meeting Abstracts, Society of Exploration Geophysicists, American Association of Petroleum Geologists, Society of Petroleum Engineers.

Alvarez, Johannes O. and Schechter, David S. 2017. Improving oil recovery in the Wolfcamp unconventional liquid reservoir using surfactants in completion fluids. *Journal of Petroleum Science and Engineering* **157**: 806-815. https://www.sciencedirect.com/science/article/pii/S0920410517300396.

Antón, Raquel, Rivas, Hercilio, and Salager, Jean-Louis. 1996. SURFACTANT-OIL-WATER SYSTEMS NEAR THE AFFINITY INVERSION. PART X: EMULSIONS MADE WITH ANIONIC-NONIONIC SURFACTANT MIXTURES. *JOURNAL OF DISPERSION SCIENCE ANDTECHNOLOGY* **17** (6): 553-566.

Antón, RE, Castillo, P, and Salager, JL. 1986. Surfactant-oil-water systems near the affinity inversion Part IV: emulsion inversion temperature. *JOURNAL OF DISPERSION SCIENCE ANDTECHNOLOGY* **7** (3): 319-329.

Antón, RE, Gomez, D, Graciaa, A et al. 1993. surfactant-oil-water systems near the affinity inversion Part IX: optimum formulation and phase behavior of mixed anionic-cationic systems. *Journal of dispersion science and technology* **14** (4): 401-416.

Antón, RE, Graciaa, A, Lachaise, J et al. 1992. SURFACTANT-OIL-WATER SYSTEMS NEAR THE AFFINITY INVERSION PART VIII: OPTIMUM FORMULATION AND PHASE BEHAVIOR OF MIXED ANIONIC-NONIONIC SYSTEMS VERSUS TEMPERATURE. *Journal of dispersion science and technology* **13** (5): 565-579.

Aoudia, Mohamed, Al-Shibli, Mohamed Nasser, Al-Kasimi, Liali Hamed et al. 2006. Novel surfactants for ultralow interfacial tension in a wide range of surfactant concentration and temperature. *Journal of Surfactants and Detergents* **9** (3): 287-293. https://doi.org/10.1007/s11743-006-5009-9.

Argüelles-Vivas, Francisco J., Wang, Mingyuan, Abeykoon, Gayan A. et al. 2020. Enhancement of Water Imbibition in Shales by use of Ketone Solvent. *Proc.,* SPE International Conference and Exhibition on Formation Damage Control. https://doi.org/10.2118/199322-MS.

Azam, Muhammad Rizwan, Tan, Isa M., Ismail, Lukman et al. 2013. Static adsorption of anionic surfactant onto crushed Berea sandstone. *Journal of Petroleum Exploration and Production Technology* **3** (3): 195-201. https://doi.org/10.1007/s13202-013-0057-y.

B. Alamdari, Baharak, Hsu, Tzu-Ping, Nguyen, Duy et al. 2018. Understanding the Oil Recovery Mechanism in Mixed-Wet Unconventional Reservoirs: Uniqueness and Challenges of Developing Chemical Formulations. *Proc.,* SPE Improved Oil Recovery Conference. https://doi.org/10.2118/190201-MS.

Bai, Jiajia, Kang, Yili, Chen, Mingjun et al. 2020. Impact of surface chemistry and pore structure on water vapor adsorption behavior in gas shale. *Chemical Engineering Journal* **402**: 126238. http://www.sciencedirect.com/science/article/pii/S1385894720323664.

Bai, Shixun, Kubelka, Jan, and Piri, Mohammad. 2020. A positively charged calcite surface model for molecular dynamics studies of wettability alteration. *Journal of Colloid and Interface Science* **569**: 128-139. http://www.sciencedirect.com/science/article/pii/S002197972030182X.

Bansal, V.K. and Shah, D.O. 1978. The Effect of Ethoxylated Sulfonates on Salt Tolerance and Optimal Salinity of Surfactant Formulations for Tertiary Oil Recovery. *Society of Petroleum Engineers Journal* **18** (03): 167-172. https://doi.org/10.2118/6696-PA.

Bao, A. and Gildin, E. 2017. Data-Driven Model Reduction Based on Sparsity-Promoting Methods for Multiphase Flow in Porous Media. Presented at the SPE Latin America and Caribbean Petroleum Engineering Conference, Buenos Aires, Argentina. 2017/5/17/. https://doi.org/10.2118/185514-MS.

Bao, Anqi, Hazlett, Randy D., and Babu, D. Krishna. 2017. A Discrete, Arbitrarily Oriented 3D Plane-Source Analytical Solution to the Diffusivity Equation for Modeling Reservoir Fluid Flow. *SPE Journal* **22** (05): 1609-1623. https://doi.org/10.2118/185180-PA.

Barati-Harooni, A., Soleymanzadeh, A., Tatar, A. et al. 2016. Experimental and modeling studies on the effects of temperature, pressure and brine salinity on interfacial tension in live oil-brine systems. *Journal of Molecular Liquids* **219**: 985-993. http://www.sciencedirect.com/science/article/pii/S0167732216302161.

Belhaj, Ahmed Fatih, Aris B M Shuhli, Juhairi, Elraies, Khaled Abdalla et al. 2020. Partitioning behaviour of novel surfactant mixture for high reservoir temperature and high salinity conditions. *Energy* **198**: 117319. https://www.sciencedirect.com/science/article/pii/S0360544220304266.

Benoit, Denise, Saputra, I Wayan, Recio III, Antonio et al. 2020. Investigating the Role of Surfactant in Oil/Water/Rock Systems Using QCM-D. *Proc.,* SPE International Conference and Exhibition on Formation Damage Control. https://doi.org/10.2118/199265-MS.

Bera, Achinta, S, Kissmathulla, Ojha, Keka et al. 2012. Mechanistic Study of Wettability Alteration of Quartz Surface Induced by Nonionic Surfactants and Interaction between Crude Oil and Quartz in the Presence of Sodium Chloride Salt. *Energy & Fuels* **26** (6): 3634-3643. https://doi.org/10.1021/ef300472k.

Bidhendi, Mehrnoosh Moradi, Kazempour, Mahdi, Ibanga, Uwana et al. 2019a. A Set of Successful Chemical EOR Trials in Permian Basin: Promising Field and Laboratory Results. Presented at the SPE/AAPG/SEG Unconventional Resources Technology Conference, Denver, Colorado, USA. 2019/7/31/. https://doi.org/10.15530/urtec-2019-881.

Bidhendi, Mehrnoosh Moradi, Kazempour, Mahdi, Ibanga, Uwana et al. 2019b. A Set of Successful Chemical EOR Trials in Permian Basin: Promising Field and Laboratory Results. *Proc.,* SPE/AAPG/SEG Unconventional Resources Technology Conference. https://doi.org/10.15530/urtec-2019-881.

Blauch, M E, Venitto, J J, Gardner, T R et al. 1993. Surfactant/solvent combination aids flow back of treatment fluids (in English). *Oil and Gas Journal; (United States)* **91:1**: Medium: X; Size: Pages: 40-44 2009-12-17. https://www.osti.gov/biblio/6883973.

Brown, C. E. and Neustadter, E. L. 1980. The Wettability of Oil/Water/Silica Systems With Reference to Oil Recovery. *Journal of Canadian Petroleum Technology* **19** (03): 12. https://doi.org/10.2118/80-03-06.

Buckley, J. S. and Liu, Y. 1998. Some mechanisms of crude oil/brine/solid interactions. *Journal of Petroleum Science and Engineering* **20** (3): 155-160. http://www.sciencedirect.com/science/article/pii/S0920410598000151.

Buckley, Jill S., Bousseau, Christophe, and Liu, Yu. 1996. Wetting Alteration by Brine and Crude Oil: From Contact Angles to Cores. *SPE Journal* **1** (03): 341-350. https://doi.org/10.2118/30765-PA.

Buckley, Jill S. and Fan, Tianguang. 2007. Crude Oil/Brine Interfacial Tensions1. *Petrophysics* **48** (03): 11. https://doi.org/.

Bui, Khoa, Akkutlu, I. Yucel, Zelenev, Andrei et al. 2016. Insights Into Mobilization of Shale Oil by Use of Microemulsion. *SPE Journal* **21** (02): 613-620. https://doi.org/10.2118/178630-PA.

Cai, B. Y., Yang, J. T., and Guo, T. M. 1996. Interfacial Tension of Hydrocarbon + Water/Brine Systems under High Pressure. *Journal of Chemical & Engineering Data* **41** (3): 493-496. https://doi.org/10.1021/je950259a.

Cao, Yu, Zhao, Rong-hua, Zhang, Lei et al. 2012. Effect of Electrolyte and Temperature on Interfacial Tensions of Alkylbenzene Sulfonate Solutions. *Energy & Fuels* **26** (4): 2175-2181. https://doi.org/10.1021/ef201982s.

Champagne, Lakia M., Zhou, Hui, Zelenev, Andrei S. et al. 2012. The Impact of Complex Nanofluid Composition on Enhancing Regained Permeability and Fluid Flowback from Tight Gas Formations and Propped Fractures. *Proc.,* SPE International Symposium and Exhibition on Formation Damage Control. https://doi.org/10.2118/151845-MS.

Chen, Weidong and Schechter, David S. 2021. Surfactant selection for enhanced oil recovery based on surfactant molecular structure in unconventional liquid reservoirs. *Journal of Petroleum Science and Engineering* **196**: 107702. https://www.sciencedirect.com/science/article/pii/S0920410520307671.

Curbelo, F., Garnica, A., and Neto, E. 2013. Salinity Effect in Cloud Point Phenomena by Nonionic Surfactants Used in Enhanced Oil Recovery Tests. *Petroleum Science and Technology* **31** (15): 1544-1552. https://doi.org/10.1080/10916466.2010.547906.

Das, S., Katiyar, A., Rohilla, N. et al. 2020. Universal scaling of adsorption of nonionic surfactants on carbonates using cloud point temperatures (in eng). *J Colloid Interface Sci* **577**: 431-440.

Das, Saikat, Adeoye, Jubilee, Dhiman, Indu et al. 2019. Imbibition of Mixed-Charge Surfactant Fluids in Shale Fractures. *Energy & Fuels* **33** (4): 2839-2847. https://doi.org/10.1021/acs.energyfuels.8b03447.

Dehghan, A. A., Masihi, M., and Ayatollahi, Sh. 2015. Phase behavior and interfacial tension evaluation of a newly designed surfactant on heavy oil displacement efficiency; effects of salinity, wettability, and capillary pressure. *Fluid Phase Equilibria* **396**: 20-27. https://www.sciencedirect.com/science/article/pii/S0378381215001508.

Deng, Lichi and King, Michael J. 2018. Theoretical Investigation of the Transition from Spontaneous to Forced Imbibition. Presented at the SPE Improved Oil Recovery Conference, Tulsa, Oklahoma, USA. 2018/4/14/.

Deng, Xiao, Kamal, Muhammad Shahzad, Patil, Shirish et al. 2020. A Review on Wettability Alteration in Carbonate Rocks: Wettability Modifiers. *Energy & Fuels* **34** (1): 31-54. https://doi.org/10.1021/acs.energyfuels.9b03409.

Drexler, Santiago, Hoerlle, Fernanda Oliveira, Silveira, Thais M. G. et al. 2019. Impact of Rock Aging Time on the Initial Wettability of Minerals and Analogue Rocks Using Pre-Salt Fluids Under Reservoir Conditions. Presented at the Offshore Technology Conference Brasil, Rio de Janeiro, Brazil. 2019/10/28/. https://doi.org/10.4043/29909-MS.

Engle, M. A., Saraswathula, V., Thordsen, J. J. et al. 2019. *U.S. Geological Survey National Produced Waters Geochemical Database v2.3*, 2.3 edition, 2019-05-22 (Reprint).

Firoozabadi, A and Ramey, H. J., Jr. 1988. Surface Tension Of Water-Hydrocarbon Systems At Reservoir Conditions. *Journal of Canadian Petroleum Technology* **27** (03): 9. https://doi.org/10.2118/88-03-03.

Fu, Qinwen, Cudjoe, Sherifa, Barati, Reza et al. 2019. Experimental and Numerical Investigation of the Diffusion-Based Huff-n-Puff Gas Injection into Lower Eagle Ford Shale Samples. *Proc.,* SPE/AAPG/SEG Unconventional Resources Technology Conference. https://doi.org/10.15530/urtec-2019-402.

Ge, Hong-Kui, Yang, Liu, Shen, Ying-Hao et al. 2015. Experimental investigation of shale imbibition capacity and the factors influencing loss of hydraulic fracturing fluids. *Petroleum Science* **12** (4): 636-650. https://doi.org/10.1007/s12182-015-0049-2.

Ghosh, Pinaki, Sharma, Himanshu, and Mohanty, Kishore K. 2018. Development of Surfactant-Polymer SP Processes for High Temperature and High Salinity Carbonate Reservoirs. *Proc.,* SPE Annual Technical Conference and Exhibition. https://doi.org/10.2118/191733-MS.

Gu, Tiren, Qin, Shoufeng, and Ma, Chiming. 1989. The effect of electrolytes on the cloud point of mixed solutions of ionic and nonionic surfactants. *Journal of Colloid and Interface Science* **127** (2): 586-588. https://www.sciencedirect.com/science/article/pii/0021979789900647.

Gu, Tiren and Sjöblom, Johan. 1992. Surfactant structure and its relation to the Krafft point, cloud point and micellization: Some empirical relationships. *Colloids and Surfaces* **64** (1): 39-46. https://www.sciencedirect.com/science/article/pii/0166662292801604.

Gupta, Ishank, Rai, Chandra S., and Sondergeld, Carl H. 2020. Impact of Surfactants on Hydrocarbon Mobility in Shales. *SPE Reservoir Evaluation & Engineering* **23** (03): 1105-1117. https://doi.org/10.2118/201110-PA.

Gupta, R.. and Mohanty, K.K.. K. 2010. Temperature Effects on Surfactant-Aided Imbibition Into Fractured Carbonates. *SPE Journal* **15** (03): 588-597. https://doi.org/10.2118/110204-PA.

Gupta, Robin and Mohanty, Kishore Kumar. 2008. Wettability Alteration of Fractured Carbonate Reservoirs. *Proc.,* SPE Symposium on Improved Oil Recovery. https://doi.org/10.2118/113407-MS.

Habibi, Ali, Esparza, Yussef, Boluk, Yaman et al. 2020. Enhancing Imbibition Oil Recovery from Tight Rocks by Mixing Nonionic Surfactants. *Energy & Fuels* **34** (10): 12301-12313. https://doi.org/10.1021/acs.energyfuels.0c02160.

Haghighi, Omid Mosalman, Zargar, Ghasem, Khaksar Manshad, Abbas et al. 2020. Effect of Environment-Friendly Non-Ionic Surfactant on Interfacial Tension Reduction and Wettability Alteration; Implications for Enhanced Oil Recovery. *Energies* **13** (15): 3988. https://www.mdpi.com/1996-1073/13/15/3988.

Hamouda, Aly Anis and Rezaei Gomari, Karam Ali. 2006. Influence of Temperature on Wettability Alteration of Carbonate Reservoirs. Presented at the SPE/DOE Symposium on Improved Oil Recovery, Tulsa, Oklahoma, USA. 2006/1/1/. https://doi.org/10.2118/99848-MS.

HanZhao, WanliKang, HongbinYang et al. 2020. Imbibition enhancing oil recovery mechanism of the two surfactants. *Physics of Fluids* **32** (4): 047103. https://aip.scitation.org/doi/abs/10.1063/5.0005106.

Hassan, M. E., Nielsen, R. F., and Calhoun, J. C. 1953. Effect of Pressure and Temperature on Oil-Water Interfacial Tensions for a Series of Hydrocarbons. *Journal of Petroleum Technology* **5** (12): 299-306. https://doi.org/10.2118/298-G.

He, Kai and Xu, Liang. 2017. Unique Mixtures of Anionic/Cationic Surfactants: A New Approach To Enhance Surfactant Performance in Liquids-Rich Shale Reservoirs. *SPE Production & Operations* **33** (02): 363-370. https://doi.org/10.2118/184515-PA.

He, Kai, Xu, Liang, Kenzhekhanov, Shaken et al. 2017. A Rock-on-a-Chip Approach to Study Fluid Invasion and Flowback in Liquids-Rich Shale Formations. *Proc.,* SPE Oklahoma City Oil and Gas Symposium. https://doi.org/10.2118/185088-MS.

Hirasaki, George and Zhang, Danhua Leslie. 2004. Surface Chemistry of Oil Recovery From Fractured, Oil-Wet, Carbonate Formations. *SPE Journal* **9** (02): 151-162. https://doi.org/10.2118/88365-PA.

Hjelmeland, O. S. and Larrondo, L. E. 1986. Experimental Investigation of the Effects of Temperature, Pressure, and Crude Oil Composition on Interfacial Properties. *SPE Reservoir Engineering* **1** (04): 321-328. https://doi.org/10.2118/12124-PA.

Houston, Nathan Allan, Blauch, Matthew Eric, Weaver, Dalton Richard et al. 2009. Fracture-Stimulation in the Marcellus Shale-Lessons Learned in Fluid Selection and Execution. *Proc.,* SPE Eastern Regional Meeting. https://doi.org/10.2118/125987-MS.

Howard, Paul R., Mukhopadhyay, Sumitra, Moniaga, Nita et al. 2010. Comparison of Flowback Aids: Understanding Their Capillary Pressure and Wetting Properties. *SPE Production & Operations* **25** (03): 376-387. https://doi.org/10.2118/122307-PA.

Huang, Hai, Babadagli, Tayfun, Chen, Xin et al. 2020. Performance Comparison of Novel Chemical Agents for Mitigating Water-Blocking Problem in Tight Gas Sands. *Proc.,* SPE International Conference and Exhibition on Formation Damage Control. https://doi.org/10.2118/199282-MS.

Huibers, Paul D. T., Shah, Dinesh O., and Katritzky, Alan R. 1997. Predicting Surfactant Cloud Point from Molecular Structure. *Journal of Colloid and Interface Science* **193** (1): 132-136. https://www.sciencedirect.com/science/article/pii/S0021979797950530.

Ivanova, Anastasia A., Cheremisin, Alexey N., Barifcani, Ahmed et al. 2020. Molecular insights in the temperature effect on adsorption of cationic surfactants at liquid/liquid

interfaces. *Journal of Molecular Liquids* **299**: 112104. https://www.sciencedirect.com/science/article/pii/S0167732219335482.

Jadhunandan, P. P. and Morrow, N. R. 1995. Effect of Wettability on Waterflood Recovery for Crude-Oil/Brine/Rock Systems. *SPE Reservoir Engineering* **10** (01): 40-46. https://doi.org/10.2118/22597-PA.

Jia, Dou, Buckley, J. S., and Morrow, N. R. 1991. Control of Core Wettability With Crude Oil. Presented at the SPE International Symposium on Oilfield Chemistry, Anaheim, California. 1991/1/1/. https://doi.org/10.2118/21041-MS.

Jia, Han, Leng, Xu, Hu, Mei et al. 2017. Systematic investigation of the effects of mixed cationic/anionic surfactants on the interfacial tension of a water/model oil system and their application to enhance crude oil recovery. *Colloids and Surfaces A: Physicochemical and Engineering Aspects* **529**: 621-627. https://www.sciencedirect.com/science/article/pii/S0927775717306179.

Jin, Lu, Hawthorne, Steven, Sorensen, James et al. 2017. Extraction of Oil From the Bakken Shales With Supercritical CO2. *Proc.,* SPE/AAPG/SEG Unconventional Resources Technology Conference. https://doi.org/10.15530/URTEC-2017-2671596.

Karnanda, Wimpy, Benzagouta, M. S., AlQuraishi, Abdulrahman et al. 2013. Effect of temperature, pressure, salinity, and surfactant concentration on IFT for surfactant flooding optimization. *Arabian Journal of Geosciences* **6** (9): 3535-3544. https://doi.org/10.1007/s12517-012-0605-7.

Kedar, Vaibhav and Bhagwat, Sunil S. 2018. Effect of salinity on the IFT between aqueous surfactant solution and crude oil. *Petroleum Science and Technology* **36** (12): 835-842. https://doi.org/10.1080/10916466.2018.1447953.

Khaksar Manshad, A., Olad, M., Taghipour, S. A. et al. 2016. Effects of water soluble ions on interfacial tension (IFT) between oil and brine in smart and carbonated smart water injection process in oil reservoirs. *Journal of Molecular Liquids* **223**: 987-993. http://www.sciencedirect.com/science/article/pii/S0167732216311370.

Kim, Jihye, Zhang, Hao, Sun, Hong et al. 2016. Choosing Surfactants for the Eagle Ford Shale Formation: Guidelines for Maximizing Flowback and Initial Oil Recovery. *Proc.,* SPE Low Perm Symposium. https://doi.org/10.2118/180227-MS.

Kim, Seongyun, Omur-Ozbek, Pinar, Dhanasekar, Ashwin et al. 2016. Temporal analysis of flowback and produced water composition from shale oil and gas operations: Impact of frac fluid characteristics. *Journal of Petroleum Science and Engineering* **147**: 202-210. https://www.sciencedirect.com/science/article/pii/S0920410516302352.

Kou, R., Moridis, G. J., and Blasingame, T. A. 2018. Analysis and Modeling of Proppant Transport in Inclined Hydraulic Fractures. Presented at the SPE Hydraulic Fracturing Technology Conference and Exhibition, The Woodlands, Texas, USA. 2018/1/23/.

Kumar, A., Neale, G., and Hornof, V. 1985. Some effects of temperature on interfacial tension between hydrocarbons and surfactant solutions. *Colloids and Surfaces* **14** (1): 11-20. https://www.sciencedirect.com/science/article/pii/0166662285800378.

Kumar, B. 2012. *Effect of salinity on the interfacial tension of model and crude oil systems* (Reprint). http://hdl.handle.net/11023/195.

Kurz, Bethany A., Sorensen, James A., Hawthorne, Steven B. et al. 2018. The Influence of Organics on Supercritical CO2 Migration in Organic- Rich Shales. *Proc.,* SPE/AAPG/SEG Unconventional Resources Technology Conference. https://doi.org/10.15530/URTEC-2018-2902743.

Lashkarbolooki, M. and Ayatollahi, S. 2018. Effects of asphaltene, resin and crude oil type on the interfacial tension of crude oil/brine solution. *Fuel* **223**: 261-267. http://www.sciencedirect.com/science/article/pii/S0016236118304204.

Lashkarbolooki, M., Riazi, M., and Ayatollahi, S. 2016. Investigation of effects of salinity, temperature, pressure, and crude oil type on the dynamic interfacial tensions. *Chemical Engineering Research and Design* **115**: 53-65. http://www.sciencedirect.com/science/article/pii/S0263876216303057.

Leung, Roger and Shah, Dinesh O. 1987. Solubilization and phase equilibria of water-in-oil microemulsions: II. Effects of alcohols, oils, and salinity on single-chain surfactant systems. *Journal of Colloid and Interface Science* **120** (2): 330-344. https://www.sciencedirect.com/science/article/pii/0021979787903614.

Li, Jing-Liang, Bai, Dong-Shun, and Chen, Bing-Hung. 2009. Effects of additives on the cloud points of selected nonionic linear ethoxylated alcohol surfactants. *Colloids and*

Surfaces A: Physicochemical and Engineering Aspects **346** (1): 237-243. https://www.sciencedirect.com/science/article/pii/S0927775709003902.

Liang, Tianbo, Achour, Sofiane H., Longoria, Rafael A. et al. 2017. Flow physics of how surfactants can reduce water blocking caused by hydraulic fracturing in low permeability reservoirs. *Journal of Petroleum Science and Engineering* **157**: 631-642. https://www.sciencedirect.com/science/article/pii/S0920410516311937.

Liang, Tianbo, Li, Qingguang, Liang, Xingyuan et al. 2018. Evaluation of liquid nanofluid as fracturing fluid additive on enhanced oil recovery from low-permeability reservoirs. *Journal of Petroleum Science and Engineering* **168**: 390-399. https://www.sciencedirect.com/science/article/pii/S092041051830367X.

Liang, Tianbo, Longoria, Rafael A., Lu, Jun et al. 2015a. The Applicability of Surfactants on Enhancing the Productivity in Tight Formations. Presented at the Unconventional Resources Technology Conference, San Antonio, Texas, USA. 2015/7/20/. https://doi.org/10.15530/URTEC-2015-2154284.

Liang, Tianbo, Longoria, Rafael A., Lu, Jun et al. 2015b. The Applicability of Surfactants on Enhancing the Productivity in Tight Formations. *Proc.,* SPE/AAPG/SEG Unconventional Resources Technology Conference. https://doi.org/10.15530/URTEC-2015-2154284.

Liang, Tianbo, Zhao, Xurong, Yuan, Shuai et al. 2021. Surfactant-EOR in tight oil reservoirs: Current status and a systematic surfactant screening method with field experiments. *Journal of Petroleum Science and Engineering* **196**: 108097. https://www.sciencedirect.com/science/article/pii/S0920410520311517.

Liang, Tianbo, Zhou, Fujian, Lu, Jun et al. 2017. Evaluation of wettability alteration and IFT reduction on mitigating water blocking for low-permeability oil-wet rocks after hydraulic fracturing. *Fuel* **209**: 650-660. https://www.sciencedirect.com/science/article/pii/S0016236117310116.

Lindman, Björn, Medronho, Bruno, and Karlström, Gunnar. 2016. Clouding of nonionic surfactants. *Current Opinion in Colloid & Interface Science* **22**: 23-29. https://www.sciencedirect.com/science/article/pii/S135902941630005X.

Liu, Junrong and Sheng, James J. 2019. Experimental investigation of surfactant enhanced spontaneous imbibition in Chinese shale oil reservoirs using NMR tests. *Journal of Industrial and Engineering Chemistry* **72**: 414-422. https://www.sciencedirect.com/science/article/pii/S1226086X18313273.

Liu, Qian, Yuan, Shiling, Yan, Hui et al. 2012. Mechanism of Oil Detachment from a Silica Surface in Aqueous Surfactant Solutions: Molecular Dynamics Simulations. *The Journal of Physical Chemistry B* **116** (9): 2867-2875. https://doi.org/10.1021/jp2118482.

Liu, Shunhua, Sahni, Vinay, Tan, Jiasen et al. 2018. Laboratory Investigation of EOR Techniques for Organic Rich Shales in the Permian Basin. *Proc.,* SPE/AAPG/SEG Unconventional Resources Technology Conference. https://doi.org/10.15530/URTEC-2018-2890074.

Liu, Zilong, Ghatkesar, Murali K., Sudhölter, Ernst J. R. et al. 2019. Understanding the Cation-Dependent Surfactant Adsorption on Clay Minerals in Oil Recovery. *Energy & Fuels* **33** (12): 12319-12329. https://doi.org/10.1021/acs.energyfuels.9b03109.

Lotfollahi, Mohammad, Beygi, Mohammad Reza, Abouie, Ali et al. 2017. Optimization of Surfactant Flooding in Tight Oil Reservoirs. *Proc.,* SPE/AAPG/SEG Unconventional Resources Technology Conference. https://doi.org/10.15530/URTEC-2017-2696038.

Macleod, D. B. 1923. *10.1039/TF9231900038*. On a relation between surface tension and density. *Transactions of the Faraday Society* **19** (July): 38-41. http://dx.doi.org/10.1039/TF9231900038.

Mahmoudkhani, Amir, O'Neil, Bill, Wylde, Jonathan J. et al. 2015. Microemulsions as Flowback Aids for Enhanced Oil and Gas Recovery after Fracturing, Myth or Reality: A Turnkey Study to Determine the Features and Benefits. *Proc.,* SPE International Symposium on Oilfield Chemistry. https://doi.org/10.2118/173729-MS.

Mandal, Ajay, Kar, Shranish, and Kumar, Sunil. 2016. The Synergistic Effect of a Mixed Surfactant (Tween 80 and SDBS) on Wettability Alteration of the Oil Wet Quartz Surface. *Journal of Dispersion Science and Technology* **37** (9): 1268-1276. https://doi.org/10.1080/01932691.2015.1089780.

Márquez, N., Bravo, B., Chávez, G. et al. 2002. Analysis of polyethoxylated surfactants in microemulsion–oil–water systems: Part II. *Analytica Chimica Acta* **452** (1): 129-141. https://www.sciencedirect.com/science/article/pii/S0003267001014398.

Márquez, Nelson, Antón, Raquel E., Graciaa, Alain et al. 1998. Partitioning of ethoxylated alkylphenol surfactants in microemulsion-oil-water systems. Part II: influence of hydrophobe branching. *Colloids and Surfaces A: Physicochemical and Engineering Aspects* **131** (1): 45-49. https://www.sciencedirect.com/science/article/pii/S0927775796039441.

Marquez, Nelson, Anton, Raquel, Graciaa, Alain et al. 1995. Partitioning of ethoxylated alkylphenol surfactants in microemulsion-oil-water systems. *Colloids and Surfaces A: Physicochemical and Engineering Aspects* **100**: 225-231. https://www.sciencedirect.com/science/article/pii/092777579503184F.

Mendez, Zuleyka, Anton, Raquel E, and Salager, Jean-Louis. 1999. Surfactant-oil-water systems near the affinity inversion. Part XI. pH sensitive emulsions containing carboxylic acids. *Journal of dispersion science and technology* **20** (3): 883-892.

Michaels, A. S. and Hauser, E. A. 1951. Interfacial Tension at Elevated Pressure and Temperature. II. Interfacial Properties of Hydrocarbon–Water Systems. *The Journal of Physical Chemistry* **55** (3): 408-421. https://doi.org/10.1021/j150486a008.

Miller, Chammi, Tong, Songyang, and Mohanty, Kishore K. A Chemical Blend for Stimulating Production in Oil-Shale Formations. In *Unconventional Resources Technology Conference, Houston, Texas, 23-25 July 2018*, 2026-2034.

Miller, Chammi, Zeng, Tongzhou, and Mohanty, Kishore. 2019. Evaluation of Chemical Blends for Shale EOR. *Proc.,* SPE Annual Technical Conference and Exhibition. https://doi.org/10.2118/195819-MS.

Mirchi, Vahideh, Saraji, Soheil, Akbarabadi, Morteza et al. 2017. A Systematic Study on the Impact of Surfactant Chain Length on Dynamic Interfacial Properties in Porous Media: Implications for Enhanced Oil Recovery. *Industrial & Engineering Chemistry Research* **56** (46): 13677-13695. https://doi.org/10.1021/acs.iecr.7b02623.

Mirchi, Vahideh, Saraji, Soheil, Goual, Lamia et al. 2015. Dynamic interfacial tension and wettability of shale in the presence of surfactants at reservoir conditions. *Fuel* **148**: 127-138. https://www.sciencedirect.com/science/article/pii/S0016236115000915.

Moeini, F., Hemmati-Sarapardeh, A., Ghazanfari, M. H. et al. 2014. Toward mechanistic understanding of heavy crude oil/brine interfacial tension: The roles of salinity, temperature and pressure. *Fluid Phase Equilibria* **375**: 191-200. http://www.sciencedirect.com/science/article/pii/S0378381214002374.

Mohammadi, Mohsen Seid, Moghadasi, Jamshid, and Kordestany, Amin. 2014. A Laboratory Investigation into Wettability Alteration of Carbonate Rock by Surfactants: The Effect of Salinity, pH, and Surfactant Concentration (in en). *Iranian Journal of Oil and Gas Science and Technology* **3** (3): 1-10. https://ijogst.put.ac.ir/article_6617.html.

Mohammadshahi, Hooman, Shahverdi, Hamidreza, and Mohammadi, Mohsen. 2020. *https://doi.org/10.1002/jsde.12372*. Optimization of Dynamic Interfacial Tension for Crude Oil–Brine System in the Presence of Nonionic Surfactants. *Journal of Surfactants and Detergents* **23** (2): 445-456. https://doi.org/10.1002/jsde.12372.

Mohanty, Kishore K., Tong, Songyang, Miller, Chammi et al. 2017. Improved Hydrocarbon Recovery using Mixtures of Energizing Chemicals in Unconventional Reservoirs. *Proc.,* SPE Annual Technical Conference and Exhibition. https://doi.org/10.2118/187240-MS.

Mohanty, Kishore, Zeng, Tongzhou, Miller, Chammi et al. 2019. Chemical Blend-CO2 Huff-n-Puff for Enhanced Oil Recovery in Shales. *Proc.,* SPE/AAPG/SEG Unconventional Resources Technology Conference. https://doi.org/10.15530/urtec-2019-362.

Mosayebi, Amir, Angaji, Mahmood Torabi, and Khadiv-Parsi, Parissa. 2016. The effect of temperature on the interfacial tension between crude oil and ethoxylated nonylphenols. *Petroleum Science and Technology* **34** (15): 1315-1322. https://doi.org/10.1080/10916466.2011.601506.

Mugele, Frieder, Bera, Bijoyendra, Cavalli, Andrea et al. 2015. Ion adsorption-induced wetting transition in oil-water-mineral systems. *Scientific Reports* **5** (1): 10519. https://doi.org/10.1038/srep10519.

Mukhina, Elena, Cheremisin, Alexander, Khakimova, Lyudmila et al. 2021. Enhanced Oil Recovery Method Selection for Shale Oil Based on Numerical Simulations. *ACS Omega* **6** (37): 23731-23741. https://doi.org/10.1021/acsomega.1c01779.

Nait Amar, M., Shateri, M., Hemmati-Sarapardeh, A. et al. 2019. Modeling oil-brine interfacial tension at high pressure and high salinity conditions. *Journal of Petroleum Science and Engineering* **183**: 106413. http://www.sciencedirect.com/science/article/pii/S0920410519308344.

Najafi-Marghmaleki, A., Tatar, A., Barati-Harooni, A. et al. 2016. On the prediction of interfacial tension (IFT) for water-hydrocarbon gas system. *Journal of Molecular Liquids* **224**: 976-990. http://www.sciencedirect.com/science/article/pii/S0167732216324679.

Nasr-El-Din, H.A. and Al-Ghamdi, A.M. 1996. Effect of Acids and Stimulation Additives on the Cloud Point of Nonionic Surfactants. *Proc.,* SPE Formation Damage Control Symposium. https://doi.org/10.2118/31106-MS.

Neog, Anirban and Schechter, David S. 2016. Investigation of Surfactant Induced Wettability Alteration in Wolfcamp Shale for Hydraulic Fracturing and EOR Applications. *Proc.,* SPE Improved Oil Recovery Conference. https://doi.org/10.2118/179600-MS.

Novosad, J. 1982. Surfactant Retention in Berea Sandstone- Effects of Phase Behavior and Temperature. *Society of Petroleum Engineers Journal* **22** (06): 962-970. https://doi.org/10.2118/10064-PA.

Okasha, T. M. and Alshiwaish, A. 2009. Effect of Brine Salinity on Interfacial Tension in Arab-D Carbonate Reservoir, Saudi Arabia. Presented at the SPE Middle East Oil and Gas Show and Conference, Manama, Bahrain. 2009/1/1/. https://doi.org/10.2118/119600-MS.

Paktinat, Javad, Pinkhouse, Joseph Allen, Johnson, Nicholas James et al. 2006. Case Studies: Optimizing Hydraulic Fracturing Performance in Northeastern Fractured Shale Formations. *Proc.,* SPE Eastern Regional Meeting. https://doi.org/10.2118/104306-MS.

Pantelides, Sokrates T., Prabhakar, Sanjay, Liu, Jian et al. 2017. Atomic-Scale Theory of Relative Wettability of Surfaces for Enhanced Oil Recovery. Presented at the Abu Dhabi International Petroleum Exhibition & Conference, Abu Dhabi, UAE. 2017/11/13/. https://doi.org/10.2118/188939-MS.

Park, Kang Han and Schechter, David S. 2020. Investigation of the Interaction of Surfactant at Variable Salinity with Permian Basin Rock Samples: Completion Enhancement and Application for Enhanced Oil Recovery. *SPE Drilling & Completion* **35** (01): 100-113. https://doi.org/10.2118/191801-PA.

Paternina, Christian A., Londoño, Alexandra K., Rondon, Miguel et al. 2020. Influence of salinity and hardness on the static adsorption of an extended surfactant for an oil recovery purpose. *Journal of Petroleum Science and Engineering* **195**: 107592. https://www.sciencedirect.com/science/article/pii/S0920410520306604.

Patil, Pramod D., Rohilla, Neeraj, Katiyar, Amit et al. 2018. Surfactant Based EOR for Tight Oil Unconventional Reservoirs Through Wettability Alteration: Novel Surfactant Formulations and Their Efficacy to Induce Spontaneous Imbibition. *Proc.,* SPE/AAPG/SEG Unconventional Resources Technology Conference. https://doi.org/10.15530/URTEC-2018-2896289.

Peng, Sheng, Liu, Yijin, Ko, Lucy Tingwei et al. 2019. Water/Oil Displacement by Spontaneous Imbibition Through Multiscale Imaging and Implication on Wettability in Wolfcamp Shale. *Proc.,* SPE/AAPG/SEG Unconventional Resources Technology Conference. https://doi.org/10.15530/urtec-2019-194.

Phaodee, Parichat, Attaphong, Chodchanok, and Sabatini, David A. 2019. *https://doi.org/10.1002/jsde.12234*. Cold Water Detergency of Triacylglycerol Semisolid Soils: The Effect of Salinity, Alcohol Type, and Surfactant Systems. *Journal of Surfactants and Detergents* **22** (5): 1175-1187. https://doi.org/10.1002/jsde.12234.

Pinnawala Arachchilage, Gayani W., Spilker, Kerry K., Tao, Emily Burdett et al. 2018. Evaluating the Effect of Temperature on Surfactant Phase Behavior and Aqueous Stability to Forecast Optimum Salinity at High Temperature. *Proc.,* SPE Improved Oil Recovery Conference. https://doi.org/10.2118/190249-MS.

Pu, Wan-Fen, Yuan, Cheng-Dong, Wang, Xiao-chao et al. 2016. The Wettability Alteration and the Effect of Initial Rock Wettability on Oil Recovery in Surfactant-

based Enhanced Oil Recovery Processes. *Journal of Dispersion Science and Technology* **37** (4): 602-611. https://doi.org/10.1080/01932691.2015.1053144.

Puerto, Maura, Hirasaki, George J., Miller, Clarence A. et al. 2011. Surfactant Systems for EOR in High-Temperature, High-Salinity Environments. *SPE Journal* **17** (01): 11-19. https://doi.org/10.2118/129675-PA.

Quintero, Harvey, Hawkes, Robert, Mattucci, Mike et al. 2018. Application of Multi-Functionalized Surfactant to Enhance Hydrocarbon Production in Tight Oil & Gas Formations Yields Successful Results. *Proc.,* SPE Argentina Exploration and Production of Unconventional Resources Symposium. https://doi.org/10.2118/191845-MS.

Quintero, Harvey, Mattucci, Mike, Hawkes, Robert et al. 2018. Nano-Particle Surfactant in Hydraulic Fracturing Fluids for Enhanced Post Frac Oil Recovery. *Proc.,* SPE Canada Unconventional Resources Conference. https://doi.org/10.2118/189780-MS.

Ramey, H. J., Jr. 1973. *Correlations Of Surface And Interfacial Tensions Of Reservoir Fluids*, Society of Petroleum Engineers (Reprint). https://doi.org/NA.

Rao, Dandina N. 1999. Wettability Effects in Thermal Recovery Operations. *SPE Reservoir Evaluation & Engineering* **2** (05): 420-430. https://doi.org/10.2118/57897-PA.

Rostami, A.. and Nasr-El-Din, H. A. 2014. Microemulsion vs. Surfactant Assisted Gas Recovery in Low Permeability Formations with Water Blockage. *Proc.,* SPE Western North American and Rocky Mountain Joint Meeting. https://doi.org/10.2118/169582-MS.

Rostami, P., Mehraban, M. F., Sharifi, M. et al. 2019. Effect of water salinity on oil/brine interfacial behaviour during low salinity waterflooding: A mechanistic study. *Petroleum* **5** (4): 367-374. http://www.sciencedirect.com/science/article/pii/S240565611830172X.

Roychaudhuri, B., Tsotsis, T. T., and Jessen, K. 2013. An experimental investigation of spontaneous imbibition in gas shales. *Journal of Petroleum Science and Engineering* **111**: 87-97. https://www.sciencedirect.com/science/article/pii/S0920410513002611.

Sadaghiania, Alireza Salehi and Khan, Ali. 1991. Clouding of a nonionic surfactant: The effect of added surfactants on the cloud point. *Journal of Colloid and Interface Science* **144** (1): 191-200. https://www.sciencedirect.com/science/article/pii/002197979190250C.

Saha, Rahul, Uppaluri, Ramgopal V. S., and Tiwari, Pankaj. 2017. Effect of mineralogy on the adsorption characteristics of surfactant—Reservoir rock system. *Colloids and Surfaces A: Physicochemical and Engineering Aspects* **531**: 121-132. https://www.sciencedirect.com/science/article/pii/S092777571730688X.

Salager, J. L. 2002. *Surfactants - Types and Uses*, Version 2 edition, 50. Merida, Venezuela: Universidad De Los Andes, Facultad De Ingenieria, Escuela De Ingenieria Quimica.

Salager, J.L., Bourrel, M., Schechter, R.S. et al. 1979. Mixing Rules for Optimum Phase-Behavior Formulations of Surfactant/Oil/Water Systems. *Society of Petroleum Engineers Journal* **19** (05): 271-278. https://doi.org/10.2118/7584-PA.

Salager, J.L., Morgan, J.C., Schechter, R.S. et al. 1979. Optimum Formulation of Surfactant/Water/Oil Systems for Minimum Interfacial Tension or Phase Behavior. *Society of Petroleum Engineers Journal* **19** (02): 107-115. https://doi.org/10.2118/7054-PA.

Salager, JL, Loaiza-Maldonado, I, Minana-Perez, M et al. 1982. Surfactant-oil-water systems near the affinity inversion part I: relationship between equilibrium phase behavior and emulsion type and stability. *JOURNAL OF DISPERSION SCIENCE ANDTECHNOLOGY* **3** (3): 279-292.

Salager, JL, Lopez-Castellanos, G, and Miaña-Pérez, M. 1990. Surfactant-Oil-Water Systems Near the Affinity Inversion: Part Vi: Emulsions Hith Viscous Hydrocarbons. *JOURNAL OF DISPERSION SCIENCE ANDTECHNOLOGY* **11** (4): 397-407.

Salager, JL, Mi~ ana-Pérez, M, Andérez, JM et al. 1983. Surfactant-oil-water systems near the affinity inversion part II: viscosity of emulsified systems. *JOURNAL OF DISPERSION SCIENCE ANDTECHNOLOGY* **4** (2): 161-173.

Salager, JL, Minana-Perez, M, Perez-Sanchez, M et al. 1983. Sorfactant-oil-water systems near the affinity inversion part iii: the two kinds of emulsion inversion. *JOURNAL OF DISPERSION SCIENCE ANDTECHNOLOGY* **4** (3): 313-329.

SalahEldin Hussien, Osman, Elraies, Khaled Abdalla, Almansour, Abdullah et al. 2019. Experimental study on the use of surfactant as a fracking fluid additive for improving shale gas productivity. *Journal of Petroleum Science and Engineering* **183**: 106426. https://www.sciencedirect.com/science/article/pii/S0920410519308472.

Sammalkorpi, Maria, Karttunen, Mikko, and Haataja, Mikko. 2009. Ionic Surfactant Aggregates in Saline Solutions: Sodium Dodecyl Sulfate (SDS) in the Presence of Excess Sodium Chloride (NaCl) or Calcium Chloride (CaCl2). *The Journal of Physical Chemistry B* **113** (17): 5863-5870. https://doi.org/10.1021/jp901228v.

Santos, Francisco Klebson G., Neto, Eduardo L. Barros, Moura, Maria Carlenise P. A. et al. 2009. Molecular behavior of ionic and nonionic surfactants in saline medium. *Colloids and Surfaces A: Physicochemical and Engineering Aspects* **333** (1): 156-162. https://www.sciencedirect.com/science/article/pii/S0927775708006456.

Saputra, I. W. R. and Schechter, D. S. 2021. SARA-Based Correlation To Describe the Effect of Polar/Nonpolar Interaction, Salinity, and Temperature for Interfacial Tension of Low-Asphaltene Crude Oils Characteristic of Unconventional Shale Reservoirs. *SPE Journal*: 1-13. https://doi.org/10.2118/206721-PA.

Saputra, I. Wayan Rakananda, Adebisi, Oluwatobiloba, Ladan, Elsie B. et al. 2022. The Influence of Oil Composition, Rock Mineralogy, Aging Time, and Brine Pre-soak on Shale Wettability. *ACS Omega* **7** (1): 85-100. https://doi.org/10.1021/acsomega.1c03940.

Saputra, I. Wayan Rakananda, Park, Kang Han, Zhang, Fan et al. 2019. Surfactant-Assisted Spontaneous Imbibition to Improve Oil Recovery on the Eagle Ford and Wolfcamp Shale Oil Reservoir: Laboratory to Field Analysis. *Energy & Fuels* **33** (8): 6904-6920. https://doi.org/10.1021/acs.energyfuels.9b00183.

Saxena, Neha, Kumar, Amit, and Mandal, Ajay. 2019. Adsorption analysis of natural anionic surfactant for enhanced oil recovery: The role of mineralogy, salinity, alkalinity and nanoparticles. *Journal of Petroleum Science and Engineering* **173**: 1264-1283. https://www.sciencedirect.com/science/article/pii/S0920410518309793.

Sayed, A. M., Olesen, K. B., Alkahala, A. S. et al. 2019. The effect of organic acids and salinity on the interfacial tension of n-decane/ water systems. *Journal of Petroleum Science and Engineering* **173**: 1047-1052. http://www.sciencedirect.com/science/article/pii/S0920410518309653.

Schechter, D. S., Zhou, D., and Orr, F. M. 1994. Low IFT drainage and imbibition. *Journal of Petroleum Science and Engineering* **11** (4): 283-300. http://www.sciencedirect.com/science/article/pii/0920410594900477.

Sharma, K. Shivaji, Patil, Sandeep R., and Rakshit, Animesh Kumar. 2003. Study of the cloud point of C12En nonionic surfactants: effect of additives. *Colloids and Surfaces A: Physicochemical and Engineering Aspects* **219** (1): 67-74. https://www.sciencedirect.com/science/article/pii/S0927775703000128.

Sheng, James J. 2013. Comparison of the effects of wettability alteration and IFT reduction on oil recovery in carbonate reservoirs. *Asia-Pacific Journal of Chemical Engineering* **8** (1): 154-161. https://onlinelibrary.wiley.com/doi/abs/10.1002/apj.1640.

Sheng, James J. 2017. What type of surfactants should be used to enhance spontaneous imbibition in shale and tight reservoirs? *Journal of Petroleum Science and Engineering* **159**: 635-643. https://www.sciencedirect.com/science/article/pii/S0920410517307726.

Singh, Robin and Miller, Joseph. 2021. Synergistic Surfactant Blends for Wettability Alteration in Wolfcamp and Eagle Ford Shale for Improved Oil Recovery. *Proc.,* SPE Western Regional Meeting. https://doi.org/10.2118/200856-MS.

Sorensen, James A., Braunberger, Jason R., Liu, Guoxiang et al. 2015. Characterization and Evaluation of the Bakken Petroleum System for CO2 Enhanced Oil Recovery. *Proc.,* SPE/AAPG/SEG Unconventional Resources Technology Conference. https://doi.org/10.15530/URTEC-2015-2169871.

Souayeh, Maissa, Al-Maamari, Rashid S., Aoudia, Mohamed et al. 2018. Experimental Investigation of Wettability Alteration of Oil-Wet Carbonates by a Non-ionic Surfactant. *Energy & Fuels* **32** (11): 11222-11233. https://doi.org/10.1021/acs.energyfuels.8b02373.

Souayeh, Maissa, Al-Maamari, Rashid S., Karimi, Mahvash et al. 2021. Wettability alteration and oil recovery by surfactant assisted low salinity water in carbonate rock: The impact of nonionic/anionic surfactants. *Journal of Petroleum Science and Engineering* **197**: 108108. https://www.sciencedirect.com/science/article/pii/S0920410520311621.

Standnes, Dag C. and Austad, Tor. 2000. Wettability alteration in chalk: 2. Mechanism for wettability alteration from oil-wet to water-wet using surfactants. *Journal of Petroleum Science and Engineering* **28** (3): 123-143. https://www.sciencedirect.com/science/article/pii/S092041050000084X.

Strand, Skule, Puntervold, Tina, and Austad, Tor. 2008. Effect of Temperature on Enhanced Oil Recovery from Mixed-Wet Chalk Cores by Spontaneous Imbibition and Forced Displacement Using Seawater. *Energy & Fuels* **22** (5): 3222-3225. https://doi.org/10.1021/ef800244v.

Strand, Skule, Standnes, Dag C., and Austad, Tor. 2003. Spontaneous Imbibition of Aqueous Surfactant Solutions into Neutral to Oil-Wet Carbonate Cores: Effects of Brine Salinity and Composition. *Energy & Fuels* **17** (5): 1133-1144. https://doi.org/10.1021/ef030051s.

Sutton, R. P. 2009. An Improved Model for Water-Hydrocarbon Surface Tension at Reservoir Conditions. Presented at the SPE Annual Technical Conference and Exhibition, New Orleans, Louisiana. 2009/1/1/. https://doi.org/10.2118/124968-MS.

Takbiri-Borujeni, Ali, Kazemi, Mohammad, Liu, Siyan et al. 2019. Molecular Simulation of Enhanced Oil Recovery in Shale. *Energy Procedia* **158**: 6067-6072. https://www.sciencedirect.com/science/article/pii/S187661021930534X.

Tang, G. Q. and Morrow, N. R. 1997. Salinity, Temperature, Oil Composition, and Oil Recovery by Waterflooding. *SPE Reservoir Engineering* **12** (04): 269-276. https://doi.org/10.2118/36680-PA.

Tang, Xianqiong, Xiao, Shaofei, Lei, Qun et al. 2019. Molecular Dynamics Simulation of Surfactant Flooding Driven Oil-Detachment in Nano-Silica Channels. *The Journal of Physical Chemistry B* **123** (1): 277-288. https://doi.org/10.1021/acs.jpcb.8b09777.

Teklu, Tadesse Weldu, Li, Xiaopeng, Zhou, Zhou et al. 2018. Low-salinity water and surfactants for hydraulic fracturing and EOR of shales. *Journal of Petroleum Science and Engineering* **162**: 367-377. https://www.sciencedirect.com/science/article/pii/S0920410517310148.

Tovar, Francisco D., Barrufet, Maria A., and Schechter, David S. 2018. Gas Injection for EOR in Organic Rich Shales. Part II: Mechanisms of Recovery. *Proc.,* SPE/AAPG/SEG Unconventional Resources Technology Conference. https://doi.org/10.15530/URTEC-2018-2903026.

Tu, Jiawei and Sheng, James. 2019a. Experimental and Numerical Study of Shale Oil EOR by Surfactant Additives in Fracturing Fluid. *Proc.,* SPE/AAPG/SEG Unconventional Resources Technology Conference. https://doi.org/10.15530/urtec-2019-295.

Tu, Jiawei and Sheng, James. 2019b. Experimental and Numerical Study of Shale Oil EOR by Surfactant Additives in Fracturing Fluid. Presented at the SPE/AAPG/SEG Unconventional Resources Technology Conference, Denver, Colorado, USA. 2019/7/31/. https://doi.org/10.15530/urtec-2019-295.

Tuero, Fernando R., Crotti, Marcelo, and Labayen, Ines. 2017. Unconventional EOR: A Capillary Based Improved Oil Recovery Case Study for Shale Oil Scenarios in the Vaca Muerta Resource Play. *Proc.,* SPE/AAPG/SEG Unconventional Resources Technology Conference. https://doi.org/10.15530/URTEC-2017-2659910.

Uzun, Ozan, Torcuk, Mehmet Ali, and Kazemi, Hossein. 2020. Enhanced Oil Recovery for Liquid-Rich Unconventional Shale Reservoirs Using Low-Salinity Surfactant and Wettability Altering Dilute Surfactants. *Proc.,* SPE Improved Oil Recovery Conference. https://doi.org/10.2118/200346-MS.

Valaulikar, B. S. and Manohar, C. 1985. The mechanism of clouding in triton X-100: The effect of additives. *Journal of Colloid and Interface Science* **108** (2): 403-406. https://www.sciencedirect.com/science/article/pii/0021979785902772.

Vatanparast, H., Alizadeh, A. H., Bahramian, A. et al. 2011. Wettability Alteration of Low-permeable Carbonate Reservoir Rocks in Presence of Mixed Ionic Surfactants. *Petroleum Science and Technology* **29** (18): 1873-1884. https://doi.org/10.1080/10916461003610389.

Velásquez, Josmary, Scorzza, Cesar, Vejar, Francia et al. 2010. Effect of Temperature and Other Variables on the Optimum Formulation of Anionic Extended Surfactant–Alkane–Brine Systems. *Journal of Surfactants and Detergents* **13** (1): 69-73. https://aocs.onlinelibrary.wiley.com/doi/abs/10.1007/s11743-009-1142-6.

Wang, Dongmei, Butler, Ray, Zhang, Jin et al. 2012. Wettability Survey in Bakken Shale With Surfactant-Formulation Imbibition. *SPE Reservoir Evaluation & Engineering* **15** (06): 695-705. https://doi.org/10.2118/153853-PA.

Wang, Dongmei, Zhang, Jin, Butler, Raymond et al. 2014. Flow Rate Behavior and Imbibition Comparison Between Bakken and Niobrara Formationsrch. *Proc.,* SPE/AAPG/SEG Unconventional Resources Technology Conference. https://doi.org/10.15530/URTEC-2014-1920887.

Wang, Dongmei, Zhang, Jin, Butler, Raymond et al. 2015. Scaling Laboratory Data Surfactant Imbibition Rates to the Field in Fractured Shale Formations. *Proc.,* SPE/AAPG/SEG Unconventional Resources Technology Conference. https://doi.org/10.15530/URTEC-2015-2137361.

Wang, Lei, Tian, Ye, Yu, Xiangyu et al. 2017. Advances in improved/enhanced oil recovery technologies for tight and shale reservoirs. *Fuel* **210**: 425-445. https://www.sciencedirect.com/science/article/pii/S0016236117310906.

Wang, Mingyuan, Abeykoon, Gayan Aruna, Vivas, Francisco Argüelles et al. 2019. Novel Wettability Modifiers for Improved Oil Recovery in Tight Oil Reservoirs. *Proc.,* SPE/AAPG/SEG Unconventional Resources Technology Conference. https://doi.org/10.15530/urtec-2019-1069.

Wang, Mingyuan, Baek, Kwang Hoon, Abeykoon, Gayan A. et al. 2020. Comparative Study of Ketone and Surfactant for Enhancement of Water Imbibition in Fractured Porous Media. *Energy & Fuels* **34** (5): 5159-5167. https://doi.org/10.1021/acs.energyfuels.9b03571.

Weissenborn, P. K. and Pugh, R. J. 1996. Surface Tension of Aqueous Solutions of Electrolytes: Relationship with Ion Hydration, Oxygen Solubility, and Bubble Coalescence. *Journal of Colloid and Interface Science* **184** (2): 550-563. http://www.sciencedirect.com/science/article/pii/S0021979796906517.

Wijaya, Nur and Sheng, James J. 2020. Surfactant selection criteria with flowback efficiency and oil recovery considered. *Journal of Petroleum Science and Engineering* **192**: 107305. https://www.sciencedirect.com/science/article/pii/S092041052030382X.

Wilson, Daniel, Poindexter, Laurie, and Nguyen, Thu. 2019. Role of Surfactant Structures on Surfactant-Rock Adsorption in Various Rock Types. *Proc.,* SPE International Conference on Oilfield Chemistry. https://doi.org/10.2118/193595-MS.

Xu, Liang, He, Kai, and Nguyen, Christina. 2015. Insights into Surfactant Containing Fracturing Fluids Inducing Microcracks and Spontaneously Imbibing in Shale Rocks. *Proc.,* SPE/CSUR Unconventional Resources Conference. https://doi.org/10.2118/175959-MS.

Xu, Liang, Ogle, James, and Collier, Todd. 2019. Fracture Hit Mitigation Through Surfactant-Based Treatment Fluids in Parent Wells. *Proc.,* SPE Liquids-Rich Basins Conference - North America. https://doi.org/10.2118/197097-MS.

Yang, Jiang, Jiang, Wei, Guan, Baoshan et al. 2014. Optimizing nanoemulsions as fluid flowback additives in enhancing tight gas production. *Journal of Petroleum Science and Engineering* **121**: 122-125. https://www.sciencedirect.com/science/article/pii/S0920410514001818.

Yarveicy, Hamidreza, Habibi, Ali, Pegov, Serge et al. 2018. Enhancing Oil Recovery by Adding Surfactants in Fracturing Water: A Montney Case Study. *Proc.,* SPE Canada Unconventional Resources Conference. https://doi.org/10.2118/189829-MS.

Yassin, Mahmood Reza, Dehghanpour, Hassan, Begum, Momotaj et al. 2018. Evaluation of Imbibition Oil Recovery in the Duvernay Formation. *SPE Reservoir Evaluation & Engineering* **21** (02): 257-272. https://doi.org/10.2118/185065-PA.

Ye, Zhongbin, Zhang, Fuxiang, Han, Lijuan et al. 2008. The effect of temperature on the interfacial tension between crude oil and gemini surfactant solution. *Colloids and Surfaces A: Physicochemical and Engineering Aspects* **322** (1): 138-141. https://www.sciencedirect.com/science/article/pii/S0927775708001635.

Yekeen, Nurudeen, Padmanabhan, Eswaran, Idris, Ahmad Kamal et al. 2019. Surfactant adsorption behaviors onto shale from Malaysian formations: Influence of silicon

dioxide nanoparticles, surfactant type, temperature, salinity and shale lithology. *Journal of Petroleum Science and Engineering* **179**: 841-854. https://www.sciencedirect.com/science/article/pii/S0920410519304334.

Yu, Yang, Li, Lei, and Sheng, James J. 2016. Further Discuss the Roles of Soaking Time and Pressure Depletion Rate in Gas Huff-n-Puff Process in Fractured Liquid-Rich Shale Reservoirs. *Proc.,* SPE Annual Technical Conference and Exhibition. https://doi.org/10.2118/181471-MS.

Yu, Yang and Sheng, James J. 2015. An Experimental Investigation of the Effect of Pressure Depletion Rate on Oil Recovery from Shale Cores by Cyclic N2 Injection. *Proc.,* SPE/AAPG/SEG Unconventional Resources Technology Conference. https://doi.org/10.15530/URTEC-2015-2144010.

Yuan, Cheng-Dong, Pu, Wan-Fen, Wang, Xiao-Chao et al. 2015. Effects of Interfacial Tension, Emulsification, and Surfactant Concentration on Oil Recovery in Surfactant Flooding Process for High Temperature and High Salinity Reservoirs. *Energy & Fuels* **29** (10): 6165-6176. https://doi.org/10.1021/acs.energyfuels.5b01393.

Yuan, Shundong, Wang, Shiyan, Wang, Xueying et al. 2016. Molecular dynamics simulation of oil detachment from calcite surface in aqueous surfactant solution. *Computational and Theoretical Chemistry* **1092**: 82-89. http://www.sciencedirect.com/science/article/pii/S2210271X16302924.

Yue, Zhiwei, Peng, Yang, He, Kai et al. 2016. Multifunctional Fracturing Additives as Flowback Aids. *Proc.,* SPE Annual Technical Conference and Exhibition. https://doi.org/10.2118/181383-MS.

Zeng, Tongzhou, S. Miller, Chammi, and Mohanty, Kishore. 2018a. Application of Surfactants in Shale Chemical EOR at High Temperatures. *Proc.,* SPE Improved Oil Recovery Conference. https://doi.org/10.2118/190318-MS.

Zeng, Tongzhou, S. Miller, Chammi, and Mohanty, Kishore. 2018b. Application of Surfactants in Shale Chemical EOR at High Temperatures. Presented at the SPE Improved Oil Recovery Conference, Tulsa, Oklahoma, USA. 2018/4/14/. https://doi.org/10.2118/190318-MS.

Zeppieri, S., Rodríguez, J., and López de Ramos, A. L. 2001. Interfacial Tension of Alkane + Water Systems. *Journal of Chemical & Engineering Data* **46** (5): 1086-1088. https://doi.org/10.1021/je000245r.

Zhang, Fan, Adel, Imad A., Park, Kang Han et al. 2018. Enhanced Oil Recovery in Unconventional Liquid Reservoir Using a Combination of CO2 Huff-n-Puff and Surfactant-Assisted Spontaneous Imbibition. *Proc.,* SPE Annual Technical Conference and Exhibition. https://doi.org/10.2118/191502-MS.

Zhang, Fan, Saputra, I. W., Parsegov, Sergei G. et al. 2019a. Experimental and Numerical Studies of EOR for the Wolfcamp Formation by Surfactant Enriched Completion Fluids and Multi-Cycle Surfactant Injection. *Proc.,* SPE Hydraulic Fracturing Technology Conference and Exhibition. https://doi.org/10.2118/194325-MS.

Zhang, Fan, Saputra, I. W. R., Adel, Imad A. et al. 2018a. Scaling for Wettability Alteration Induced by the Addition of Surfactants in Completion Fluids: Surfactant Selection for Optimum Performance. *Proc.,* SPE/AAPG/SEG Unconventional Resources Technology Conference. https://doi.org/10.15530/URTEC-2018-2889308.

Zhang, Fan, Saputra, I. W. R., Adel, Imad A. et al. 2018b. Scaling for Wettability Alteration Induced by the Addition of Surfactants in Completion Fluids: Surfactant Selection for Optimum Performance. In *Unconventional Resources Technology Conference, Houston, Texas, 23-25 July 2018*, 971-987. SEG Global Meeting Abstracts, Society of Exploration Geophysicists, American Association of Petroleum Geologists, Society of Petroleum Engineers.

Zhang, Fan, Saputra, I. W. R., Parsegov, Sergei G. et al. 2019b. Experimental and Numerical Studies of EOR for the Wolfcamp Formation by Surfactant Enriched Completion Fluids and Multi-Cycle Surfactant Injection. Presented at the SPE Hydraulic Fracturing Technology Conference and Exhibition, The Woodlands, Texas, USA. 2019/1/29/. https://doi.org/10.2118/194325-MS.

Zhang, Jin and Wang, Dongmei. 2018a. Chemical Stimulation With Driving Process to Extract Oil From Tight Formation. *Proc.,* SPE/AAPG/SEG Unconventional Resources Technology Conference. https://doi.org/10.15530/URTEC-2018-2903115.

Zhang, Jin and Wang, Dongmei. 2018b. Chemical Stimulation With Driving Process to Extract Oil From Tight Formation. Presented at the SPE/AAPG/SEG Unconventional

Resources Technology Conference, Houston, Texas, USA. 2018/8/9/. https://doi.org/10.15530/URTEC-2018-2903115.

Zhang, Jin, Wang, Dongmei, and Butler, Ray. 2013. Optimal Salinity Study to Support Surfactant Imbibition into the Bakken Shale. *Proc.,* SPE Unconventional Resources Conference Canada. https://doi.org/10.2118/167142-MS.

Zhong, Jie, Wang, Pan, Zhang, Yang et al. 2013. Adsorption mechanism of oil components on water-wet mineral surface: A molecular dynamics simulation study. *Energy* **59**: 295-300. http://www.sciencedirect.com/science/article/pii/S0360544213006038.

Zhou, Jia, Cutler, Jennifer, Hughes, Baker et al. 2014. Enhancing Well Stimulation with Improved Salt Tolerant Surfactant for Bakken Formation. *Proc.,* SPE Improved Oil Recovery Symposium. https://doi.org/10.2118/169141-MS.

Zhou, Xiam-min, Torsaeter, Ole, Xie, Xina et al. 1995. The Effect of Crude-Oil Aging Time and Temperature on the Rate of Water Imbibition and Long-Term Recovery by Imbibition. *SPE Formation Evaluation* **10** (04): 259-266. https://doi.org/10.2118/26674-PA.

Zhou, Xianmin, Morrow, N. R., and Ma, Shouxiang. 2000. Interrelationship of Wettability, Initial Water Saturation, Aging Time, and Oil Recovery by Spontaneous Imbibition and Waterflooding. *SPE Journal* **5** (02): 199-207. https://doi.org/10.2118/62507-PA.

Ziegler, Victor M. and Handy, Lyman L. 1981. Effect of Temperature on Surfactant Adsorption in Porous Media. *Society of Petroleum Engineers Journal* **21** (02): 218-228. https://doi.org/10.2118/8264-PA.